Novel mechanisms for the post-transcriptional regulation of monocyte-macrophage tissue factor expression

by
M. Bilal Iqbal
BSc MBBS MRCP(UK)

A thesis submitted for the
Degree of Doctor of Philosophy (PhD)

Imperial College London
2013

Imperial Centre for Translational and Experimental Medicine,
National Heart and Lung Institute,
Imperial College London,
Hammersmith Hospital,
Du Cane Road,
London W12 0NN.

Abstract

Post-transcriptional regulation of mRNA is an important determinant of net gene expression. Tissue factor (TF) is the key stimulus for thrombus formation and plays critical roles in atherothrombosis. Little is known about its post-transcriptional regulation. Tristetraprolin (TTP) is the most widely studied mRNA-binding protein, and binds to the adenylate-uridylate rich elements (AREs) in the 3' untranslated region (3'UTR) of target mRNAs and promotes degradation. Poly(ADP-ribose)-polymerase-14 (PARP-14), belongs to a family of ~17 proteins with a PARP domain that generates negatively charged poly(ADP-ribose) adducts on intracellular proteins – a post-translational modification implicated in diverse cellular functions. Preliminary findings in our laboratory have identified PARP-14 as a novel RNA-binding protein, and found it to regulate inflammatory mRNA. This study sought to establish the roles for TTP and PARP-14 in regulating TF mRNA stability in LPS-stimulated monocyte-macrophages.

Preliminary experiments demonstrated that TF mRNA, TF protein and TF mRNA stability were increased in *Ttp*$^{-/-}$ and *Parp14*$^{-/-}$ macrophages. Similarly, TF expression was increased *in vivo* in *Parp14*$^{-/-}$ mice. Furthermore, intravital microscopy demonstrated accelerated thrombosis following ferric-chloride injury in LPS-stimulated *Parp14*$^{-/-}$ mice. RNP immunoprecipitation, RNA biotin pulldown and co-immunoprecipitation assays demonstrated an interdependency for PARP-14 and TTP to form a ternary complex with TF mRNA. Both proteins interacted within the same 3'UTR segment containing a highly conserved palindromic ARE (AUAAUUUAUUUAAUA) comprising 2 overlapping AUUUAUUUA and UUAUUUAAU nonamers, both of which

appeared to be critical in mediating this interaction. Inhibition of p38, which classically results in accelerated decay of TTP-regulated transcripts, reduced TF mRNA stability in WT but not *Ttp*$^{-/-}$ or *Parp14*$^{-/-}$ macrophages. Inhibition of PARP activity reduced TF mRNA stability in WT but not in *Parp14*$^{-/-}$ macrophages. Interestingly, PARP-14 conferred selectivity for TTP to degrade TF mRNA, as PARP-14 had no effect on TNFα expression, an established target of TTP. Similarly, PARP inhibition had no effect on TNFα mRNA decay.

These data define novel roles for TTP and PARP-14 in the selective regulation of TF mRNA turnover, and demonstrates for the first time how the actions of TTP may be selectively regulated. PARP-14 functions as an accessory RNA-binding protein which is required for TTP to bind and degrade TF mRNA. Inhibition of either p38 or PARP catalytic activity accelerated TF mRNA decay. Thus one may propose that both PARP-14-mediated ADP-ribosylation and p38-mediated phosphorylation events are necessary for inactivating TTP-mediated TF mRNA decay. The selective destabilization of TF mRNA via pharmacological inhibition of PARP-14 may offer a novel therapeutic strategy in atherosclerosis and cardiovascular disease where thrombosis is linked to TF expression.

CONTENTS

Abbreviations

ABC	ATP -binding cassette (family of transporters)
ACAT-1	Acyl CoA: cholesterol acyltransferase-1
ACE	Angiotensin converting enzyme
ACS	Acute coronary syndrome
ActD	Actinomycin D
ADP	Adenosine diphosphate
Ago	Argonaute (family of proteins)
Akt/PKB	Protein kinase B
AMP	Adenosine monophosphate
AngII	Angiontesin II
AP-1	Activator protein 1
APC	Activated Protein C
ARE	Adenylateuridylate-rich elements
ARH	ADP-ribosyl hydrolase
AUF1	AU-rich binding factor 1
βME	β–mercaptoethanol
BMDM	Bone-marrow derived macrophage
BRF	Butyrate response factor
CAF1	CCR4-associated factor
CCR-2	C-C chemokine receptor type 2
CCR4	Carbon catabolite repressor-4
CG	Cytosine-guanine (haplotype)
COX-2	Cyclo-oxygenase-2
CRP	C-reactive protein
Dex	Dexamethasone
DIC	Disseminated intravascular coagulation
DNA	Deoxyribonucleic acid
DUSP	Dual specificity phosphatase

EDTA	Ethylenediaminetetraacetic acid
eIF	Eukaryotic translation initiation factor
ERK	Extracellular-signal-regulated kinase
FCS	Fetal calf serum
FSAP	Factor VII activating protein
GC	Glucocorticoid
GM-CSF	Granulocyte-macrophage colony-stimulating factor
GR	Glucocorticoid receptor
GRE	Glucocorticoid response element
GSK-3b	Glycogen synthase kinase 3
HDAC	Histone deacetylase
HDL	High-density lipoprotein
HePTP	Haemopoietic tyrosine phosphatase
HuR	Hu protein R
ICAM-1	Intercellular adhesion molecule-1
IFNγ	Interferon γ
IL	Interleukin
JAM-C	Junctional adhesion molecule C
JNK	c-Jun N-terminal kinases
KSRP	KH-type splicing regulatory protein
LDL	Low density lipoprotein
LDLR	Low density lipoprotein receptor
$Ldlr^{-/-}$	LDLR knock out
LPS	Lipopolysaccharide (endotoxin)
mAb	Mono-clonal antibody
MAPK	Mitogen-activated protein kinase
MAPKAPK-2	MAPK-activated protein kinase (MK2)
MCP-1	Monocyte chemoattractant protein-1
MFI	Mean fluorescence intensity
MI	Myocardial infarction
miRISC	MiRNA-containing RNA-induced silencing complex

miRNA	MicroRNA
mmLDL	Minimally modified low density lipoprotein
MMP	Matrix-degrading metalloproteinases
mRNA	Messenger ribonucleic acid
mTOR	Mammalian target of rapamycin
MyD88	Myeloid differentiation primary response gene 88
NAD+	Nicotinamide adenine dinucleotide
NES	Nuclear export signals
NFAT	Nuclear factor for activated T cells
NF-κB	Nuclear factor kappa-light-chain-enhancer of activated B cells
NUDIX	Nucleoside diphosphate linked to another moiety X
oxLDL	Oxidized low density lipoprotein
PABP	Poly(A)-binding protein
PAF	Platelet-activating factor
PAI	Plasminogen activator inhibitor
PAN-2	Poly(A) nuclease-2
PAN-3	Poly(A) nuclease-3
PAR	protease-activated receptors
PAR	Poly(ADP-ribose)
PARP	Poly(ADP-ribose) polymerase
PARG	Poly(ADP-ribose) glycohydrolase
Parp14$^{-/-}$	PARP-14 knock out
PB	Processing body
PBMC	Peripheral blood mononuclear cell
PBS	Phosphate-buffered saline
PCR	Polymerase chain reaction
PDGF	Platetlet derived growth factor
PDI	Protein disulphide isomerase
PGE_2	Prostaglandin E_2
PI3K	Phosphatidylinositide 3-kinase
PIP_2	Phosphatidylinositol 4,5-bisphosphate

PIP_3	Phosphatidylinositol (3,4,5)-triphosphate
PKC	Protein Kinase C
PN-1	Protease nexin-1
PPP	Platelet-poor plasma
PRP	Platelet-rich plasma
PS	Phosphatidylserine
PSDK1	Phosphoinositide dependent kinase 1
PSGL-1	P-selectin glycoprotein ligand-1
PTP-SL	Protein tyrosine phosphatase SL
RANTES	Regulated on activation, normal T cell expressed and secreted
RLMFI	Relative mean fluoresence intensity
RNA	Ribonucleic acid
RNP	Ribonucleoprotein
ROS	Reactive oxygen species
RT	Reverse transcriptase
RT-PCR	Reverse transcriptase polymerase chain rection
SAPK	Stress-activated protein kinase
SG	Stress granule
siRNA	Small interfering RNA
STAT	Signal transducer and activator of transcription
STEP	Striatal enriched tyrosine phosphatase
SUMO	Small ubiquitin-like modifier
TF	Tissue factor
TFPI	Tissue factor pathway inhibitor
TGFβ	Transforming growth factor-β
TIMI	Thrombolysis in myocardial infarction (score)
TIMP	Tissue inhibitors of metalloproteinase
TLR-4	Toll-like receptor-4
TNFα	Tumor necrosis factor alpha α
TNFR	TNFα receptor
tPA	Tissue-type plasminogen activator

TREM-1	Triggering receptor expressed on myeloid cells 1
TTP	Tristetraprolin
Ttp$^{-/-}$	TTP knock out
uPA	Urokinase-type plasminogen activator
UTR	Untranslated region
VCAM-1	Vascular cell adhesion protein 1
VEGF	Vascular endothelial growth factor
VSMC	Vascular smooth muscle cell
vWF	Von willebrand factor
ZF	Zinc finger

List of Figures

List of Tables

Acknowledgements

All work relating to this thesis was conducted over the course of three years under the British Heart Foundation Chairholder's Scholarship and Junior Clinical Research Fellowship at the Imperial Centre for Translational and Experimental Medicine, Hammersmith Hospital, London. The work presented in this thesis represents my own work and all else has been appropriately referenced..

I cannot be grateful enough to my supervisor, Professor Dorian Haskard, for his everlasting guidance, support and encouragement without which this work would never have been possible. I am also grateful to Mike Johns and Yu Liu who orientated me in the basic science laboratory and taught me the basic science and molecular techniques. In particular, I worked closely with Mike Johns throughout the three years, and if it was not for his patience, guidance and advice on a daily basis this project would certainly not have been where it is today. I am also grateful to Graeme Birdsey and Richard Starke for their advice and support throughout my time in the basic science laboratory. I would like to thank Felicity Gavins and Kevin Woollard for help with the intravital microscopy experiments.

This project has allowed me to develop many national and international academic collaborations, and I am particularly grateful to Mike Laffan and Nigel Mackman who provided advice on all aspects of thrombosis; Jon Dean and Andy Clark who provided guidance on all aspects of post-transcriptional regulation; Jon Dean and Perry Blackshear for providing the *Ttp*$^{-/-}$ mice; and Mark Boothby for providing the *Parp14*$^{-/-}$ mice.

Whilst aspiring to become an interventional cardiologist, this three year period of basic science research was, perhaps, the most important factor in potentially shaping my future career pathway. The importance of basic science research as the fundamental building block upon which clinical and translational research is based became apparent. My research training has equipped me with valuable basic science research techniques

and general research principles that would one day enable me to become an independent academic interventional cardiologist.

Finally, I am forever grateful to my wonderful wife, Nabila, and two adorable children, Adam and Anna, for their patience, love and support at home throughout my research period without which I would never have been able to complete this work.

I would like to dedicate my thesis to my wife and children, Nabila, Adam and Anna.

Copyright declaration

Chapter 1

Introduction

1.1 ATHEROSCELROSIS

1.1.1 Introduction to atherosclerosis

Atherosclerosis is a progressive disease which is characterized by the accumulation of lipids and fibrous elements within large and medium-sized arteries of the vascular beds (aorta, carotid, coronary and peripheral arteries) and represents the pathological basis for cardiovascular disease (coronary artery disease, stroke and peripheral vascular disease)[1, 2]. It is not a disease of the 21st century man, as calcified coronary lesions have been documented dating back to Egyptian mummies, and as for much of the last century, it was widely considered to be a disorder of lipid storage as a natural component of aging[3]. With the advancing modern era of cell biology, atherosclerosis is now understood to represent a mutlifactorial complex disease process. In a broad outline, it can be considered as a form of chronic inflammation resulting from the interaction between modified lipoproteins, macrophages, T cells and normal cellular elements of the arterial wall[4]. Several risk factors such as hyperlipidaemia, diabetes, hypertension, smoking, inflammation, age and gender contribute to the development and progression of atherosclerosis[5].

1.1.2 Burden of atherosclerosis

Atherosclerosis is associated with significant morbidity and mortality. Cardiovascular disease is predicted to be the principal cause of death worldwide by the year 2030, accountable for 25 million deaths per year[6]. Coronary artery disease is now the leading cause of death worldwide with a high clinical, social and economic burden. An estimated 2.6 million people in the UK have coronary artery disease and accounts for over 88,000 deaths per year (an average of 224 people each day or one death every six minutes). Approximately 1.3 million people in the UK have had a myocardial infarction, 2 million people suffer from angina, and over 230,000 new myocardial infarctions are diagnosed every year[7].

1.1.3 Development of the atherosclerotic plaque

Inflammation is now recognized as central to the development of atherosclerosis[8]. As early as 1958, experimental observations in rabbits showed that monocytes adhered to

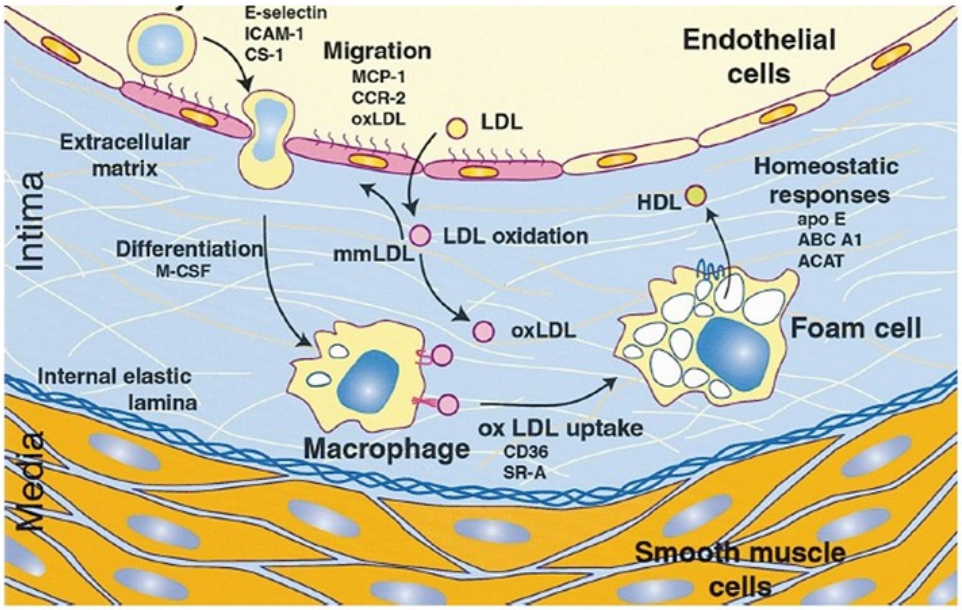

Figure 1-1: Development of the foam cell within an atherosclerotic plaque
Endothelial dysfunction results in induction of cell adhesion molecules. Monocytes adhere to the endothelium and migrate into the sub-endothelial space and differentiate into macrophages. LDL is subject to modification progressing from minimally modified (mmLDL) to oxidised LDL (oxLDL). Macrophages take up the oxLDL via scavenger receptors resulting in foam cell formation. OxLDL is subject to esterification by ACAT-1and storage as lipid droplets or exported to extracellular HDL acceptors via cholesterol transporters, such as ATP -binding cassette family of transporters (ABC-A1). Monocytes attach to endothelial cells. Secretion of apo E contributes to formation of HDL, thereby increasing extracellular acceptors. Adapted from [23].

the intact endothelium in early atherosclerotic lesions[9]. Leukocyte recruitment does not generally occur in the presence of normal endothelium. The endothelium is a metabolically active organ system, and by virtue of its location and size (~700m^2 in an average sized adult) plays a critical role in maintaining vascular homeostasis by regulating thrombotic, inflammatory and reparative responses to local injury[10, 11]. Thus, endothelial dysfunction represents the initial promoter of atherosclerosis[12]. At the onset of atherosclerosis, lipoproteins become trapped by the proteoglycans in the intima and accumulate in the arterial wall, resulting in intimal thickening. Endothelial dysfunction promotes an inflammatory environment, where the lipoproteins are modified by oxidation, lipolysis, proteolysis and aggregation[8]. Pro-inflammatory cytokines are released in response to the infiltrated oxidized lipoproteins to recruit circulating monocytes. Cells within the atherosclerotic lesion express many chemotactic factors for monocytes. There is overwhelming evidence to support the critical role for MCP-1 as

the most important mediator of monocyte recruitment[13, 14]. Vascular endothelial cells produce MCP-1, anchoring it on the cell surface. Monocytes, activated T-cells and activated natural killer cells express CCR-2, a receptor for MCP-1, and thus MCP-1/CCR-2 are important in monocyte recruitment into atherosclerotic lesions[15]. Furthermore, adhesion molecules (ICAM-1, VCAM-1, P-selectin and E-selectin) essential for monocyte recruitment are up-regulated on vascular endothelial cells[16-18]. Once monocytes exit the circulation to enter the atherosclerotic lesion, they differentiate into macrophages. In atherosclerotic lesions, M-CSF is criticial for monocyte-macrophage differentiation[19]. Oxidized lipoproteins are taken up by macrophages via macrophage scavenger receptors (SR-A and CD-36)[20], where they are transported into lysosomes and degraded into amino acids and free cholesterol[21]. The free cholesterol is released back into the cytosol, and given that excess free cholesterol is toxic to macrophages[22], it is converted to cholesterol esters by acyl CoA: cholesterol acyltransferase-1 (ACAT-1) and stored in this form in the cytosol[21, 23]. This intracytoplasmic accumulation of cholesterol ester as membrane-free lipid droplets transforms macrophages into foam cells (figure 1-1)[22]. Foam cells in atherosclerotic lesions eventually undergo apoptosis, because intracellular accumulation of free cholesterol is toxic to them[24]. This is mainly seen within the central lipid core of the lesion. Macrophages and T cells secrete cytokines and growth factors which promote smooth muscle cell migration, proliferation and extracellular matrix production[23]. This growing mass of smooth muscle cells embedded in extracellular matrix results in fibrous cap formation that protects the deeper thrombogenic lipid core from contact with the circulating blood. Disruption of this fibrous cap results in activation of the coagulation cascade and thrombosis.

1.2 COAGULATION CASCADE

The coagulation cascade is characterized by sequential, rapid and highly localized activation of serine proteases resulting in the generation of thrombin, which subsequently converts fibrinogen to fibrin. Following endothelial injury, collagen and tissue factor (TF) become exposed to the flowing blood. Collagen triggers the

accumulation and activation of platelets, whereas TF initiates the generation of thrombin via the “extrinsic pathway”[25].

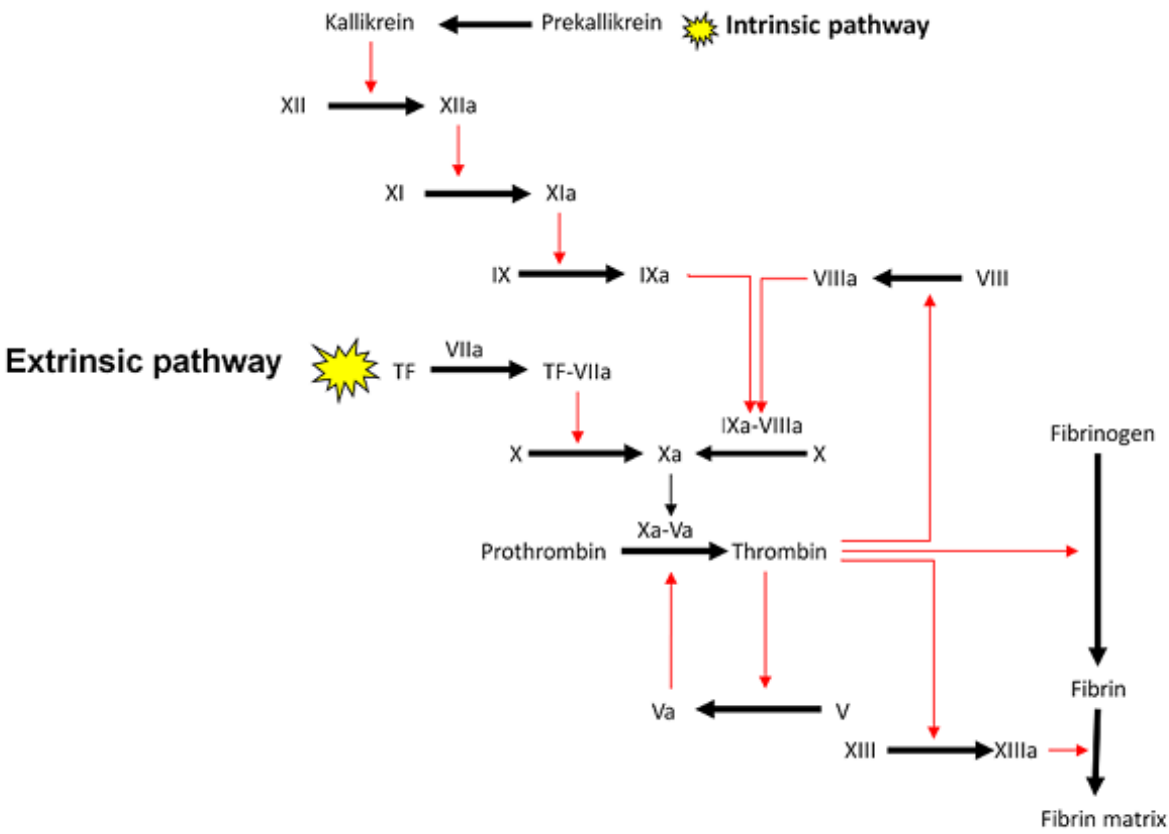

Figure 1-2: The coagulation cascade
The extrinsic and intrinsic pathways ultimately converge to activate factor X. This results in cleavage of prothrombin to thrombin which results in thrombus formation.

1.2.1 Platelet activation

Platelets adhere to the site of endothelial damage via platelet glycoprotein VI that interacts directly with collagen, and platelet glycoprotein 1b-V-IX that interacts with collagen-bound von Willebrand factor (vWF)[26]. These platelet-endothelial cell interactions result in platelet activation[27]. Thrombin can directly activate platelets, independently of vWF and platelet glycoprotein VI, by cleaving protease-activated receptors (PARs)[28, 29]. Platelet activation results in a conformational change of the platelet integrin $\alpha_{IIb}\beta_3$, increasing the affinity for its ligands, fibrinogen and von Willebrand factor[30]. This mediates platelet-platelet interactions and recruits platelets to the developing thrombus. Activated platelets release granules containing ADP,

serotonin, and thromboxane A_2 which leads to further platelet activation[31]. The activated platelet membrane provides a surface rich in negatively charged phosphatidylserine (PS) to act as a catalytic surface for activation of coagulation factors[25].

1.2.2 Extrinsic pathway

The "extrinsic" pathway plays an important role in thrombosis, resulting in the rapid production of thrombin and subsequent thrombus formation. TF is the key stimulus that drives the extrinsic pathway. TF activates factor VII and complexes with its activated form (VIIa) and to activate factors IX and X (IXa and Xa). Factor VIIa is a very weak serine protease, but upon binding to TF, its catalytic activity is enhanced over a million fold. Factor Xa binds with factor V, which converts prothrombin into thrombin. Initially, the extrinsic pathway is inefficient as factors VIII and V, the circulating pro-factors for the tenase (factor VIIIa-factor IXa) and prothrombinase (factor Xa-factor Va) complexes are not activated. The amount of thrombin produced by factor Xa-factor V complex is a 100 times less that that seen with factor Xa-factor Va complex, and therefore the initial yield of thrombin is very small. However, thrombin subsequently activates factors VIII and V (factors VIIIa and Va), and the tenase and prothrombinase complexes proceed efficiently to generate a large burst of thrombin[32]. Thrombin cleaves fibrinogen into soluble fibrin monomers and also activates factor XIII (factor XIIIa) that cross-links soluble fibrin monomers into a fibrin matrix[25].

1.2.3 Intrinsic pathway

The "intrinsic pathway" or "contact activation pathway" plays a minor role in initiating thrombus formation, due to a slower activation process. However, its latent activation may play an important role in thrombus propagation. Furthermore, the initial burst of thrombin following TF exposure (via the extrinsic pathway) can directly activate components of the intrinsic pathway. The intrinsic pathway begins with the formation of the primary complex on collagen comprising kininogen, prekallikrein, and factor XII. Prekallikrein is converted to kallikrein and this activates factor XII (factor XIIa). Factor XIIa activates factor XI (factor XIa) that activates factor IX (factor IXa) which complexes with factor VIIIa to from the tenase complex. Thrombin can additionally activate factor XI and thus contribute to the intrinsic pathway[33].

1.2.4 Feedback mechanisms and regulation of thrombosis

The coagulation cascade is regulated by several naturally occurring anticoagulants, TF pathway inhibitor (TFPI), Protein C and anti-thrombin. TFPI inhibits the TF-factor VIIa complex, by initially binding with factor Xa, and then TFPI-factor Xa complexes TF-factor VIIa to form a stable quaternary complex[34]. In this way, TFPI is also a direct inhibitor of factor Xa. TFPI provides a mechanism to ensure that a small procoagulant stimulus does not produce an uncontrolled burst of thrombin. However, once the coagulation cascade is triggered, thrombin provides a positive-feedback amplification mechanism, through the activation of factors V, VIII and XI, and allows the coagulation cascade to continue in the absence of functionally active TF[35]. It is not TFPI, but the inhibitory actions of Protein C and anti-thrombin that become more prevalent in controlling thrombin generation and eventually switching off the coagulation cascade. Protein C is converted to activated Protein C (APC) by the thrombin-thrombomodulin complex. APC in association with its cofactor Protein S cleaves and inactivates factors Va and VIIIa[36]. The primary target of anti-thrombin is thrombin, but it can also inactivate other coagulation factors, including factors IXa, Xa, XIa, and XIIa[25, 36]. The coagulation cascade is outlined in figure 1-2.

1.3 MONOCYTE-MACROPHAGES IN ATHEROTHROMBOSIS

1.3.1 Plaque instability and rupture

Plaque rupture is a recognized complication of atherosclerosis. It exposes thrombogenic material to the flowing blood and initiates the coagulation cascade and thrombosis (hence the term “atherothrombosis”)[37]. Although this can lead to occlusive thrombus formation and acute ischaemia, accounting for the most serious clinical manifestations of atherosclerosis[37, 38], repeated episodes of plaque rupture and thrombosis can contribute to asymptomatic plaque growth. If thrombus formation remains mural rather than occlusive and its lysis is incomplete, then re-endothelialization followed by thrombus organization results in plaque growth[39]. Similarly, plaque growth can occur following intraplaque haemorrhage from plaque neovessels. Cells in the growing plaque

receive oxygen by diffusion, but when intimal thickness increases beyond a diffusion limit, this stimulates growth of new vessels (neovessels). These neovessels can rupture or leak resulting in intraplaque haemorrhage. Consequently, the plaque increases in size with the redevelopment of plaque hypoxia and stimulation of further neovascularization predisposing to further intraplaque haemorrhage. Thus intraplaque haemorrhage can contribute to exponential plaque growth and predispose to plaque instability[40].

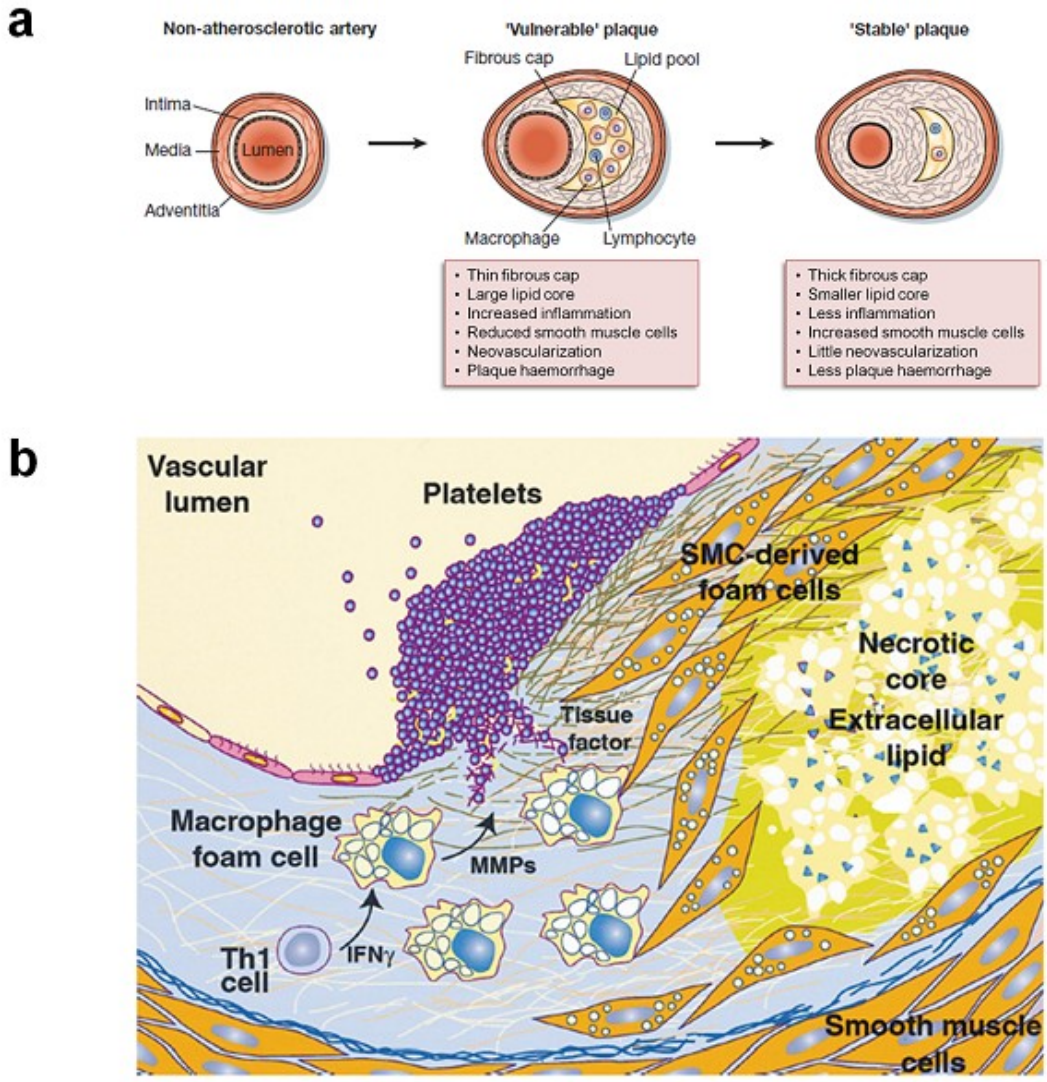

Figure 1-3: Plaque instability, rupture and thrombosis
(a) Features of the "vulnerable" versus "stable" plaque. Adapted from [44]; (b) Weakening and thinning of the fibrous cap can ultimately result in plaque rupture. This exposes TF and initiation of thrombus formation. Adapted from [23]

It is plaque composition rather than size and severity of the resulting stenosis that plays a critical role in plaque rupture [41, 42]. In advanced atheromatous plaques, the lipid core contains abundant free cholesterol, oxidised lipids and apoptotic cells. This necrotic lipid core is rich in TF, which is primarily derived from macrophages and foam cells[43]. Following plaque rupture, TF is the key trigger for initiating thrombosis. Factors associated with plaque instability include, a large lipid core, thin fibrous caps, increased inflammation of the fibrous cap, increased plaque neovascularization and intraplaque haemorrhage(figure 1-3)[44, 45]. Increased plaque inflammation is central to the pathogenesis of plaque rupture[46]. Ruptured plaques contain more inflammatory cells than intact plaques and these primarily include monocytes/macrophages but also include activated T cells and mast cells. Increased expression of inflammatory mediators such as adhesion molecules, cytokines and chemokines can be demonstrated at sites of plaque rupture[46, 47].

The fibrous cap of an atherosclerotic plaque protects the deeper thrombogenic lipid core from contact with the circulating blood. Its structural components include collagen, elastin and proteoglycans that are derived from smooth muscle cells. Thinning of the fibrous cap is considered to be a prelude to plaque rupture and fibrous caps from ruptured plaques contain less extracellular matrix and fewer smooth muscle cells[48]. This reduction in extracellular matrix can result from decreased synthesis and/or increased breakdown. Decreased extracellular matrix synthesis results from a reduction in smooth muscle cells with a reduction in their synthetic function[48-50]. Inflammatory cytokines, particularly INF-γ, inhibit collagen synthesis by smooth muscle cells in atherosclerotic plaques[51]. TGF-β is expressed by macrophages, smooth muscle and endothelial cells and promotes plaque stability by inducing collagen synthesis. With plaque development, there is a reduction in TGF-β receptors and thus a reduction in TGF-β-mediated collagen synthesis thereby promoting plaque instability and rupture[52]. Increased extracellular matrix breakdown is attributed to a number of proteases that include matrix-degrading metalloproteinases (MMPs), cathepsins, tryptase, elastase and chymase that are primarily expressed by macrophages and to a lesser extent by smooth muscle and endothelial cells[53-58]. Studies have consistently demonstrated the

colocalization of MMPs in unstable plaques[57-59]. MMPs can additionally promote plaque neovascularization[60] that predisposes to plaque haemmorhage and instability.

1.3.2 Monocyte-macrophages as modulators of thrombosis

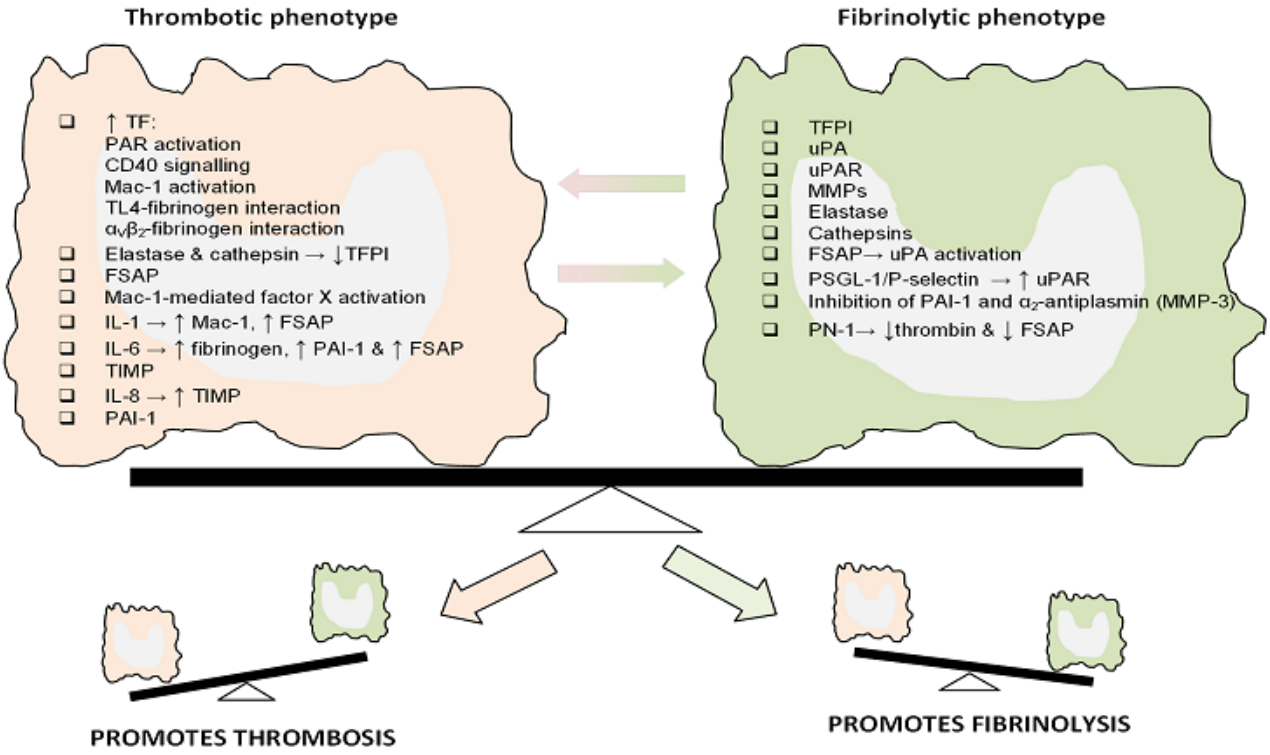

Figure 1-4: Monocyte-macrophages in thrombosis-fibrinolysis
Monocyte-macrophages express many thrombotic and fibrinolytic effector mechanisms that may contribute to the local thrombosis-fibrinolysis balance.

Thrombus formation is a dynamic process characterized by a continuous balance between thrombotic and fibrinolytic mechanisms. Monocyte-macrophages possess both thrombotic and fibrinolytic activity[61-72], and thus may modulate thrombus formation (figure 1-4). Recent studies examining thrombi from culprit coronary lesions show that the age of thrombus can be greater than 7 days[73-76]. It is important to understand the evolution of the developing thrombus and the factors that may govern its fate. What factors determine the outcomes of thrombosis are unclear, but in simple terms, thrombus propagation probably results from imbalances between thrombotic and fibrinolytic activities, at least at a local level, and the contributory role of monocyte-

macrophages in this setting may be crucial. The formation of a cross-linked fibrin matrix approximates cells and allows complex interactions to occur between macrophages, platelets and endothelial cells. With up-regulation of adhesion molecules, receptors, inflammatory cytokines, secretory enzymes and with activated clotting factors and products of the coagulation cascade, there is considerable potential for modulation of macrophage function, both in an autocrine and paracrine fashion. Figure 1-5 summarizes the complex interplaying mechanisms between different cells in inflammatory and thrombotic milieu of plaque rupture and thrombosis.

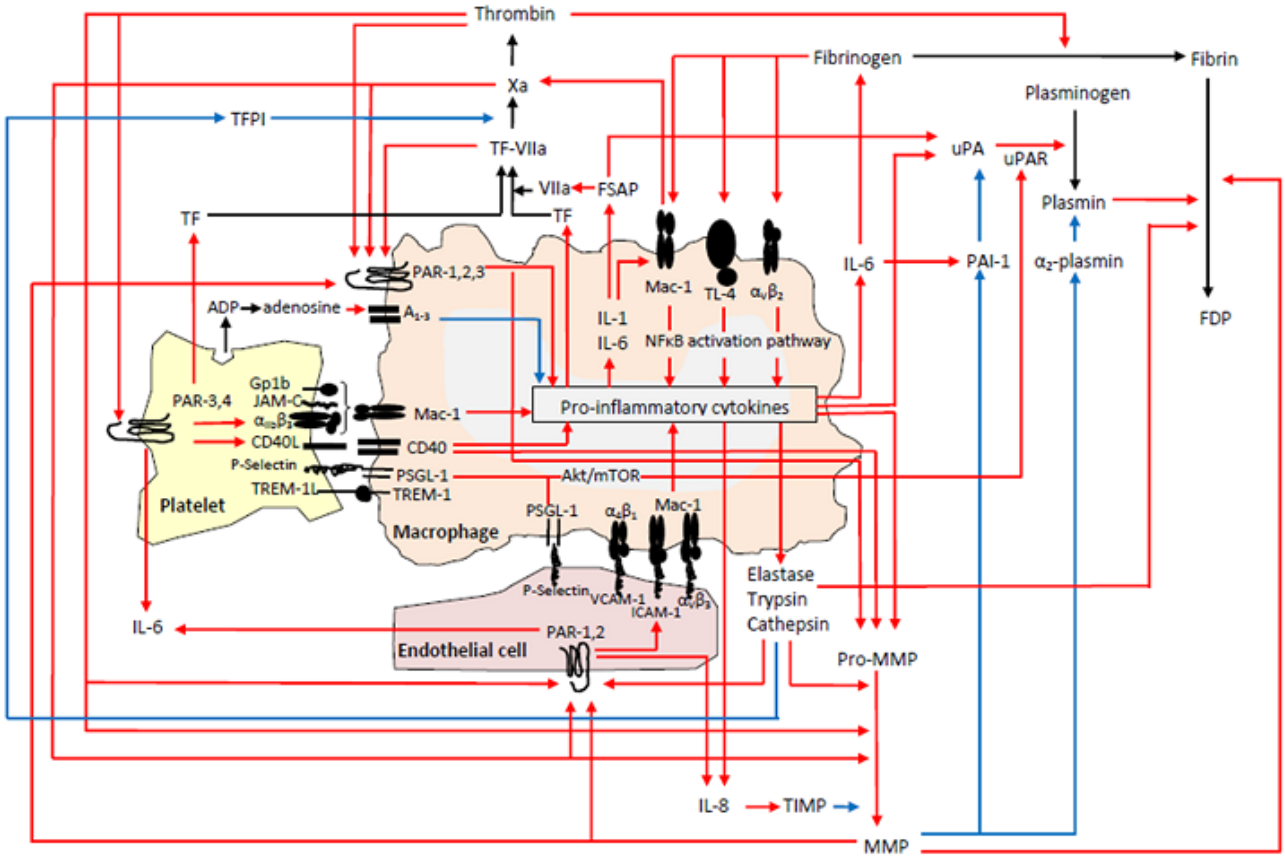

Figure 1-5: Monocyte-macrophages in thrombosis-fibrinolysis
Integrative model showing the multiple interactions of monocyte-macrophages in thrombosis (▬ denotes activation; ▬ denotes inhibition).

1.3.2a Macrophages and tissue factor

TF is the key trigger for thrombosis. Monocyte-macrophages are an important source of TF in atherothrombosis, both within the plaque and the circulating blood. In the blood,

TF is expressed on monocytes and microparticles[63]. Microparticles (MPs) are small membrane vesicles, less than 1000nm in diameter that are derived from activated and apoptotic cells. They are predominantly derived from monocytes/macrophages but can also be released by lymphocytes, vascular smooth muscle cells, endothelial cells and platelets[77, 78]. They express negatively charged phosphatidylserine (PS) and antigen markers representative of cellular origin. PS is a procoagulant phospholipid necessary for the assembly of blood clotting enzyme complexes[25], and together with TF, microparticles serve as catalytic surfaces for thrombosis[79]. In atherosclerotic plaques, the necrotic lipid core is rich in TF, which is primarily derived from apoptotic macrophages and foam cells[43]. In atherosclerosis, monocyte differentiation into macrophages is itself associated with a significant increase in TF expression via the NF-κB and AP1 transcription factor pathways[80]. CD40 and its ligand, CD40L, are co-expressed by macrophages and vascular smooth muscle cells[66, 81, 82]. Oxidised lipoproteins increase the expression of CD40 and CD40L[83], and increased CD40 signalling enhances thrombogenicity by decreasing thrombomodulin and increasing TF production in vascular smooth muscle cells and macrophages[84, 85]. In macrophages, the activation of protease-activated receptors (PARs)[28] and ligation of PSGL-1, Mac-1 and TREM-1 receptors[67, 86] through macrophage-platelet-endothelial cell interactions results in increased expression of TF.

In atherosclerotic plaques, TFPI is co-expressed by endothelial cells, vascular smooth muscle cells, macrophages and foam cells[70]. Both TF and TFPI-positive macrophages can be demonstrated within the necrotic core of atherosclerotic plaques[87]. There are no studies that have specifically explored TFPI activity in the context of plaque rupture and thrombosis, but differential expression of TF and TFPI has been demonstrated in atherosclerotic plaques, thus implicating a role for TFPI in modulating plaque thrombogenicity[68, 88, 89]. This concept may be extended to thrombosis, and a relative deficiency of TFPI may promote thrombosis. Macrophages produce elastase and cathepsins, which can cleave and inactivate TFPI[90, 91], and this provides a potential role for macrophages in regulating and modulating thrombosis.

1.3.2b Macrophages and thrombin

Although thrombin is the key effector of the coagulation cascade, it contributes significantly to inflammation in atherosclerosis and thrombosis. The predominant mechanism mediating this pro-inflammatory response is via activation of PARs. These receptors have four sub-types (PAR 1-4) and are expressed on macrophages, endothelial cells, vascular smooth muscle cells and platelets[71]. They require proteolytic cleavage for their activation, and although thrombin is the primary activating protease, other proteases including factors Xa and VIIa and those derived from macrophages (tryptase, cathepsins, MMPs, plasmin) can additionally activate these receptors[71, 92] (table 1-1). Thus, macrophages play important roles in PAR activation, both in a paracrine and autocrine fashion, and PAR activation integrates macrophage function with neighbouring cells and different components of the coagulation cascade. In macrophages, PAR-1, PAR-2 and PAR-3 activation stimulates a pro-inflammatory and pro-thrombotic response with increased expression of chemo-attractants (MCP-1), inflammatory cytokines (IL-1, IL-6, IL-8), MMPs and TF[93-95].

Activation of endothelial PAR-1 and PAR-2 elicits a pro-inflammatory and pro-thrombotic response with increased expression of adhesion molecules (ICAM-1, VCAM-1 P-selectin and E-selectin), chemo-attractants (MCP-1), cytokines (IL-6 and IL-8), vWF, TF and PAI-1[92, 96, 97]. By stimulating an acute-phase response, IL-6 can further promote thrombogenicity by increasing circulating fibrinogen and plasminogen activator inhibitor (PA-I)[98]. Furthermore, endothelial PAR activation induces cell retraction and reorganization of cadherins at endothelial junctions, increasing endothelial permeability and promoting monocyte extravasation[99]. Activation of platelet PAR-3 and PAR-4, results in granule release, formation of microparticles, secretion of a number of cytokines (PDGF, PF4, and RANTES), expression of TF, up-regulation and activation of $\alpha_{IIb}\beta_3$ complex and increased expression of P-selectin and CD40L[28, 86, 92, 100, 101]. Thrombin interacts with gp1b and P-selectin, and these may serve to localize thrombin to the platelet surface to promote PAR activation[102]. PAR activation promotes CD40 signalling and this induces the expression of pro-inflammatory cytokines including IL-1, IL-6, and IL-8, adhesion molecules, MMPs and TF[83].

	LOCATION				ACTIVATING PROTEASES	
	Endothelial cell	Platelet	Leukocyte	VSMC	Primary	Others
PAR-1	•		•	•	Thrombin	Trypsin Factor Xa MMP-1
PAR-2	•		•	•	Trypsin Tryptase	Factor Xa Factor VIIa
PAR-3		•			Thrombin	
PAR-4		•			Thrombin Trypsin	Plasmin Cathepsin

Table 1-1: Distribution and activation of PARs
PAR 1-4 are expressed on different cells and can be activated by a number of different proteases.

Thrombin influences all aspects of monocyte-macrophage function and intricately modulates their inflammatory, thrombotic and fibrinolytic activity. Conversely, macrophages may play important roles in modulating thrombin function. Both platelets and macrophages produce PAI-1 and protease nexin-1 (PN-1) that can inhibit thrombin, thereby mediating anti-thrombotic effects[65]. Although PAI-1 predominantly inhibits urokinase-type plasminogen activator (uP)A, by binding to vibronectin, it can alter its substrate specificity, allowing it to inhibit thrombin[103]. PN-1 is a serine protease and is a powerful inhibitor of thrombin but can also inhibit uPA and plasmin. In the presence of glycosaminoglycans, thrombin becomes the preferential target of PN-1[104]. PN-1 is a more potent thrombin inhibitor than anti-thrombin[105], and there is evidence that it exerts a predominant anti-thrombotic effect[106].

1.3.2c Macrophages and clotting factors

Macrophages can initiate coagulation via the Mac-1 (CD11b/CD18, $\alpha_M\beta_2$) receptor[69] and through the expression of factor VII activating protein (FSAP)[72]. Mac-1 is a cell surface receptor that is up-regulated by pro-inflammatory cytokines and platelet-macrophage interactions through P-selectin/PSGL-1, CD40L/CD40 and TREM-1L/TREM-1[67]. Mac-1 can bind to factor X and following exposure to ADP, macrophages can catalyse the activation of cell-bound factor X to factor Xa, independent of TF and factor VIIa[69]. FSAP is a serine protease, secreted as an inactive zymogen that can be activated by

polyanions and uPA[72]. It is secreted by macrophages, and its expression is increased by pro-inflammatory cytokines, particularly IL-1 and IL-6[107]. It is rapidly inactivated by α_2-antiplasmin, anti-thrombin, PN-1 and PAI-1, after which it is internalised by receptor-mediated endocytosis[72, 108]. The primary substrates for FSAP are factor VII and uPA[72], and therefore, FSAP plays important roles in initiating the extrinsic pathway and mediating fibrinolysis, although there is greater evidence for the later. Another potential substrate is fibrinogen, implicating FSAP in fibrin formation[72]. Immunostaining studies show that FSAP is not present in normal arteries, but increased intracellular and extracellular FSAP is present in vulnerable atherosclerotic plaques, confined predominantly to macrophages[107]. FSAP inhibits vascular smooth muscle cell proliferation by cleaving and inactivating PDGF[109], and this in conjunction with its pro-fibrinolytic actions, may promote plaque instability.

1.3.2d Macrophages and platelets

During thrombus formation, activated platelets express P-selectin, $\alpha_{IIb}\beta_3$, gp1b, JAM-C, CD40L and TREM-1 that can bind to receptors on macrophages. Platelet-macrophage interactions activate intracellular signalling pathways that stimulate pro-inflammatory and pro-thrombotic responses in macrophages[85]. P-selectin can bind to PSGL-1 on monocyte-macrophage derived microparticles, resulting in fusion of microparticles with activated platelets[110]. Platelet-macrophage interactions, through P-selectin/PSGL-1, CD40L/CD40 and TREM-1L/TREM-1, up-regulate macrophage integrin expression, particularly the Mac-1 receptor. Mac-1 binding to platelet $\alpha_{IIb}\beta_3$ is mediated by fibrinogen, but can additionally bind with platelet gp1b and JAM-C independently of fibrinogen. Ligation of macrophage PSGL-1, Mac-1, CD40 and TREM-1 activates the NF-κB transcription factor pathways promoting proinflammatory and prothrombotic responses with up-regulation of IL-1β, IL-8, TNF-α, MCP-1 and TF[85].

1.3.2e Macrophages and fibrinolysis

Plasmin is the most important mediator of fibrinolysis, and exists in its inactive form, plasminogen, that requires activation by plasminogen activators - tissue PA (tPA) and

urokinase-type PA (uPA). tPA-mediated plasminogen activation is primarily involved in fibrinolysis in the circulation, whereas uPA activates cell-bound plasminogen by binding with a specific cell surface receptor, u-PAR[111]. Macrophages contribute to fibrinolysis through plasmin-dependent and plasmin-independent mechanisms. Besides its fibrinolytic function, plasmin can cleave and activate annexin A2 heterotetramer on macrophages stimulating a proinflammatory response[112]. Fibrinolysis is regulated by α_2-antiplasmin and plasminogen activator inhibitors, PAI-1 and PAI-2[113, 114]. Macrophages play important roles in regulating fibrinolysis, contributing to mechanisms that promote and inhibit fibrinolysis. Importantly, they produce uPA and tPA, which mediate plasmin-dependent fibrinolysis, and PAI-1, the predominant inhibitor of fibrinolysis[115]. TGFβ1 can induce the formation of reactive oxygen species (ROS), which can both directly and indirectly upregulate the expression of PAI-1[116, 117]. Ligation of macrophage PSGL-1 receptor by P-selectin on platelets and endothelial cells can enhance macrophage fibrinolytic activity by activating Akt signalling to the mammalian target of rapamycin (mTOR) kinase complex, resulting in the upregulation of uPAR[118]. Macrophages express FSAP, which promotes fibrinolysis by activating uPA[72].

Macrophages contribute to alternative plasmin-independent fibrinolytic pathways that can account for up to a third of total fibrinolysis[119, 120]. Both soluble and insoluble fibrin can bind with Mac-1, and following endocytosis, fibrin is degraded via lysosomal cathepsin[62, 121]. Mac-1 mediated fibrin degradation can account for up to 20% of total fibrinolysis[122]. Additionally, macrophages release fibrinolytic enzymes that include elastase and cathepsins[123, 124]. Ligation of Mac-1 by fibrin also results in the release of elastase, which has potent fibrinolytic properties[125]. Elastase can cleave plasminogen, removing the first 4 kringle domains, to yield mini-plasminogen. Mini-plasminogen is readily cleaved by uPA to form mini-plasmin, and compared to plasmin, mini-plasmin is more efficient in forming fibrin, and is 10 times less sensitive to inactivation by α_2-antiplasmin[126-128]. Elastase has further anti-thrombotic characteristics, by cleaving and inactivating factors VIIa, VIIIa, IXa, XIIa and XIIIa[129, 130]. Certain MMPs expressed by macrophages possess direct fibrinolytic activity and can further promote fibrinolysis by inactivating PAI-1 and α_2-antiplasmin[131].

1.3.2f Macrophages and MMPs

MMPs constitute a group of zinc-dependent endopeptidases that degrade most components of the extracellular matrix predisposing to plaque instability and rupture. At present, there are 23 members of the MMP family. They are synthesized and secreted as zymogens that are activated by several proteases including, plasmin, trypsin, cathepsins, kallikrein, chymase, thrombin, factor Xa and other MMPs[132]. Monocytes express very little MMPs, but contact with cells and extracellular matrix stimulates PGE_2 production. This acts in an autocrine fashion to activate the monocyte EP4 receptor that increases the expression of MMPs[133].

Several MMPs (MMP-1, MMP-2, MMP-3, MMP-7, MMP-8, MMP-9, MMP-12, MMP-14) are expressed by macrophages in atherosclerotic plaques. The expression of MMPs is up-regulated by oxidised lipoproteins, ROS, CD-40L, TNFα and IL-1β through activation of the NF-κB pathway[134-136]. Cytokines exert variable influences on the expression of different MMPs. TGF-β and IL-10 down-regulate MMP expression and this may explain their atheroprotective effects[60]. IL-4 down-regulates MMP-1 and MMP-9 production[137], whilst being a potent stimulus for MMP-12 production[138]. IFN-γ is a pro-inflammatory cytokine that promotes atherosclerosis[139], but interestingly, reduces the production of MMP-9 and MMP-12[137, 140]. Tissue inhibitors of matrix MMPs (TIMP) 1-4 are expressed in atherosclerotic plaques and regulate extracellular matrix breakdown. Macrophages constitutively express TIMPs, and oxidised lipoproteins have been shown to decrease TIMP secretion through the autocrine action of IL-8[141].

MMPs can promote fibrinolysis with MMP-3 and MMP-7 having direct fibrinolytic activity. In addition, MMP-3 specifically inactivates PAI-1 and α_2-antiplasmin, further enhancing its fibrinolytic effect. On the other hand, MMP-3 and MMP-7 can also inhibit fibrinolysis by cleaving uPA to remove the uPAR binding domains, thus preventing uPA from activated cell-bound plasminogen. MMP-2 can cleave and inactivate thrombin, thus providing an additional mechanism to inhibit thrombus formation[131]. Certain MMPs (MMP-2, MMP-9 and MMP-14) stimulate vascular smooth muscle cell proliferation, and therefore confer plaque stability[142]. Thus, although MMPs are strongly implicated in

plaque instability, their diverse functions can both promote and prevent plaque rupture, and posses both thrombotic and fibrinolytic characteristics. Which actions predominate may depend on the differential expression of MMPs and TIMPs by different cells and their levels of activity.

1.3.2g Macrophages and adenosine

Platelet activation results in the release of α-granules and dense granules that carry components critical for thrombus formation. Dense granules contain ADP that stimulates further platelet recruitment and activation through platelet ADP receptors, P2Y1 and P2Y2[143]. In addition to endothelial cells and macrophages, platelets serve as major sources of extracellular adenosine. Adenosine receptors are present on macrophages (A_1, A_{2A}, A_{2B} and A_3), and through these receptors, adenosine can modulate macrophage function. In macrophages, adenosine inhibits the production of TNF-α, IL-12, TF and ROS and stimulates the production of IL-10[61]. Thus adenosine provides a negative feedback mechanism in an autocrine and paracrine fashion to limit the inflammatory and thrombotic responses in macrophages.

1.3.2h Macrophages and fibrinogen

Fibrinogen and fibrin are ligands for ICAM-1, Mac-1 (CD11b/CD18, $\alpha_M\beta_2$) and $\alpha_V\beta_2$ (CD11c/CD18) that are expressed on macrophages, lymphocytes and neutrophils, and thus acts as adhesion substrates for these cells[144-148]. In macrophages, both fibrinogen and fibrin can stimulate the Mac-1-dependent activation of the NF-κB transcription pathway that increases pro-inflammatory cytokines, particularly TNF-α and IL-1β[149, 150]. By binding with fibrin, Mac-1 also provides a mechanism for plasmin-independent fibrinolysis[122]. Fibrinogen can bind TLR-4, expressed on macrophages, that activates NF-κB transcription factor pathway, stimulating the expression of pro-inflammatory cytokines[151]. Thus fibrinogen and fibrin, although critical for thrombus formation, can additionally induce pro-inflammatory responses in macrophages.

1.4 TISSUE FACTOR

Tissue factor (TF) (thromboplastin/F3/CD142) is a 47kDa transmembrane cell surface glycoprotein and is the key trigger for the coagulation cascade[152, 153]. Besides its critical role in coagulation, it plays important roles in angiogenesis, wound healing, intracellular signaling, tumour metastasis and inflammation. Its role in angiogenesis, is clearly demonstrated by the fact that the TF knockout mouse dies between day 8.5 and 10.5 of embryogenesis as a consequence of defects in vascular integrity[154].

1.4.1 Structure of TF

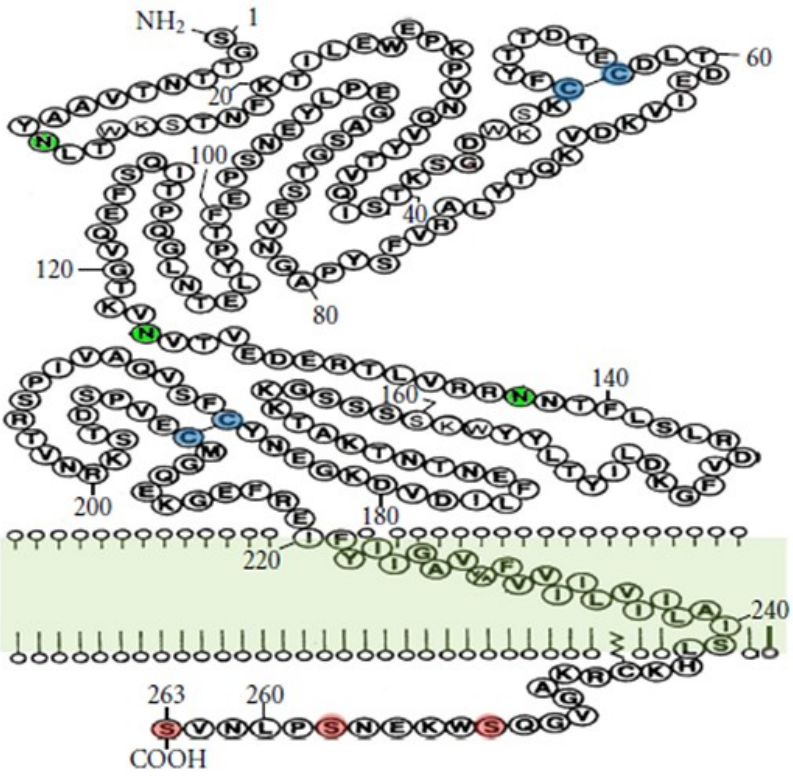

Figure 1-6: Structure of the mature human TF polypeptide chain (263αα)
The TF chain consists of extracellular, transmembrane and cytoplasmic domains. There are 2 disulphide bridges within the extracellular domain (Cys49-Cys57 and Cys186-Cys209, shown in blue). There are 3 serine residues (shown in red) in the cytoplasmic domain which are phosphorylation sites. The 3 potential glycosylation sites are shown in green (Asn11, 124 and 137). Adapted from [156].

The complete gene sequence for human TF gene (12.2kb) was first reported in 1989, and is located on chromosome1 at 1p22-23[152]. The complete gene sequence for murine TF (11.5kb) was reported in 1992 and is located on chromosome 3 at locus

52.94cM[155]. Both the human and murine TF genes are organized into six exons separated by five introns[152, 155]. The human TF gene encodes a 295αα polypeptide chain, whilst the murine TF gene encodes a 294αα polypeptide chain. Most of our detailed understanding of the structure of TF is centered on human TF[156]. The human TF 295 αα poypeptide chain comprises of a 32αα leader sequence and a 263αα mature TF protein (figure 1-6) [152]. The mature protein also contains the (1) extracellular domain (219 αα); (2) transmembrane domain (23αα); and (3) cytoplasmic domain (21 αα)[157-159]. The extracellular domain comprises of 2 fibronectin type III (FNIII) modules joined by an interdomain hinge[160]. It is classified as a class II cytokine receptor, based on its homology to the IFN-γ receptor[160]. The extracellular domain binds factor VII/VIIa and contains 4 potential N-linked glycosylation sites. It contains 4 cysteine residues that form 2 disulphide bonds which may be important for factor VII/VIIa binding. The cytoplasmic domain contains three serine residues (potential phosphorylation sites), and a single cysteine residue that is thioester-linked to palmitate that may contribute to anchoring of TF to the membrane[161]. The cytoplasmic domain also plays important roles in intracellular signalling.

1.4.2 Distribution of TF

1.4.2a Tissues

TF is expressed widely in both vascular and extra-vascular tissues. Under physiological conditions, the endothelium expresses very little TF, if at all. Extensive immunohistochemical studies of human arteries have failed to detect TF in normal vascular endothelium[162-164], and others have also noted an absence of endothelial TF in diseased atherosclerotic vessels[163, 165-167]. Similarly, *in vivo* animal studies have not provided consistent evidence for endothelial TF both under physiological and agonist-induced conditions[168-173]. However, certain pathological conditions such as invasive breast tumours have been reported to induce endothelial TF[162]. Nevertheless, endothelial cells can produce TF *in vitro* following stimulation with TNFα[174], LPS[175], IL-1β[176], CD40L[177], thrombin[178], histamine[179], oxLDL[180] and VEGF[181]. Within blood vessels, TF is constitutively expressed in the vessel wall, confined to adventitial

fibroblasts and medial smooth muscle cells[163, 165, 166]. This provides a haemostatic procoagulant envelope around the vessel wall, ready to activate the coagulation cascade when the integrity of the vascular endothelium is disrupted. TF is also constitutively expressed in richly vascularized organs such as the placenta, brain, kidneys, lungs and heart[163].

1.4.2b Peripheral blood cells

Monocytes represent a major source of TF within the circulating blood. Other blood cells that have been reported to express TF are neutrophils and eosinophils[182, 183]. Monocytes express TF under basal conditions, and stimulation with TNFα[184], LPS[185], CD40L[84], PDGF[186], AngII[187], oxLDL[188] and CRP[189] has been shown to upregulate TF expression. Perhaps the most widely studied stimulus in this context is LPS, which induces monocyte TF expression through both transcriptional and post-transcriptional mechanisms[190, 191]. Disseminated intravascular coagulation (DIC) is a recognized complication of severe sepsis, where multiple intravascular thrombotic events result from increased monocyte TF expression[192]. Mature blood eosinophils have been shown to express TF under basal conditions, and following stimulation with GM-CSF and PAF, TF expression is increased[182]. On the other hand, neutrophils express very little TF under basal conditions[183], but may express increased TF following specific stimuli, e.g. complement component C5a[193]. Another important source of blood-borne TF is MPs. These small membrane vesicles can express TF, which is derived from the cell membranes of their parent cells. Monocytes and platelets represent the major source of circulating TF-containing microparticles[78]. Whether platelets express TF is still a matter of controversy. Some investigators have failed to identify TF in platelets, whereas others have reported TF in platelet membranes[194, 195], in the matrix of α-granules and in the open canalicular system[183]. As platelets do not contain TF mRNA, it is possible that platelet TF may be derived from other cells e.g. circulating monocytes and neutrophils[196]. For example, TF-bearing microparticles released from monocytes may bind and fuse with activated platelets through a P-selectin/PSGL-1 dependent mechanism[110]. Increased TF-containing microparticles have been demonstrated in

acute coronary syndromes (ACS)[197, 198], anti-phospholipid syndrome[199], sickle cell disease[200] and sepsis[201]. Soluble TF is yet another source of TF in the blood. This has been identified as an alternatively spliced form of TF (asTF) and is not associated with microparticles. This isoform is generated by exon 4 directly splicing onto exon 6 and the protein contains most of the extracellular domain of TF but lacks the transmembrane domain, rendering it soluble[202]. asTF is produced in several cell types such as monocytes, smooth muscle cells and cancer cells and can be detected in plasma, lungs and placenta. As yet, it is still debated whether asTF has any intrinsic procoagulant activity[203]. However, asTF exhibits procoagulant activity when exposed to phospholipids, following thrombus initiation, it may be incorporated into the developing thrombus, and contribute to thrombus propagation.

1.4.3 "Encrypted" vs. "decrypted" TF

Many studies have reported a discrepancy between the amount of TF present and the amount of procoagulant activity. However, it is becoming increasingly recognized that not all cell surface expressed TF is functional. Within a cell, it is TF exposed on the cell surface that possesses functional activity. Within intact cells, approximately one third of the total cellular TF is inside the cells, whilst two thirds is on the surface, and of this fraction, only 50% was found to be active[204]. This has lead to the concept of inactive ("encrypted") vs. active ("decrypted") forms of TF. Both encrypted and decrypted TF can bind FVIIa with similar affinity, but it has been proposed that only the decrypted TF–FVIIa complex can proteolytically activate the factor X. The molecular differences between these two forms and mechanisms responsible for "activation" are not entirely clear and remain controversial[205]. There are many theories to explain how the activity of TF may be regulated. One theory suggests that cell membrane lipid composition plays a crucial role in TF decryption, where exposure to clusters of PS activates TF. Whilst PS exposure in response to multiple stimuli, such as cell lysis, calcium ionophores and apoptotic signals, has been shown to increase TF activity[206-209], there is no direct experimental evidence of a TF-PS interaction that would translate into a TF conformational change to support TF decryption. One may argue that PS may still contribute to the initiation of coagulation through direct interaction with FVIIa or FX and

as such PS-induced decryption may not involve changes in TF at all. Another theory implicates a key role for the Cys^{186}-Cys^{209} disulfide bond in the TF extracellular domain, where shuffling between the reduced and oxidized states of this allosteric bond induces a conformational change that supports TF encryption-decryption[210, 211]. Accordingly, TF containing reduced cysteines is “encrypted”, whilst intramolecular cystine within the bond represents the “decrypted”, highly procoagulant form of TF. Disruption of this bond by the oxidoreductase activity of protein disulphide isomerase (PDI) has been shown to disable coagulation[212, 213]. Consistent with this observation, oxidation of these cysteine residues with resultant formation of the bond has been shown to increase TF activity. However, this redox switch model has been recently debated[214] as (1) there is no direct evidence that the disulfide bond affects TF conformation and subsequent binding and activity of FVIIa; (2) the redox agents may have multiple effects on both TF, FVIIa, FX and the cellular environment; (3) TF mutants with impaired disulfide bond formation still retain procoagulant activity comparable to native TF[215]; (4) redox modulation can alter the phospholipid dynamics at the plasma membrane which may affect coagulation[216]; and (5) in the encrypted TF-VIIa complex, the allosteric cysteines are buried in the complex, such that it may not be possible for PDI to modulate their redox status during decryption[217]. Given these inconsistencies, the precise role the cysteine bonds play in determining TF activity and function remains controversial.

1.4.4 Role of TF in cardiovascular disease

Throughout the process of plaque formation, the inflammatory milieu induces TF expression in plaque macrophages, foam cells and smooth muscle cells. TF is found in extracellular spaces surrounding cholesterol clefts and within the necrotic core. TF-containing microparticles are released from monocyte-macrophages and lymphocytes. Given that TF is the key stimulus for thrombus formation, all these factors contribute significantly to plaque thrombogenicity[218]. Accordingly, examination of coronary atherectomy specimens from patients with ACS have shown increased TF content when compared to those with stable coronary disease[219]. Furthermore, PAR signalling

mechanisms provide an important means for TF to mediate cross-talk between coagulation and inflammation[71]. TF may also contribute to plaque development through coagulation-independent mechanisms. TF/VIIa complex has been shown to be a stimulus for smooth muscle migration in atherosclerotic plaques, and overexpression of TFPI has been shown to counter this effect[220, 221]. TF may promote plaque neovascularization[154], that may contribute to plaque growth, haemorrhage and instability.

Whilst TF within the plaque plays roles in plaque inflammation, development and thrombogenicity, it is now recognized that many risk factors for atherosclerosis may contribute to increased TF expression. Compared to normoglycaemic individuals, those with established diabetes have increased plasma TF activity[222], TF-containing MPs[223] and monocyte TF expression[223, 224]. Accordingly, hyperglycaemia has been shown to increase TF expression in monocytes derived from healthy volunteers[225, 226]. Hyperglycaemia results in advanced glycation end products (AGEs) and these can interact with receptors for AGE (RAGEs) and induce TF expression in monocytes through NFκB activation[227-229]. Patients with hypercholesterlolaemia, have increased plasma TF activity, that can be inhibited by statin therapy[230, 231]. Conversely, the protective effects of HDL can be demonstrated by the fact that HDL inhibits TF expression through activation of the P13K pathway[232]. Hypertensive patients demonstrate increased plasma TF activity, when compared to normotensive patients[233]. Angiontesin II (Ang-II) is a naturally occurring vasoconstrictor produced by the renin-angiotensin system, and plays an important role in the development of hypertension. Ang-II increases TF expression in monocytes and vascular smooth muscle cells-an effect mediated by the AT1 receptor[234]. Consistent with this, angiotensin converting enzyme (ACE) inhibitor therapy has been shown to reduce LPS-induced TF expression in monocytes[235]. Smoking has also been shown to increase plasma TF activity, and analysis of carotid plaques from smokers were found to have increased TF content compared to those from non-smokers[236].

In patients with ACS, increased TF expression is not limited to the plaque[218, 237, 238] but also seen in circulating monocytes[239]. Similarly, plasma TF levels are increased in patients with unstable angina compared to those with stable disease. In the context of ST-elevation MI, there is a positive correlation between the TIMI score (a marker of risk) and plasma TF levels[240]. Furthermore, higher plasma levels of TF have been shown to correlate with adverse outcomes following non-ST-elevation MI[198, 241]. *In vitro* stent thrombosis models show that circulating TF plays a critical role in stent thrombosis, and in this setting, monocytes appeared to be the main source of TF. Monocyte depletion of blood reduced TF staining in thrombi by 83% (p=0.01)[242]. Analysis of TF gene polymorphisms from patients in the FRISC II trial, demonstrated that the CG haplotype was associated with a 3-fold increased risk of death, and in these subjects, monocytes demonstrated increased TF activity[243].

1.4.5 Transcriptional regulation of TF

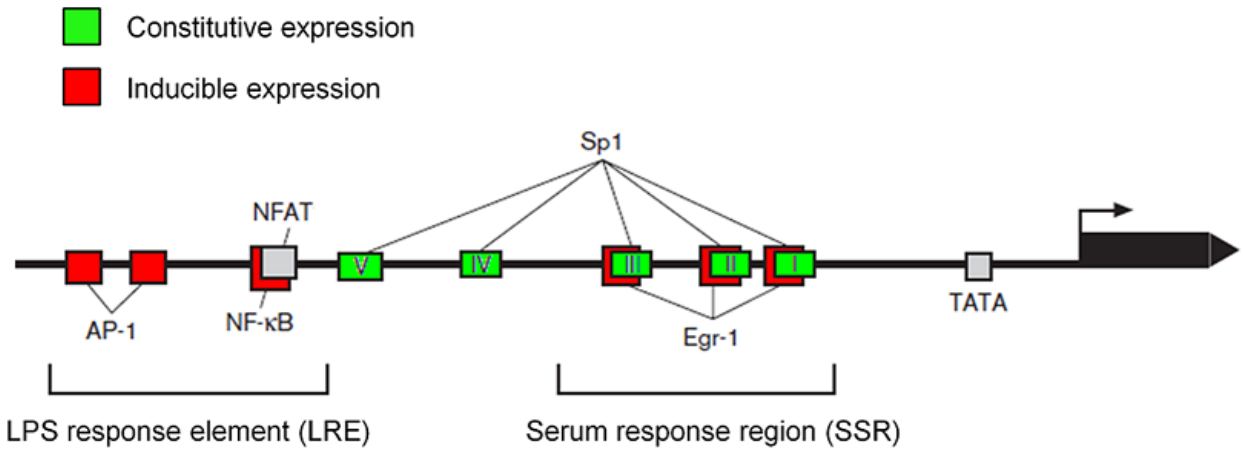

Figure 1-7: The human TF promoter
Schematic representation of the human TF promoter. The boxes represent different transcription factors sites. The transcription initiation site is shown with the arrow. Adapted from [244].

The human TF promoter contains binding sites for different transcription factors (figure 1-7): 2 activated protein-1 (AP-1) binding sites; 1 NFκB binding site; 3 Egr-1 binding sites; 5 Sp1 binding sites[244, 245]; and 1 nuclear factor for activated T cells (NFAT) binding site (overlapping NFκB binding site)[246]. The 5' of the TF promoter region contains a CpG island[247], and methylation of this site can prevent TF gene expression in

B and T cells[152]. The transcriptional activity can be broadly classified into constitutive or inducible expression.

1.4.5a Constitutive expression

The Sp1 sites are considered to be responsible for basal constitutive TF expression. The three Sp1 binding sites ($Sp1_{III}$, $Sp1_{IV}$ and $Sp1_{V}$) are conserved between human, mouse, rat and pig. Sp1 is a constitutively expressed transcription factor, and multiple Sp1 sites act in synergy, where at least two sites are required for constitutive expression[244]. There are four members of the Sp family of transcription factors: Sp1-4. Sp1, Sp3, Sp4 are known to bind to same DNA segment. Sp3 is thought to generally act as a repressor of Sp1, and given the levels of Sp1 and Sp3 vary in different cells, the cell-specific Sp1:Sp3 ratio may ultimately determine the net basal TF transcription[248].

1.4.6b Inducible expression

There are two regions in the human TF promoter that are implicated in inducible TF expression. The first is a distal 56bp enhancer region (-227 to -172), also termed the LPS response element, which contains the NFκB and AP-1 binding sites[244], and this mediates transcriptional activation following LPS, phorbol ester, TNFα, CD40L and IL-1β stimulation[249-251]. This enhancer region is conserved between human and mouse[244]. The second is a more proximal 50bp region (-109 to -59), also termed the serum response region, which contains the Egr-1 binding sites, and this mediates transcriptional activation in response to serum, shear stress, LPS, phorbol ester, oxLDL, and VEGF[252-255]. LPS, phorbol ester, TNFα, IL-1β, CD40L, oxLDL, thrombin and VEGF stimulation results in activation of MAPK pathways (p38, ERK and JNK), which leads to the activation of transcription factors AP-1 and Egr-1. LPS also activates NFκB signalling through the MyD88-dependent pathway which results in phosphorylation and release of the inhibitory component IκB. LPS, TNFα, histamine and thrombin act through activation of all 3 MAPK pathways[178, 179, 256], whereas, VEGF only activates p38 and ERK pathways[256]. VEGF and TNFα also activate PKC, which can increase TF expression either directly through activation of transcription factors or indirectly via MAPK activation[256]. The PI3K pathway is a negative regulator of TF expression[257]. PI3K

phosphorylates PIP_2 to form PIP_3 which results in the phosphorylation of downstream targets, Akt and GSK-3β. PIP_3 binds Akt allowing it to be phosphorylated by its activating kinases, phosphoinositide dependent kinase 1 (PSDK1) and mTORC2. Phosphorylation of GSK-3β promotes beta-catenin degradation and inhibits TF protein synthesis. In addition to MAPK activation, stimulation with LPS, TNFα, histamine, thrombin or VEGF also inhibit the PI3K pathway, thereby providing a cooperative mechanism for enhancing TF expression[178, 232, 257, 258].

1.4.6 Post-transcriptional regulation of TF

LPS is the most widely used stimulus to study TF expression, providing a powerful and consistent TF induction in different cell types. Although LPS mediates both transcriptional and post-transcriptional effects[190], it is generally considered that LPS-induced TF expression is mainly a result of increased mRNA stability[191]. Following LPS stimulation, there is a rapid but transient induction in TF mRNA, with levels peaking at 2-4 hours, following which the mRNA levels fall rapidly. This time-course provides robust post-transcriptional mechanisms where dynamic changes in mRNA stability allow rapid increase in steady state mRNA levels followed by a rapid decline.

The TF transcript is considered to be intrinsically unstable[152, 259, 260]. The 3'UTR contains several AREs that may serve as potential binding sites for ARE-binding proteins, and indeed TF mRNA has been assigned to the group III cluster of the ARED database[261]. These AREs are conserved in both human and mouse. TF mRNA levels are "super-induced" and mRNA stability prolonged by stimulating cells in the presence of cycloheximide (a protein synthesis inhibitor), suggesting down-regulation of mRNA stability with time by an induced protein[260, 262, 263]. The TF 3'UTR has been shown to confer instability, and specifically, it has been demonstrated that the destabilizing element within the 3'UTR is confined to the last 150bp sequence[260]. It is interesting to note that this sequence contains a palindromic ARE which comprises 2 overlapping nonameric sequences: AUUUAUUUA and UUAUUUAAU, the latter representing a site with high predictive binding for ARE-binding proteins[264-266]. This particular ARE exhibits significant conservation throughout different species, further specifying its importance.

In a study examining TF mRNA stability in lung epithelial cells, the TF 3'UTR was shown to bind 37 and 87kDa proteins, where the 37kDa protein was postulated to confer instability whilst the 87kDa protein was thought to confer stability[267]. However , to date, these proteins have not been characterized. Recently, the roles for microRNAs (mir-19 and mir-20) in regulating TF mRNA stability have been reported[268].

1.5 POST-TRANSCRIPTIONAL REGULATION

1.5.1 Physiological importance

Messenger RNA (mRNA) mediates the transfer of genetic information from the cell nucleus to ribosomes in the cytoplasm, where it serves as a template for protein synthesis. This passage of genetic information from DNA through to the effector protein molecule is highly regulated at multiple stages. In addition to transcriptional and translational control, there is overwhelming evidence for the role of mRNA turnover in determining net gene expression. Once mRNAs enter the cytoplasm, they are translated, stored for later translation, or degraded. The mRNA serves as a template for translation, and in general terms, there is positive correlation between the levels of mRNA and translated protein. It follows that the levels of steady mRNA present in a cell depends on the balance between its rate of formation and rate of decay. The concept of mRNA decay gives rise to the concept of mRNA stability and mRNA half-life. When mRNA was first discovered in E. Coli over 40 years ago, a key feature of mRNA was its unstable nature[269]. Indeed, mRNA half lives in *E. Coli* range from 20 seconds to 20 minutes. In eukaryotes, mRNA turnover is slower with half-lives ranging from 20 minutes to over 24 hours. Following mRNA transcription and translation, mechanisms must be in place to ensure mRNA is degraded after it has performed its function, otherwise there would be an exaggerated protein response. This would be particularly important following an inflammatory stimulus, to prevent an overwhelming inflammatory response thereby limiting chronic inflammation. Following an inflammatory stimulus, there is a rapid induction of the immediate response mRNAs, followed by a rapid decline in levels. Many such mRNAs are intrinsically unstable. However, the regulation of mRNA stability

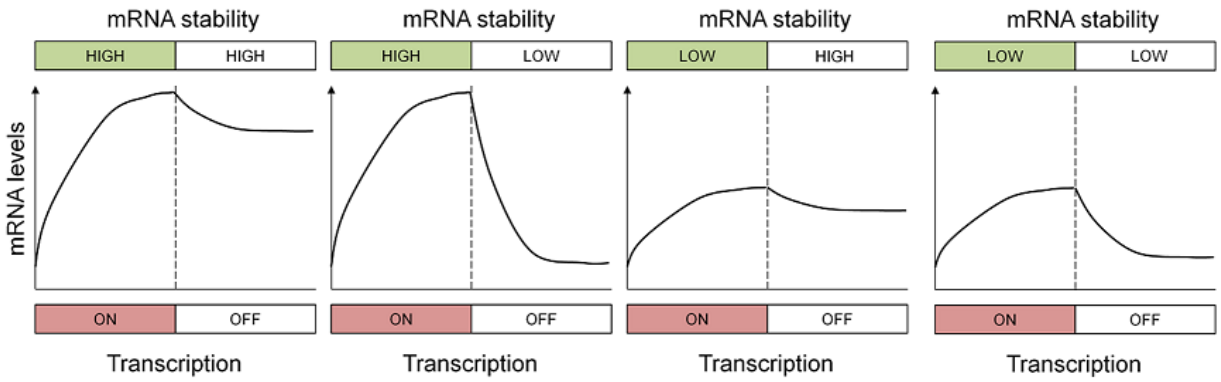

Figure 1-8: The effect of varying mRNA stability on the net mRNA response
Effect of mRNA stability on mRNA levels, assuming the rate of transcription is fixed. The second panel from the left is representative of an inflammatory response gene, where stabilization of an unstable transcript results in high levels. When transcription is switched off, destabilization of the transcript results in rapid decline in mRNA levels.

in this setting that provides a means for "fine tuning" gene expression[270]. Figure 1-8 shows that by transiently stabilizing an unstable transcript, the steady state levels can be increased efficiently, and subsequent destabilization results in rapid decline in levels. Regulation of mRNA stability provides a robust mechanism to regulate net gene expression, e.g. doubling mRNA half-life can result in100-1000-fold increase in mRNA abundance[270]. What determines mRNA stability and how is this regulated? In the broadest terms, mRNA stability is governed by specific sequences in the 3'UTR of the transcripts and their interaction with different RNA-binding proteins, which depending on their function, mediate mRNA stabilization or decay.

1.5.2 Adenylate uridylate-rich elements (AREs)

AREs represent major *cis*-elements in the 3'UTR of mRNAs that are essential determinants of mRNA stability[271-273]. Different ARE-binding proteins (ARE-BP) can bind these sequences on target mRNAs, and depending on their function, either promote stabilization or degradation. A common trait of ARE-containing mRNAs is that they are short-lived[274] and rapidly disappear once their critical role in gene regulation is accomplished - important in processes requiring transient rapid responses such as inflammatory and immune responses and cellular proliferation. The first evidence for the functional role of AREs was provided by demonstrating rapid mRNA degradation of the otherwise stable β-globin mRNA, when its 3'UTR was replaced with the 3'UTR of GM-

Figure 1-9: Examples of ARE-containing mRNAs in the ARED database
Examples of different ARE-containing mRNAs are listed according to the ARE classification. AREs are classified into 5 groups based on the number of continuous AUUUA pentamers: Group I: ≥5; Group II: 4; Group III: 3; Group IV: 2 and group V: 1 AUUUA pentamer. A complete list is available from http://rc.kfshrc.edu.sa/ared. Adapted from [261].

CSF[275]. It is estimated that approximately 7% of human and 5% of murine mRNAs contain AREs[276]. A general feature of functional AREs is that they contain a variable number of, often overlapping, AUUUA pentamers, usually in a U-rich context. It has been shown that an isolated presence of an AUUUA motif does not guarantee a destabilizing function. It has been proposed that the minimal nonameric sequence that represents the optimal binding site for a destabilizing protein thereby conferring instability is UUAUUUA(U/A)(U/A)[264-266]. This consensus was based on limited number of ARE-containing mRNAs e.g. GM-CSF, TNFα and c-fos etc. However, this sequence

does not represent the key minimal core sequence that confers instability, as many transcripts with functional AREs do not contain it, e.g. c-myc, c-jun and junB[277]. According to the ARE database (ARED), which contains the complete entries of human ARE-containing full-length mRNAs, AREs are classified into 5 groups based on the number of continuous AUUUA pentamers: Group I: ≥5; Group II: 4; Group III: 3; Group IV: 2 and group V: 1 AUUUA pentamer[261]. In ARED, clustering was performed in such a way that, for example, Group 1 included not only exact five or more continuous ARE pentamers but also those with 10% ambiguity, so that a stretch of WUUUAUUUAUUUAUUUAUUUW would also fall in this category. Figure 1-9 gives example of transcripts within these groups.

1.5.3 mRNA binding proteins

To date, many mRNA binding proteins that regulate mRNA turnover have been identified[278]. The main ARE-BPs that promote decay of ARE-containing mRNAs include tristetraprolin (TTP), butyrate response factor 1 (BRF1), AU-rich binding factor 1 (AUF1) and KH-type splicing regulatory protein (KHSRP or KSRP). So far, only Hu protein R (HuR) has been shown to play a role in stabilizing ARE-containing mRNAs[279].

1.5.4 microRNAs

Another important mechanism for regulating mRNA turnover is via microRNAs (miRNAs). miRNAs are small non-coding RNA molecules that act as post-transcriptional repressors by binding to specific target sequences within the 3' UTRs of their target genes and either block translation or promote mRNA degradation[280]. miRNAs are transcribed by RNA polymerase II as long primary transcripts referred to as 'pri-miRNAs' that fold into hairpins[281]. Little is known about the transcriptional regulation of pri-miRNAs, except that certain pri-miRNAs are located within introns of host genes, including both protein-coding genes and non-coding genes, and might therefore be transcriptionally regulated through their host-gene promoters[282]. In addition, certain miRNAs are clustered in polycistronic transcripts, indicating that these miRNAs are coordinately regulated during development[282]. Following transcription, the pri-miRNAs

stem-loop is cleaved by Drosha, an RNase III family member, to generate ~70 nucleotide precursors called pre-miRNAs[283]. Pre-miRNAs are exported by Exportin-5 (a Ran-GTP dependent nucleo/cytoplasmic cargo transporter) to the cytoplasm[284], where they are further processed by Dicer[285], another RNase III enzyme, to generate ~22 nucleotide single-stranded intermediates that enter effector complexes called miRISC (miRNA-containing RNA-induced silencing complex)[286]. Argonaute2 (AGO2) proteins[286, 287], which directly interact with miRNAs, and glycine-tryptophan protein of 182 kDa (GW182) proteins[288, 289], which act as downstream effectors in the repression, are key factors in the assembly and function of miRISCs. As part of miRISC, miRNAs base-pair to target mRNAs and induce their translational repression or degradation[290-292]. Furthermore, there may be functional overlap between ARE- and miRNA-mediated pathways. ARE binding proteins may either (1) alter mRNA structure and thereby facilitate miRISC binding to mRNA; (2) directly interact with miRISC components; or (3) directly interact with the miRNA/mRNA complexes. For example, HuR can bind AREs present in c-myc 3′UTR at a site proximal to that recognized by let-7 miRNA, facilitating let-7 binding and c-Myc mRNA breakdown[293]. Similarly, when HuR binds to the ARE in the CAT-1 3′-UTR, it can relieve miR-122-mediated translational silencing[294]. DND1 is an ARE-BP that can antagonize the miR-430-mediated translational repression of *NANOS1* and *TDRD7* mRNAs by binding to sequences that overlap with miRNA binding sites[295]. Another example is the cooperation of TTP and miR-16 in TNFα mRNA for ARE-mediated mRNA degradation. miR16, contains an UAAAUAUU sequence that is complementary to the ARE sequence. TTP does not bind directly with miR-16 but it forms a complex with miRISC, which recruits the deadenylase complex and the exosome for mRNA degradation[296].

1.5.5 mRNA degradation

There are three major classes of intracellular RNA-degrading enzymes: (1) endonucleases that cut RNA internally; (2) 5′ exonucleases that degrade RNA from the 5′ end; and (3) 3′ exonucleases that degrade RNA from the 3′ end. In mammalian cells, mRNAs are formed with two integral stability components — the 5' 7-methylguanosine cap and the 3' poly(A) tail. These two structures interact with the cytoplasmic

proteins eIF4E and the poly(A)-binding protein (PABP) respectively, to protect the transcript from exonucleases and to enhance translation initiation[297, 298]. To initiate decay, either one of these two structures must be compromised or the mRNA must be cleaved internally by endonucleases. In mammalian cells, both 3' and 5' exonucleases have been identified, indicating bidirectional degradation, but 3'-to-5' degradation is considered to be the major pathway. Deadenylation is the major step in triggering mammalian mRNA degradation (figure 1-10).

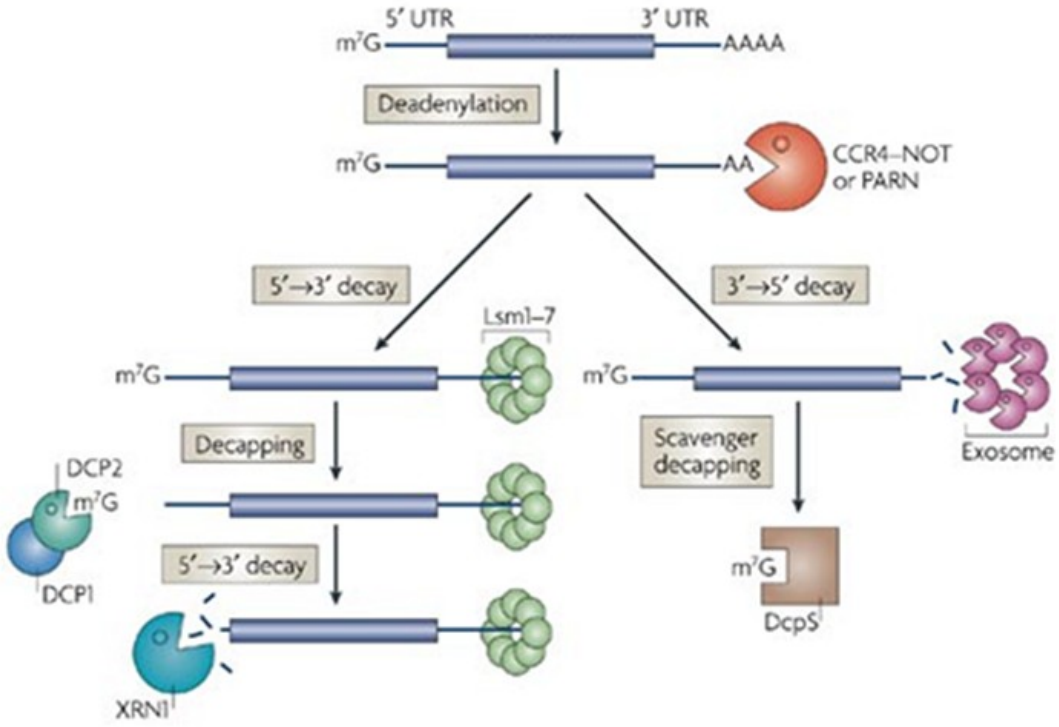

Figure 1-10: Deadenylation-dependent mRNA decay
Deadenylation is the key step triggering mRNA degradation. Following deadenylation, mRNA degradation occurs via 2 pathways: 3'-5' decay and/or 5'-3' decay. Adapted from [304].

Several deadenylases have been identified in eukaryotes: (1) poly(A) nuclease (PAN)2-PAN3; (2) carbon catabolite repressor protein 4 (CCR4)-NOT-a complex of 9 proteins of which 2 are CCR4 and CCR4-associated factor 1 (CAF1); and (3) poly(A)-specific ribonuclease (PARN). Deadenylation is a biphasic process involving two distinct deadenylase complexes- PAN2-PAN3, and CCR4-CAF1. First, the poly(A) tail is slowly shortened by the PAN2-PAN3 complex to ~100 nt; then the remaining tail is rapidly degraded by the CCR4-CAF1 complex to 8–12 nt[299, 300]. The first step in deadenylation

is unique in that it is reversible — transcripts can be readenylated and return to polysomes. Nevertheless, once the mRNA fate is set for destruction, one of two irreversible pathways are taken: (1) the 5' cap is removed (decapping) by the Dcp1–Dcp2 complex. Lsm1-7 is heptameric complex that binds to the 3' end of the mRNA and induces decapping by the Dcp1-Dcp-2 complex[301]. Following this, the mRNA is degraded in the 5'-to-3' direction by the 5′ exonuclease Xrn1; or (2) the deadenylated 3' end is attacked by a large complex of 3'-to-5' exonucleases known as the exosome[302], with the remaining cap structure being hydrolyzed by the scavenger decapping enzyme, DcpS[303]. PARN is unique in that it has cap-dependent deadenylase activity, i.e. its activity is enhanced by the presence of a 5' cap, whilst its activity is inhibited by cap-binding proteins. Decapping and subsequent 5′-to-3′ decay may occur during and/or after the second phase of deadenlyation and serves as an additional mechanism promoting mRNA degradation, especially where the deadenylation process has been inefficient. ARE-BPs have been shown to directly activate deadenylation; decapping; 5'-to-3' exonucleolytic decay; and 3′-to-5′ exonucleolytic decay[304].

1.6 TRISTETRAPROLIN

TTP (Tis11/Zfp36/NUP475/GOS24) is the most widely studied ARE-BP. It was discovered over 20 years ago by screening for genes that could be induced rapidly in fibroblasts following stimulation with growth factors and mitogens[305-308]. Its name derives from the fact that it contains three characteristic PPPPG motifs (tris-tetra-proline).

1.6.1 Structure of TTP

The human TTP gene is located on chromosome 19 and encodes a 326αα protein and the murine gene is on chromosome 7 and encodes a 316αα protein. TTP belongs to the TIS11 (tetradeconoyl phorbol acetate (TPA-Induced Sequence 11) family of proteins with 2 other members: butyrate response factor 1 (BRF1/Tis11b/ZFP36L1/ERF1) and butyrate response factor 2 (BRF2/Tis11d/ZFP36L2/ERF2) which are also ARE-binding proteins[308]. In addition to these well-described members, rodents possess another member (ZFP36L3) specifically expressed in the placenta[309]. The common feature of

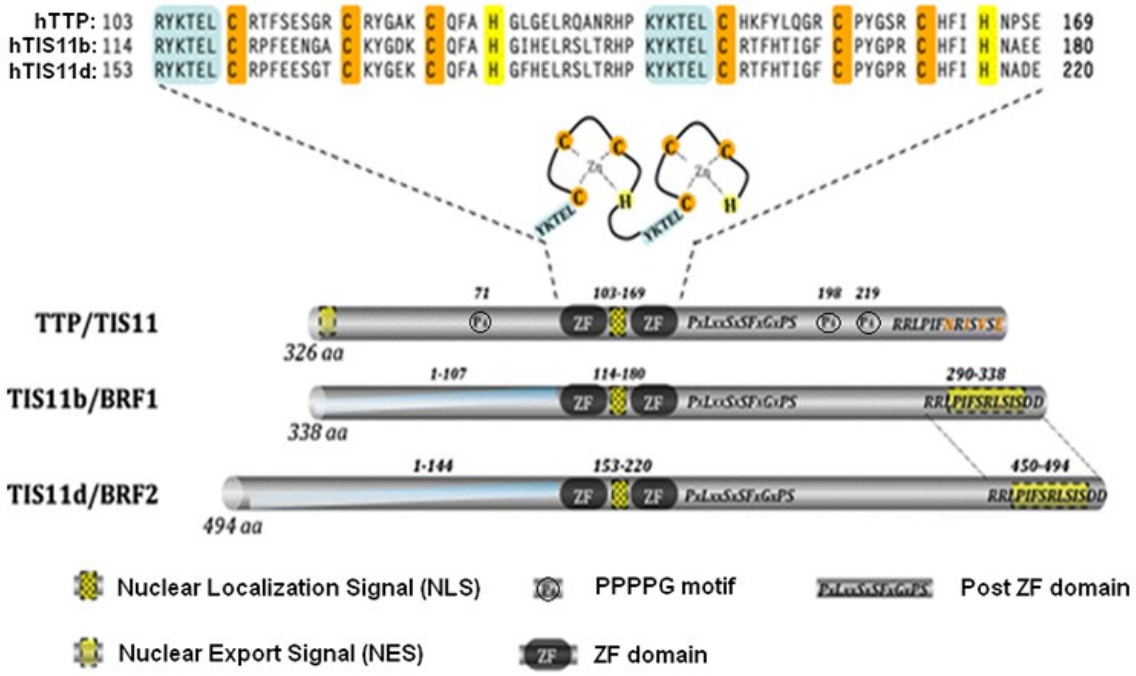

Figure 1-11: Protein domains of the TTP family members
The sequence of the tandem ZF domains, which are characteristic of the TTP family, are shown. Tristetraprolin has been named after the particular repeated motif (PPPPG) of the protein. Each protein of the family contains a nuclear localization signal (NLS) inside the much-conserved ZF domain and a conserved post-ZF domain of unknown function. Nuclear export signals (NES) are located in the C-termini of BRF1 and BRF2 and in the N-terminus of TTP. Adapted from [310].

the Tis11 family members is the presence of two CCCH zinc finger (ZF) motifs ($CX_8CX_5CX_3H$, where X represents various amino acids) each preceded by a conserved YKTEL leader sequence[307, 310] (figure 1-11). In addition to the ZF motifs, two other homologous domains are present in the three proteins. One is a stretch of 14 amino acids that contains a functional nuclear export sequence (NES). This sequence is C-terminal in BRF1 and BRF2, whereas for TTP it is located in the N-terminus of the protein. The second homologous motif is located immediately downstream of the ZF domains and is composed of the PxLxxSxSFxGxPS sequence, where x represents one member of a closely related family of amino acids. The exact function of this domain is unknown, but contains (at least for TTP and BRF1) a binding site for 14-3-3 proteins[311, 312].

1.6.2 Functions of TTP

1.6.2a TTP functions as an ARE-binding protein

Following the discovery of TTP, very little was known about its function until the development of the TTP knockout (*Ttp*$^{-/-}$) mouse in 1996[313]. These mice were normal at birth, but developed weight loss, severe erosive polyarthritis, myeloid hyperplasia, alopecia, conjunctivitis, dermatitis and autoimmunity[313]. In contrast to TTP knockout phenotype, loss of BRF1 induces embryonic lethality with neural tube abnormalities, failure of chorioallantoic fusion, and angiogenesis defects[314], and loss of BRF2 induces lethality within 2 weeks after birth due to diverse haemorrhages, probably caused by defective hematopoiesis[315]. These studies showed that (at least for some of their physiological functions) members of the TTP family cannot compensate for each other. A link between TTP and TNFα was suggested by the facts that (a) the *Ttp*$^{-/-}$ phenotype could be prevented by treatment of young mice with anti-TNFα antibody[313, 316]; (b) the symmetrical arthritis with erythematous swollen paws, was similar to that observed previously in TNFα excess syndromes[317, 318]; and (c) the direct demonstration of increased TNFα expression in the *Ttp*$^{-/-}$ mice[319].

Subsequent studies revealed that TNFα mRNA stability was increased in the *Ttp*$^{-/-}$ mice, and further work revealed that TTP could bind to an ARE in the 3'UTR of TNFα transcript – a process dependent on the two ZFs[320]. TTP exists in two forms: dephosphorylated (active) and phosphorylated (inactive). Initially, it was speculated that phosphorylation of TTP would modulate its RNA-binding capacity, however, experimental results have been contradictory. Nevertheless, the phosphorylation status of TTP, does indeed, regulate its destabilizing function. Although many phosphorylated forms exist, phosphorylation of TTP at Ser^{52} and Ser^{178} [321, 322], leads to binding to 14-3-3 adaptor protein that reduces its destabilizing activity[311, 323]. The phosphatase PP2A competes with 14-3-3 protein and dephosphorylates TTP, rendering it active[324]. Thus the proportion of TTP in the phosphorylated and dephosphorylated form remains in equilibrium (figure 1-12), and the disruption of this equilibrium, through either increased or decreased phosphorylation, affects overall TTP activity.

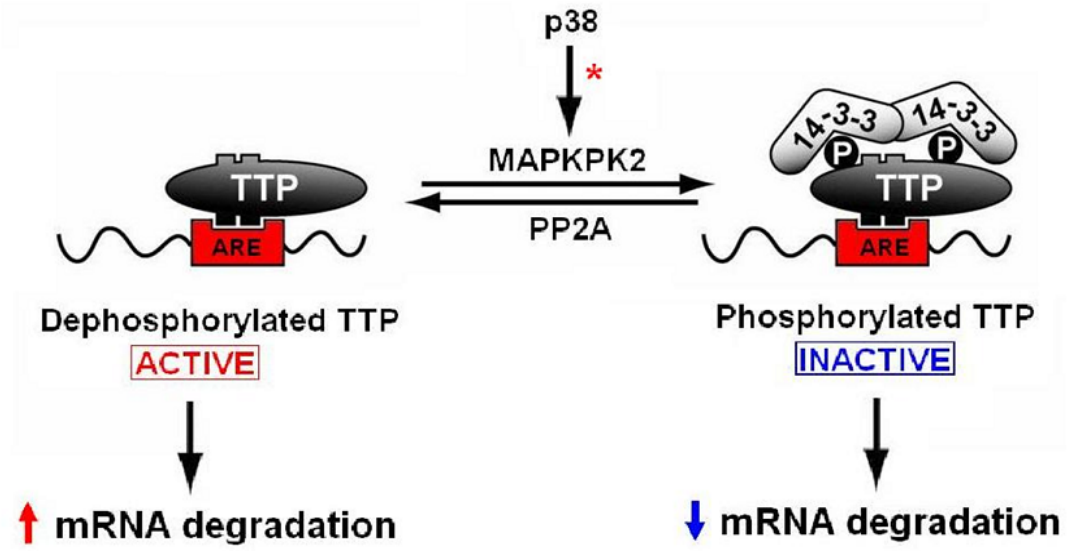

Figure 1-12: Phosphorylation of TTP regulates TTP activity and function
TTP exists in two forms: dephosphorylated (active) and phosphorylated (inactive). The proportion of TTP in the phosphorylated and dephosphorylated form remains in equilibrium, and the disruption of this equilibrium, through either increased or decreased phosphorylation, affects overall TTP activity.

1.6.2b TTP regulates mRNA decay

TTP promotes mRNA degradation by interacting with various components of the 3'-5' and 5'-3' mRNA degradation pathways (figure 1-13)[325]. However, its predominant role in mRNA degradation is facilitating deadenylation. PABP protects the mRNA poly(A) tail from degradation and is involved in maintaining mRNA circularization through binding to eukaryotic translation initiation factor 4G (eIF4G), and may inhibit TTP-directed deadenylation[326, 327]. This TTP–PABP interaction has been further confirmed and characterized by yeast two-hybrid analyses and shown to be RNA-independent[328]. Therefore this interaction with TTP may displace PABP from the poly(A) tail and potentially promote 3′-to-5′ mRNA degradation.

CCR4-NOT deadenylase complex has been implicated in ARE-mediated decay as knockdown of CAF1 has been shown to abrogate the deadenylation and decay of the ARE-containing α-globin mRNA[329, 330]. Furthermore, the phosphorylation of TTP has

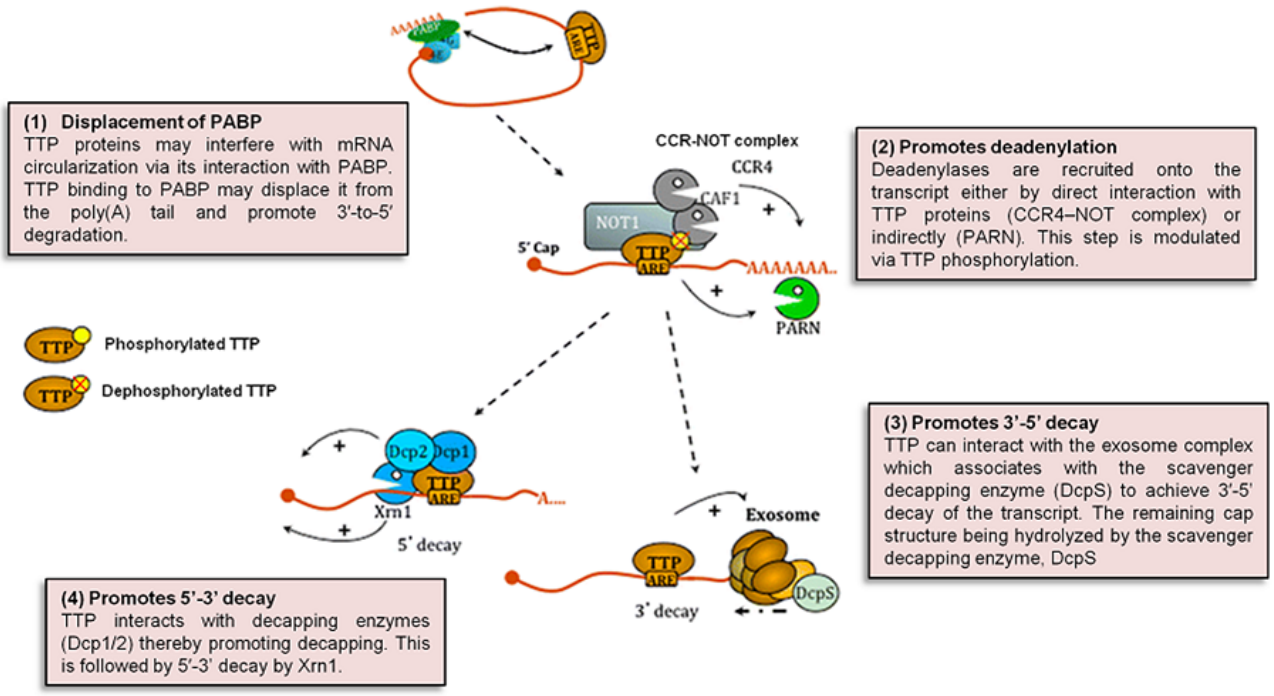

Figure 1-13: Involvement of TTP in deadenylation –dependent mRNA degradation
TTP promotes mRNA degradation by interacting with various components of the 3'-5' and 5'-3' mRNA degradation pathways. However, its predominant role in mRNA degradation is by facilitating deadenylation. Adapted from [325].

been shown to reduce its ability to promote deadenylation by inhibiting the recruitment of CAF1 deadenylase, specifically indicating that the CCR4-NOT complex is responsible for TTP-directed deadenylation[331]. TTP interacts with various components of processing bodies (PBs) where mRNA are degraded[332]. PB-associated proteins that interact with TTP include those that are involved in deadenylation (CCR4)[333]; decapping (Dcp1/Dcp2, Edc3 and Xrn1)[333, 334] and miRNA-induced silencing (Ago2 and Ago4)[296]. TTP associates with other components of RNA decay enzymes not present in PBs, e.g. the two subunits of the exosome, PM-Scl75 and Rrp4[333, 335, 336]. *In vitro* studies demonstrate that TTP can also promote deadenylation of ARE-containing mRNAs by PARN[337]. However, given a direct interaction between TTP and PARN has not been identified, it is possible that TTP binding to AREs may modify RNA conformation that may favor the recruitment of this deadenylase[326, 333, 337].

TTP can also associate with cytoplasmic foci called stress granules (SGs). SGs form when a cell shuts down bulk mRNA translation following a cellular stress response. It contains untranslated mRNAs which may be stored for later use or transported to PBs for degradation. During the stress response, TTP is recruited to SGs in its dephosphorylated form, when it is not bound to 14-3-3 protein[311]. Given that TTP interacts with PB components, TTP provides a mechanism for PB and SG interaction[338]. Following phosphorylation of TTP, it is excluded from SGs and consequently PBs are released from their tight association with SGs. Interestingly, TTP remains in PBs irrespective of its phosphorylation status[338].

1.6.2c TTP binds non-ARE segments

It has been shown that TTP may bind to a subset of mRNAs which contain a CTTGTG motif in the 3'UTR, and deletion of such motif in the 3′-UTR abrogated the TTP response in reporter gene experiments[339]. This observation may be further supported by findings from genome wide screening studies, where many TTP-targets have been identified but are devoid of AREs[340]. Alternatively, TTP may associate with other mRNA-binding proteins that target distinct ARE/non-ARE sequences, or may modulate mRNA expression independently of its mRNA-binding activity. A direct interaction between TTP and KSRP has been demonstrated, such that interaction with KSRP inhibits its recruitment onto the ARE and therefore prevents mRNA degradation via the exosome[341]. Moreover, it has recently been shown that binding of different isoforms of AUF1 to TTP via its ZF domain can modulate TTP-binding affinity to its target mRNA sequence, thereby promoting TTP-dependent mRNA degradation[342].

1.6.2d TTP regulates transcription

Due to the presence of two putative ZFs, TTP was originally thought to be a transcription factor. Although subsequent work focused primarily on its role in mRNA turnover, more recent work seems to have sustained this hypothesis. TTP has been shown to activate transcription when fused to the GAL4 DNA binding domain[343]. More recently, TTP has been shown to modulate NF-κB signaling. Following NF-κB

activation, TTP can bind to the p65 subunit and impair either its nucleocytoplasmic shuttling or its acetylation resulting in attenuation of NF-κB signaling[344, 345].

1.6.3 Regulation of TTP activity by p38 MAPK pathway

AREs provide a means for ARE-binding proteins to bind target mRNA and promote degradation or stablisation. However, the function(s) of ARE-binding proteins may be modulated, and this allows dynamic regulation of mRNA stability following extracellular stimuli. This is primarily mediated by modulating the function of ARE-binding proteins. The phosphorylation status of TTP is the key determinant for its function. This is mediated by the p38-MAPK pathway (figure 1-14).

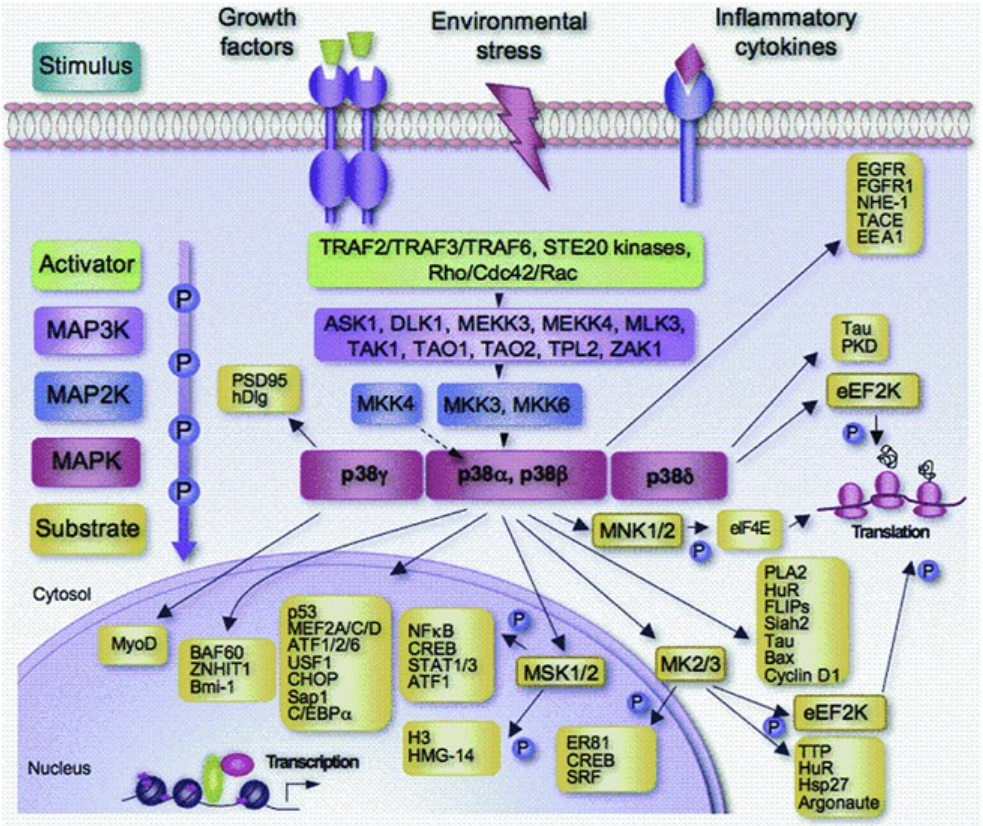

Figure 1-14: The p38 MAPK pathway

Different stimuli such as growth factors, inflammatory cytokines or a wide variety of environmental stresses can activate p38 MAPKs. A number of representative downstream targets, including protein kinases, cytosolic substrates, transcription factors and chromatin remodellers, are shown. CHOP, C/EBP-homologous protein; DLK1, dual-leucine-zipper-bearing kinase 1; EEA1, early-endosome antigen 1; eEF2K, eukaryotic elongation factor 2 kinase; eIF4E, eukaryotic initiation factor 4E; HMG-14, high-mobility group 14; NHE-1, Na/H exchanger 1; PLA2, phospholipase A2; PSD95, postsynaptic density 95; Sap1, SRF accessory protein 1; STAT, signal transducer and activator of transcription; TAO, thousand-and-one amino acid; TPL2, tumour progression loci 2; TTP, tristetraprolin; ZAK1, leucine zipper and sterile-α motif kinase 1; ZNHIT1, zinc finger HIT-type 1. Adapted from [346].

The mitogen-activated protein kinases (MAPKs) family comprises three main groups: (1) p38 MAPK pathway; (2) Jun N-terminal kinase (JNK) pathway; and (3) extracellular-signal-regulated kinase (ERK) pathway, and are involved in most signal transduction pathways[346]. There are 4 members of the p38 MAPK family which are approximately 60% identical in their amino acid sequence and include: (1) p38α (MAPK14); (2) p38β (MAPK11); (3) p38γ [SAPK (stress-activated protein kinase) 3, ERK (extracellular-signal-regulated kinase) 6 or MAPK12]; and (4) p38δ (SAPK4 or MAPK13), of which the p38α being the most widely expressed and studied isoform[347-352]. The p38 MAPK pathway is activated by numerous stimuli including LPS, pro-inflammatory cytokines, toxins, UV light and toxins. MAPKs are evolutionarily conserved enzymes, the activation of which requires dual phosphorylation of the Thr-X-Tyr motif that is catalysed by MAP2K kinases. This phosphorylation on a flexible loop termed the phosphorylation lip or activation loop, induces conformational changes that relieve steric blocking and stabilize the activation loop, thereby facilitating substrate binding. Of the MAP2K kinases, MKK6 can phosphorylate all four p38 isoforms, whereas MKK3 activates p38α, p38γ and p38δ, but not p38β[352, 353]. In addition, p38α can be phosphorylated by MKK4, and through autophosphorylation[354]. The MAP2K kinases are activated by upstream kinases, termed MAP3K kinases that include ASK1, DLK1, TAK1, TAO 1 and 2, TPL2, MLK3, MEKK 3/4, and ZAK1[355]. Upstream of the cascade, the regulation of MAP3Ks is more complex, involving phosphorylation by STE20 family kinases and binding of small GTP-binding proteins of the Rho family as well as ubiquitination-based mechanisms[355].

Down-regulation of p38 MAPK activity is critical in regulating signal intensity. Termination of kinase activity involves several phosphatases that target the activation loop threonine and tyrosine residues, include generic phosphatases that dephosphorylate serine/threonine residues (e.g. PP2A and PP2C), or tyrosine residues (e.g. STEP (striatal enriched tyrosine phosphatase), HePTP (haemopoietic tyrosine phosphatase) and PTP-SL (protein tyrosine phosphatase SL). These lead to monophosphorylated forms of p38, which have reduced activity (p38α phosphorylated on both Thr^{180} and Tyr^{182} is 10–20-fold more active than p38α phosphorylated only on Thr^{180}, whereas p38α phosphorylated on Tyr^{182} alone is inactive)[356]. p38α activity can

also be down-regulated by Wip1, a serine/threonine phosphatase of the PP2C family[357]. The activity of MAPKs is also regulated by the MAPK phosphatase/dual specificity phosphatases (DUSP) family[358, 359]. DUSP 1, 4, 5 and 7 can dephosphorylate p38α and p38β, however, the most important negative regulator of p38 activity is considered to be DUSP1[360, 361].

After activation, MAPKs phosphorylate specific serine and threonine residues of target substrates, which include other protein kinases and many transcription factors (figure 1-13). Of the downstream kinases, MAPKAPK-2/3 are implicated in post-transcriptional regulation. MAPKAPK-2 has been shown to phosphorylate Ago2 on Ser-387 (a major Ago2 phosphorylation site, as mutation of Ser-387 to Ala-387 impairs Ago2 localization to PBs)[362]. The p38 MAPK pathway plays a pivotal role in the regulation of TTP activity. Both MAPKAPK-2 and to a lesser extent p38 can phosphorylate and inactivate TTP (the primary target for MAPKAPK-2)[363]. Thus following an inflammatory stimulus, p38 activity can stabilize ARE-containing transcripts. However, there is also a parallel induction of DUSP1, providing a negative feedback mechanism to limit p38 activation, and this may result in subsequent destabilization of these transcripts. This modulation of TTP phosphorylation and function results in dynamic changes in mRNA stability allowing rapid induction of inflammatory transcripts, followed by a rapid decline, thereby preventing a perpetuating inflammatory response.

1.6.4 TTP-regulated genes

In recent years, many studies have revealed numerous targets for TTP. Microarray analysis of RNA from wild-type and TTP-deficient mouse embryonic fibroblast cell lines after serum stimulation and treatment with actinomycin D, identified 250 mRNAs that were stabilized in the absence of TTP[364]. Of these genes only 33 containes AREs. In one study, a genome-wide approach combining RNA immunoprecipitation and microarray analysis identified 137 mRNAs as targets for TTP[340]. Sequence analysis revealed a significant enrichment of AU-rich element motifs, with AUUUA pentamers present in 96% and UUAUUUAUU nonamers present in 44% of TTP-associated mRNAs. Using a similar strategy, another study identified 393 mRNAs as putative TTP

mRNA targets in human dendritic cells[339]. In this analysis, only 37 of the 393 genes identified as putative TTP ligands were present in the ARED database. Whilst these studies demonstrate diverse TTP targets, the low percentage of ARE-containing genes indicates that TTP is likely to bind to additional non-ARE mRNA sequence elements[339], as predicted using in vitro binding studies[365], as well as with TTP interacting with mRNA ligands via a protein bridge, as reported for the iNOS mRNA[366].

1.7 PARP-14

1.7.1 Introduction to the PARP superfamily

Poly(ADP-ribosyl)ation is a unique post-translational modification where negatively charged ADP-ribose moieties are adducted onto proteins. This occurs in almost every nucleated cell of mammals, plants, lower eukaryotes, but is absent from yeast[367]. The transfer of ADP-ribose to proteins was originally discovered in bacterial toxins such as *C. diphtheriae* toxin, which inactivates eIF-2 by ADP-ribosylation[368]. Poly(ADP-ribosyl)ation is of central importance to a wide variety of cellular processes, e.g. DNA repair[369, 370], transcriptional regulation[371, 372], proteasomal protein degradation[373], vesicle trafficking and apoptosis[374]. This process is catalyzed by a family of NAD+ ADP-ribosyl transferases, the poly(ADP-ribose) polymerases (PARPs).

To date, 17 PARP members have been identified on the basis of homology to PARP1, the founding member (figure 1-15)[375, 376]. Analysis of the catalytic domains of chicken PARP1 and murine PARP2 has shown that these proteins have structural homology with the active site of bacterial ADP-ribosylating toxin from *C. diphtheria*[377, 378]. The β-α-loop-β-α NAD+ fold which is the most conserved region is considered to be the PARP signature[379]. The PARP domain is located at the C terminus of the protein, except in PARP4[380]. Not all PARP members are enzymatically active and some function as mono(ADP-ribosyl) transferases rather than poly(ADP-ribosyl) transferases (PARPs 1, 2, 4, 5A, 5B catalyze poly(ADP-ribosyl)ation, whereas PARP 3, 10, 14 and 15 catalyze mono(ADP-ribosyl)ation). Hence a new nomenclature has been proposed that refers to PARPs as ADP-ribosyl transferases (ARTDs)[380].

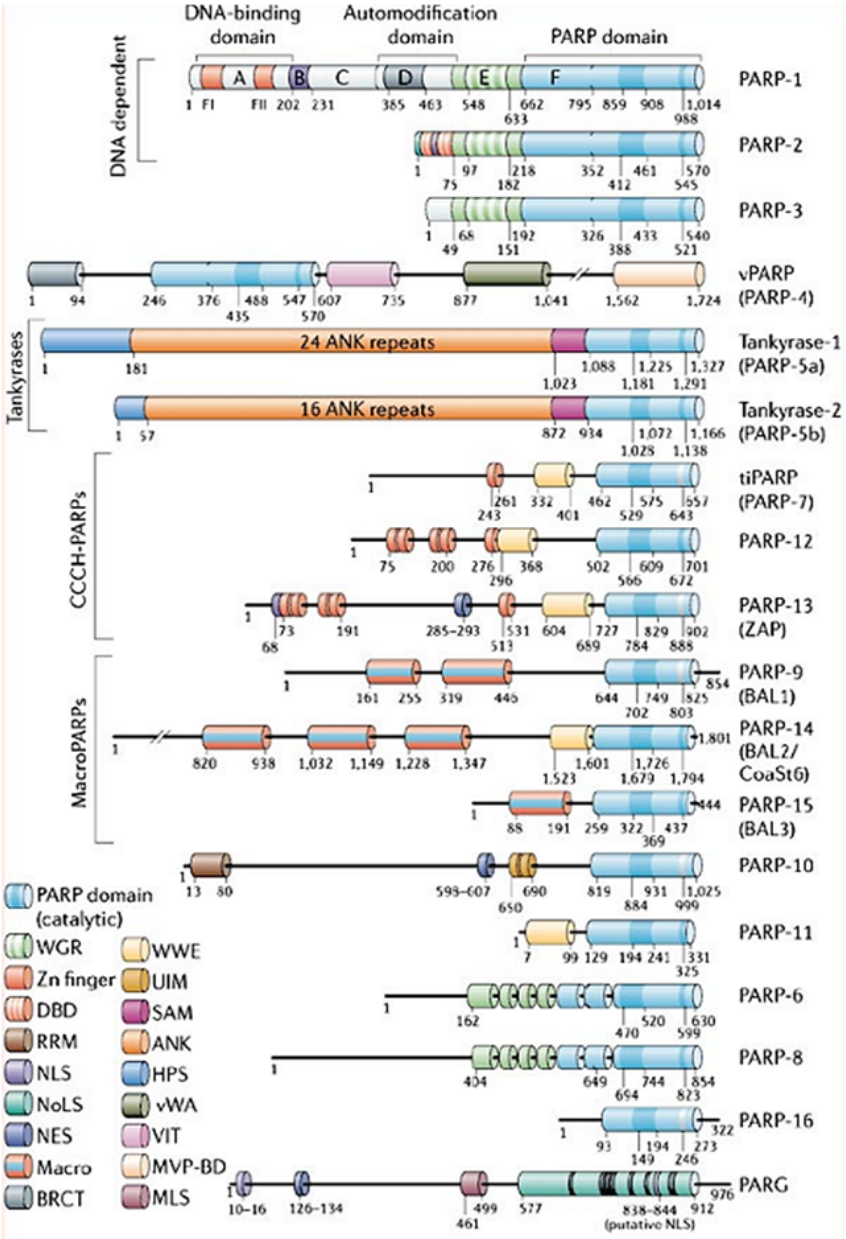

Figure 1-15: The PARP superfamily

The domain architecture of the 17 members of the poly(ADP-ribose) polymerase (PARP) superfamily and of poly(ADP-ribose) glycohydrolase (PARG). Within each putative PARP domain, the region that is homologous to the PARP signature (residues 859–908 of PARP-1) as well as the equivalent of the PARP-1 Glu988 catalytic residue (when present) are darkened. The WGR domain is defined by the conserved Trp, Gly and Arg residues, but its function is still unknown. The Zn fingers can be either DNAbinding (CX2CX28,30HX2C, noted as FI and FII in PARP-1) or putative RNA-binding (CX7-11CX3-9CX3H; PARP-12, PARP-13 and tiPARP) modules. DBD is a DNA-binding domain of unknown structure in PARP-2. RRM is an RNA-binding motif. Some macro domains have been described as ADP, ADP-ribose, poly(ADP-ribose) or *O*-acetyl-ADP-ribose binding modules. The BRCT (BRCA1 C terminus) domain is a protein–protein interaction domain. The WWE domain is probably a protein–protein interaction motif, and UIM interacts with ubiquitin. Both SAM (sterile α-motif) and ANK (ankyrin) are protein-interaction modules. The HPS domain, the function of which is unknown, contains homopolymeric runs of His, Pro and Ser residues. The vWA (von Willebrand factor type A) domain is proposed to be a metal-ion-dependent site for binding proteins, and the VIT (vault inter-α-trypsin) domain has no known function. MVP-BD is a binding site for major vault protein (MVP). MLS, mitochondrial localization signal; NES, nuclear export signal; NoLS, nucleolar localization signal; NLS, nuclear localization signal. Figure from [380].

The PARP family is divided into four subfamilies based on their domain architectures: (1) DNA-dependent PARPs (PARP1,2 and 3); (2) tankyrases (PARP5a and 5b); (3) CCCH PARPs (PARP7, 12, 13.1 and 13.2); and (4) macro PARPs (PARP9, 14 and 15)[380]. The DNA-dependent PARPs are activated by DNA damage through their DNA-binding domains[381]. The tankyrases contain large ankyrin domain repeats that mediate protein-protein interaction[382]. The CCCH PARPs contain ZFs that can bind RNA, as well as WWE domains (putative protein-protein interaction motifs that contain two tryptophans (W) and a glutamic acid (E)) that can bind PARs. The macroPARPs are characterized by 1-3 macrodomains that link to a PARP domain. The macrodomains, named through homology to the histone variant macro-H2A, have been shown to bind ADP-ribose and facilitate localization of these PARPs to sites of poly- or mono(ADP-ribosyl)ation[383]. A summary of all the PARP members is given in table 1-2 [380].

1.7.2 Mechanism of ADP-ribosylation

Of all the PARPs, PARP1 has been most extensively studied in the context of DNA damage[376]. It catalyzes the formation of ADP-ribose from NAD+ (oxidized form of nicotinamide) by cleavage of the glycosidic bond between nicotinamide and ribose. These ADP-ribose moieties are then covalently attached to glutamate, aspartate and lysine residues of target proteins through formation of an ester bond(figure 1-16) [384, 385]. For poly(ADP-ribosyl)ation, PARP1 catalyzes an elongation and branching reaction where additional ADP-ribose units are added through ribosyl-ribosyl linkages eventually resulting in the formation of branching polymers. PAR polymers can grow over 200 units in size, with branching reactions occurring every 20-50 elongation reactions[386, 387]. In the elongation reaction, the adenine-proximal ribose (A-ribose) units from the PAR chain termini are joined in an α(1→2) O-glycosidic bond, whereas in the branching reaction, the ADP-ribose junction occurs between two nicotinamide-proximal ribose (N-ribose) rings. Adduction of ADP-ribose moieties is typically transient as they are rapidly degraded predominantly by poly(ADP-ribose) glycohydrolase (PARG), an enzyme with both exo- and endoglycosidase activity[388, 389]. The exoglycosidase activity results in free ADP-ribose monomers, whilst the endoglycosidase activity results in the formation of free poly(ADP-ribose) polymers. There are three isoforms of PARG in mammalian cells,

$PARG_{99}$, $PARG_{102}$ and $PARG_{110}$ (99, 102 and 110kDa respectively). $PARG_{99}$ and $PARG_{110}$ localize to the cytoplasm, whereas $PARG_{110}$ predominantly localizes to the nucleus[390]. Free ADP-ribose monomers are potent at glycating proteins and therefore can result in protein damage[391]. This is prevented by ADP-ribose pyrophosphatase that converts the ADP-ribose monomers to AMP and ribose 5-phosphate[392]. Other PAR-degrading enzymes include ARH (ADP-ribosyl hydrolase) and NUDIX (nucleoside diphosphate linked to another moiety X) family of proteins[393].

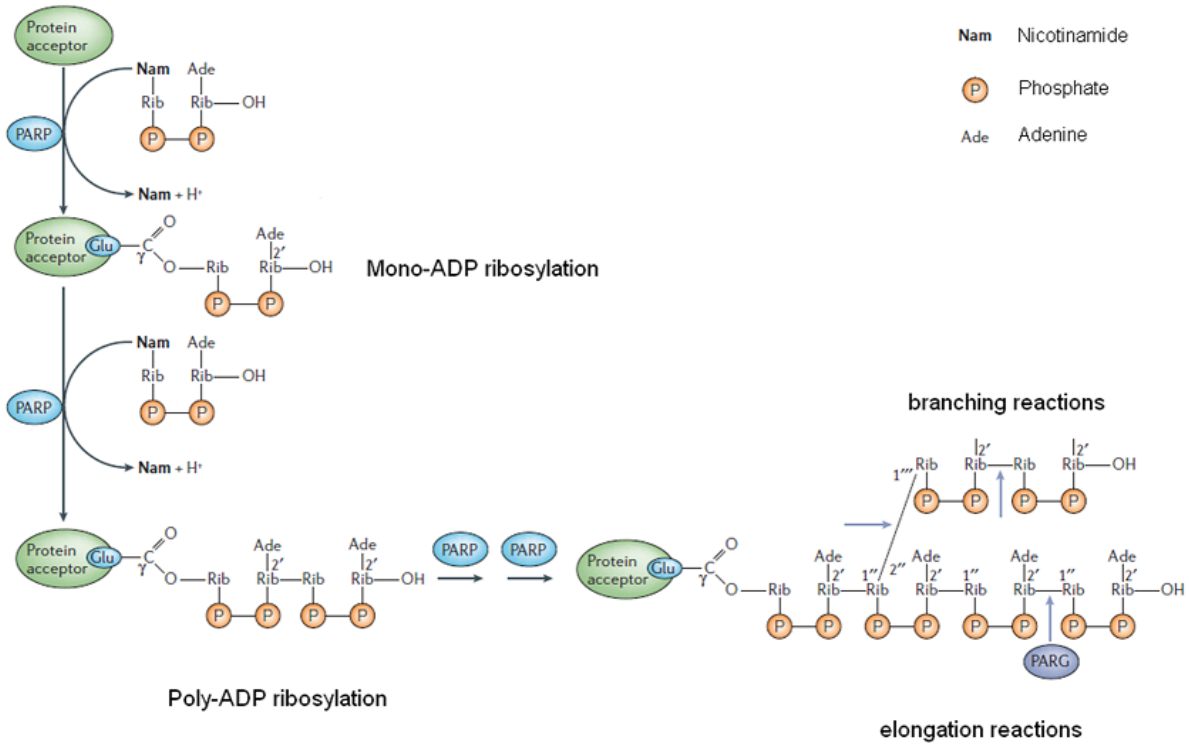

Figure 1-16: ADP ribosylation
PARP enzymes catalyze the successive transfer of the ADP-ribose moiety to protein acceptors. The reaction is initiated by the formation of an ester bond between the amino-acid acceptor (Glu, Asp or COOH-Lys) and the first ADP-ribose (mono-ADP ribosylation); polymer elongation involves the catalysis of a 2′–1″ glycosidic bond (poly-ADP ribosylation); polymer branching occurs on average after 20 ADP-ribose units and branching points are located at regular distances (every 20–50 ADP-ribose units). PARG has endo- and exo-glycolytic activities that cleave glycosidic bonds between ADP-ribose units (blue arrows). Adapted from [380].

1.7.3 Cellular functions of ADP ribosylation

PARs are bulky, negatively charged and flexible, and these features make them suitable for post-translational signals capable of mediating rapid cellular responses. ADP ribosylation can regulate two broad classes of cellular processes, protein-nucleic acid and protein-protein interactions. The highly negative charge resembling nucleic acids

can allow PARs to repulse DNA/RNA as well as attracting DNA/RNA binding proteins. ADP-ribosylation of target proteins can result in formation of a molecular scaffold that allows recruitment and promotes interactions between cellular proteins. In the context of PARP1, following DNA damage, the PAR chains and branches result in a complex scaffold which allows recruitment of different components of DNA repair components, ATM and e3 SUMO ligase, both of which contain PAR-binding domains[394]. ATM interacts with IκB kinase-γ, triggering its activation through SUMOlyation and phosphorylation. Thus the PAR scaffold helps promote NF-κB signaling following DNA damage[394]. PAR-dependent scaffold also affects the formation and function of SGs. Following a stress response, the RNA-binding PARPs cooperate with PARP5A and macroPARPs to help form SGs. This can be elegantly demonstrated by the fact that over-expression of any one these PARPs results in SG formation and that this can be inhibited by over-expression of the cytoplasmic PARGs[395]. Various RNA-binding proteins, e.g. Ago2, G3BP1, and TIA-1 have been shown to be modified by ADP-ribosylation, and such modification may allow recruitment of RNA-binding proteins to SGs, thus functioning as a scaffold for protein recruitment[395]. Other important examples of PAR scaffolds in the cell include spindle pole protein recruitment by PARs at the mitotic spindle during mitosis[396] and Cajal bodies, a nuclear organelle enriched in nucleic acid-binding proteins[397]. PARs play an important role in ubiquitinylation and subsequent degradation of target proteins[398, 399]. This is exemplified by RNF146, a PAR-binding E3 ligase, which plays an important role in tankyrase-dependent protein degradation pathway. RNF146 can bind PARs through its WWE domain, and subsequently ubiquitinylate the protein, targeting it for degradation[400]. Many other ubiquitin ligases contain WWE domains, which permits PAR-dependent ubiquitinylation[398].

1.7.4 Current understanding of PARP-14

PARP-14 is one of the three macroPARPs and will be the focus of this thesis. Most of our current understanding on the biology of PARPs is primarily centered on PARP-1. As yet, there is very little published data on the structure and function(s) of PARP-14. Work

in our laboratory identified PARP-14 by subtractive hybridisation of cDNA from TNFα-activated *versus* unstimulated porcine aortic endothelial cells.

1.7.4a Structure of PARP-14

PARP-14 is a ~205kDa protein, where the linear domain structure is identical in both human and mouse[401]. The published salient features are three macro domains; a WWE domain; and a C-terminal PARP domain (catalytically active). In addition, work in our department has identified three previously unrecognized KH-like domains and a RRM domain in PARP-14. We have shown that PARP-14 associates with RNA via its N-terminal RRM domain. Typically an RRM is structurally characterized by the packing of two α helices on a 4-stranded β sheet with β1αβ2β3αβ4 topology[402, 403]. The β sheets are thought to contact RNA, whilst the α helices may interact with associated proteins (e.g. RRM2 of PTB binds Raver1). KH domains are common in RNA-binding proteins, and indeed may contact RNA directly[404]. However the three PARP-14 KH-like domains do not have a canonical GxxG motif between the α1 and α2 helices that is considered crucial for RNA binding of KH domains (hence we have named them "KH-like")[405]. They may therefore mediate protein-protein interactions rather than bind RNA directly.

1.7.4b Functions of PARP-14

Research into the biology of PARP family proteins has mainly focused on their nuclear functions, especially of PARP-1. In comparison, the biology of the other "orphan PARPs" has received much less attention. PARP-14 deficient mice have been generated and found to be viable and to support a role for nuclear PARP-14 as a co-activator of IL-4/Stat-6-mediated transcription in B lymphocytes[401, 406, 407]. In this context, PARP-14 acts as a transcriptional switch by ADP-ribosylating HDAC 2 and 3, which are then released from IL-4 responsive promoters to allow access of histone acetyl transferases. Recently, several PARP family members, including PARP-14, have been shown to be expressed in the cytoplasm and have roles in RNA regulation[395, 408]. However, in unpublished work, we have found that PARP-14 plays a role in regulating mRNA stability of the chemokine IP-10 following IFNγ stimulation.

1.8 HYPOTHESIS AND AIMS

1.8.1 Development of the hypothesis

The TF 3'UTR contains several AREs. The final palindromic ARE is highly conserved with sequences predicted to have high affinity for RNA-binding proteins. Despite significant advances in molecular biology and our understanding of the regulatory mechanisms in mRNA turnover, the precise molecular mechanisms involved in ARE-mediated TF mRNA decay have not been fully elucidated. In particular: (i) although p38 signaling plays an important role in TF expression, whether it regulates TF mRNA stability has not been clearly defined; (ii) although there are AREs in the 3'UTR that appear to be functional, the role of ARE-binding proteins has not been investigated; and (iii) whether or not other inducible proteins besides ARE-binding proteins are required is not known.

With the above background in TF, TTP and PARP-14, the following hypothesis was formulated:

"TTP and PARP-14 regulate TF mRNA stability"

1.8.2 Aims

This hypothesis would allow us to test whether a key established protein in post-transcriptional regulation (TTP) and a novel protein in RNA biology (PARP-14) would regulate TF, an important protein in thrombosis and cardiovascular biology. To strategically dissect this study, the following aims were set:

1. To establish the effect of p38 inhibition on TF expression and mRNA stability

Given that p38 activity is an important regulator of TTP activity and function, the first stage was to establish the effect of p38 inhibition on TF mRNA and protein expression and its effect on TF mRNA decay. The precise role for TTP in regulating TF mRNA and protein expression was investigated and, specifically, its effect on TF mRNA stability. The interaction of TTP with TF 3'UTR and specific interactions with AREs were determined. [CHAPTER 3]

2. To determine the role for PARP-14 in regulating TF expression and mRNA stability

Preliminary work in our department has identified the role for PARP-14 in regulating mRNA stability of the chemokine IP-10, and that TF expression was increased in LPS-stimulated *Parp14*$^{-/-}$ murine macrophages. Thus, the role of PARP-14 in regulating TF mRNA and protein expression was investigated and, specifically, its effect on TF mRNA stability. Furthermore, the effect of PARP-14 deficiency on TF expression and thrombosis was examined *in vivo*. The interaction of PARP-14 with TF 3'UTR and specific interactions with AREs were determined. [CHAPTER 4]

3. To determine the TTP-PARP-14 interaction and its relevance to the regulation of TF mRNA stability

Having established the roles for TTP and PARP-14 in the post-transcriptional regulation of TF, the precise molecular mechanisms underlying their interaction and the interdependency of both proteins was examined. Furthermore, the role of PARP-14 enzymatic activity, i.e. ADP ribosylation, on the regulation of TF mRNA stability was tested both in the absence and presence of p38 inhibition. Finally, the roles for PARP-14, ADP ribosylation, and the TTP-PARP-14 complex was tested for TNFα, a well-established TTP-regulated transcript. [CHAPTER 4]

4. To establish the effect of glucocorticoids on TF expression

Glucocorticoids (GCs) are negative regulators of p38 activity and have been used as experimental tools to study p38-dependent post-transcriptional regulatory mechanisms, particularly in the setting of TTP-regulated transcripts. Having established a role for p38 activity in the post-transcriptional regulation of TF, whether these results would be applicable to GCs was investigated. The candidate GC used for this analysis was dexamethasone (Dex). [CHAPTER 5]

1.8.3 Structure of thesis

In the following chapters, a detailed section on generic methods and experimental protocols is presented. This is followed by three results chapters, each comprising of a small introduction, abbreviated methods specific to the chapter; experimental findings and results; and a discussion focusing specifically on the results. This is followed by a general discussion chapter where all the findings from the three results chapters are collated and discussed in the context of the wider literature. This is followed by a conclusions chapter which closes the thesis.

Chapter 2

General methods & protocols

2.1 PRIMARY HUMAN MONOCYTE ISOLATION AND CULTURE

2.1.1 Reagents

Sodium citrate (Sigma-Aldrich, Gillingham, UK); PBS (Invitrogen, Paisley, UK); Histopaque-1077 (Sigma-Aldrich, Gillingham, UK); 0.5M EDTA (Invitrogen, Paisley, UK); Bovine Serum Albumin (BSA, Invitrogen, Paisley, UK); Iscove's Modified Dulbecco's Media (IMDM, Invitrogen, Paisley, UK); Fetal Calf Serum (FCS, Innov-Research, Missouri, USA); CD14 MicroBeads (Miltenyi Biotec, Surrey, UK)

2.1.2 Isolation of PBMCs

Monocytes were isolated from citrated venous blood derived from healthy donors (with local ethical approval) with citrate:blood ratio of 1:9. 50mL of venous blood was venesected from a large vein in the antecubital fossa and immediately citrated. The citrated blood was centrifuged at 400g for 20 minutes at room temperature, and the platelet rich plasma (PRP) supernatant was removed from the cell fraction. The cell fraction (~30 mL was divided into 2 portions and each made up to 35mL using PBS. Peripheral blood mononuclear cells were (PBMCs), were isolated from the cell fraction by Ficoll–Paque density-gradient centrifugation using Histopaque-1077. 2 x 15mL Histopaque-1077 was placed into 2 x 50mL tubes respectively, and the 35mL PBS-blood mixture was carefully pipetted over the Histopaque-1077 into each tube ensuring that the interface between the two layers was not disrupted. The tubes were centrifuged at 800g for 20 minutes at room temperature. The buffy coat and surrounding fluid was carefully pipetted from each tube without disrupting the red cell fraction and centrifuged at 800g for 10 minutes at room temperature to pellet the PBMCs. The PBMCs were pooled from both tubes, and washed with PBS twice by centrifuging at 300g for 10 minutes at room temperature.

2.1.3 Labeling with magnetic CD14 Microbeads

The PBMCs were resuspended in 10mL MACS buffer (0.5% BSA-PBS, 2mM EDTA) and counted using light microscopy. The suspension was centrifuged at 300g for 10 minutes at 4°C, the supernatant completely removed and the PBMC pellet resuspended in 80µL MACS buffer per 10^7 cells. 20µl CD14 Microbeads per 10^7 cells were added to

the cell suspension and thoroughly mixed followed by an incubation at 4°C for 15 minutes. The cells were resuspended in ice cold 10mL MACS buffer, centrifuged at 300g for 10 minutes at 4°C and the supernatant was completely aspirated. The cells were resuspended in 500µL ice cold MACS buffer.

2.1.4 Magnetic separation using MS column

Magnetic separation was performed using a MACS Separator (Miltenyi Biotec, Surrey, UK) according to the manufacturer's instructions. Briefly, a magnetic MS column (Miltenyi Biotec, Surrey, UK) was placed in a magnetic field and primed with 500µl MACS buffer. The cell suspension was applied to the column. Following this, the column was washed with 0.5mL aliquots of MACS buffer 3 times. The unlabelled effluent cells were collected at the bottom of the column and discarded. Next, the magnetic column was removed from the magnetic field, placed into a 15mL collection tube. 1mL PBS was placed into the column and using the supplied plunger, the labeled cells were immediately flushed out of the column. The cells were immediately added to 9mL IMDM [10% FCS] and counted. Depending on the experimental protocol, the concentration of the cells was adjusted with the culture medium and plated out into tissue culture plates. The plates were placed in a 37°C incubator with 5% CO_2 atmosphere overnight to allow the monocytes to adhere, ready for experiments the following day.

2.2 BONE-MARROW DERIVED MACROPHGE ISOLATION AND CULTURE

2.2.1 Reagents

Dulbecco's minimal essential medium (DMEM, Invitrogen, Paisley, UK); FCS (Innov-Research, Missouri, USA); PBS (Invitrogen, Paisley, UK); L-Glutamine (Sigma-Aldrich, Gillingham, UK); Penicillin (Sigma-Aldrich, Gillingham, UK); Streptomycin (Sigma-Aldrich, Gillingham, UK); L929 Conditioned medium

2.2.2 Mice

Ttp$^{-/-}$ mice were generated as previously described[313]. *Ttp*$^{-/-}$ mice were of mixed 129 and C57BL/6 background and maintained as heterozygous breeding pairs. The *Parp14*$^{-/-}$ mice were generated as previously described[406], and had a C57BL/6 background, and maintained as heterozygous breeding pairs. All experiments were conducted using age- and sex-matched wild-type (WT) progeny as littermate controls.

2.2.3 Bone marrow culturing medium

For culturing bone marrow cells, the “bone marrow culture medium” referred to in this protocol comprises of DMEM, 10% FCS, 2 mM L-Glutamine, 100 U/ml penicillin, 100 µg/ml streptomycin and 10% L929-conditioned medium, a source of granulocyte/macrophage colony-stimulating factor.

2.2.4 Harvesting bones from mice

Femurs and tibia were obtained from 15-20 week old C57BL/6 mice. The mice were sacrificed using cervical dislocation. After euthanasia, the mice were sprayed with 70% ethanol and the femurs were dissected using sterile scissors, cutting through the knee joints as well as through the pelvic bone close to the hip joint. The tibia were dissected in a similar fashion cutting through the knee joints as well as through the calcaneum. Muscles connected to the bones were removed using sterile gauze and the epiphyses were removed using sterile scissors and forceps. The bones were placed into a polypropylene tube containing sterile PBS on ice. The bones were placed in 70% ethanol for 1 minute, and then immersed into bone marrow culture medium.

2.2.5 Preparing bone marrow cell suspension

The bones were then flushed with a syringe filled with bone marrow culture medium to extrude bone marrow into 15 mL sterile tubes. The tubes were centrifuged at 300g for 10 minutes at room temperature to pellet the bone marrow. 10ml of bone culture medium was added and a 5 ml pipette was used to gently homogenize the bone marrow cells. This suspension was applied to a 70µM cell strainer to obtain a uniform single-cell bone marrow cell suspension.

2.2.6 Culturing bone marrow cells

1mL of bone marrow cell suspension was added to 19mL bone marrow culture medium into a T75 culture flask and placed in a 37°C incubator in a 5% CO_2 atmosphere. In this way, 10 x T75 flasks were obtained per mouse, and the cells were cultured for 6 days . On day 6, the overlying culture medium was removed to ensure removal of dead cells and debris. 20mL PBS was added, the adherent macrophages were harvested by scraping. The cells were counted and the cell suspension was centrifuged at 300g for 10 minutes. The cells were resuspended in the bone marrow culture medium at a density dependent on the experimental protocol, and plated in culture dishes/flasks for experiments to be conducted on day 7.

2.3 RNA EXTRACTION

2.3.1 Reagents required

β-mercaptoethanol (Sigma-Aldrich, Gillingham, UK); Molecular grade ethanol (Sigma-Aldrich, Gillingham, UK); RLT lysis buffer (Qiagen, Crawley, UK); RW1 buffer (Qiagen, Crawley, UK); R-PE buffer (Qiagen, Crawley, UK); RNase-free DNase (Qiagen, Crawley, UK); Molecular grade water (Invitrogen, Paisley, UK); RNase-free DNase 1 (Qiagen, Crawley, UK): Proteinase K (Qiagen, Crawley, UK); Trizol reagent (Sigma-Aldrich, Gillingham, UK); Chloroform (Sigma-Aldrich, Gillingham, UK); Isopropanolol Sigma-Aldrich, Gillingham, UK); 20 µg/µl Ultra-pure Glycogen (Invitrogen, Paisley, UK).

2.3.2 Extraction of RNA from cells

Following the experimental treatment of cells, the culture supernatants were removed and cells washed in 1mL aliquots of ice cold PBS in the tissue culture wells to remove overlying medium, ensuring the adhering cells were not disrupted. 350µL RLT lysis buffer, freshly supplemented with 1% β-mercaptoethanol, was added to the cells. The RLT buffer was gently pipetted up and down ensuring dissociation of cells from the tissue culture plate. The RLT lysates were transferred to 1.5mL RNase-free eppendorfs. RNA was subsequently isolated using RNeasy Mini kits (Qiagen, Crawley, UK) according to manufacturer's instructions, incorporating an on-column DNase digestion using RNase-free DNase. Briefly, the samples were initially homogenized by passing

the lysate at least 5 times through a blunt 20-gauge needle (0.9 mm diameter) fitted to an RNase-free syringe, following which the lysates were added to an equal volume of 70% ethanol (~350µL). The samples were mixed well and applied to the RNeasy spin columns (Qiagen, Crawley, UK). The columns were spun on a table-top centrifuge at 13000g for 30 seconds. The flow-through was discarded. 350 µl of RW1 buffer was added to the RNeasy spin column and centrifuged at 13000g for 15 seconds, again discarding the flow-through. 80µl of RNase-free DNase 1 was added to the spin column membrane and allowed to incubate for 15 minutes at room temperature, followed by a repeat wash with 350 µl of RW1 buffer and centrifugation at 13000g for 15 seconds, again discarding the flow-through. 500 µl of RPE-buffer was then added to the RNeasy spin column and centrifuged at 13000g for 30 seconds, again discarding the flow-through. A second wash step with 500 µl of RPE-buffer was performed followed by centrifugation at 13000g for 2 minutes, again discarding the flow-through. The RNeasy spin column was placed in a new 2 ml collection tube and centrifuged at 13000g for 1 minute to remove any residual wash buffer. The RNeasy spin column was now placed in a new 1.5 ml RNase-free eppendorf, and 50 µl RNase-free water was added directly to the spin column membrane, ensuring the pipette tip did not touch the membrane, and centrifuged at 13000g for 1 minute to elute the RNA. The concentration and quality of the RNA were determined using Nanodrop 1000 (Thermo Scientific, Loughborough, UK), ensuring a 260/280 ratio >1.8 and a 260/230 ratio >1.9.

2.3.3 Extraction of RNA from tissues

All tissue samples were immediately snap-frozen and stored at -80°C until RNA extraction. For the extraction of RNA from tissues, 30mg tissue samples were initially homogenized in 300µL RLT buffer (supplemented with 1% β-mercaptoethanol) using the TissueLyser and 5mm stainless steel beads (Qiagen, Crawley, UK) according to the manufacturer's instructions. Briefly, the tissue samples with the RLT buffer and stainless steel beads were placed into 2mL RNase-free eppendorfs and placed into the TissueLyser adapter set (2 x 24). The TissueLyser was operated for 2 min at 20Hz. The adapter set was disassembled and the tubes rearranged so that the tubes nearest to

the TissueLyser were now outermost, and the adapter set re-assembled. The TissueLyser was operated for another 2 min at 20Hz.

RNA was subsequently isolated using the RNeasy Fibrous Tissue Mini kit (Qiagen, Crawley, UK) according to manufacturer's instructions, again incorporating an on-column DNase digestion using RNase-free DNase. Briefly, the homogenate was carefully pipetted into new 2mL eppendorfs, discarding the remaining tube with the stainless steel bead. 590 µl RNase-free water was added to the lysate. 10 µl proteinase K solution was then added, thoroughly mixed and incubated at 55°C for 10 minutes. The lysates were centrifuged at 10,000g for 3 minutes at room temperature. The supernatant (~900µL) was carefully removed and placed into a new microcentrifuge tube, avoiding the transfer of the pellet. Next 450µL 100% ethanol was added to the cleared lysate, making the total volume of the lysate ~1.4mL. 700µL of the lysate was applied to the RNeasy spin column, and centrifuged at 13000g for 30 seconds. The flow-through was discarded and the remainder of the lysate was applied to the columns followed by a repeat spin, again discarding the flow-through. 350 µl of RW1 buffer was added to the RNeasy spin column and centrifuged at 13000g for 15 seconds, discarding the flow-through. The subsequent steps were as for RNA extraction from cells (see above).

2.3.4 RNA extraction using Trizol reagent

This method of RNA extraction was used following the RNP immunoprecipitation assays (see below), where the RNA was extracted from supernatants. 300µL of supernatant was added to 500µL of Trizol reagent in a 1.5mL eppendorf. This mixture was left at room temperature for 5 minutes and then briefly vortexed. Next, 100µL chloroform was added and briefly vortexed and allowed to stand at room temperature for 15 minutes. Following this, the mixture was centrifuged at 17,000g for 30 minutes at 4°C. The aqueous phase (top layer) was carefully removed and transferred to a fresh 1.5mL eppendorf. Next, an equal volume (~300µL) of isopropanolol was added. This was briefly vortexed and left overnight at -20°C. The addition of 1µL glycogen was optional, facilitating the visibility of the RNA pellet. The following day, the tube was centrifuged at

17000g for 30 minutes at 4°C to pellet the RNA. The supernatant was completely removed, and the RNA pellet was resuspended in 500µL 70% ethanol, and centrifuged at 17000g for 15 minutes at 4°C. The supernatant was completely removed, and the RNA pellet air-dried for 15-20 minutes. The RNA pellet was resuspended in 15-25µL water. The concentration and quality of the RNA were determined using Nanodrop 1000 (Thermo Scientific, Loughborough, UK), ensuring a 260/280 ratio >1.8 and a 260/230 ratio >1.9.

2.4 FIRST STRAND cDNA SYNTHESIS

2.4.1 Reagents required

10 mM dNTP Mix (Roche Diagnostics, Sussex, UK); 100pM Oligo dT (Eurofins, Ebersberg, Germany); Molecular grade water (Invitrogen, Paisley, UK); 5X First-Strand Buffer (Invitrogen, Paisley, UK); 0.1 M DTT (Invitrogen, Paisley, UK); SuperScript™ III Reverse Transcriptase (200 units/µl) (Invitrogen, Paisley, UK)

2.4.2 Protocol

1µg of total RNA was used for first strand cDNA synthesis using SuperScript III reverse transcriptase enzyme according to the manufacturer's reverse transcriptase protocol. To minimize pipetting errors for multiple reactions, 2 master mixes were made. Master mix A comprised 1µL dNTP and 1µL oligo dT per reaction. Master mix B comprised 4µL first strand buffer, 1µL DTT, 1µL water and 1µL SuperScript III reverse transcriptase (added just before use). 11µL RNA was added to 2µL of mastermix A, and reaction mixture vortexed and briefly centrifuged. The reaction mixture was heated to 65°C for 5 min following which the reaction was immediately placed on ice for 1 minute. Next, 7µL of master mix B was added, reaction mixture vortexed and briefly centrifuged and incubated at 50°C for 60 minutes, followed by inactivation at 70°C for 15 minutes using a thermal cycler (Applied Biosystems, Warrington, UK). The cDNA was stored at -20°C until use.

2.5 QUANTITATIVE REVERSE-TRANSCRIPTASE PCR (qRT-PCR)

2.5.1 Reagents

Molecular grade water (Invitrogen, Paisley, UK); 10pM forward and reverse primers (Eurofins, Ebersberg, Germany); iQ SYBR green PCR Fastmix (VWR, Lutterworth, UK)

2.5.2 Protocol

Comparative qRT-PCR was performed using 5 µL template cDNA (1:20 dilution with molecular grade water), 0.5 µL forward primer, 0.5 µL reverse primer, 6.5µL molecular water and 12.5 µL SYBR green PCR Fastmix, with a total volume of 25µL per reaction. Reactions were performed in triplicate in Hard-Shell ® 96-well PCR plates (Biorad-Laboratories, Hercules, CA) using Biorad CFX96 Thermal Cycler (Biorad-Laboratories, Hercules, CA). The gene specific primer sequences, their amplicon lengths and reaction conditions are listed in table 2-1 . Primers were designed and optimized such that they all required the same reaction conditions. A typical reaction protocol incorporating a melt curve analysis is shown in figure 2-1. All primers were validated with standard curves for serial cDNA dilutions (10-fold dilutions), negative control (water only template) and non-reverse transcription controls (to exclude genomic DNA contamination). The slopes of the standard curves were calculated using BioRad CFX Manager Software Version 1.6 (Biorad-Laboratories, Hercules, CA), and slopes between -3.1 to -3.6 giving reaction efficiencies between 90 to 110% were considered acceptable. As part of the optimization protocol, the products of the reaction were separated in a 1% agarose gel containing ethidium bromide and visualized under UV light to confirm the amplicon length respectively. Figure 2-1 illustrates the validation of the primers using the murine TF primers as an example, with construction of a standard curve for murine TF with appropriate controls, and the RT-PCR products as run on a 1% ethidium bromide gel.

2.5.3 Data analysis

Data was analysed using BioRad CFX Manager Software Version 1.6 (Biorad-Laboratories, Hercules, CA). All reactions were performed in triplicate, and the mean threshold cycle values (C_T values) were calculated per sample for the test gene and

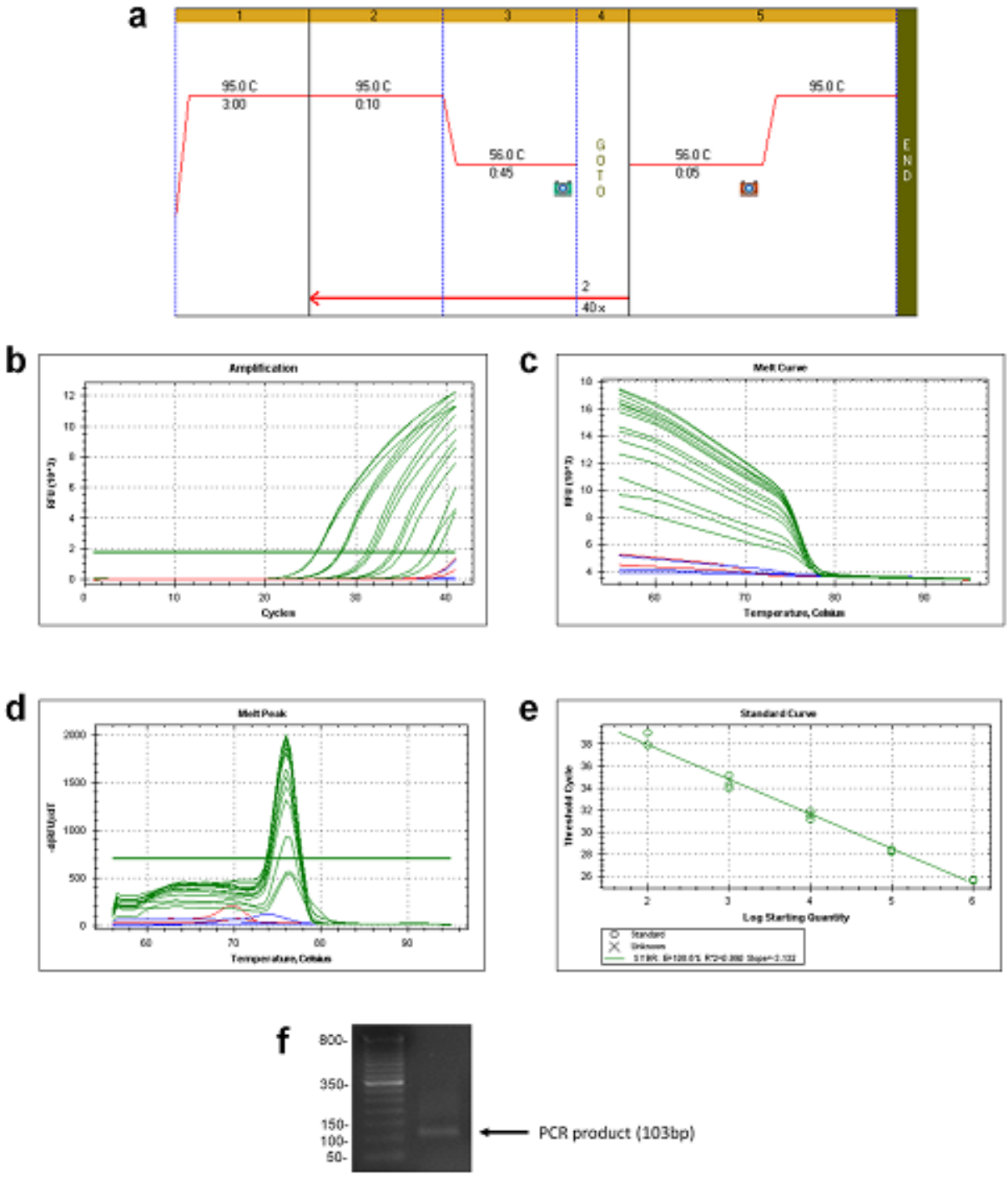

Figure 2-1: Protocol for quantitative RT-PCR using the Biorad CFX96 Thermal Cycler (Biorad-Laboratories,) **(a)** Typical protocol for quantitative RT-PCR for primers used in this study (including murine TF) with an annealing temperature of 56°C. The protocol incorporated 40 cycles followed by a melt-curve analysis protocol (from 56°C in 0.5°C increments up to 95°C); Standard curves were generated using 10 fold serial dilutions of cDNA as template (prepared from WT macrophages stimulated with LPS 1µg/mL for 2h), water as a negative control (shown in red) and no RT-controls (shown in blue); **(b)** The amplification process through 40 cycles; **(c)** Melt curves of the respective PCR products; **(d)** Melt peaks of the respective PCR products; **(e)** The generated standard curve for mouse TF; and **(f)** Visualization of the PCR product which corresponds to the amplicon size of 103bp.

housekeeping control gene. Data was validated using 2 housekeeping controls, GAPDH and HPRT. Relative gene expression was calculated by comparing the number of thermal cycles that were necessary to generate threshold amounts of product using the ΔΔCt method[409].

2.6 WESTERN BLOTTING ANALYSIS

2.6.1 Reagents

Cell Lytic M Cell lysis buffer (Sigma-Aldrich, Gillingham, UK); Cell Lytic MT Cell lysis buffer (Sigma-Aldrich, Gillingham, UK); Protease inhibitor cocktail (Sigma-Aldrich, Gillingham, UK); NuPAGE® LDS Sample Buffer (4x) (Invitrogen, Paisley, UK); PBS (Invitrogen, Paisley, UK); 20x running buffer MES /Tris-Acetate (Invitrogen, Paisley, UK); 20x transfer buffer (Invitrogen, Paisley, UK); Full range molecular weight rainbow marker (GE Healthcare, Amersham, UK); Methanol (Sigma-Aldrich, Gillingham, UK); Tween-20 (Sigma-Aldrich, Gillingham, UK); ECL (Plus)™ Western Blotting Detection Reagents (GE Healthcare, Amersham, UK); 5% dried milk powder (Sainsburys, London, UK); 20% SDS solution (Sigma-Aldrich, Gillingham, UK); Molecular grade water (Invitrogen, Paisley, UK); 0.5M TRIS-HCl (pH 6.8) (Ambion); β-mercaptoethanol (Sigma-Aldrich, Gillingham, UK); Stripping buffer (Invitrogen, Paisley, UK)

2.6.2 Buffers

- Running buffer (1L): 50mL 20x running buffer + 950mL water
- Transfer buffer (1L): 50mL 20x transfer buffer + 900mL water + 100mL methanol
- PBS-T (1L): 999mL water + 1mL Tween-20
- Blocking buffer (100mL): 100mL PBS (0.1% Tween) + 5g 5% dried milk powder
- Stripping buffer (100mL): 77.5mL water + 10mL 20% SDS + 12.5mL 0.5M TRIS (pH=6.8) +800μL β-mercaptoethanol

2.6.3 Preparation of cell lysates

Following the experimental protocol and treatment of cells, the supernatant culture medium was removed and cells were gently washed twice in ice-cold PBS to remove culture medium, ensuring the adherent cells were not disrupted. The cells were lysed

with 100µL of Cell Lytic M lysis buffer with 1µL of protease inhibitor cocktail using a plastic policeman. The lysates were carefully transferred to 1.5mL eppendorfs, and left on ice for 10 minutes. The lysates were centrifuged at 17,000g for 20 minutes at 4ºC to pellet cell debris. The supernatant was carefully removed and stored at -80ºC until analysis.

2.6.4 Preparation of tissue lysates

All tissue samples were immediately snap-frozen and stored at -80°C until preparation of tissue lysates. 50-100mg of tissue were added to 300µL of Cell Lytic MT lysis buffer and 3 µL protease inhibitor cocktail into a 2mL eppendorf. The sample was homogenized by adding a stainless steel bead (Qiagen, Crawley, UK) and operating a TissueLyser (Qiagen, Crawley, UK) for 2 min at 20Hz. The tubes were centrifuged at 17,000g for 20 minutes at 4ºC to pellet cell debris with the stainless steel bead. The supernatant was carefully removed and stored at -80ºC until analysis.

2.6.5 Preparation of samples

The concentrations of protein lysates were determined using a Jenway Genova Life Science Analyser (Bibby Scientific Limited, Stone, UK) with direct uv mode (260:280nm ratio). 20µg of protein was used per sample, and each sample was added to 4x SDS loading buffer (supplemented with 2.5% β-mercaptoethanol) at a ratio of V_{sample}:$V_{loading\ buffer}$ = 3:1. The samples were boiled at 100°C for 4 minutes and placed on ice.

2.6.6 Gel Electrophoresis

A Novex XCell II Mini Gel System (Invitrogen, Paisley, UK) was used. The proteins were separated by gel electrophoresis in pre-cast polyacrylamide gels (Invitrogen, Paisley, UK). Depending on the size of the proteins, the precast gels were chosen appropriately. For separation of higher molecular weight proteins (>150kDa), NuPAGE® Novex 3-8% Tris-Acetate Gels were used, otherwise NuPAGE® Novex® 4–12% Bis-Tris Gels were used. The running buffer was chosen in accordance with the gel system used (MES running buffer for 4–12% Bis-Tris Gels and Tris-Acetate running buffer for 3-8% Tris-Acetate Gels. The pre-cast gels were rinsed with water, positioned into the Mini-Cell gel

tanks such that the notched “well” side of the cassette faced inwards toward the buffer core. The gels were seated on the bottom of the Mini-Cell and locked into place with the gel tension Wedge. If one gel was being used, the plastic buffer dam replaced the second gel cassette. Ensuring a tight seal, the upper buffer chamber (inner side) was filled with the appropriate 1x running buffer to a level exceeding that of the level of the wells. Similarly, the lower buffer chamber (outer side) was filled with 600 ml of the appropriate 1x running buffer. 5-10µL of the molecular weight marker was added to the first well (5µL for 15 lane gels systems and 10µL for 10 lane gel systems). Protein samples were added carefully to the remaining wells. The electrophoresis conditions were dependent on the gel system used. For NuPAGE® Novex 4-12%Bis-Tris Gels with MES Running Buffer, the voltage was set to 150-200V, which resulted in an approximate running time of 45-60 minutes. For NuPAGE® Novex 3-8% Tris-Acetate Gels, the voltage was set to 120-150V, which resulted in an approximate running time of 60-90 minutes. Following the electrophoresis, the cassettes were removed from the Mini-Cell gel tank.

2.6.7 Preparation for blotting gels

The polyvinylidene difluoride membranes (Millipore, Dundee, UK) were cut to the same size as the blotting pads and immersed in methanol. The methanol was discarded and the membrane was immersed in 1x transfer buffer. 2 similarly sized filter papers were cut and added to the transfer buffer. The three bonded sides of the cassettes were separated by inserting the gel knife into the gap between the cassette’s two plates. The gel was carefully removed and placed in transfer buffer (same container as the membrane and filter papers). In a separate container 6-8 blotting pads were immersed in 1x transfer buffer.

2.6.8 The blotting protocol

3 soaked blotting pads were placed on the cathode (-) core of the blot module. A pre-soaked filter paper was placed on top of the pads ensuring to remove any air bubbles. The gel was carefully placed over the filter paper in the correct orientation. The membrane was positioned over the gel followed by the second pre-soaked filter paper

ensuring to remove any trapped air bubbles. 3 soaked blotting pads were placed over the second filter paper. The anode (+) core was placed on top of the pads. The blot module held firmly together was positioned into the into the guide rails on the lower buffer chamber of the Mini-Cell gel tank. The gel tension Wedge was inserted into the lower buffer chamber and locked into position. The blot module was filled with 1x transfer buffer, until the gel/membrane assembly was fully immersed. The outer buffer chamber was filled with 600-700mL water. The transfer was performed at 30V constant for 90 minutes.

2.6.9 Blocking the membrane

Following the transfer process, the membrane was carefully removed and allowed to air dry for 15 minutes. The membrane was immersed in 20mL blocking buffer for 1 hour at room temperature, or overnight at 4°C.

2.6.10 Primary and secondary antibodies

After blocking the membrane, the primary antibody was added in blocking buffer at the recommended concentration and incubated according to the recommended instructions. Following this, the membrane was washed with 20mL PBS-T for 10 minutes (3 times). HRP-conjugated secondary antibodies were then added to the membranes in blocking buffer at recommended concentrations and incubated for 1 hour at room temperature. The membranes were washed with 20mL PBS-T for 10 minutes (3 times). For list of primary and secondary antibodies used please see table 2-2.

2.6.11 Detection using chemiluminescence

The Amersham ECL detection reagent was prepared by mixing an equal volume of detection solution 1 with detection solution 2 allowing sufficient total volume to cover the membranes (the recommended final volume required is ~0.125 ml/cm^2 membrane). The excess PBS-T from the washed membrane was drained, and placed on a transparency film with the protein side facing up. The mixed detection reagent was pipetted onto the membrane and incubated for 1 minute at room temperature. The excess detection reagent was removed by blotting using filter paper. Another transparency was

positioned over the membrane and transferred to an X-ray film cassette. Film exposure was conducted in a dark room. A sheet of autoradiography film (Sigma-Aldrich, Gillingham, UK) was placed on top of the membrane. The cassette was closed for the duration of exposure and the film was developed using X-O-Mat processor (Kodak, Cambridge, UK).

2.6.12 Stripping and reprobing a membrane

To reprobe the membrane, the membrane was immersed in 100mL striping buffer at 50°C with gentle agitation. The membrane was washed 2 times with PBS-T for 10 minutes prior to proceeding to blocking and application of primary and secondary antibodies as above.

2.6.13 Protein quantification

Protein quantification was performed using densitometry using ImageJ software (National Institutes of Health, Bethesda, Maryland, USA). The immunodensity of the protein band was normalized to the immunodensity of tubulin.

2.7 TF ACTIVITY ASSAY

2.7.1 Reagents

Pooled human platelet poor plasma (PPP); Pooled murine PPP (Seralab, Sussex, UK); Factor VII-deficient human PPP (Alphalabs, Eastleigh, UK); Corn trypsin inhibitor (Sigma-Aldrich, Gillingham, UK); Sodium citrate (Sigma-Aldrich, Gillingham, UK); 1M $CaCl_2$ (Sigma-Aldrich, Gillingham, UK); Chromgenic TF activity assay (Abcam); Relipidated TF (Innovin®, Dade Behring, Milton-Keynes, UK); N-octyl β-D-glucopyranoside (Sigma-Aldrich, Gillingham, UK); 1M HEPES (Sigma-Aldrich, Gillingham, UK); 5M NaCl (Ambion, Paisley, UK); Molecular grade water (Invitrogen, Paisley, UK)

2.7.2 Buffers

- HN-Buffer (25mM HEPES, 175mM NaCl) – for 10mL HN buffer: 250µL 1M HEPES + 350 µL 5M NaCl + 9.4mL water

- 15mM N-octyl β-D-glucopyranoside – 8.8mg N-octyl β-D-glucopyranoside + 1mL HN-buffer

2.7.3 Principle of the turbimetric assay

Many clotting assays exist to assess the thrombogenicity of cells in culture. The most commonly used is a turbimetric clotting assay, where clot formation can be assessed by following changes in clot turbidity as it forms, using absorption spectrophotometry (A_{405}). A turbimetric clot assay was used to determine TF activity, with minor adaptation of a validated one-step plasma recalcification clotting assay[410]. Figure 2-2a shows a clot turbidity curve. The lag phase of the turbidity curve (T_{lag}) is the time to exponential increase in clot turbidity, representing the time required for fibrin protofibrils to grow to sufficient length to allow lateral aggregation to occur, and is the most sensitive clot turbimetric parameter[411]. The maximum rate of turbidity change (V_{max}), i.e. the steepest portion of the curve, corresponds to the peak clotting rate. By determining the steepest portion of turbidity curve, the intersection point of a tangent drawn at this point to the arbitrary baseline absorbance (ABS_{min}) line corresponds to T_{lag}[411, 412]. The maximum absorbance at plateau (ABS_{max}) reflects the number of protofibrils per fibre[411, 412]. The clot turbidity curves were modelled mathematically using TableCurve2D v5.0 (Systat) where ABS was a function of T, ABS=*f*(T), to determine V_{max}, T_{Vmax}, ABS_{max} and AB_{min}. Using V_{max}, T_{Vmax} and ABS_{min}, T_{lag} was derived using coordinate geometry:

$$T_{lag} = \frac{ABS_{min} - [f(T_{vmax}) - V_{max}.T_{Vmax}]}{V_{max}} \quad \text{where } ABS=f(T)$$

In general, if the turbimetric profiles shift to the left, this is indicative of increased procoagulant activity, whilst a shift to the right is indicative of reduced procoagulant activity (figure 2-2b). The intrinsic coagulation pathway has a delayed onset due to a slower activation process[33] (figure 2-2c).

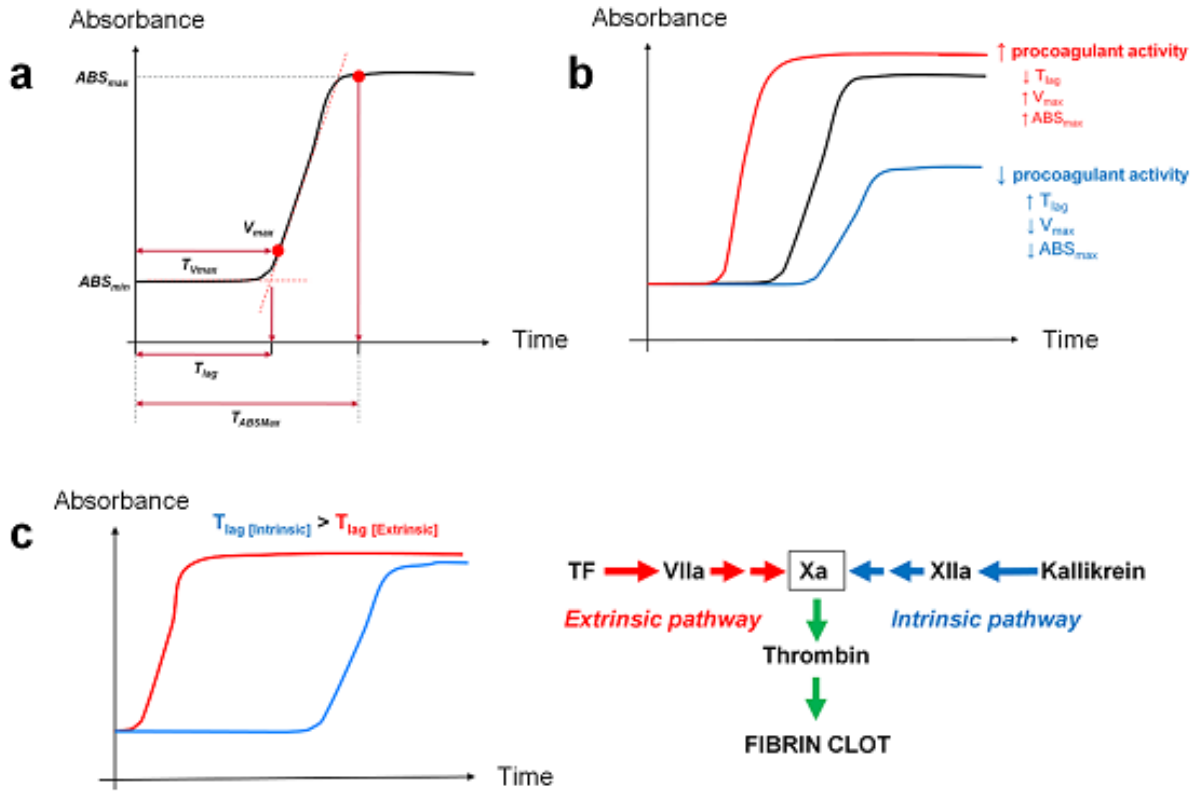

Figure 2-2: The principles of the turbimetric clot assay
(a) Clot turbidity curves can be analyzed using many turbimetric parameters. The lag phase of the turbidity curve (T_{lag}) is the time to exponential increase in clot turbidity and is the most sensitive clot turbimetric parameter. The maximum rate of turbidity change (V_{max}), i.e. the steepest portion of the curve, corresponds to the peak clotting rate. By determining the steepest portion of turbidity curve, the intersection point of a tangent drawn at this point to the arbitrary baseline absorbance (ABS_{min}) line corresponds to T_{lag}. The maximum absorbance at plateau (ABS_{max}) reflects the number of protofibrils per fibre. Other parameters used include T_{Vmax} and T_{ABSmax}; **(b)** Schematic representation to show shifts in the turbimetric curves indicative of change in procoagulant activity; and (c) The intrinsic pathway is more slower in onset than the extrinsic pathway and is therefore often associated with greater T_{lag} values.

2.7.4 Plasma preparation for turbimetric assay

For assessing procoagulant activity of human cells, pooled citrated human PPP was used. Platelet rich plasma (PRP) was obtained from citrated venous blood (citrate:blood=1:9) following centrifugation at 400g for 20 minutes at room temperature. PPP was made by centrifuging PRP at 5000g for 20 minutes at 4°C. Pooled normal

PPP was formed by pooling PPP from 10 different healthy human volunteers. For assessing procoagulant activity of murine cells, human plasma cannot be used, as murine TF cannot effectively activate human VII[413]. Using mouse plasma for clot turbibity assays has been variably reported, but the disadvantage is that mouse plasma is darker and less clear compared to human plasma. This does not result in the characteristic clot turbimetric profiles to allow reliable derivation of clot turbimetric parameters. Thus, a combination of citrated pooled human PPP (as above) and murine PPP (available commercially from Seralab, UK) was used (human plasma:mouse plasma = 9:1). The 10% mouse plasma provides sufficient factor VII for clot formation to subsequently occur (see below).

2.7.5 Determining TF activity of cells in culture

To determine TF activity of cells in culture, cells were cultured in 96 well plates (cell density=$2x10^4$ cells per well) according to the experimental protocol. Following the experiment, the supernatant was removed, with the cells remaining adherent to the base of the wells, and washed with PBS twice to remove any culture medium and serum. The surface of the cells provided procoagulant stimulus for the subsequent clotting reaction. 100 µL of the citrated plasma was added to the wells and recalcified with 2 µL of 1.0M $CaCl_2$ to initiate clotting (20mM final well concentration). Clotting was assessed using clot turbidity by measuring absorbance (A_{405}) every minute for 60 minutes in a spectrophotometer (Synergy HT, Biotek, Potton, UK) with internal thermostatic control at 37°C. The clot turbidity curves were modeled mathematically using TableCurve2D v5.0 (Systat, Chicago, IL, USA) where ABS was a function of T, ABS=*f*(T), to determine T_{lag}. A TF standard curve was generated using relipidated TF (Innovin®) to provide a correlation between T_{lag} and TF concentration. The concentration of TF in the Innovin® preparation was initially determined using a chromogenic TF activity assay (see below). Each experimental condition was performed in triplicate providing 3 T_{lag} values and, therefore, 3 TF activity values accordingly. The mean TF activity values were used for subsequent analyses.

2.7.6 Determining TF activity of tissue samples

To determine TF activity of tissues samples, tissue were harvested and snap frozen and stored at -80°C until analysis. The tissue sample were dissolved in 300µl 15 mM N-octyl β-D-glucopyranoside in HN-Buffer in 2mL round-bottomed eppendorfs. The tissues were homogenized by adding a stainless steel bead (Qiagen, Crawley, UK) and operating a TissueLyser (Qiagen, Crawley, UK) for 2 min at 20Hz. The tubes were centrifuged at 17,000g for 20 minutes at 4ºC to pellet cell debris with the stainless steel bead. The supernatant (homogenate) was carefully removed and transferred to a fresh eppendorf, followed by repeat centrifugation at 17,000g for 20 minutes at 4ºC to pellet any remaining debris. The homogenate was carefully transferred to a fresh eppendorf. Total protein content of the tissue homogenates was determined and homogenates were made to a working concentration of 1 mg/mL total protein using HN-Buffer as a dilutent. 5µL of the homogenate was mixed with 100µl citrated plasma as above and recalcified. TF activity was determined as above.

2.7.7 Chromogenic TF activity assay

A chromogenic TF activity assay (Abcam, Cambridge, UK) was used to determine the TF concentration of the Innovin® preparation, as TF concentration of this commercially available preparation is not provided. First, the TF standards were made using the stock TF preparation (250pM) with sample dilutent which were provided in the assay kit. The standards used were 250, 125, 62.5, 31.25, 15.63 and 0pM TF. All reactions were performed in triplicate. For the total number of wells, a master mix was made using reagents provided in the kit which comprised of 50µL assay dilutent, 10µL factor VII and 10µL factor X per well. 70µL of this master mix was added to each well. 10µL of TF standard or sample was added to each well and allowed to incubate at 37°C for 30 minutes. Next, 20µL of factor Xa substrate (provided in the kit) was added to each well and gently mixed. The absorbance (A_{405}) was measured in a spectrophotometer (Synergy HT, Biotek, Potton, UK) with internal thermostatic control at 37°C. A standard curve was constructed using the A_{405} values and TF concentration and modeled mathematically using TableCurve2D v5.0 (Systat). The TF concentration of the

Innovin® preparation was determined from the standard curve. The TF concentration of the Innovin preparation was used to prepare [TF]-T_{lag} standard curve.

2.7.8 Validation experiments for turbimetric clot assay

2.7.8a Investigating [$CaCl_2$] for plasma re-calcification

The concentration of $CaCl_2$ for re-calcifying plasma was based on standard concentrations used in our laboratory. As a validation exercise, the effect of increasing calcium concentrations was investigated on the intrinsic coagulation cascade, where 100µL human PPP was recalcified and clot turbimetric profiles were established. The clot turbidity curves were modeled mathematically to determine T_{lag}, V_{max} and ABS_{max}. The concentrations of $CaCl_2$ used were 10-50mM. Figure 2-3 shows the clot turbimetric profiles and analyses of T_{lag}, V_{max} and ABS_{max}. It is interesting to note for concentrations ranging from 10-25mM there was no significant change in clot turbimetric profiles, however beyond these values there was a suggestion that excess $CaCl_2$ was inhibiting intrinsic coagulation. For $CaCl_2$ > 35mM, the T_{lag} was increasing; for $CaCl_2$ > 25mM, the V_{max} was decreasing; and for $CaCl_2$ > 30mM, the ABS_{max} was decreasing. These results indicate that the a concentration of 20mM $CaCl_2$ used for re-calcification represents concentration at the higher end of concentration range where little adverse effect is observed on clot turbimetric parameters. The observation that increasing $CaCl_2$ concentration beyond 25-30mM appears to have an inhibitory effect on intrinsic coagulation certainly warrants an explanation. One possibility is that the excess positive charge provided by the Ca^{2+} ions may neutralize the negative charge on the surface of the wells that is important for contact activation in the intrinsic pathway.

2.7.8b Validation of murine TF turbimetric assay

In experiments where murine TF needed to be quantified, a combination of citrated pooled human PPP (as above) and mouse PPP (as above) was used (human plasma:mouse plasma = 9:1). The rationale for using this combination is that (a) human plasma cannot be used, as murine TF cannot effectively activate human VII[413]; and (b) using mouse plasma for clot turbidity assays has the disadvantage that it is darker and

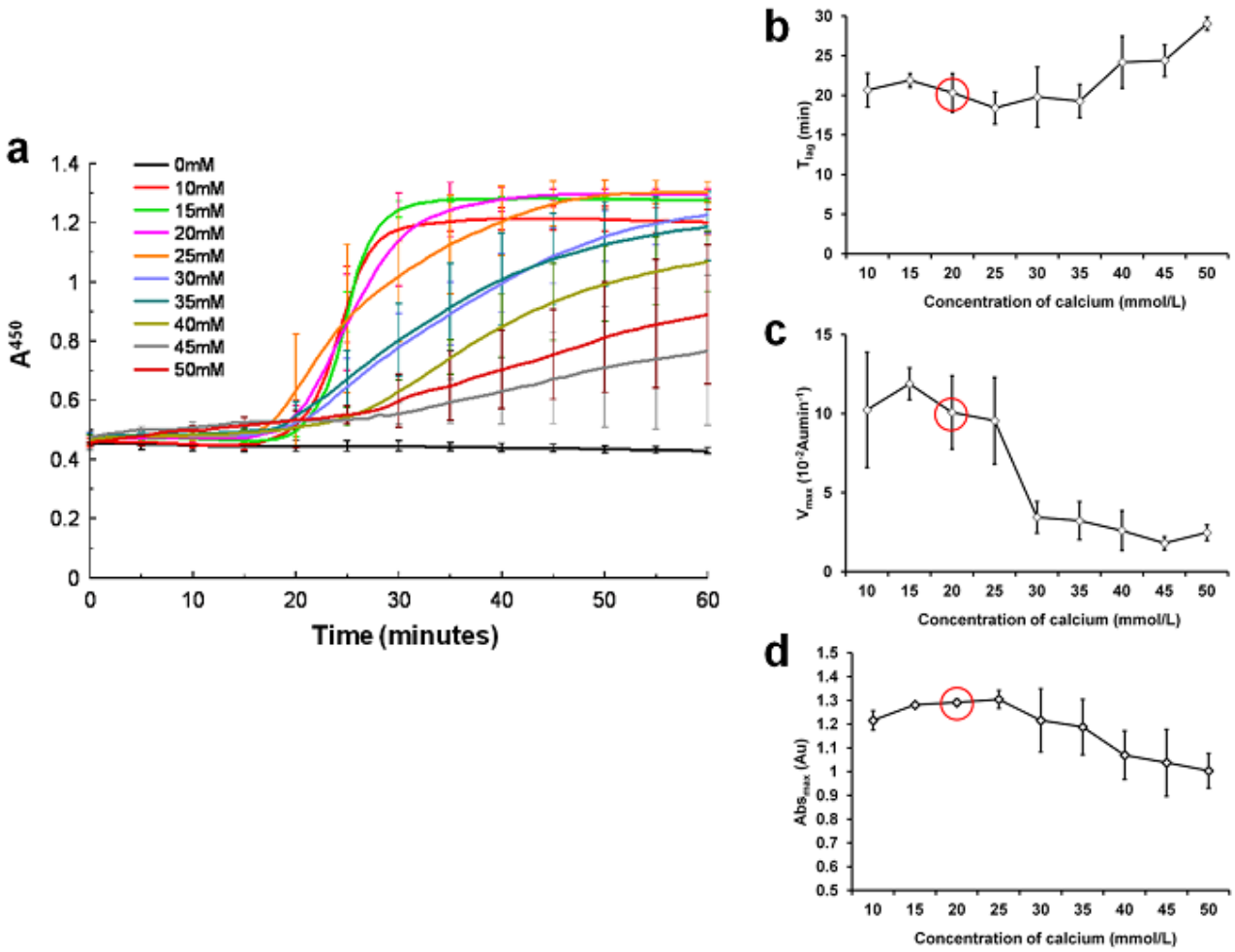

Figure 2-3: Investigating the concentration of $CaCl_2$ for plasma re-calcification
The effect of increasing calcium concentrations (10-50mM) for plasma re-calcification was investigated on the intrinsic coagulation cascade (n=4). 100µL human PPP was recalcified and clot turbimetric profiles were established. The clot turbidity curves were modeled mathematically to determine T_{lag}, V_{max} and ABS_{max}. The turbimetric profiles are shown in **(a)** and turbimetric parameters are shown in **(b-d)**. The standard $CaCl_2$ concentration used in all experiments is 20mM (highlighted with red circle). Data is expressed as mean ± SEM.

less clear compared to human plasma resulting in sub-optimal clot turbimetric profiles to allow reliable derivation of clot turbimetric parameters. For this reason, a small amount of mouse plasma (10%) was added to human plasma to provide sufficient factor VII for clot formation to subsequently occur, whilst still retaining the clearer nature of human plasma, making it favorable for optimal turbimetric profiling. Figure 2-4a demonstrates this principle where different combinations of 100µL citrated plasma were added to wells containing LPS stimulated murine macrophages (1µg/mL for 8 hours) - a source of murine TF. Following removal of the culture medium, the adherent LPS-stimulated

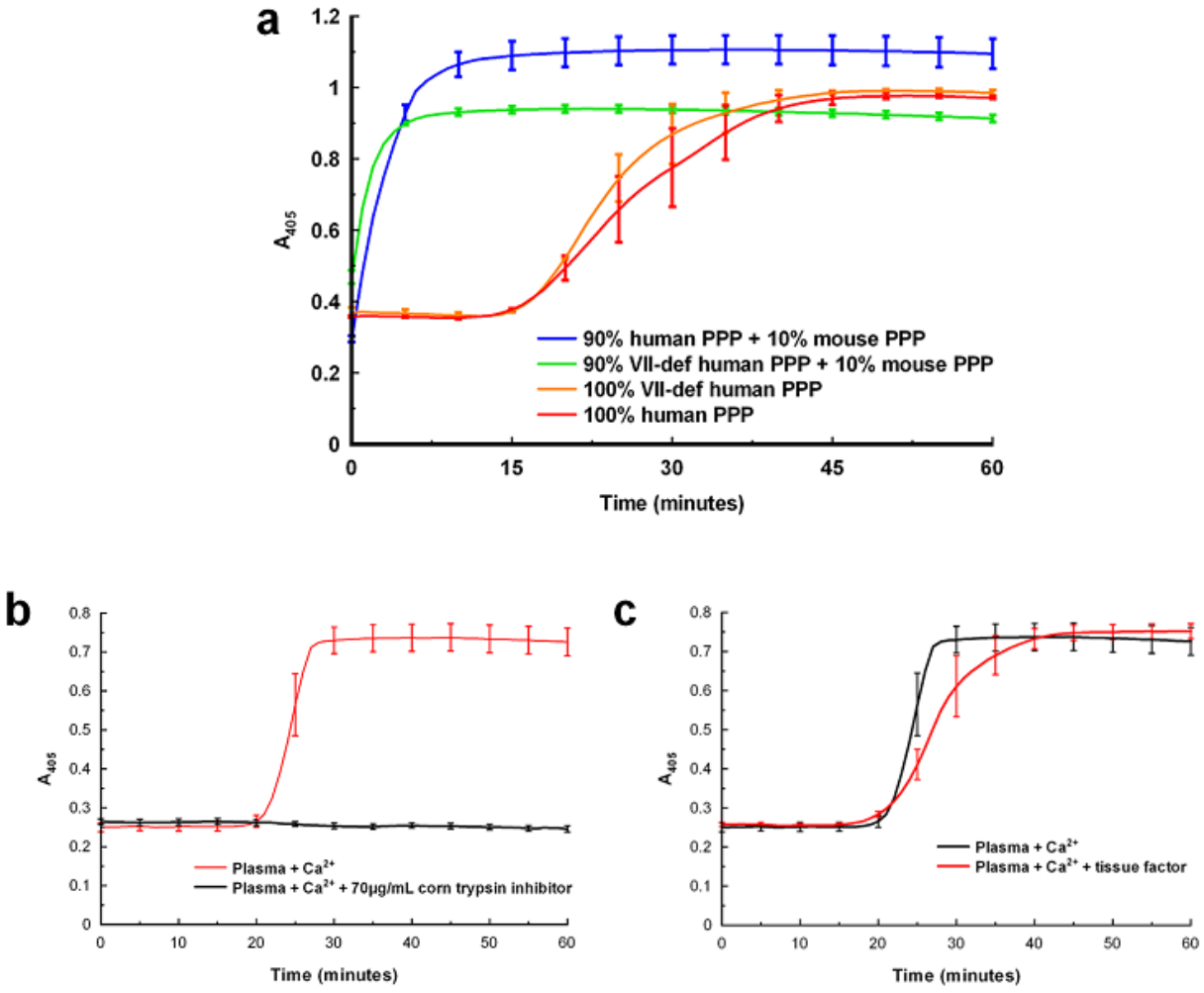

Figure 2-4: Validation of mouse:human plasma combination for detection of murine TF
(a) All wells contained LPS stimulated murine macrophages (1µg/mL for 8 hours), providing a source of murine TF. 100µL plasma was added and re-calcified. Clot turbimetric profiles established (n=4). All experiments were conducted in the presence of corn trypsin inhibitor (70µg/mL) which inhibits the intrinsic coagulation pathway. Efficient clotting, representative of extrinsic coagulation, did not occur using either pooled human PPP or using pooled human VII-deficient PPP (Alpha Laboratories). Addition of 10% murine plasma to VII-deficient human plasma and pooled human plasma completely restored extrinsic clotting; **(b)** Corn trypsin inhibitor (70µg/mL) inhibits the intrinsic coagulation cascade when added to factor VII deficient plasma (n=4); and **(c)** Exogenous TF does not affect clotting when added to factor VII deficient plasma validating the absence of factor VII in the assay (n=4). Data is expressed as mean ± SEM.

murine macrophages were washed with PBS and 100µL PPP was added and re-calcified, allowing clot turbimetric profiles to be established. All experiments were conducted in the presence of corn trypsin inhibitor (70µg/mL) which inhibits the intrinsic coagulation pathway. The corn trypsin inhibitor was added to the plasma before adding the plasma to the wells. Efficient clotting, representative of extrinsic coagulation, did not

occur using either pooled human PPP or using pooled human VII-deficient PPP. It is important to note that some clotting was seen at with T_{lag} ~ 15min, and given that intrinsic coagulation was inhibited using corn trypsin inhibitor, this may represent very weak extrinsic coagulation, as murine TF has been reported to activate human factor VII to some extent[413]. However adding 10% murine plasma to VII-deficient human plasma and pooled human plasma completely restored clotting. Using corn trypsin inhibitor (70µg/mL) effectively abolishes the intrinsic coagulation cascade, and obviates any issues where the intrinsic coagulation cascade may confound interpretation of these results. This principle is demonstrated in figure 2-4b, where corn trypsin inhibitor abolished coagulation of re-calcified factor VII-deficient plasma. The factor VII deficient plasma was also validated by experiments where the addition of exogenous TF did not accelerate coagulation (figure 2-4c).

2.7.8c Determining sensitivities of the crude clot turbimetric parameters

Amongst the different turbimetric parameters, T_{lag}, V_{max} and ABS_{max} are the most commonly used. Of these, T_{lag} represents the most sensitive clot turbimetric parameter[411]. Whilst T_{lag} has been used as the index parameter against which a TF standard curve is generated to provide a concentration of TF, it is important to have an understanding of how these turbimetric parameters behave throughout a range of TF concentrations. To test this, different concentrations of exogenous TF (Innovin®) were used. The neat concentration of the commercially available preparation was arbitrarily set at 1. 10-fold serial dilutions were made using PBS (10^{-4}U to 1U). 100µL of TF solution was added to each well of a 96-well plate and allowed to incubate at 37°C for 1 hour. This allowed the TF to become adsorbed onto the plate surface. After the incubation period, the TF solution was removed carefully using a pipette and washed once with 100µL PBS. 100 µL of the citrated plasma was added and re-calcified. Clot turbimetric profiles were established, and turbidity curves were modeled mathematically to determine T_{lag}, V_{max} and ABS_{max}. In these set of experiments corn-trypsin inhibitor was not used, and thus the clot turbimetric profile with [TF]=0 represents intrinsic coagulation. Figure 2-5a shows the turbimetric profiles throughout the range of TF concentrations. With increasing TF concentrations the curves shift to the left in keeping

with increased procoagulant activity. Analysis of the clot turbimetric profiles demonstrates T_{lag} being the most sensitive clot turbimetric parameter, being able to detect differences throughout the TF concentration spectrum including very low TF concentrations (figure 2-5b). V_{max} appears to the next most sensitive, but was not able to detect differences below 10^{-2}U (figure 2-5c). ABS_{max} appeared to be the least sensitive parameter (figure 2-5d). These experiments corroborate previously reported findings, and support the use of T_{lag} as the index turbimetric parameter against which TF standard curves can be generated[411].

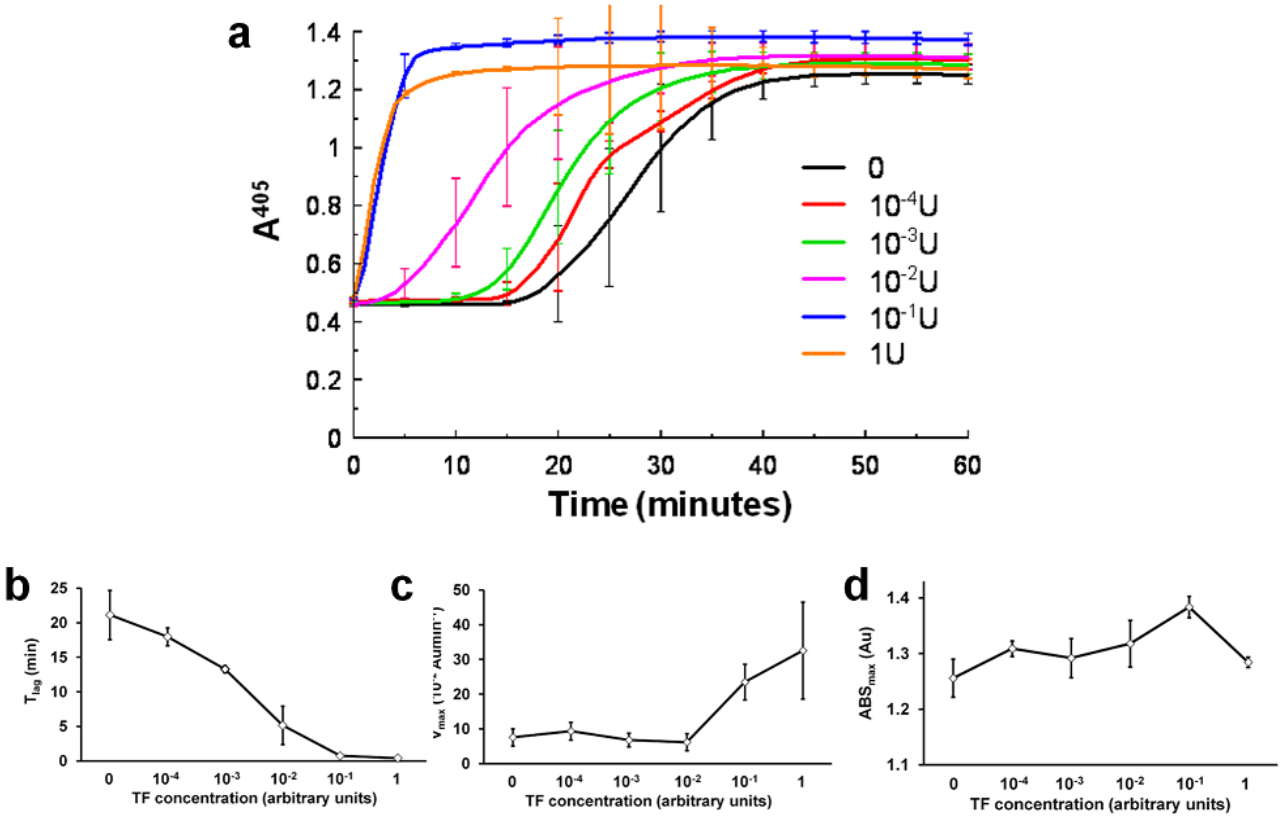

Figure 2-5: Sensitivities of the clot turbimetric parameters
Different concentrations of exogenous TF were adsorbed onto the plate surface in a 96-well plate. 100 µL of the citrated plasma was added and re-calcified and clot turbimetric profiles were established (n=4). **(a)** Turbimetric profiles throughout the range of TF concentrations (10^{-4}U to 1U); Analyses of T_{lag}, V_{max} and ABS_{max} are shown in **(b-d)**. Data is expressed as mean ± SEM. T_{lag} appears to be the most sensitive clot turbimetric parameter, being able to detect differences throughout the TF concentration spectrum including very low TF concentrations.

2.8 MOUSE TNFα ELISA

TNFα proteins levels in cell culture supernatants and mouse sera were measured using a mouse TNFα Duo-set sandwich ELISA kit (RND systems, Abingdon, UK) according to

the manufacturer's instructions. Briefly, 96 wells plates were coated overnight with 100µL of goat anti-mouse TNFα antibody (144 µg/mL) at room temperature, dependent on the final number of wells required (all samples or standards were tested in triplicate). The wells were washed with wash buffer [PBS (0.05% Tween)] and blocked with 1% BSA in PBS at room temperature for 1 hour. The wells were washed with wash buffer and the sample or standard was added and incubated for 2 hours at room temperature. The standards were prepared from the stock TNFα provided in the kit, and the concentrations used for the standard were 2000, 1000, 500, 250, 125, 62.5 and 31.25 pg/mL. The wells were washed with wash buffer and 100µL of biotinylated goat anti-mouse TNFα (72 µg/mL) was added and incubated for 2 hours at room temperature. The wells were washed with wash buffer and 100µL of Streptavidin-HRP antibody was added and incubated for 20 minutes at room temperature (avoiding light). The wells were washed and 100µL of Substrate Solution was added to each well and incubated for 20 minutes at room temperature. 50 µL of Stop Solution (2 N H_2SO_4) was added. the optical density of each well was determined immediately (A_{450}) using a spectrophotometer (Synergy HT, Biotek, Potton, UK). A standard curve was constructed using the A_{450} values and TNFα concentration and modeled mathematically using TableCurve2D v5.0 (Systat, Chicago, IL, USA). The TNFα concentration of the samples were determined from the standard curve.

2.9 FLOW CYTOMETRIC ANALYSIS

2.9.1 Detection of murine TF

The cells were treated according to the experimental protocol, following which the culture medium was removed. The cells were washed twice with 500µL ice cold PBS. The PBS aliquots were added above the cells and carefully removed using a pipette without disrupting the adherent cells. 500µL ice cold PBS was added to each well and the cells harvest by scraping. The cell suspensions were transferred to 1.5mL eppendorfs, and washed with 1 mL aliquots of ice cold PBS each time centrifuging on a table top centrifuge at 8000g for 5 minutes at 4°C. Following the final wash, the cells were resuspended in 100µL of PBS. The cells were blocked with goat serum (Dako UK Ltd, Cambridge, UK) at 1:50 dilution for 30 minutes at 4°C , and stained for 30 minutes

at 4°C with either 1µg/ml rabbit IgG control antibody (Santa Cruz, Insight Biotechnology, Wembley, UK) or 1µg/ml rabbit anti-mouse TF antibody (American Diagnostica, Alere, Manchester, UK) with 1 mL aliquots of ice cold PBS each time centrifuging on a table top centrifuge at 8000g for 5 minutes at 4°C. Following the final wash, the cells were resuspended in 100µL of PBS and stained with 1µg/ml FITC-conjugated F(ab')2 fragment of goat anti-rabbit antibody (Invitrogen, Paisley, UK) for 30 minutes at 4°C .The cells were again washed with 1 mL aliquots of ice cold PBS twice, and resuspended in 500 µl PBS for flow cytometric analysis. The cells were read on a Coulter EpicsXL flow cytometer, FL1–600V, FL2–600V. The maximum event rate was set to 10,000. Data were analyzed and presented using WinMDI software (Scripps Research Institute, CA, USA). Relative mean fluorescence intensity (RLMFI) values were obtained as ratio of the geometric mean of the fluorescence intensity with anti-TF antibody to the geometric mean of fluorescence intensity obtained with the control antibody.

2.9.2 Detection of human TF

The supernatant culture medium was removed and cells washed twice in cold PBS, and harvested in 500µL ice cold PBS (as above). For detection of surface human TF expression, the cells were incubated with either FITC-conjugated TF or FITC-conjugated isotype control antibodies (AdD Serotec, Kidlington, UK) for 30min at 4ºC. The cells were washed with cold PBS and resuspended in 500µL cold PBS and subjected to flow cytometric analysis. The cells were read on a Coulter EpicsXL flow cytometer, FL1–600V, FL2–600V. The maximum event count was set at 10,000. Data were analyzed and presented using WinMDI software (as above).

2.10 RNP IMMUNOPRECIPTATION

2.10.1 Reagents

2M KCl (Ambion, Paisley, UK); 5M NaCl (Ambion, Paisley, UK); 1M MgCl2 (Ambion, Paisley, UK); 1M HEPES; 100mM TRIS (pH=7.4) (Calbiochem. Nottingham, UK); IGEPAL (Sigma-Aldrich, Gillingham, UK); RNase Out (Invitrogen, Paisley, UK); Superasin (Ambion, Paisley, UK); Protease inhibitor cocktail (Sigma-Aldrich, Gillingham,

UK); 1M DTT (Ambion, Paisley, UK); Protein-G agarose beads (Sigma-Aldrich, Gillingham, UK); 10mg/mL Proteinase K (Qiagen, Crawley, UK); RNase-free DNase 1 (Qiagen, Crawley, UK); 20% SDS (Sigma-Aldrich, Gillingham, UK); Molecular grade water (Invitrogen, Paisley, UK)

2.10.2 Buffers

- Polysome Lysis buffer (100mM KCl, 5mM $MgCl_2$, 10mM HEPES, pH 7.0, 0.5% NP-40) – for 50mL buffer: 0.5mL 1M HEPES + 2.5mL 2M KCl + 250µL 1M $MgCl_2$ + 1.25mL 20% IGEPAL +45.5mL water
- NT-2 Buffer (50mM Tris–HCl (pH 7.4), 150mM NaCl, 1mM $MgCl_2$ and 0.05% NP-40) – for 50mL buffer: 25mL 100mM TRIS + 1.5mL 5M NaCl + 50µL 1M MgCl2 + 125µL 20% IGEPAL + 23.325mL water

2.10.3 Preparation of RNP lysate from cultured cells

RNP immunoprecipitation was performed as previously described for immunoprecipitation of TTP using rabbit anti-TTP (H-120, Santa Cruz, Insight Biotechnology, Wembley, UK)[414]. Briefly, the cells were seeded in T75 culture flasks at a density of $1x10^7$ cells per flask and treated as per the experimental protocol. The overlying culture medium containing dead cells and debris was removed. 20mL ice cold PBS was added to the flask. The adherent cells were removed by scraping. The cell suspension was transferred to 50mL tube and centrifuged at 300g for 10 minutes at 4°C. The supernatant was completely aspirated. The cells were washed again in 50mL ice cold PBS and pelleted and transferred to a 1.5mL eppendorf. The cells were pelleted and lysed with 500µL polysome lysis buffer (1mL of buffer supplemented with 1µL 1M DTT, 10µL RNase Out, 10µL Superasin and 10µL protease inhibitor cocktail immediately prior to use). The lysis buffer was added to the pellet and gently mixed by pipetting up and down (without vortexing). The lysate was kept on ice for 15 minutes and centrifuged at 17000g at 4°C for 30 minutes to pellet cell debris. The supernatant was carefully removed. Protein concentration was determined and adjusted with lysis buffer to achieve a concentration of 3mg per 100µl. 100 µl of lysate were aliquoted and either used immediately for immunoprecipitation or stored at -80°C until use.

2.10.4 Preparation of beads

100µL of Protein-G agarose beads were used per immunoprecipitation reaction. 2 x 100µL beads were transferred to 2 x 1.5mL RNase-free eppendorfs (for control and anti-TTP antibody reactions respectively) and centrifuged at 10,000g for 30 seconds at 4°C. The supernatant was completely removed and 4 washing steps were repeated, each time resuspending in 500µL NT-2 buffer, centrifuged at 10,000g for 30 seconds at 4°C and completely aspirating the supernatant. The beads were resupended in 200µL NT-2 buffer and 20µg of the protein-specific antibody or IgG control was added to each of the tubes. The tubes were mixed with rotation overnight at 4°C. The following day, the beads were washed with 1mL aliquots of ice-cold NT-2 buffer at 14000g for 5 minutes at 4°C (5 times). After the final wash, the NT-2 buffer was completely removed and the beads were ready to use.

2.10.5 Immunoprecipitation of RNPs

700µL NT-2 buffer was added to the pre-coated beads. In a separate tube 10µL 0.1 DTT, 10µL RNase Out and 33µL 0.5M EDTA was added and mixed. The mix was then added to the pre-coated beads. 100µL of the lysate was added and the total volume made up to 1mL with ice-cold NT-2 buffer. The tube was mixed with rotation for 1 hour at 4°C. Following the incubation, the beads were pelleted at 5000g for 5 minutes at 4°C. The beads were washed with 1mL aliquots of ice-cold NT-2 buffer and pelleted at 5000g for 5 minutes at 4°C (5 times). After the final wash the beads were incubated in 100ml of NT2 buffer containing 20U of RNase-free DNase I at 37°C for 10 minutes to remove genomic DNA contamination. 1mL ice cold NT2 buffer was added and centrifuged at 5000g for 5 minutes at 4°C. In a separate tube 5µL 10mg/mL Proteinase K, 0.5µL 20% SDS and 100µL NT-2 buffer were added and mixed. The mix was then added to the beads and incubated at 55°C for 15 minutes with mixing. The beads were pelleted by centrifugation at 500g for 5 minutes and the supernatant collected (~100µL). A further 200µL of NT-2 buffer was added to the beads and beads were pelleted by centrifugation at 5000g for 5 minutes and again the supernatant collected (~200µL). Both supernatants were combined (total supernatant volume ~300µL).

2.10.6 RNA extraction and cDNA synthesis

RNA was extracted from the supernatants using Trizol preparation (as above). The final RNA pellet was resuspended in 22µL of water. RNA concentration and quality was determined using Nanodrop 1000 (Thermo Scientific, Loughborough, UK). 11µL of RNA was used for first strand cDNA synthesis (as above), whilst the remaining RNA was stored at -80°C for use as non-RT controls in subsequent control PCR reactions.

2.10.7 Analysis of protein-bound mRNAs species

Gene specific primers used for qRT-PCR were used to determine the presence or absence of protein-bound mRNA species and control transcripts (HPRT and GAPDH). The reaction protocol used was identical to the qRT-PCR reactions with SYBG green (as above), but the cDNA dilutions used were 1:10 and reactions were performed in duplicate. To determine specificity for mRNA, the samples were run in parallel with non-RT samples to control for genomic DNA contamination. The PCR reaction products were separated in a 2% agarose gel containing ethidium bromide and visualized under UV light.

2.11 CLONING OF TF 3'UTR

2.11.1 Reagents

10pM Forward and reverse PCR primers (Eurofins, Ebersberg, Germany); Advantage 2 DNA Polymerase (Clontech, Oxford, UK); Advantage 2 PCR buffer (Clontech, Oxford, UK); 10mM dNTP mix (Roche Diagnostics, Sussex, UK); DNA gel loading buffer (Invitrogen, Paisley, UK); 1kB Plus DNA ladder (Invitrogen, Paisley, UK); 10X Tris-Borate-EDTA (TBE) buffer (Invitrogen, Paisley, UK); Ultrapure agar (Invitrogen, Paisley, UK); 10mg/mL Ethidium bromide (Sigma-Aldrich, Gillingham, UK); Gel extraction Kit (Qiagen, Crawley, UK); Isopropanolol (Sigma-Aldrich, Gillingham, UK); (pCRII-TOPO vector (Invitrogen, Paisley, UK); Salt solution (200 mM NaCl, 10 mM $MgCl_2$) (Invitrogen, Paisley, UK); One Shot TOP10 Electrocompetent E. Coli (Invitrogen, Paisley, UK); Agar (Sigma-Aldrich, Gillingham, UK); LB Broth (Sigma-Aldrich, Gillingham, UK); Molecular grade water (Invitrogen, Paisley, UK); Kanamycin (Invitrogen, Paisley, UK)

2.11.2 Amplification of DNA sequences

The murine and human TF 3'UTR sequences/truncations/mutations were amplified from total murine or human macrophage cDNA with PCR primers listed in tables 2-3 and 2-4 using the Advantage 2 PCR cloning kit (Clontech) according to the manufacturer's protocol. For the template, cDNA from 2 hour LPS-stimulated macrophages was used at a 1:10 dilution. The PCR reaction comprised of 1μL forward primer, 1μL reverse primer, 1μL template, 1μL 10mM dNTP mix, 1μL Advantage 2 DNA polymerase, 40μL water and 5μL Advantage 2 PCR buffer (total reaction volume = 50 μL). The components were placed in PCR tubes followed by brief spin and placed in a thermal cycler (Applied Biosystems, Warrington, UK) using the following protocol: 94°C (1 minute) followed by 30 cycles of 94°C (30 seconds), 60°C (30 seconds) and 72°C (1 minute).

2.11.3 Preparation of agarose gels

Agarose gels were prepared by adding the appropriate amount of ultrapure agarose to 1xTBE buffer and heating in a microwave until the agarose was fully dissolved. For "x" % gels, "x" grams of ultrapure agarose was added per 100mLs of 1x TBE buffer. The agarose solution was allowed to cool to 50-60°C and 4μl of 10mg/ml ethidium bromide was added per 100ml agarose solution. A gel caster was prepared with the appropriate comb(s) to make the wells and sealed, following which the agarose-ethidium bromide gel solution was carefully poured into the gel caster under a fume hood. The gel was allowed to set and solidify for 30 minutes, before removal of the gel caster and combs. The gel was immersed into 1X TBE buffer in an electrophoresis tank, ensuring the wells were positioned at the cathode pole of the tank.

2.11.4 Purification of amplified DNA sequences

The PCR reaction products were separated in a 1% agarose gel containing ethidium bromide and visualized under UV light, and the corresponding PCR fragment was carefully excised using a clean scalpel under UV guidance. The excised DNA band was carefully transferred to a 1.5mL eppendorfs and kept on ice. The DNA was subsequently extracted using Gel Extraction Kit (Qiagen, Crawley, UK) according to the manufacturer's instructions. Briefly, 300μL of Buffer QG was added to the excised gel

band and incubated at 50°C for 10 minutes to dissolve the gel. 100µL isopropanolol was added and mixed by pipetting, and then the total volume applied to a gel extraction spin column. The spin columns were centrifuged at 13000g for 1 minute, and the flow-through discarded. 0.5mL Buffer QG was added to the column and centrifuged at 13000g for 1 minute, again discarding the flow-through. 0.75mL of buffer PE was added to the spin column and centrifuged at 13000g for 1 minute, again discarding the flow-through, followed by repeat dry centrifugation at 13000g for 1 minute to remove any excess wash buffer. The spin column was placed in a clean 1.5mL eppendorfs, and 30µL of water was applied to the spin column membrane, allowed to incubate for 1 minute at room temperature before a final centrifugation at 13000g for 1 minute to elute the DNA. The concentration and quality of the DNA were determined using Nanodrop 1000 (Thermo Scientific, Loughborough, UK), ensuring a 260/280 ratio >1.8.

2.11.5 Cloning reaction

All DNA fragments in this study were cloned into the pCRII-TOPO vector (Invitrogen, Paisley, UK) using the TOPO TA Cloning Kit (Invitrogen, Paisley, UK) using the manufacturer's protocol. The map for the pCRII vector is shown in figure 2-6. This vector was chosen as it contains T7 and SP6 promoters appropriate for *in vitro* RNA transcription to generate sense and anti-sense strands. It contains both kanamycin and ampicillin resistance for choice of selection in E. coli. The cloning reaction comprised of 2µL DNA, 2µL water, 1µL salt solution and 1µL of pCRII vector (total reaction volume = 6µL). The components were placed in a 0.2mL PCR tube and briefly spun and allowed to incubate at room temperature for 20 minutes.

2.11.6 Transformation of bacteria

All transformations were performed using One Shot TOP10 Electrocompetent E. Coli (Invitrogen, Paisley, UK) according to the manufacturer's instruction. Firstly, one vial of bacteria was taken and allowed to thaw on ice for 10 minutes. Next, 2µL of the cloning reaction was taken and gently added to the bacteria and mixed by swirling using a pipette tip (no vortexing), and placed on ice for 30 minutes. Following the incubation, the cells were heat-shocked for 30 seconds at 42°C without shaking, and immediately

transferred to ice. 250 µL of S.O.C. medium (held at room temperature) was added to the reaction mixture. The tube cap was closed tightly and placed horizontally in a shaking incubator (200 rpm) at 37°C for 1 hour.

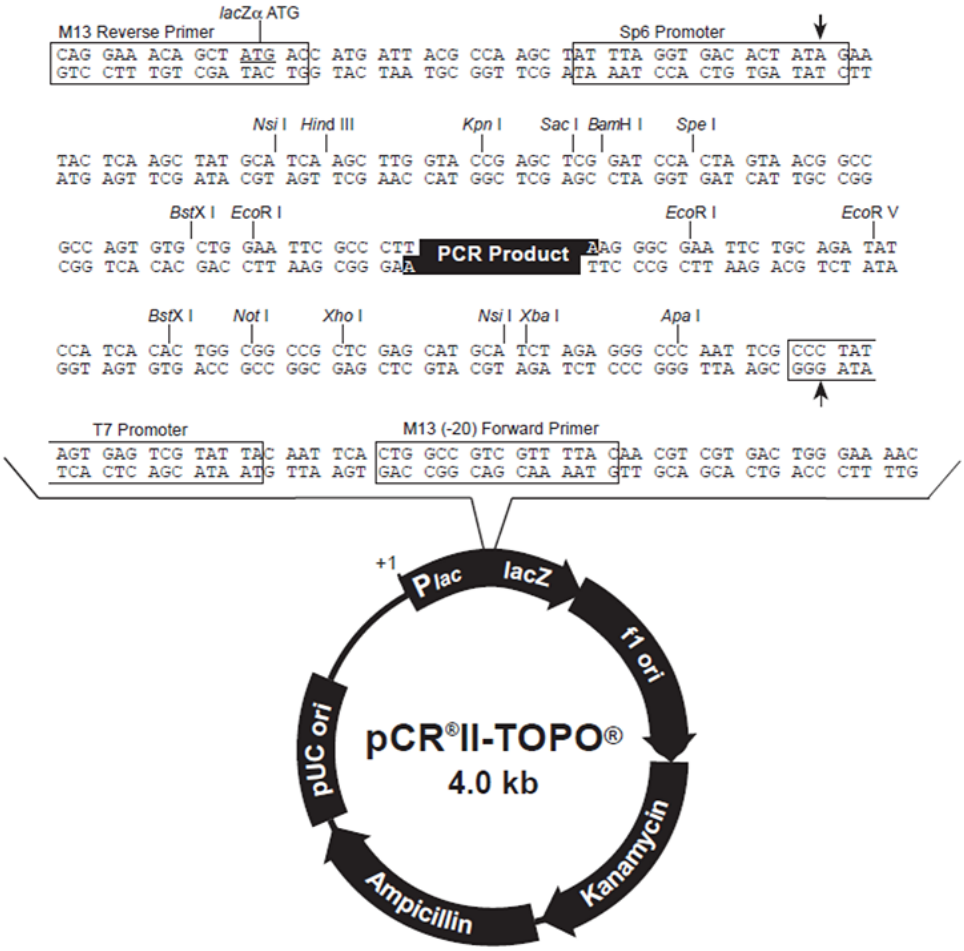

Figure 2-6: The pCRII-TOPO vector
Map of the pCR II-TOPO vector with restriction sites shown. T7 and SP6 polymerase sites allow the generation of *in vitro* sense and anti-sense RNA strands depending on the orientation of the insert . Linearization of the vector was necessary prior to in vitro transcription, as using intact non-linearized plasmid DNA would otherwise result in heterogenous transcripts of varying lengths. For the murine sequences, restriction digestion was with either Hind III or EcoRV; and for human sequences, restriction digestion was with either Sac1 or EcoRV.

2.11.7 Preparation of agar plates

Agar was prepared by adding 1 agar tablet per 50mL of sterile water and autoclaved. As a general rule 30mL of agar solution was deemed appropriate per agar plate. Following the autoclave process, the agar was allowed to cool to 50-60°C at which point the appropriate volume of antibiotic (50-100µg/mL ampicillin or kanamycin, depending on

the vector resistance) was added to the agar under sterile conditions. The agar was carefully poured into sterile agar plates in sterile conditions (dedicated tissue culture hood) and allowed to set for 30 minutes. After the 1 hour transformation reaction, the bacterial suspension from each transformation was taken and 120µL of the suspension was spread on each agar plate under sterile conditions, and incubated overnight at 37°C without shaking.

2.11.8 Analyzing the colonies

The LB broth medium was made by adding 1 tablet of LB broth tablet per 50mL sterile water followed by autoclaving. 50 µg/mL ampicillin or kanamycin was added to LB broth depending the required resistance. 5mL of LB broth was added to sterile tubes. Approximately 10 colonies were selected per agar plate, and using a sterile pipette tip, carefully transferred to the LB broth under sterile conditions, ensuring no cross contamination between the colonies occurred. The LB broth was incubated overnight in a shaking incubator (200 rpm) at 37°C. The following day, DNA was extracted from the colonies using Plasmid Mini Kit (Qiagen, Crawley, UK) according to the manufacturer's instructions. Briefly, the bacteria were pelleted in 1.5mL eppendorfs from the overnight bacterial culture by centrifuging at 10000g for 3 minutes at room temperature. The bacterial pellet was resuspended in 250µL Buffer P1 (ensuring RNase had been added prior to use). 250µL Buffer P2 was added and mixed thoroughly by vigorously inverting the sealed tube 4–6 times. The lysis reaction was not allowed to proceed for more than 5 minutes. 350µL Buffer N3 was added and mix immediately and thoroughly by vigorously inverting 4–6 times, and incubate on ice for 5 minutes. The tubes were centrifuged at 17000g for 10minutes, and the supernatant carefully transferred to a QIAprep spin column and centrifuged at 17000g for 1 minute, discarding the flow-through. 500µL Buffer PB was added to the spin column and centrifuged at 17000g for 1 minute, discarding the flow-through. Next, 750µL Buffer PE was added to the spin column and centrifuged at 17000g for 1 minute, discarding the flow-through. The column was centrifuged for an additional 1 minute to remove residual wash buffer, and transferred to clean 1.5mL eppendorf. 50µl of water was carefully pipette onto the spin column membrane and left to incubate at room temperature for 1minute before final

centrifugation at 17000g for 1minute to elute the purified DNA plasmids. The concentration and quality of the DNA were determined using Nanodrop 1000 (Thermo Scientific, Loughborough, UK), ensuring a 260/280 ratio >1.8. The plasmids were sequenced using establish M13 (-20) sequencing primers (forward: GTAAAACGACGGCCAG, reverse: CAGGAAACAGCTATGAC).

2.11.9 Generation of ARE mutant sequences

Both mouse and human TF 3'UTR contain 4 conserved ARE segments. For the purpose of this study, the murine TF 3'UTR was used for detailed ARE analyses. The final palindromic ARE was found to be functional in the TF 3'UTR, and thus mutations relating to this ARE were constructed. This palindromic ARE (AUAAUUUAUUUAAUA) comprises 2 overlapping AUUUAUUUA and UUAUUUAAU nonamers. 4 mutant sequences were generated (ARE_{Mut1-4}) which tested whether the complete palindromic sequence or the individual nonamers had functional importance: ARE_{Mut1}, **GGG**AUUUAUUUAAUA; ARE_{Mut2}, AUAAUUUAUUUA**GGG**; ARE_{Mut3}, AUAA**GGG**AUUUAAUA; and ARE_{Mut4}, AUAAUUUA**GGG**AAUA. The ARE was close to the 3' end of the sequence, and this property was utilized in generating the mutant sequences, employing larger than usual reverse primer sequences. The PCR primers for cloning the different ARE mutants and corresponding WT sequence are shown in table 2-4. The PCR amplification reactions, cloning, transformation, plasmid purifications and sequencing were as detailed above.

2.12 GENERATION OF BIOTINYLATED TRANSCRIPTS

2.12.1 Reagents

Restriction enzymes: EcoRV, Sac1 and HindIII (Promega, Southampton, UK); 10x Restriction enzyme buffers D, E and J (Promega, Southampton, UK); Acetylated BSA (Promega, Southampton, UK); Molecular water (Sigma); Phenol:Chloroform:Isoamyl Alcohol 25:24:1 (Sigma-Aldrich, Gillingham, UK); Chloroform:Isoamyl alcohol 24:1(Sigma-Aldrich, Gillingham, UK); Ethanol (Sigma-Aldrich, Gillingham, UK); 3M Sodium acetate (Ambion, Paisley, UK); 20 µg/µl Ultra-pure Glycogen (Invitrogen, Paisley, UK); SP6 or T7 polymerase (Roche Diagnostics, Sussex, UK); Biotinylated

oligonucleotides mix (Roche Diagnostics, Sussex, UK); RNase inhibitor (Roche Diagnostics, Sussex, UK); DNase 1 (Roche Diagnostics, Sussex, UK); 10X transcription buffer (Roche Diagnostics, Sussex, UK); 0.5M EDTA (Ambion, Paisley, UK)

2.12.2 Linearization of the plasmid

For generation of both sense anti-sense RNA strands for the respective DNA sequence, the dual promoter sites in the pCRII vector were utilized, where the T7 and SP6 reactions would give the sense and anti-sense RNA strand depending on the orientation of the insert (figure2-6). First, 3µg pCRII vector was linearized by restriction digestion using enzymes dependent on the insert, ensuring the insert sequence did not contain any restriction sites. Using intact non-linearized plasmid DNA would otherwise result in heterogenous transcripts of varying lengths. For the murine sequences, restriction digestion was with either Hind III or EcoRV; and for human sequences, restriction digestion was with either Sac1 or EcoRV, all according to manufacturer's instructions. The restriction digestion reaction for 3µg intact plasmid comprised the following: 42µL water, 6µL 10X buffer, 6µL acetylated BSA, 3µL (3µg) plasmid and 3µL restriction enzyme. The choice of buffer was dependent on the restriction enzyme used and compatibility according to the manufacturer's protocol (EcoRV-Buffer D; HindIII-Buffer E; and Sac1-Buffer J). The separate restriction digest reactions were set up in 0.2mL PCR tubes and briefly spun, and incubated at 37°C for 90 minutes. The integrity of the linearized bands were visualized in a 1% agarose gel containing ethidium bromide and visualized under UV light.

2.12.3 Purification of DNA using phenol-chloroform extraction

The restriction digest reaction was made up to 300µL using molecular water in a 1.5mL eppendorf. Next, 300µL of Phenol:Chloroform:Isoamyl Alcohol (lower layer) was added, vortexed and centrifuged at 17000g for 15 minutes at 4°C. Following this, the top aqueous layer was carefully removed and transferred to a new 1.5mL eppendorf. Next, 250µL Chloroform:Isoamyl Alcohol was added, vortexed and centrifuged at 17000g for 15 minutes at 4°C. Again, the top aqueous layer was carefully removed and transferred to a new 1.5mL eppendorf. 25µL 3M sodium acetate solution and 625µL of 100%

ethanol was added and vortexed and left for overnight precipitation at -20°C. The addition of 1µL glycogen was optional, facilitating the visibility of the DNA pellet. The following day, the tube was centrifuged at 17000g for 30 minutes at 4°C to pellet the DNA. The supernatant was completely removed, and the DNA pellet was resuspended in 500µL 70% ethanol, and centrifuged at 17000g for 15 minutes at 4°C. The supernatant was completely removed, and the pellet air-dried for 15-20 minutes. The DNA pellet was resuspended in 15-20µL water. The concentration and quality of the DNA were determined using Nanodrop 1000 (Thermo Scientific, Loughborough, UK), ensuring a 260/280 ratio >1.8.

2.12.4 *In vitro* transcription of RNA

1µg of the linearized DNA was *in vitro* transcribed using the SP6/T7 transcription kit (Roche Diagnostics, Sussex, UK) in the presence of biotinylated oligonucleotides according to the manufacturer's *in vitro* transcription protocol. SP6 or T7 polymerase was used according to the orientation of the insert and restriction digest enzyme used ensuring the sequence was in direct continuity with the respective SP6/T7 promoter site. The *in vitro* transcription reaction was set up as follows: 1µg linearized DNA (1-10µL dependent on the concentration), 2µL biotinylated oligonucleotides mix, 1µL RNA inhibitor, 2µL 10X transcription buffer, and 2µL of the appropriate polymerase (Sp6 or T7). The reaction volume was made up to 20µL using molecular water. The components were added to 0.2mL PCR tube and briefly spun, followed by an incubation at 37°C for 2 hours. Next, 2µL DNase 1 was added and incubated at 37°C for 15 minutes. This ensured the DNA template for RNA was destroyed. Finally, the reaction was inactivated by the addition of 0.8µL 0.5M EDTA and heated at 65°C for 10 minutes. The biotinylated transcripts were extracted from the reaction mixture using ethanol precipitation. The reaction mixture was transferred to a 1.5mL eppendorfs, and volume made up to 250µL using water. 25µL 3M sodium acetate solution and 625µL of 100% ethanol was added and vortexed and left for overnight precipitation at -20°C. The addition of 1µL glycogen was optional, facilitating the visibility of the RNA pellet. The following day, the tube was centrifuged at 17000g for 30 minutes at 4°C to pellet the RNA. The supernatant was completely removed, and the RNA pellet was resuspended in 500µL 70% ethanol, and

centrifuged at 17000g for 15 minutes at 4°C. The supernatant was completely removed, and the RNA pellet air-dried for 15-20 minutes. The RNA pellet was resuspended in 15-20µL water. The concentration and quality of the RNA were determined using Nanodrop 1000 (Thermo Scientific, Loughborough, UK), ensuring a 260/280 ratio >1.8 and a 260/230 ratio >1.9.

2.13 RNA-BIOTIN PULLDOWN ASSAY

2.13.1 Reagents

Dynabeads® M-280 Streptavidin (Invitrogen, Paisley, UK); 100mM TRIS pH=7.4 (Calbiochem, Nottingham, UK); 5M NaCl (Ambion, Paisley, UK); 1M $MgCl_2$ (Ambion, Paisley, UK); Triton X-100 (Sigma-Aldrich, Gillingham, UK); RNase Out (Invitrogen, Paisley, UK); Superasin (Ambion, Paisley, UK); Protease inhibitor cocktail (Sigma-Aldrich, Gillingham, UK); 1M DTT (Ambion, Paisley, UK); 2M NaF (Sigma-Aldrich, Gillingham, UK); 1M $NaVO_4$ (Sigma-Aldrich, Gillingham, UK); SDS Loading buffer (Invitrogen, Paisley, UK)

2.13.2 Buffers

- Lysis buffer (Triton 0.5%, 10mM TRIS, 2.5mM $MgCl_2$ and 150mM NaCl) – for 50mL buffer: 250µL Triton, 5mL 100mM TRIS, 125µL MgCL2, 1.5mL 5M NaCl and 43.125mL water)

2.13.3 Preparation of lysates

To determine proteins bound to the TF 3'UTR, an RNA-biotin pulldown assay was used as previously described, with minor adaptation[415]. Briefly, the cells were seeded in T75 culture flasks at a density of $1x10^7$ cells per flask and treated as per the experimental protocol. The overlying culture medium containing dead cells and debris was removed. 20mL ice cold PBS was added to the flask. The adherent cells were removed by scraping. The cell suspension was transferred to 50mL tube and centrifuged at 300g for 10 minutes at 4°C. The supernatant was completely aspirated. The cells were washed again in 50mL ice cold PBS and pelleted and transferred to a 1.5mL eppendorf. The cells were pelleted and lysed with 1mL of lysis buffer supplemented with 1µL 1M DTT,

10µL RNase Out, 10µL Superasin, 2µL 2M NaF, 1µL 1M $NaVO_4$ and 10µL protease inhibitor cocktail immediately prior to use). The lysis buffer was added to the pellet and gently mixed by pipetting up and down (no vortexing). The lysate was kept on ice for 15 minutes and centrifuged at 17000g at 4°C for 30 minutes to pellet cell debris. The supernatant was carefully removed. Protein concentration was determined and adjusted with lysis buffer to achieve a concentration of 1mg/mL. 100 µl of lysate were aliquoted and either used immediately or stored at -80°C until use.

2.13.4 Preparation of beads

20µL of magnetic streptavidin beads were used per reaction. The beads were isolated from the storage medium using magnetic separation and washed with 500µL aliquots of ice cold lysis buffer (3 times), using magnetic separation. The beads were resuspended in the original volume (20µL per reaction) of lysis buffer and placed on ice.

2.13.5 RNP isolation

For each sample of RNA, 2 parallel reactions were performed – one for the sense RNA and one for the anti-sense (control) RNA strand. All reaction were performed in 0.2mL PCR tubes. First, 1µL RNase Out, 1µL Superasin and 1µL 0.1M DTT were added to each of the tubes. 100µl of lysate was added to each tube, followed by 2µg of either the sense or anti-sense biotinylated transcript. The contents were briefly spun and incubated at 4°C for 1 hour with rotation. Next, 20µl of the prepared magnetic streptavidin-coated beads were then added to each tube and incubated at 4°C for 1 hour with rotation. Following this, the beads were separated using magnetic separation and washed 5 times in ice cold lysis buffer. The proteins bound to the beads/transcripts were eluted by boiling the beads in 30µL 1x SDS loading buffer at 100°C for 4 minutes. The candidate RNA binding proteins were detected using Western blotting and immunodetection methods as described above. The anti-sense strands in this study did not contain any AREs and therefore served as an internal controls for their respective reactions. The experiment was further controlled by detecting for tubulin which serves as a marker for non-specific binding.

2.14 CO-IMMUNOPRECIPITATION ASSAY

2.14.1 Reagents

Dynabeads® Protein G (Invitrogen, Paisley, UK); 100mM TRIS pH=7.4 (Calbiochem, Nottingham, UK); 5M NaCl (Ambion, Paisley, UK); 1M $MgCl_2$ (Ambion, Paisley, UK); Triton X-100 (Sigma-Aldrich, Gillingham, UK); RNase Out (Invitrogen, Paisley, UK); Superasin (Ambion); Protease inhibitor cocktail (Sigma-Aldrich, Gillingham, UK); 1M DTT (Ambion, Paisley, UK)

2.14.2 Buffers

- IP lysis buffer (0.5% Triton, 20mM TRIS, 150mM NaCl) - for 50mL buffer: 250µL Triton, 10mL 100mM TRIS, 1.5mL 5M NaCl and 38.5mL water
- IP wash buffer (0.5% Triton, 20mM TRIS, 150mM NaCl) - for 50mL buffer: 50µL Triton, 10mL 100mM TRIS, 1.5mL 5M NaCl and 38.7mL water

2.14.3 Preparation of lysates

The cells were seeded in T75 culture flasks at a density of $1x10^7$ cells per flask and treated as per the experimental protocol. The overlying culture medium containing dead cells and debris was removed. 20mL ice cold PBS was added to the flask. The adherent cells were removed by scraping. The cell suspension was transferred to 50mL tube and centrifuged at 300g for 10 minutes at 4°C. The supernatant was completely aspirated. The cells were washed again in 50mL ice cold PBS and pelleted and transferred to a 1.5mL eppendorf. The cells were pelleted and lysed with 1mL of lysis buffer, supplemented with 1µL 1M DTT, 10µL RNase Out, 10µL Superasin and 10µL protease inhibitor cocktail immediately prior to use. The lysis buffer was added to the pellet and gently mixed by pipetting up and down (no vortexing). The lysate was kept on ice for 15 minutes and centrifuged at 17000g at 4°C for 30 minutes to pellet cell debris. For experiments were RNase treatment was necessary, RNase A (Invitrogen, Paisley, UK) was added to the lysis buffer (prior to lysis) at a final concentration of 5µg/mL. The supernatant was carefully removed. Protein concentrations were determined and adjusted with lysis buffer to achieve a concentration of 2mg/mL. 500 µl of lysate were aliquoted and either used immediately or stored at -80°C until use.

2.14.4 Preparation of beads

50µL of magnetic streptavidin beads were used per reaction. The beads were isolated from the storage medium using magnetic separation and washed with 500µL aliquots of ice cold IP lysis buffer (3 times), using magnetic separation. The beads were resuspended in the original volume (50µL per reaction) of IP lysis buffer and placed on ice.

2.14.5 Immunoprecipitation

For each reaction, 500µL of lysate was used. The lysate was added to either 5µg of protein specific antibody or 5µg IgG control and incubated at 4°C for 1 hour with rotation. 50µL of prepared magnetic protein G beads were added to the antibody-lysate mixture and incubated for 15 minutes at room temperature with rotation. The beads were isolated using magnetic separation and washed with ice cold IP wash buffer (3 times). The proteins bound to the beads were eluted by boiling the beads in 20-30µL 1x SDS loading buffer at 100°C for 4 minutes. The (co-)immunoprecipitated proteins were detected using Western blotting and immunodetection methods as described above.

2.15 INTRAVITAL MICROSCOPY & FERRIC CHLORIDE INJURY MODEL

All *in vivo* procedures were covered by approval from the UK Home Office. WT and *Parp14*$^{-/-}$ mice were injected with LPS 10 µg i.p. or a corresponding volume of the saline vehicle control. Anaesthesia was induced 4 hours after LPS injection by administration of ketamine (150mg/kg i.p. Fort Dodge Animal Health, Southampton, UK) and xylazine (7.5mg/kg i.p. Bayer Healthcare, Newbury, UK). The mouse cremaster muscle was prepared for intravital microscopy as described previously[416]. Briefly, the cremaster was dissected free of skin and fascia, opened longitudinally, and then pinned out flat against the viewing platform of a plexiglass stage. The preparation was mounted on an Olympus BW61WI microscope with a water-immersion objective lens (magnification of x40; LUMPlan FI/R, Olympus, Japan), which was used to observe the arterioles in the cremaster muscle. Superfusion of the cremaster muscle with bicarbonate-buffered solution (BBS; g/L: 7.71 NaCl, 0.25 KCl, 0.14 $MgSO_4$, 1.51 $NaHCO_3$, and 0.22 $CaCl_2$,

pH 7.4, at 37°C, gassed with 5% CO_2/95% N_2) at a rate of 2 ml/min began immediately. After the preparation of the cremaster muscle, the mice were allowed to recover from surgical preparation for 30 minutes. Then, induction of thrombus formation was performed in randomly chosen arterioles. Due to the rapid spreading of ferric chloride solution only 1 arteriole per preparation was observed within each animal. Microscopic images were acquired by a black-and-white camera (model CoolSNAP HQ (Photometrics, Tucson, AZ, US), coupled to a Windows XP-based computer for recording by Slidebook 4.2 (Intelligent Imaging Innovations, Inc., Denver, CO, US) for off-line evaluation. Resting blood flow was monitored in individual arterioles (diameter range 30-50µm), followed by superfusion with 30µl of a 25M ferric chloride solution (Sigma-Aldrich, Gillingham, UK)[417]. Recording of vessels was discontinued after blood flow in the vessel ceased.

2.16 LIST OF PRIMERS FOR qRT-PCR

Table 2-1: Primers for qRT-PCR

Gene	Primers for qRT-PCR
Human TF [418]	Forward: GAGTGTATGGCCCAGGAGAA Reverse: GCCAGGATGATGACAAGGAT
Human TNFα	Forward: GCCCATGTTGTAGCAAACCCTC Reverse: ATCTCTCAGCTCCACGCCATT
Human HPRT	Forward: TTGGTCAGGCAGTATAATCC Reverse: GGGCATATCCTACAACAAAC
Human GAPDH	Forward: CAAGGTCATCCATGACAACTTTG Reverse: GGGCCATCCACAGTCTTCTG
Mouse TF (primer set 1)	Forward: AGCCTGCCAATCCTAGCTCAGAG Reverse: CGGTTTCCGTTCGTCCTAACGTGAC
Mouse TF (primer set 2) [171]	Forward: TCAAGCACGGGAAAGAAAAC Reverse: CTGCTTCCTGGGCTATTTTG
Mouse TNFα	Forward: AGCCCACGTCGTAGCAAACCA Reverse: CGGGGCAGCCTTGTCCCTTG
Mouse TTP [419]	Forward: AATCCCTCGGAGGACTTTGGAACA Reverse: AGTTGCAGTAGGCGAAGTAGGTGA
Mouse PARP-14	Forward: TCCGCCTGGTAGAAGAAG Reverse: GCCCACATCAACAGAGAC
Mouse HPRT	Forward: GTTAAGCAGTACAGCCCCAAAATC Reverse: TCAAGGGCATATCCAACAACAAAC
Mouse GAPDH	Forward: CAAGGTCATCCATGACAACTTTG Reverse: GGGCCATCCACAGTCTTCTG

2.17 LIST OF ANTIBODIES

Table 2-2: Antibodies used in this study

ANTIBODY	SUPPLIER	DILUTION
PRIMARY ANTIBODIES		
Rabbit anti-mouse TF [420]	American Diagnostica, (Alere, Manchester, UK)	1:1000 (WB) 1:10 (FC)
Rabbit anti-PARP14	Eurogenetec, Seraing, Belgium	1:700
Rabbit anti-TTP (SAK21A) [421]	Kennedy Institute of Rheumatology, Oxford, UK	1: 2000 (WB)
Rabbit anti-TTP (H-120)	Santa Cruz (Insight Biotechnology, Wembley, UK)	1:200 (WB)
Goat anti-TTP (N-18)	Santa Cruz (Insight Biotechnology, Wembley, UK)	1:1000 (WB)
Rabbit anti- total p38 MAPK	Cell Signalling (New England Biolabs, Hitchin, UK)	1:1000 (WB)
Rabbit anti-phospho-p38 MAPK	Cell Signalling (New England Biolabs, Hitchin, UK)	1:1000 (WB)
Rabbit anti- total JNK MAPK	Cell Signalling (New England Biolabs, Hitchin, UK)	1:1000 (WB)
Rabbit anti-phospho-JNK MAPK	Cell Signalling (New England Biolabs, Hitchin, UK)	1:1000 (WB)
Mouse anti-human TF (IgG_1)	Abcam, Cambridge, UK	1: 500 (WB)
Mouse anti-human TF (IgG_1) (FITC-conjugated)	AdD Serotec, Kidlington, UK	1:50 (FC)
Mouse IgG_1 isotype control (FITC-conjugated)	AdD Serotec, Kidlington, UK	1:50 (FC)
SECONDARY ANTIBODIES		
Rabbit anti-goat-HRP	Dako UK Ltd, Cambridge, UK	1:2000 (WB)
Rabbit anti-mouse-HRP	Dako UK Ltd, Cambridge, UK	1:2000 (WB)
Goat anti-rabbit-HRP	Dako UK Ltd, Cambridge, UK	1:2000 (WB)
Goat anti-rabbit F(ab')2 fragment-FITC	Invitrogen, Paisley, UK, Paisley, UK	1:200 (FC)

WB=Western blotting

FC= Flow cytometry

2.18 LIST OF PRIMERS FOR CLONING

Table 2-3: Primers for cloning the murine and human TF 3'UTR

Sequence	PCR Primers (forward and reverse)
ARE_{WT}	Forward: AGGAAAGGCTGAAGCCG Reverse: CCCAATCACCTTTATTTATATAAAAGTATATTAAATAAATTATCTCAAAATATAC
ARE_{Mut1}	Forward: AGGAAAGGCTGAAGCCG Reverse: CCCAATCACCTTTATTTATATAAAAGTATATTAAATAAATCCCCTCAAAATATAC
ARE_{Mut2}	Forward: AGGAAAGGCTGAAGCCG Reverse: CCCAATCACCTTTATTTATATAAAAGTACCCTAAATAAATTATCTCAAAATATAC
ARE_{Mut3}	Forward: AGGAAAGGCTGAAGCCG Reverse: CCCAATCACCTTTATTTATATAAAAGTATATTAAATAACCCATCTCAAAATATAC
ARE_{Mut4}	Forward: AGGAAAGGCTGAAGCCG Reverse: CCCAATCACCTTTATTTATATAAAAGTATATTCCCTAAATTATCTCAAAATATAC

Table 2-4: Primers for generating mutants for final ARE in murine TF 3'UTR

Sequence	PCR Primers (forward and reverse)
ARE_{WT}	Forward: AGGAAAGGCTGAAGCCG Reverse: CCCAATCACCTTTATTTATATAAAAGTATATTAAATAAATTATCTCAAAATATAC
ARE_{Mut1}	Forward: AGGAAAGGCTGAAGCCG Reverse: CCCAATCACCTTTATTTATATAAAAGTATATTAAATAAATCCCCTCAAAATATAC
ARE_{Mut2}	Forward: AGGAAAGGCTGAAGCCG Reverse: CCCAATCACCTTTATTTATATAAAAGTACCCTAAATAAATTATCTCAAAATATAC
ARE_{Mut3}	Forward: AGGAAAGGCTGAAGCCG Reverse: CCCAATCACCTTTATTTATATAAAAGTATATTAAATAACCCATCTCAAAATATAC
ARE_{Mut4}	Forward: AGGAAAGGCTGAAGCCG Reverse: CCCAATCACCTTTATTTATATAAAAGTATATTCCCTAAATTATCTCAAAATATAC

Chapter 3

Results:

TTP regulates TF mRNA stability

3.1 INTRODUCTION

Regulation of TF gene transcription provides one of the primary mechanisms for governing its level of expression and hence cellular procoagulant activity. In monocytes and macrophages, TF gene transcription is stimulated by inflammatory cytokines (e.g. IL-1β, TNFα) or by LPS [249-251]. LPS activates macrophages via toll-like receptor 4, and is commonly used as a canonical stimulus for studying TF expression. Following LPS stimulation, increased transcription of the TF gene occurs via the activation of AP-1, NFκB and Egr-1 transcription factor pathways. However, following LPS stimulation, increased levels of TF mRNA are transient, with peak levels occurring at 2-4 hours followed by a rapid decline. This time-course implies robust post-transcriptional mechanisms that destabilize and degrade TF mRNA, the control of which is likely to be as important as the transcriptional regulation in ultimately determining the net gene expression.

TF mRNA transcripts are intrinsically unstable, but show a transient increase in stability over two hours following LPS treatment in THP-1 monocytic cells[190] and in endothelial cells[191], providing a means for fresh mRNA transcripts to be converted into TF protein [259, 260]. The TF 3'UTR contains several AREs that may serve as potential binding sites for ARE-binding proteins, and indeed TF mRNA has been assigned to the group III cluster of the ARED database[261]. These AREs are functional and conserved in both human and mouse. Although, the roles for microRNAs in regulating TF mRNA stability have recently been reported[268], the precise molecular mechanisms involved in ARE-mediated TF mRNA decay have not been fully elucidated. The p38 pathway is one of the three MAPK pathways that affect mammalian gene expression[347-352]. LPS stimulation results in phosphorylation and activation of p38, which promotes inflammatory gene response through both transcriptional and post-transcriptional mechanisms. The p38 pathway stabilizes mRNA by activating MAPKAPK-2 that subsequently phosphorylates and inactivates TTP (the primary target for MAPKAPK-2) [363]. TTP is the most widely studied mRNA binding proteins that classically binds to a consensus nonamer ARE sequence, UUAUUUA(A/U)(A/U), in the 3'UTR of target transcripts promoting their degradation[264-266]. Following analyses of the putative AREs

we hypothesized that TTP, a well established ARE-binding protein, would bind and regulate the TF transcript. In this chapter, the specific roles for p38 and TTP in the post-transcriptional regulation of TF were investigated.

3.2 METHODS

Detailed generic methods have been described in Chapter 2. In this section, the methods and experimental protocols specific to this chapter are briefly described.

3.2.1 Primary human monocyte isolation and culture

Monocytes were isolated from citrated venous blood derived from healthy donors (with local ethical approval). PBMCs were isolated from the cell fraction by Ficoll–Paque density-gradient centrifugation and CD14+ monocytes were separated using magnetic separation with CD14 MicroBeads and a MACS Separator column. Monocytes were plated into tissue culture plates according to the experimental protocol in IMDM with 10% FCS ($25x10^4$ cells/well in 24 well plates, $2X10^4$/well in 96-well plates or $1x10^7$cells/T75 flask) and incubated overnight in a 37°C incubator, for experiments the following day.

3.2.2 Bone marrow-derived macrophage (BMDM) isolation and culture

WT and *Ttp*$^{-/-}$ mice were sacrificed using cervical dislocation. Bone marrow cells were flushed from the femur and tibia and cultured in bone marrow culture medium for 6 days. On day 6, the cells were harvested, resuspended in the bone marrow culture medium, and plated in culture dishes/flasks as per the experimental protocol ($25X10^4$ cells/well in 24 well plates or $1x10^7$cells/T75 flask) and incubated overnight in a 37°C incubator, for experiments the following day.

3.2.3 RNA extraction and quantitative reverse-transcriptase PCR (qRT-PCR)

RNA was isolated from cells using RNEasy Mini kits, incorporating an on-column DNase digestion using RNase-free DNase. 1µg of total RNA was used for cDNA synthesis using SuperScript III reverse transcriptase protocol. Comparative qRT-PCR was performed using SYBR green and gene specific primers (table 2-1). Data was

normalized to 2 housekeeping controls, GAPDH and HPRT. For mouse TF mRNA expression, data were validated using 2 primer sets. Relative gene expression was calculated using the ΔΔCt method[409].

3.2.4 mRNA decay experiments

All mRNA decay experiments were performed with an identical protocol. Cells were stimulated with LPS 1μg/mL. Actinomycin D (5μg/mL) was added at 2 hours following LPS stimulation to induce transcriptional arrest. The 2 hour time point was chosen for 2 reasons: (a) TF mRNA levels peak at 2-4 hours following LPS stimulation, and (b) TF mRNA half-life has previously been shown to be very stable up to 2 hours following LPS stimulation in THP-1 cells (t½~120minutes), following which the t½ rapidly declines. A relatively stable baseline decay profile would thus allow one to better observe the destabilizing effects of particular treatments, e.g. p38 inhibitors. For p38 inhibition, the following compounds were used: SB203580, SB202190, BIRB796 and LY2228800. Where SB203580/SB202190 compounds were used, an inactive analogue compound SB202474 was used as a control. In experiments specifically examining the effect of these signaling inhibitors on mRNA decay, the inhibitors were all added at the time of actinomycin D, except for BIRB796 and LY2228800 which were added 15 minutes prior to actinomycin D due to their slower onset of action. Following actinomycin D, RNA was isolated at time 0, 15, 30, 60 and 90 minutes. mRNA was quantified using qRT-PCR, and levels were normalized to levels at time 0. Both HPRT and GAPDH levels remained stable following transcriptional arrest, validating the use of these housekeeping genes for mRNA decay analyses (data not shown). The mRNA decay profiles were modeled mathematically using non-linear regression analysis and mRNA half-lives calculated.

3.2.5 Western blotting analysis

Following the experimental protocol, the cells were lysed with 100μL of Cell Lytic M lysis buffer with 1μL of protease inhibitor cocktail. The lysates were centrifuged at 17,000g for 20 minutes at 4ºC to pellet cell debris. The supernatants were carefully removed and stored at -80ºC until analysis. A Novex XCell II (Invitrogen) mini gel system was used. 20μg of protein was used per lane, and proteins were separated by gel electrophoresis

using pre-cast polyacrylamide gels, and electrotransferred to polyvinylidene difluoride membranes. The membranes were blocked using blocking buffer and primary and secondary antibodies were applied in blocking buffer at the appropriate dilutions (table 2-2). Protein bands were detected using chemiluminescence. Protein quantification was performed using densitometry using ImageJ software (National Institute of Health Bethesda, Maryland, USA) normalized to tubulin.

3.2.6 TF activity assays

A turbimetric clot assay was used to determine TF activity. Cells were cultured in 96 well plates (cell density=$2x10^4$ cells per well) according to the experimental protocol. The supernatant was removed and cells were washed with PBS twice. 100 µL of the citrated PPP was added to the wells and recalcified with 2 µL of 1.0M $CaCl_2$ to initiate clotting. Clot turbidity was measured by absorbance (A_{405}) every minute for 60 minutes in a spectrophotometer (Synergy HT, Biotek) with internal thermostatic control at 37°C. The clot lag time (T_{lag}) was determined and correlated to a TF standard curve generated using relipidated TF (Innovin®, Dade) to determine TF activity.

3.2.7 RNP immunoprecipitation

Cells were seeded in T75 culture flasks at a density of $1x10^7$ cells per flask and stimulated with LPS 1µg/mL for 2 hours. Cells were washed with ice cold PBS twice, lysed with polysome lysis buffer supplemented with RNase and protease inhibitors and centrifuged at 17000g at 4°C for 30minutes to pellet cell debris.100 µl (3mg protein) of lysate was incubated for 2 hours with 100 µl of preswollen Protein-G agarose beads (Sigma-Aldrich) precoated with either 20µg of rabbit anti-TTP (H-120) or normal rabbit IgG. The beads were washed with NT2 buffer and then incubated in 100ml NT2 buffer containing 0.1% SDS and 0.5 mg/ml proteinase K (15 minutes, 55°C). The beads were pelleted, and the supernatant carefully removed. RNA was extracted using Trizol reagent. cDNA synthesis and qRT-PCR was performed using gene-specific primers as above. To determine specificity for mRNA, the samples were run in parallel with non-RT samples to control for genomic DNA contamination. The PCR reaction products were

separated in a 2% agarose gel containing ethidium bromide and visualized under UV light.

3.2.8 *In vitro* transcription

The murine and human TF 3'UTRs, truncated and mutant 3'UTR segments were amplified from total murine or human macrophage cDNA with PCR primers listed in tables 2-3 and 2-4 using the Advantage 2 PCR cloning kit and cloned using the TOPO TA Cloning Kit into the pCRII-TOPO vector. The plasmids were purified using Plasmid Miniprep Kit (Qiagen), linearized by restriction digestion using (Hind III or EcoRV for the murine sequences, and Sac1 or EcoRV for human sequences). Biotinylated transcripts were formed using the SP6/T7 transcription kit in the presence of biotinylated oligonucleotides. For competition experiments where cold (non-biotinylated transcripts were necessary, the in vitro transcription reaction was performed replacing the biotinylated nucleotide mix with a standard non-biotinylated nucleotide mix. The RNA was purified from the reaction mixture using ethanol precipitation.

3.2.9 RNA-biotin pulldown assays

Cell lysates were produced from LPS-stimulated murine and human macrophages. The cells were seeded in T75 culture flasks at a density of $1x10^7$ cells per flask and stimulated with LPS 1μg/mL for 2 hours. In experiments where p38 inhibition was necessary, SB203580 1μM was added 15 minutes prior to lysis. The adherent cells were harvested by scraping, washed twice with ice cold PBS and lysed with 1mL lysis buffer supplemented with RNase and protease inhibitors. 100μl (100μg protein) of lysate was incubated with either the sense or anti-sense biotinylated transcript (2μg) for 1 hour. In the competition experiments, parallel reactions were set up where 1, 5 and 10 fold excess cold transcripts were added in addition to the 2μg of biotinylated WT 3'UTR transcripts. 20μl of magnetic streptavidin-coated beads (Dynabeads®, Invitrogen) were added and incubated at 4°C for 1 hour. Following 1 hour incubation, the Dynabeads® were added according to the standard protocol, and the associated proteins resolved by Western blotting as above. The beads were separated using magnetic separation, washed with lysis buffer and boiled in 1x SDS loading buffer at

100°C for 4 minutes. The proteins were detected using Western blotting and immunodetection.

3.2.10 Statistical analyses

All continuous variables were expressed as mean ± SEM. Statistical analyses were performed using GraphPad Prism v5.0 (GraphPad Software, San Diego, CA, USA) and Microsoft Excel 2007 (Microsoft, Washington, USA). All continuous variables were confirmed to be normally distributed by the Shapiro-Wilk statistic. Thus for comparison of groups, the unpaired Student's t-test (2-tailed) was used. Statistical significance was set at $p<0.05$.

3.3 RESULTS

3.3.1 p38 inhibition reduces TF expression in primary human monocytes

Monocytes were stimulated with LPS (1µg/mL) and concurrently treated with increasing concentrations (0.1, 1 and 10µM) of SB202190, SB203580 and SB202474. TF mRNA levels were determined at 2 hours following LPS stimulation, and TF activity and protein levels were determined at 8 hours following LPS stimulation (figures 3-1 and 3-2). Using the control analogue compound SB202474, there was no significant difference in TF TF activity (figures 3-1a,b), mRNA levels (figure 3-2a) and TF protein levels (figure 3-2b). However, p38 inhibition with SB202190 and SB203580 was associated with a significant reduction in TF mRNA, TF activity and TF protein levels. Following LPS stimulation there was a 13% ($p=0.03$), 45% ($p=0.002$), and 60% ($p<0.001$) reduction in TF mRNA levels at 2 hours; and a 57% ($p=0.005$), 87% ($p<0.001$) and 90% ($p<0.001$) in TF activity levels at 8 hours with SB203580 at 0.1,1 and 10µM respectively. Similarly, following LPS stimulation there was a 11% ($p=0.24$), 55% ($p<0.001$), and 68% ($p<0.001$) reduction in TF mRNA levels at 2 hours; and a 77% ($p=0.001$), 92% ($p<0.001$) and 94% ($p<0.001$) reduction in TF activity levels at 8 hours with SB202190 at 0.1, 1 and 10µM respectively. In general terms, TF activity serves a surrogate marker for TF protein levels. However, to confirm the findings for TF activity, western blotting analyses were also performed to assess TF protein levels at 8 hours following LPS

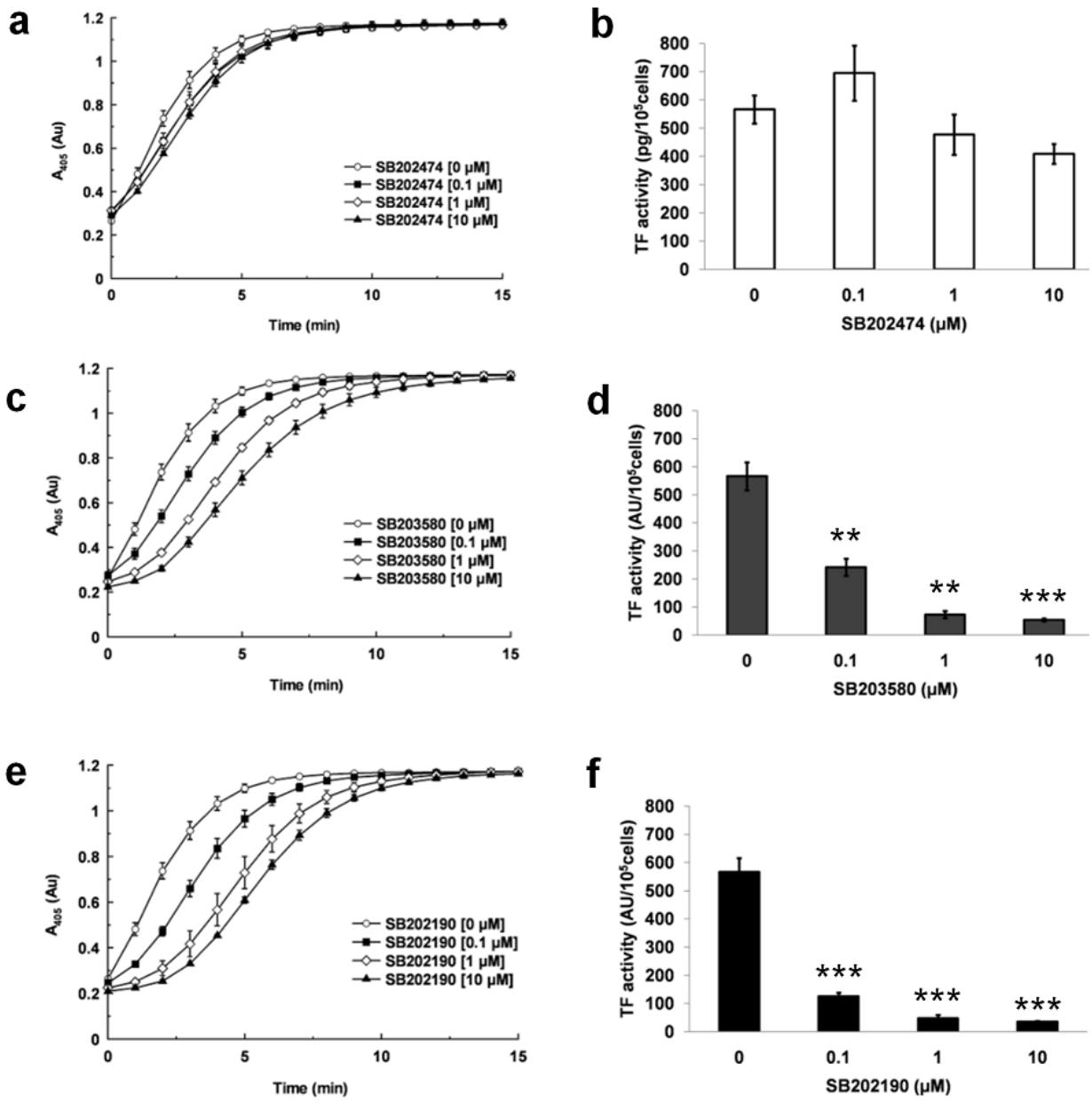

Figure 3-1: The effect of p38 inhibition on procoagulant activity in LPS-stimulated human monocytes.
Monocytes were stimulated with LPS 1µg/mL. Increasing concentrations of 3 different SB compounds: SB202474 0. 1 and 10µM **(a,b)**; SB203580 0.1, 1 and 10µM **(c,d)**; and SB202190 0.1, 1 and 10µM **(e,f)** were added 30min aft LPS. TF activity was determined 2h after LPS stimulation using a turbimetric clotting assay. Turbimetric curves show are on the left **(a,c,e,)** and TF activity determined from corresponding T_{lag} on the right **(b,d,f)**. Data expressed as mea ± SEM and analysed using a 2-tailed Student's t-test. * $p<0.05$, ** $p<0.01$, *** $p< 0.001$ compared to control arm of th experiment.

stimulation with each compounds (SB202474, SB203580 and SB202190) 0.1, 1 and 10µM respectively. In keeping with the TF activity data, figure 3-2 confirms that SB202474 has no effect on LPS-induced TF protein expression whilst SB203580 and SB202190 produce a concentration-dependent reduction in TF protein levels. Based on

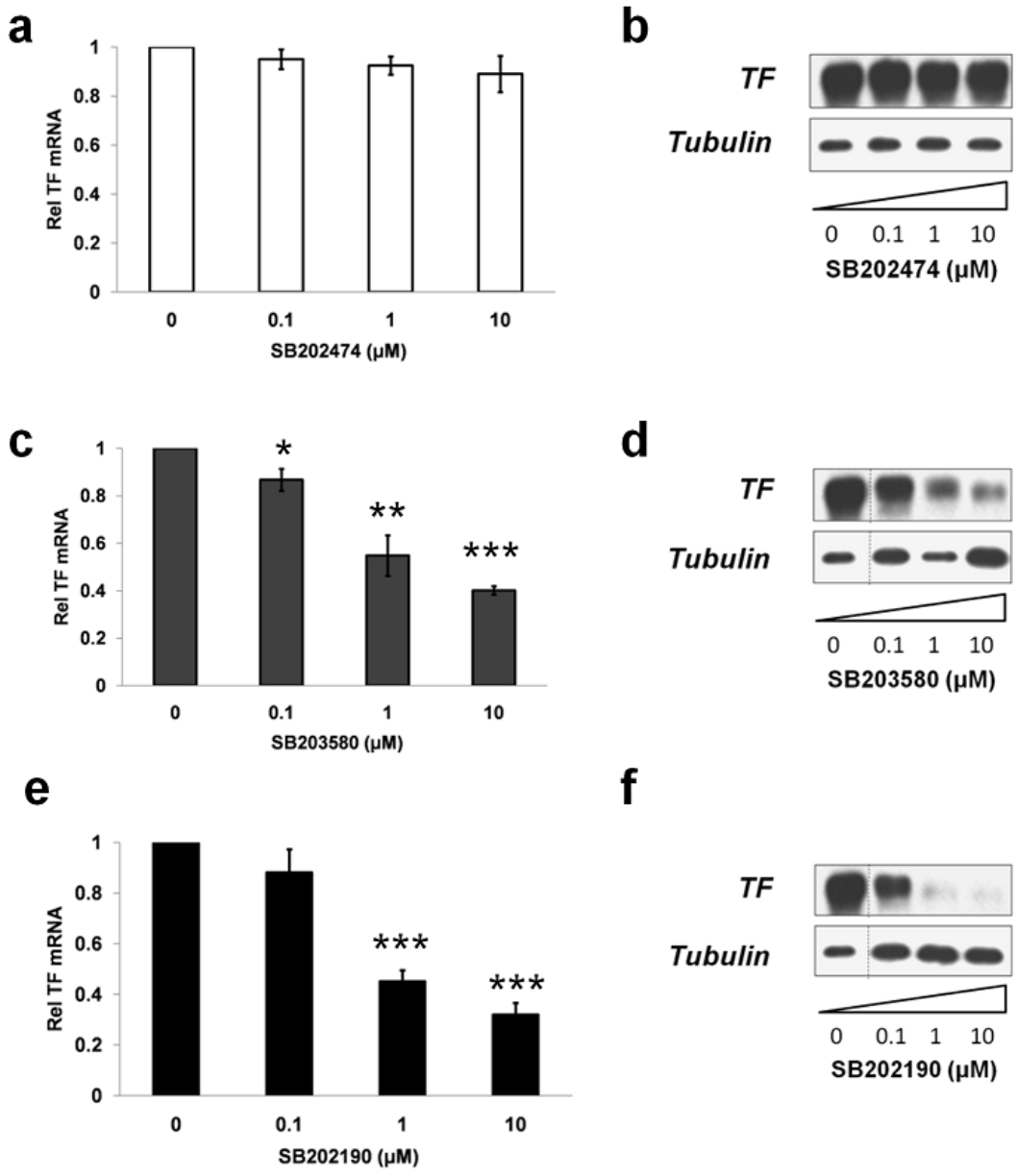

Figure 3-2: The effect of p38 inhibition on TF expression in LPS-stimulated human monocytes. Monocytes were stimulated with LPS 1μg/mL. Increasing concentrations of 3 different SB compounds: SB202474 0.1, 1 and 10μM **(a,b)**; SB203580 0.1, 1 and 10μM **(c,d)**; and SB202190 0.1, 1 and 10μM **(e,f)** were added 30min after LPS. TF mRNA levels were determined 2h after LPS stimulation using RT-PCR **(a,c,e,)**. TF protein levels were determined at 8h following LPS stimulation using western blotting **(b,d,f)**. All the TF and tubulin blots were run on the same gel. The LPS-treated sample without any SB compound was run on the same gel but has been spliced into each blot for clarity. The dotted lines indicate where the blots have been spliced. Representative blot of 3 independent experiments. Data expressed as mean ± SEM and analysed using a 2-tailed Student's t-test. * $p<0.05$, ** $p<0.01$, *** $p< 0.001$ compared to control arm of the experiment.

previously published literature, SB203580 and SB202190 compounds have been used in concentrations up to 25μM, and non-specific effects on other kinases, particularly JNK have been reported with higher concentrations. Given this, and based on published data, a concentration of 1μM was chosen for use in subsequent experiments. To test whether these compounds were specific for p38 inhibition at this concentration, phospho-p38:total p38 and phospho-JNK:total JNK ratios were determined by Western blotting following LPS stimulation (1μg/mL for 90 minutes) followed by a 30 minute incubation with 1μM SB compound. Figure 3-3 shows the phospho-p38:total p38 and phospho-JNK:total JNK ratios as determined by densitometric analyses. Both SB2023580 and SB202190 at 1μM were found to be specific for p38 inhibition with little effect on JNK, whilst SB202474 had no significant effect.

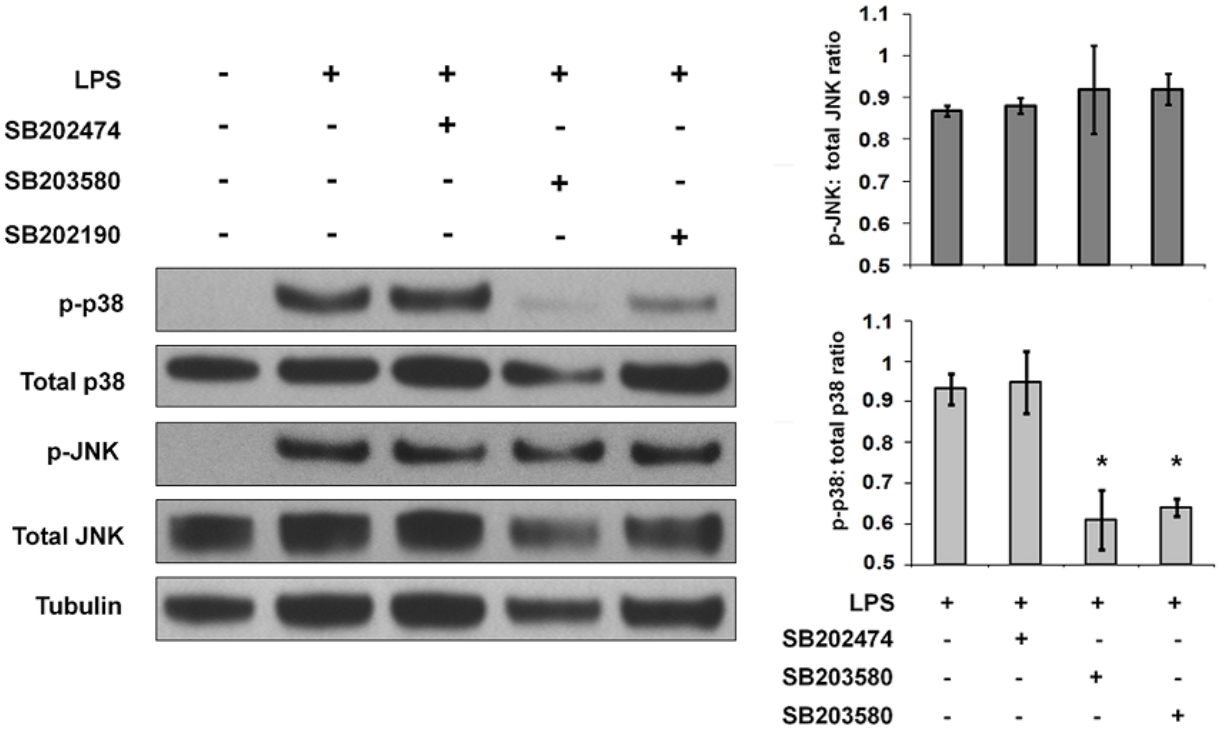

Figure 3-3: The effect of SB compounds on phospho-p38 and phospho-JNK levels.
Monocytes were stimulated with LPS 1μg/mL. Different SB compounds: SB202474 1μM, SB203580 1μM and SB202190 1μM were added 30min after LPS. Total p38, phospho-p38, total JNK and phospho-JNK were determined at 2h after LPS stimulation using western blotting. Representative blot of 3 independent experiments is shown on the left with densitometric analyses on the right. Inhibition of p38 using SB203580 1μM and SB202190 1μM resulted in reduced phopsho-p38: total p38 without a significant reduction in phospho-JNK: total JNK, indicating relative selectivity for p38 inhibition at this concentration. Representative blot of 3 independent experiments. Data expressed as mean ± SEM and analysed using a 2-tailed Student's t-test. * $p<0.05$, ** $p<0.01$, *** $p< 0.001$ compared to control arm of the experiment.

3.3.2 p38 inhibition reduces TF mRNA stability in primary human monocytes

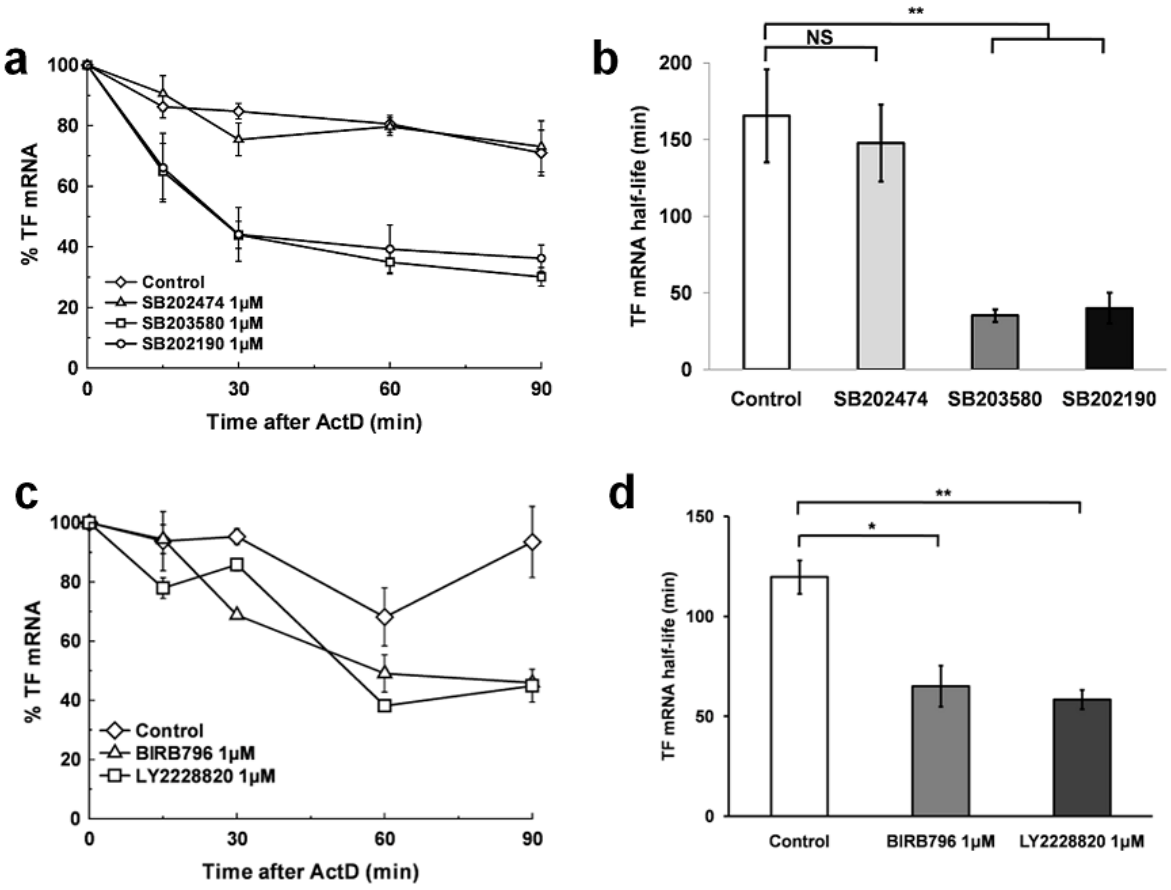

Figure 3-4: The effect of p38 inhibition on TF mRNA stability in primary human monocytes.
Monocytes were stimulated with LPS 1μg/mL. for 2h. Actinomycin D (5μg/mL) was added at 2h to induce transcriptional arrest. Inhibition of p38 was achieved using SB compounds 1μM which were added with actinomycin D (n=4) **(a,b)** and BIRB796 1μM and LY2228820 1μM which were added 15 minutes prior to actinomycin D due to their slower onset of action (n=3) **(c,d)**. TF mRNA levels were determined at each time point and normalized to levels at time point 0 to obtain mRNA decay profiles **(a,c)**. The decay profiles were modelled mathematically using non-linear regression analysis to determine mRNA half-life. Inhibition of p38 consistently demonstrated a significant reduction in TF mRNA half-life. Data expressed as mean ± SEM and analysed using a 2-tailed Student's t-test. * $p<0.05$, ** $p<0.01$, *** $p< 0.001$.

To specifically address the role of p38 activation in the post-transcriptional regulation of TF, TF mRNA decay profiles were established following LPS stimulation both in the absence and presence of p38 inhibitors. Monocytes were stimulated with LPS (1μg/mL), and actinomycin D (5μg/mL) was added at 2 hours to induce transcriptional arrest. Given the rapid onset of action of the SB compounds, SB202474, SB202190 and SB203580 1μM were added concurrently with actinomycin D, to minimize any effect on mRNA transcription. Given that these compounds were water soluble, water was added as a vehicle control to the control arm of the experiment. TF mRNA levels were

quantified at time 0, 15, 30, 60 and 90 minutes after actinomycin D and TF mRNA decay profiles determined. The TF mRNA half-life in the absence of any SB compound was 166±30minutes. With the control analogue SB202474, there was no significant difference in TF mRNA half-life, 148±25 minutes (p=0.72). With the p38 inhibitors, SB203580 and SB202190, there was a significant reduction in TF mRNA half-life to 35±4minutes (p=0.007) and 40±10 minutes (p=0.01) respectively (figures 3-4 a,b). To exclude a compound class effect, other novel p38 inhibitors, BIRB796 and LY2228800 were tested. These compounds are insoluble in water, and were therefore dissolved in DMSO, necessitating the use of DMSO as a vehicle control in the control arm of the experiments. These compounds were dissolved such that the final DMSO concentration was 0.5% of the final volume in the wells. The TF mRNA half-life was 120±8minutes in the control arm of the experiment. With the specific p38 inhibitors, BIRB796 1μM and LY2228800 1μM, there was a significant reduction in TF mRNA half-life to 65±10minutes (p=0.007) and 58±5 minutes (p=0.001) respectively (figures 3-4 c,d). Collectively, these data indicate that the p38 MAPK pathway post-transcriptionally regulates TF expression, and that specific inhibition of p38 reduces TF mRNA stability.

3.3.3 TF mRNA stability falls with increasing duration of LPS stimulation

TF mRNA decay kinetics have previously been reported in LPS-stimulated THP-1 cells, where TF mRNA half-life was found to be very stable up to 2 hours following LPS-stimulation (t½~120 minutes) following which the half-life falls rapidly to 25±5 minutes by 4-6 hours[190]. These data would suggest that LPS stabilizes TF mRNA when TF mRNA levels are increasing and that this effect contributes to the overall rate and magnitude of the TF mRNA response. Given that important difference exist between THP-1 cells and primary human monocytes[422], similar detailed analyses of TF mRNA kinetics have not been reported in primary human monocytes or murine macrophages. Thus, TF mRNA decay curves were determined in LPS-stimulated primary human monocytes and WT murine macrophages, where actinomycin D was added 2 hours, 4 hours and 6 hours following LPS stimulation (1μg/mL). In primary human monocytes, TF mRNA half-lives fell progressively with increasing duration of LPS stimulation (t½= 141±2, 88±16 and 36±18 minutes at 2, 4 and 6 hours respectively (r^2=0.998) (Figures 3-

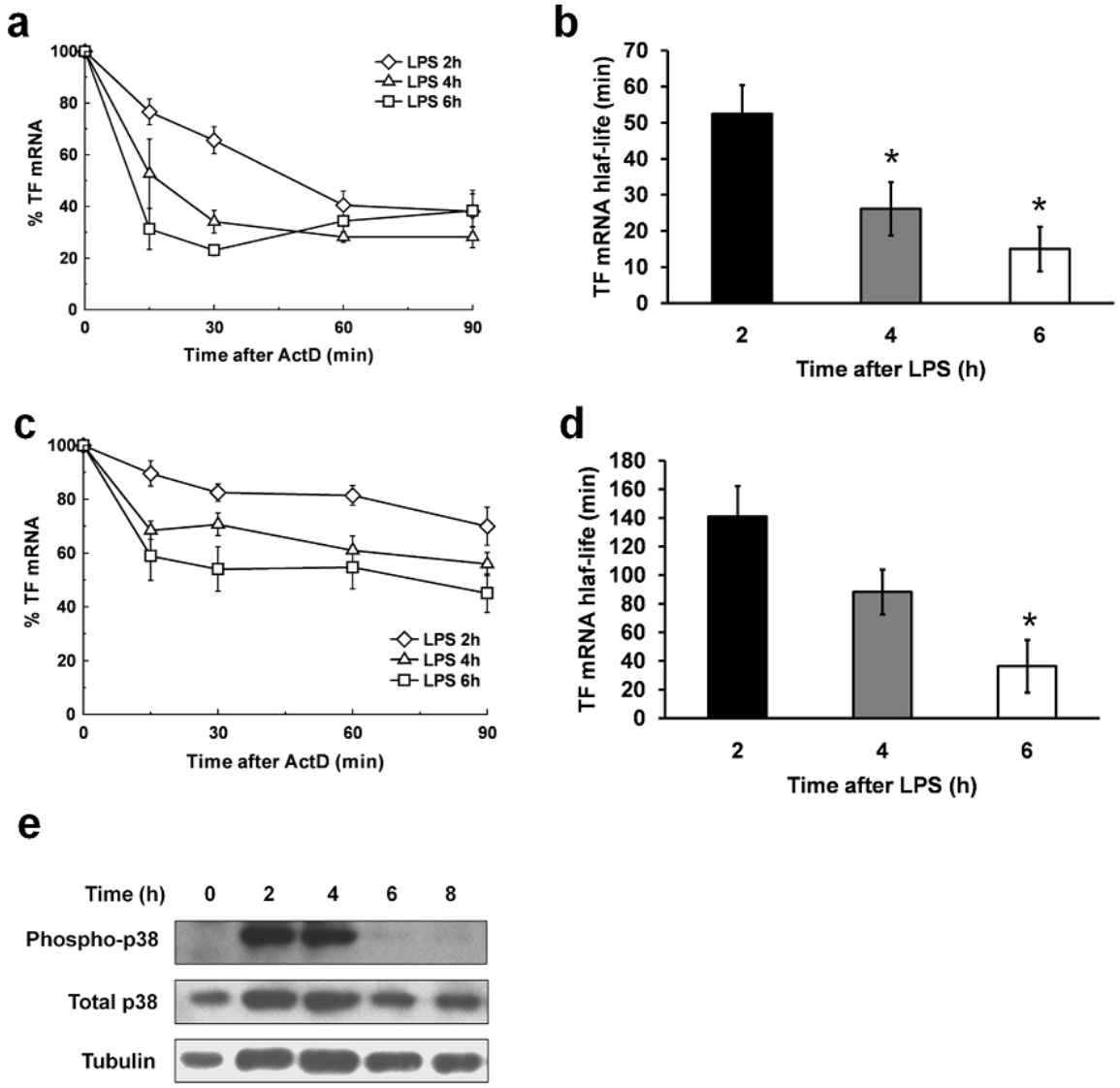

Figure 3-5: TF mRNA decay curves at different times after LPS stimulation.
Primary human monocytes **(a,b)** and murine macrophages **(c-d)** were stimulated with LPS 1µg/mL for 2,4 or 6h prior to induction of transcriptional arrest with actinomycin D (5µg/mL). TF mRNA levels were determined at each time point and normalized to levels at time point 0 to obtain mRNA decay profiles **(a,c)**. The decay profiles were modelled mathematically using non-linear regression analysis to determine mRNA half-life (n=3) as shown in **(b,d)**. Data expressed as mean ± SEM and analysed using a 2-tailed Student's t-test. * $p<0.05$, ** $p<0.01$, *** $p< 0.001$ compared to half-life at 2h. There appears to be a reduction in TF mRNA stability with increasing time following LPS stimulation. (e) Western blotting analysis of phospho-p38 at times shown following LPS stimulation in murine macrophages. Representative blot of 3 independent experiments. There appears to be a progressive reduction in phospho-p38 levels with increasing time following LPS stimulation.

5a,b). A similar pattern was observed with murine macrophages (t½= 52±8, 26±7 and 15±6 minutes at 2, 4 and 6 hours respectively (r^2=0.948) (Figures 3-5c,d). Given the above observation that p38 activity modulates TF mRNA half-life, one possible explanation would be the decline in phospho-p38 levels, i.e. p38 activity, with time

following LPS stimulation. To demonstrate this, total and phospho-p38 levels were determined using western blotting analyses at 2, 4 and 6 hours following LPS stimulation. Figure 3-5e shows a progressive reduction in phospho-p38 levels over 6 hour period, providing a potential explanation for the observed reduction in TF mRNA half-life over this period.

3.3.4 TTP deficiency results in increased TF expression

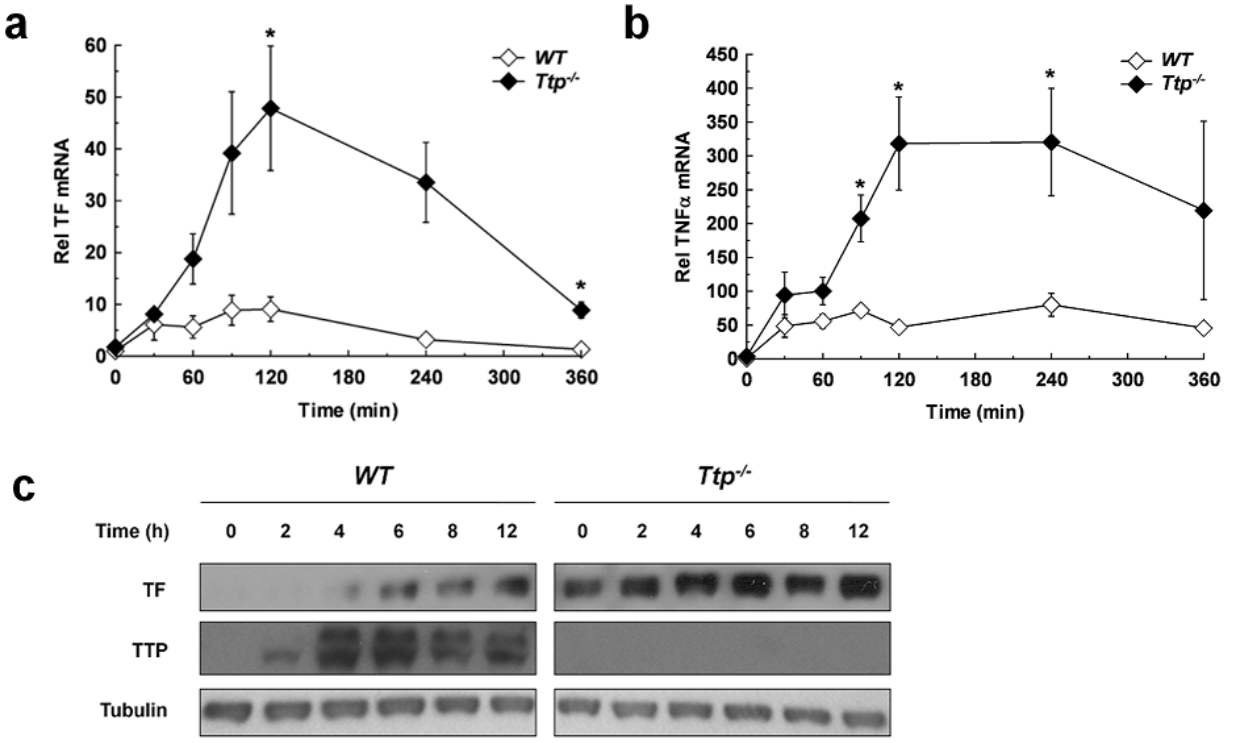

Figure 3-6: The effect of TTP deficiency on TF expression in LPS stimulated murine macrophages.
WT and *Ttp*$^{-/-}$ murine macrophages were stimulated with LPS 1µg/mL for times shown. **(a)** TF mRNA levels were determined at each time point and normalized to levels in unstimulated WT macrophages (n=3); **(b)** TNFα mRNA levels were determined at each time point and normalized to levels in unstimulated WT macrophages (n=3). This served as a control experiment as TNFα expression is known to be increased in *Ttp*$^{-/-}$ cells. Data expressed as mean ± SEM and analysed using a 2-tailed Student's t-test. * $p<0.05$, ** $p<0.01$, *** $p< 0.001$ compared to TF mRNA levels in WT macrophages at time=0; **(c)** Western blotting analysis of TF protein expression at times shown following LPS stimulation. Representative blot of 3 independent experiments. For each protein, the bands from WT and *Ttp*$^{-/-}$ cells are on the same blot, but have been separated for clarity. TF expression is increased at both mRNA and protein level in *Ttp*$^{-/-}$ macrophages.

If p38 inhibition reduces TF mRNA stability, then one can propose that the p38 MAPK pathway is phosphorylating and inactivating an mRNA-binding protein. Potential targets for which such a mechanism would be applicable are TTP, AUF1 and KSRP. Given the strong association with p38 activity and TTP function, and the bioinformatic analyses

the putative AREs upon which the original hypothesis was based, the potential role for TTP in regulating TF expression was examined. Given that TTP negatively regulates its targets, then if TTP does regulate TF expression, then the absence of TTP should increase TF expression. Thus, steady state TF mRNA and protein levels were determined in WT and *Ttp*$^{-/-}$ murine macrophages. Murine macrophages were stimulated with LPS 1μg/mL and TF mRNA levels were determined. There was no statistically significant difference in the basal levels of TF mRNA in *Ttp*$^{-/-}$ compared to WT macrophages. To establish the TF mRNA induction profiles and allow easier comparison between WT and *Ttp*$^{-/-}$ cells, TF mRNA levels in both WT and *Ttp*$^{-/-}$ macrophages were normalized to levels in the unstimulated WT macrophages within each experiment. Figure 3-6a shows that TF mRNA levels were significantly increased in *Ttp*$^{-/-}$ vs. WT macrophages at 2 and 6 hours after LPS stimulation ($p<0.05$). Perhaps the most widely studied transcript in the context of TTP is TNFα, and TTP deficiency is known to result in increased TNFα expression. In a series of control parallel experiments, TNFα mRNA levels were measured following LPS stimulation in WT and *Ttp*$^{-/-}$ macrophages following LPS stimulation, as above. Figure 3-6b confirms increased TNFα mRNA levels in *Ttp*$^{-/-}$ macrophages, corroborating previously published findings. TF protein levels were determined using western blotting analyses. Figure 3-6c shows that TF protein levels were significantly increased in *Ttp*$^{-/-}$ vs. WT macrophages in resting cells and following LPS stimulation.

3.3.5 p38 inhibition reduces TF mRNA stability in a TTP-dependent manner

The increased TF expression in *Ttp*$^{-/-}$ macrophages, could be a result of increased transcription; increased TF mRNA stability; or both. As demonstrated above TNFα expression is increased in *Ttp*$^{-/-}$ macrophages and this may account for increased TF transcription. Thus to dissect this, the specific role for TTP in regulating TF mRNA stability was examined. Murine macrophages were stimulated with LPS 1μg/mL and actinomycin D (5μg/mL) was added at 2 hours to induce transcriptional arrest. As above, SB202190 and SB203580 1μM were added concurrently with actinomycin D, to minimize any effect on mRNA transcription and TF mRNA decay profiles were determined (figure 3-7). In WT murine macrophages, the TF mRNA half-life was 97±15

minutes. p38 inhibition with SB2023580 1μM and SB202190 1μM resulted in a significant reduction in TF mRNA half-life to 43±10 minutes (p=0.016) and 35±7 minutes (p=0.012) respectively. Compared to WT macrophages, in the *Ttp*$^{-/-}$ macrophages, there was a significant increase in TF mRNA half-life to 352±82 minutes (p=0.016), and p38 inhibition with either SB203580 or SB202190 had no significant effect on TF mRNA half-life, with mRNA half-lives of 301±52 minutes (p=0.618) and 360±57 minutes (p=0.944) respectively. These data (a) confirm a similar effect of p38 inhibition on TF mRNA stability as seen in human monocytes; (b) provide evidence that TTP regulates TF mRNA stability; and (c) confirm that the effect of p38 inhibition is TTP-dependent.

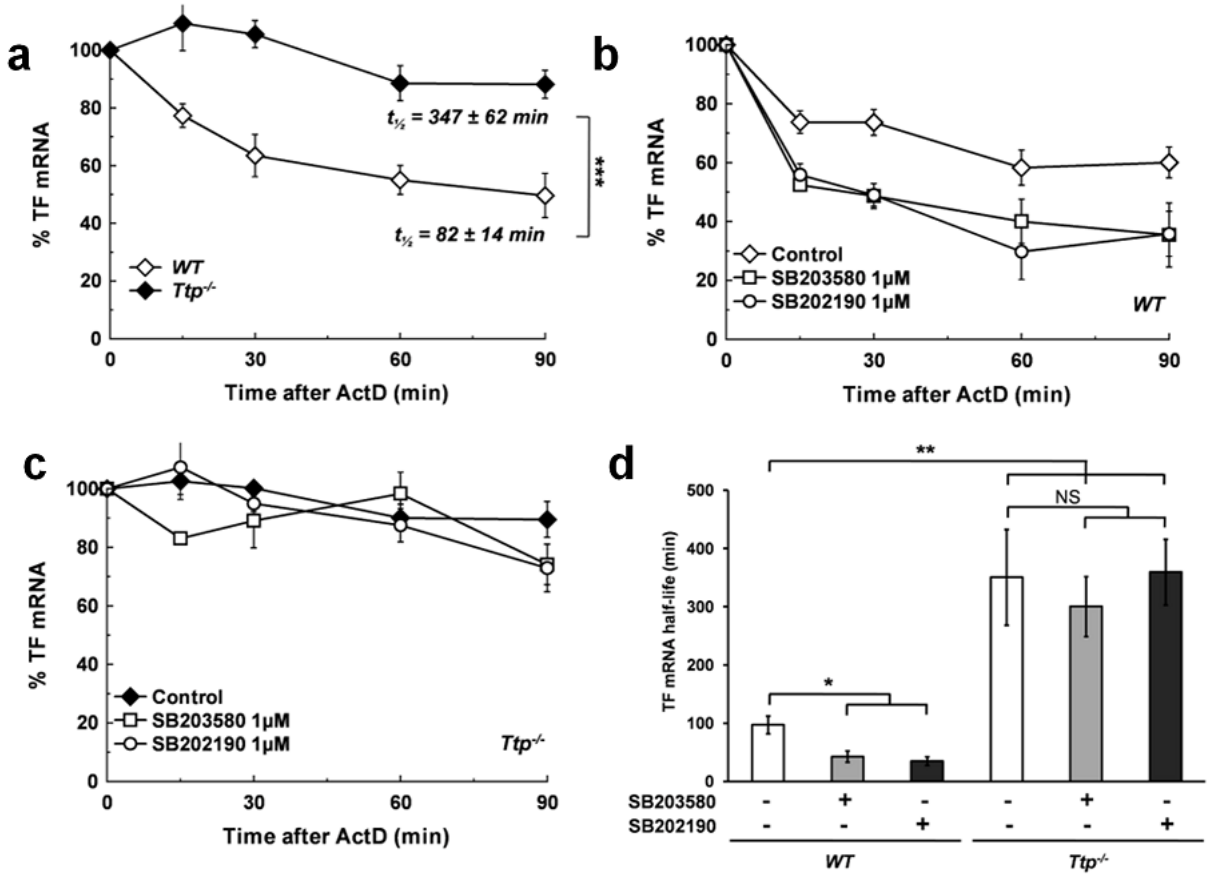

Figure 3-7: The effect of TTP deficiency on TF mRNA stability in LPS stimulated murine macrophages. WT and *Ttp*$^{-/-}$ murine macrophages were stimulated with LPS 1μg/mL for 2h. Actinomycin D (5μg/mL) was added at 2h to induce transcriptional arrest. Inhibition of p38 was achieved using SB203580 and SB202190 (both 1μM) which were added with actinomycin D (n=5). TF mRNA levels were determined at each time point and normalized to levels at time point 0 to obtain mRNA decay profiles. The decay profiles were modelled mathematically using non-linear regression analysis to determine mRNA half-life. **(a)** TF mRNA decay profiles in WT vs. *Ttp*$^{-/-}$ macrophages (n=7); **(b)** Effect of p38 inhibition in WT macrophages; **(c)** Effect of p38 inhibition in *Ttp*$^{-/-}$ macrophages; and **(d)** Comparison of TF mRNA half lives in WT and *Ttp*$^{-/-}$ macrophages with or without p38 inhibition. Data expressed as mean ± SEM and analysed using a 2-tailed Student's t-test. * $p<0.05$, ** $p<0.01$, *** $p< 0.001$. TF mRNA stability is increased in *Ttp*$^{-/-}$ macrophages and p38 inhibition reduces TF mRNA stability in WT but not *Ttp*$^{-/-}$ macrophages.

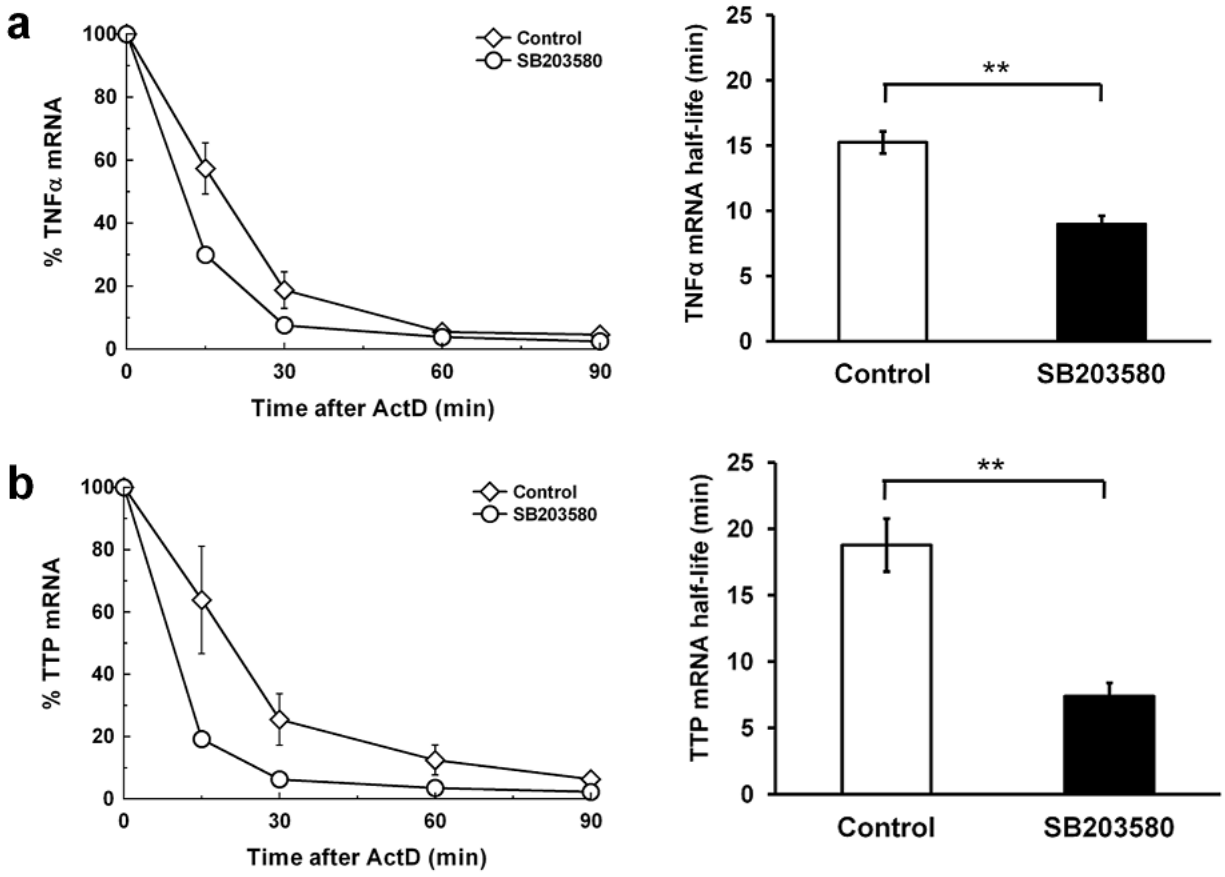

Figure 3-8: The effect of p38 inhibition on TNFα and TTP mRNA stability in LPS-stimulated murine macrophages.

These control experiments served to demonstrate a reduction in mRNA half-life with p38 inhibition for already established TTP targets, TNFα and TTP. WT murine macrophages were stimulated with LPS 1μg/mL for 2h. Actinomycin D (5μg/mL) was added at 2h to induce transcriptional arrest. Inhibition of p38 was achieved using SB203580 1μM which were added with actinomycin D. TF mRNA levels were determined at each time point and normalized to levels at time point 0 to obtain mRNA decay profiles. The decay profiles were modelled mathematically using non-linear regression analysis to determine mRNA half-life. **(a)** TNFα mRNA decay profiles in LPS-stimulated macrophages (n=6); and **(b)** TTP mRNA decay profiles in LPS-stimulated macrophages (n=6). Data expressed as mean ± SEM and analysed using a 2-tailed Student's t-test. * $p<0.05$, ** $p<0.01$, *** $p< 0.001$. p38 inhibition results in significant reduction in both TNFα and TTP mRNA half-life.

Both TNFα and TTP mRNA stability is regulated by TTP, and these transcripts are known to be destabilized through the inhibition of p38[363]. Thus in a series of control parallel experiments, designed primarily to demonstrate the effect of p38 inhibition on established TTP target transcripts, TNFα and TTP mRNA decay profiles were established in LPS-stimulated WT murine macrophages, and the effect of p38 inhibition on decay profiles was examined. The experimental protocol was as above. Figure 3-8 confirms that p38 inhibition with SB203580 1μM results in significant reduction in TNFα and TTP mRNA stability in LPS-stimulated murine macrophages as expected.

3.3.6 TTP interacts with TF mRNA

Having demonstrated that TTP regulates TF mRNA stability, it was crucial to establish whether TTP indeed interacts with TF mRNA. This was tested using RNP immunoprecipitation assays. RNP immunoprecipitation was performed using a rabbit anti-TTP (H-120) and rabbit IgG control antibody using lysates prepared from LPS-stimulated human monocytes. Following immunoprecipitation, the mRNA species bound to TTP were separated, reverse transcribed to form cDNA templates, and then amplified using TF and TNFα specific primers. TNFα was chosen as it is known to bind TTP and would serve as a positive control. HPRT and GAPDH were also amplified using the appropriate primers to control for non-specific pulldown. The PCR products were visualized on a 2% agarose gel with ethidium bromide. To ensure that the amplified products were not as a result of amplification of genomic DNA, parallel control PCR reactions were conducted on pulled down material that had not been reverse transcribed (no RT control). Figure 3-9a demonstrates that both the human TNFα and TF transcripts were bound to TTP, which was not observed with the IgG control. This confirmed that TTP associates with TF mRNA in human monocytes. To test whether TTP interacts with TF mRNA in murine macrophages, RNP immunoprecipitation was performed again using the rabbit anti-TTP (H-120) antibody and rabbit IgG control using lysates prepared from LPS-stimulated WT and *Ttp*$^{-/-}$ macrophages. Figure 3-9b demonstrates again that both the murine TNFα and TF transcripts were bound to TTP, which was not observed with the IgG control or from lysates from *Ttp*$^{-/-}$ macrophages. The RNP immunoprecipitation assays therefore confirmed that TTP interacts with TF mRNA in both human and murine macrophages.

3.3.7 TTP interacts with TF 3'UTR

Having determined that TTP interacts with TF mRNA, to specifically test whether TTP associates with TF 3'UTR, an RNA-biotin pulldown assay was used. TF 3'UTR sequences for both mouse and human TF 3'UTR were cloned and corresponding biotinylated sense and anti-sense RNA strands were synthesized using in vitro transcription. The anti-sense strand served as an internal control for each reaction. The biotinylated RNA strands were incubated with lysates prepared from LPS-stimulated

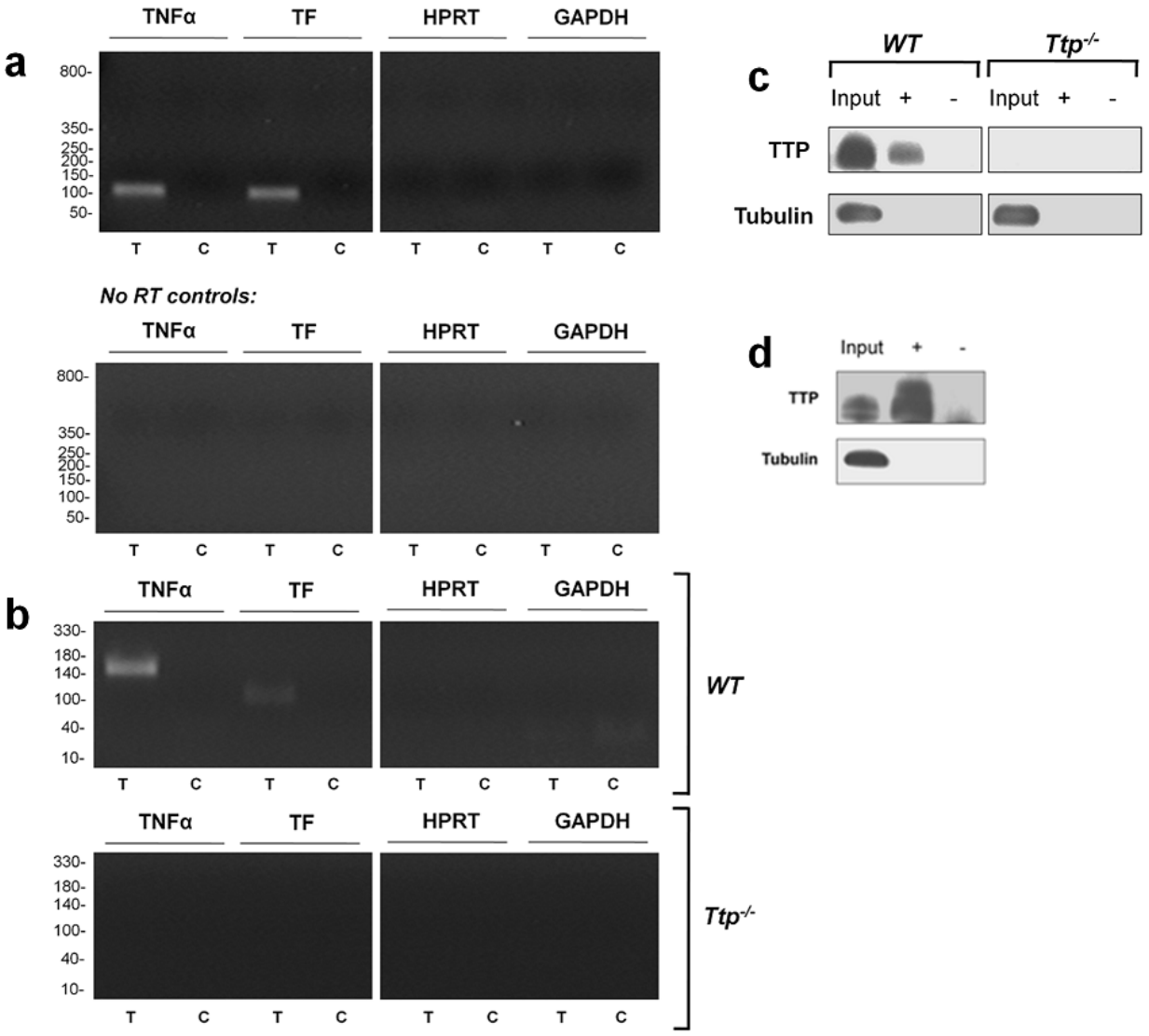

Figure 3-9: TF mRNA interacts with TTP

Interaction of TTP with TF mRNA as shown with RNP immunoprecipitation assays **(a,b)** and RNA-biotin pulldown assays **(c,d)**. **(a)** RT-PCR of TF mRNA immunoprecipitated by anti-TTP (T) antibody compared to rabbit IgG control (C) from lysates of LPS-treated primary human monocytes (1 µg/ml for 2 h). The amplicon length of human TF PCR product is 98bp and human TNFα PCR product is 96bp. TNFα provides a positive control as it is known to interact with TTP. Human HPRT (amplicon length=133) and GAPDH (amplicon length=90) provide a negative control mRNA. Also shown is a gel from a similar experiment when performing RT-PCR of immunoprecipitated material but without reverse transcription (no RT controls). This demonstrated that the bands observed for TF and TNFα were not due to contamination with genomic DNA. Representative of 3 independent experiments; **(b)** RT-PCR of TF mRNA immunoprecipitated by anti-TTP (T) antibody compared to rabbit IgG control (C) from lysates of LPS-treated WT and *Ttp*$^{-/-}$ macrophages (1µg/ml for 2 h). The amplicon length of murine TF PCR product is 105bp and murine TNFα PCR product is 173bp. TNFα provides a positive control. Murine HPRT (amplicon length=134bp) and GAPDH (amplicon length=90bp) provide a negative control mRNA. Representative of 3 independent experiments.; **(c)** Western blots of proteins isolated from lysates of LPS-treated WT and *Ttp*$^{-/-}$ macrophages (1 µg/ml for 2 h) by streptavidin beads coated with biotinylated sense (+) or anti-sense (-) murine TF 3'UTR. In this and other figures, tubulin serves as a negative marker for non-specific protein binding to beads; and **(d)** Western blots of proteins isolated from lysates of LPS-treated WT macrophages (1 µg/ml for 2 h) by streptavidin beads coated with biotinylated sense (+) or anti-sense (-) human TF 3'UTR. The TTP-TF 3'UTR interaction demonstrates species cross-reactivity. Representative of 3 independent experiments.

murine macrophages. The biotinylated transcripts were captured using Dynabeads® and the associated proteins resolved by Western blotting. Figure 3-9c shows that TTP associates with murine TF 3'UTR in lysates prepared from WT macrophages. The experiment was controlled by detecting for tubulin which serves as a marker for non-specific binding. The 3'UTR sequence is highly conserved between mouse and human. To test whether inter-species specificity exists for the TTP and TF 3'UTR interaction, an RNA-biotin pulldown assay was performed where biotinylated human 3'UTR sequences were incubated with WT murine macrophage lysates. Figure 3-9d demonstrates that murine TTP interacts with human TF 3'UTR sequence, confirming cross-species specificity for the TTP and TF 3'UTR interaction. These data provide evidence that TTP interacts specifically with the 3'UTR of TF.

3.3.8 TTP interacts with 2 nonameric sequences

Both mouse and human TF 3'UTR contain many ARE segments (figure 3-10a). The most highly conserved ARE across a variety of species including mouse and human is the final palindromic ARE sequence (figure 3-10b). For the remainder of this study, the murine TF 3'UTR was used for detailed ARE analyses. There are 7 AREs in the murine TF 3'UTR. These were grouped into 4 hypothetical ARE segments (ARE1-4). To test which ARE is functional and mediates TTP binding, the murine TF 3'UTR was divided to yield 6 constructs: 0-5. Constructs 0-1 were devoid of AREs and served as control constructs. Constructs 2-5 contained the 4 AREs in progressive summation with construct 5 containing all 4 AREs, i.e. the complete 3'UTR sequence. RNA-biotin pulldown assays were performed with both sense and anti-sense RNA strands corresponding to each 3'UTR segment and lysates prepared from LPS-stimulated WT murine macrophages. Figure 3-10b shows that TTP associates only with transcripts that contain the final ARE. This ARE has a palindromic sequence (AUAAUUUAUUUAAUA) which contains 2 overlapping AUUUAUUUA and UUAUUUAAU nonamers, each of which represent potential TTP binding sites. Accordingly, 4 mutant sequences were generated (ARE_{Mut1-4}) which tested whether (a) the complete palindromic sequence had functional importance (ARE_{Mut1}, **GGG**AUUUAUUUAAUA) or the individual nonamers alone or in combination had functional importance (ARE_{Mut2}, AUAAUUUAUUUA**GGG**;

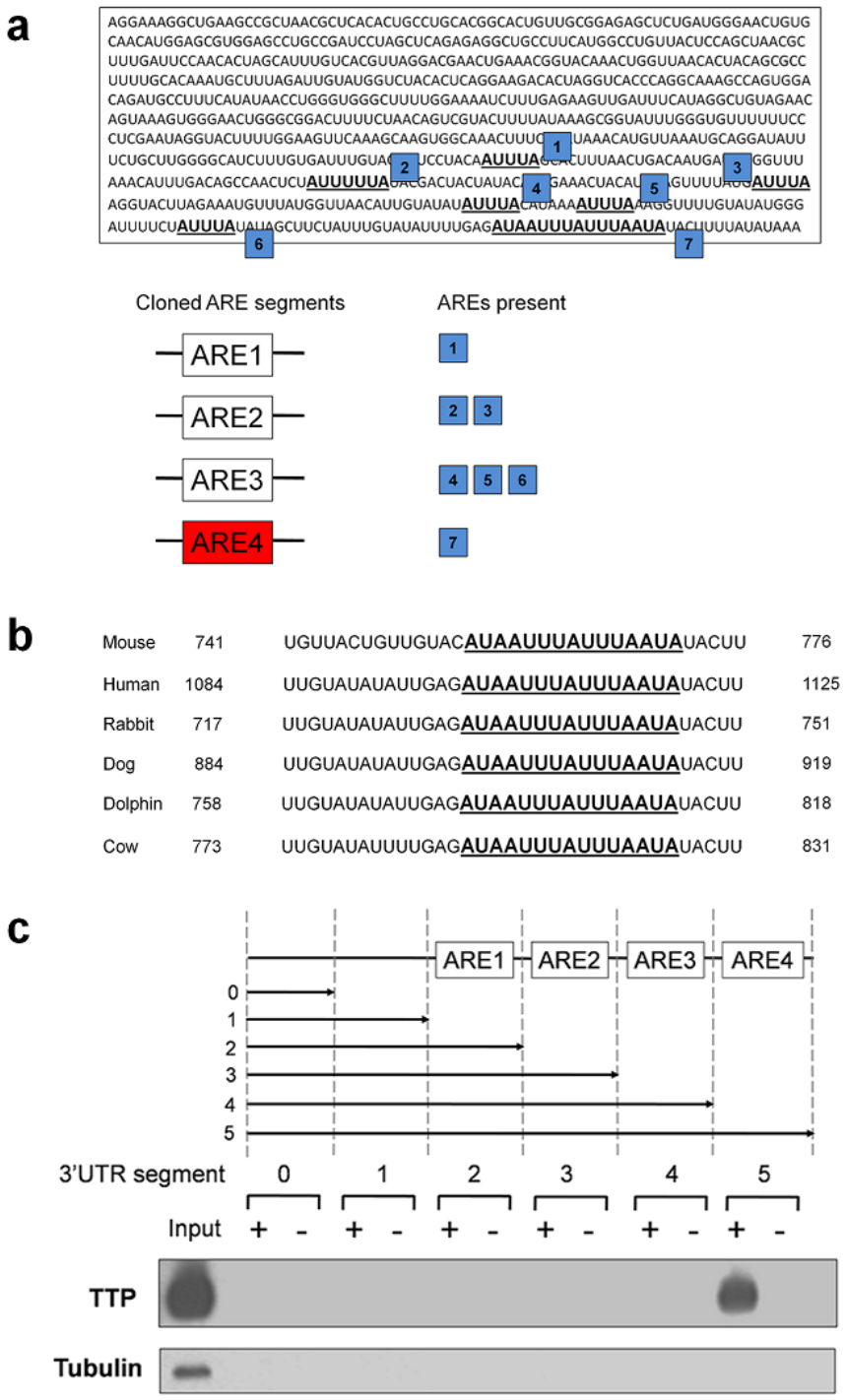

Figure 3-10: The specifics of the interaction between TTP and TF 3'UTR
RNA-biotin pull down assays conducted with lysates of LPS-treated WT macrophages (1 μg/ml for 2 h) by streptavidin beads coated with biotinylated sense (+) or anti-sense (-) human TF 3'UTR. The biotinylated RNA sequences represent different cloned 3'UTR segments. **(a)** Figure showing the cloned ARE segments and the specific AREs contained within the murine TF 3'UTR. ARE 4 contains the final palindromic ARE sequence; **(b)** Conservation of the palindromic ARE is seen throughout a number of different species; **(c)** RNA –biotin pulldown assays performed for different cloned 3'UTR segments and western blots of proteins isolated. TTP appears to interact with the 3'UTR sequence that contains the final palindromic ARE. Representative of 2 independent experiments.

ARE $_{Mut3}$, AUAA**GGG**AUUUAAUA; and ARE $_{Mut4}$, AUAAUUUA**GGG**AAUA). RNA-biotin pulldown assays were performed with both sense and anti-sense RNA strands corresponding to the WT TF 3'UTR and each of ARE mutant sequences. As above, the lysates were prepared from LPS-stimulated WT murine macrophages.

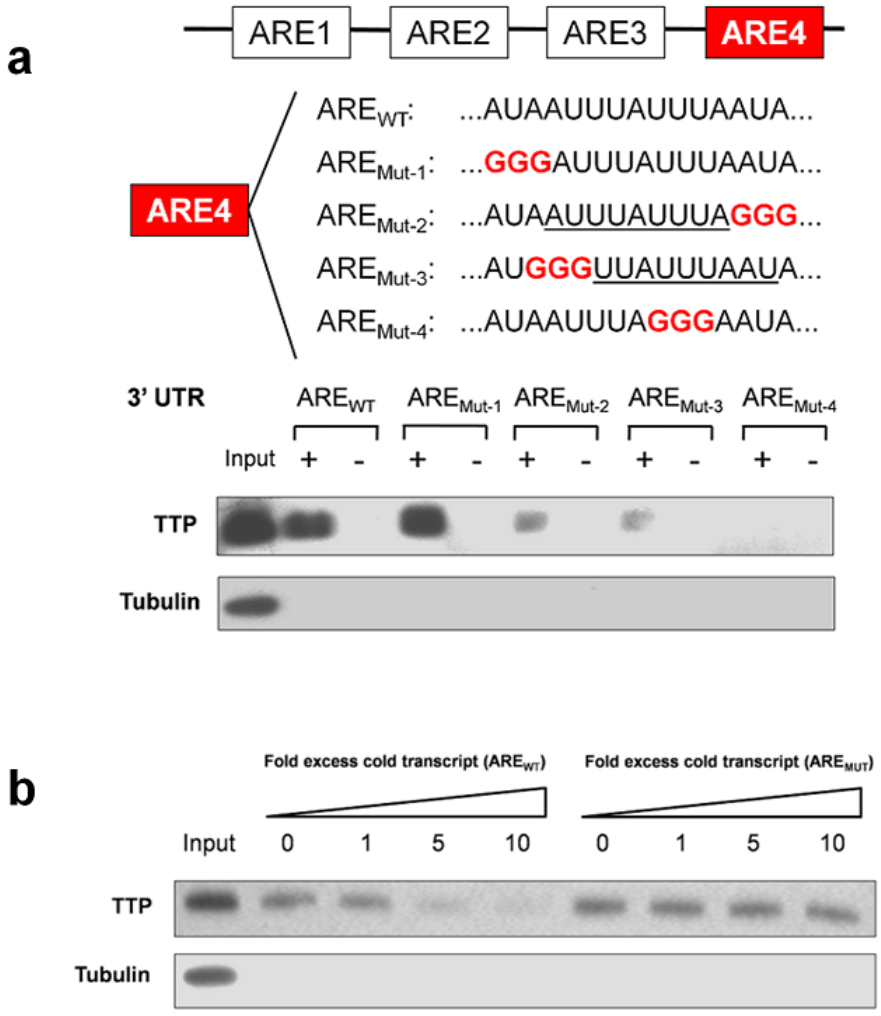

Figure 3-11: Defining the specific ARE sequences within TF 3'UTR that mediate binding to TTP
The final ARE contains 2 overlapping nonameric sequences with high predictive binding to ARE-binding proteins (underlined). Focusing on this ARE, 4 mutated sequences were generated as shown, and binding to TTP was interrogated using RNA-biotin pulldown assays. RNA-biotin pull down assays were conducted with lysates of LPS-treated WT macrophages (1 µg/ml for 2h) by streptavidin beads coated with biotinylated sense (+) or anti-sense (-) murine TF 3'UTR (WT or mutant sequences). **(a)** Western blots of proteins isolated. Tubulin acts as a control for non-specific pull-down. TTP appears to interact with the 3'UTR sequence that contains the final palindromic ARE. Representative of 2 independent experiments. Mutations of each of the separate nonamers reduced, but did not abolish, TTP binding. Mutations of both nonamers by substituting the shared UUU with GGG (ARE$_{Mut-4}$) completely abolished TTP binding; **(b)** Competition RNA-biotin pulldown assay was performed, using cold unlabelled transcripts (WT and ARE$_{Mut-4}$) which if able to bind TTP would compete with the biotin-labelled WT transcripts coated on the streptavidin beads. Western blots of proteins isolated show that the cold mutant transcripts do not affect TTP binding, whilst the cold WT transcripts compete with binding. Representative of 2 independent experiments.

Figure 3-11a shows that TTP binding was not affected by mutations within the palindromic sequences as long as the nonameric sequences were preserved. However, mutations of each of the separate nonamers reduced, but did not abolish, TTP binding. Finally, mutations of both nonamers by substituting the shared UUU with GGG completely abolished TTP binding. These data would suggest that both sequences mediate binding to TTP in a cooperative fashion. To further test this, a competition RNA-biotin pulldown assay was performed, using cold unlabelled transcripts (figure 3-11b). The principle underlying these experiment was, if the final ARE was indeed functional and mediated binding to TTP, then the addition of excess WT cold transcripts would compete with the biotinylated transcripts for TTP binding, whilst the mutant transcripts (ARE_{Mut-4}) would have no effect. Figure 3-11b demonstrates that the addition of the cold WT transcripts significantly reduced TTP binding to the biotinylated transcripts captured by the beads. However, the cold mutant transcripts did not affect TTP binding to the biotinylated transcripts captured by the beads. These data provide further evidence that the 2 nonameric sequences within the final palindromic ARE in TF 3'UTR bind TTP in a cooperative fashion.

3.3.9 p38 inhibition does not alter TTP binding to TF 3'UTR

The above data indicates that p38 inhibition results in destabilization of the TF transcript in a TTP-dependent manner. To test whether p38 inhibition directly impairs the ability of TTP to bind with the TF transcript, RNA-biotin pull-down assay were used. In these experiments, the preparation of the lysates were critical. Lysates were prepared form WT murine macrophages which were either treated with LPS 1μg/mL or LPS 1μg/mL and SB203580 1μM. First, the cells were cultured with LPS for 90 minutes, and then in the p38 inhibitor arm of the experiment, SB203580 was added, with vehicle control in the control arm of the experiment. This was allowed to incubate for 30 minutes prior to preparation of lysates. Due to the rapid action of SB compounds, this strategy has been demonstrated above to efficiently reduce phospho-p38 levels by western blotting techniques (figure3-3). Furthermore, the SB compounds were added concurrently with actinomycin D in the mRNA decay experiments with an appreciable reduction in TF and TNF α mRNA stability, again demonstrating their rapid onset of action and inhibition of

TTP activity. p38 inhibitors could not be added concurrently with LPS as this would inhibit LPS-induced transcription and potentially reduce TTP protein levels in the lysates. Figure 3-12 shows that a short treatment with SB203580 1μM did not produce an appreciable reduction in TTP in the lysate, and more importantly had no effect on TTP binding to TF 3'UTR. These findings are in keeping with previously reported findings[331].

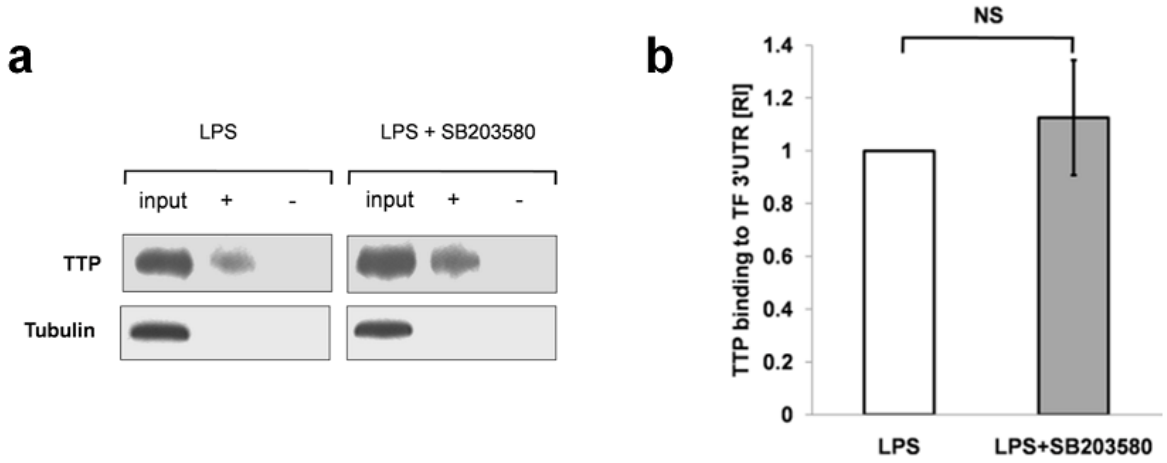

Figure 3-12: TTP binding to TF 3'UTR is independent of p38 phosphorylation status
RNA-biotin pull down assays were conducted with lysates of either LPS-treated WT macrophages (1 μg/ml for 2h) or LPS-treated WT macrophages (1 μg/ml for 2h) treated with 15 min SB203580 1μM prior to lysate extraction. Streptavidin beads were coated with biotinylated sense (+) or anti-sense (-) human TF 3'UTR. **(a)** Western blots of proteins isolated. Tubulin acts as a control for non-specific pull-down. TTP appears to interact with the 3'UTR sequence irrespective of p38 phosphorylation status. Representative blot from 3 independent experiments; **(b)** Densitometric analysis with immunodensity of pulled down TTP relative to the immunodensity of TTP in the input lane. This is then normalized to the ratio to the LPS arm of the experiment. Data expressed as mean ± SEM and analysed using a 2-tailed Student's t-test. * $p<0.05$, ** $p<0.01$, *** $p< 0.001$.

3.4 DISCUSSION

The above data demonstrate the specific role for the p38 MAPK pathway and TTP in the post-transcriptional regulation of TF. Preliminary experiments demonstrated that inhibition of p38 led to a reduction in TF expression, both at the level of mRNA and protein. This was paralleled by a reduction in procoagulant activity. The p38 pathway plays important roles in transcriptional regulation, therefore this observed effect was likely a combination of both transcriptional repression coupled with its post-transcriptional effects. However, the specific role for p38 in the post-transcriptional regulation of TF was demonstrated by the ability of a variety of inhibitors (SB202190,

SB203580, BIRB796 and LY2228800) to reduce TF mRNA half-life in human monocytes. The SB compounds represent an important tool for investigating p38 function(s) in experimental laboratory science. The drawbacks of these compounds are that they may have non-specific effects on other kinases, particularly JNK. However, adopting a 1μM dose for all SB compounds, little effect on phospho-JNK levels were observed, indicting relative selectivity for p38. These are the standard concentration for SB compounds in the reported literature. However, despite the specificity demonstrated using western blotting analyses, it is possible that western blotting may not have been sensitive enough to demonstrate inhibition specificity for p38. This may have been more robustly demonstrated using dedicated kinase assays. Nevertheless, the effect of p38 inhibition on TF mRNA stability was confirmed and substantiated using more novel and different classes of compounds, BIRB796 and LY2228800.

Although the TF transcript is unstable, its half-life has previously shown to be dynamic in THP-1 cells, where it is relatively stable early in the LPS induction phase, but it becomes unstable later in the response[190]. This observation has not previously been described in primary human and murine macrophages. In this chapter, this was demonstrated in primary human monocytes and murine macrophages following LPS stimulation, where the TF transcript appeared to be relatively stable at 2 hours, but by 6 hours the half-life has fallen to less than 30%. This dynamic change in half-life implies robust post-transcriptional regulatory mechanisms. Having established a role for p38 in regulating TF mRNA half-life, it was intriguing to speculate that a progressive reduction in phospho-p38 levels as seen late in the LPS response may in part explain this observation.

Following LPS stimulation, steady state TF mRNA and protein levels were increased in *Ttp*$^{-/-}$ macrophages. Whilst this observation may imply a role for TTP in the post-transcriptional regulation of TF, this has confounded interpretation as TTP deficiency results in increased TNFα production which can mediate transcriptional effects. However, the specific role for TTP was demonstrated by the observation that the TF mRNA half-life was significantly increased in *Ttp*$^{-/-}$ macrophages. Furthermore, p38

inhibitors were able to reduce TF mRNA stability in WT but not in *Ttp*$^{-/-}$ macrophages. This has two important interpretations, (a) the effect of p38 inhibition on TF mRNA decay is TTP-dependent; and (b) the effect of p38 inhibition on TF mRNA decay does not involve any other RNA-binding proteins whose functions are regulated by p38-dependent phosphorylation, e.g. AUF1, BRF1 and KSRP[278].

Using RNP immunoprecipitation and RNA-biotin pulldown assays, TTP was shown to associate with TF mRNA and specifically with TF 3'UTR. Using truncated murine 3'UTR sequences with AREs in progressive summation, RNA-biotin assays confirmed that TTP binds the sequence that contains the final ARE segment (ARE4 in figure 3-10c). This has two interpretations, (a) the final ARE is functional and mediates binding to TTP; or (b) all the AREs are required to mediate binding to TTP. The later explanation is unlikely, as the 3'UTR spanning all the AREs is ~700 nucleotides in length, and studies have shown that RNA binding to TTP involves short nucleotide sequences[423, 424]. The final ARE segment contains a palindromic ARE, which contains 2 overlapping nonamers (AUUUAUUUA and UUAUUUAAU) [264-266]. These nonamers have high predictive binding for ARE-binding proteins, the later bearing striking resemblance to the consensus nonameric sequence with high predictive binding to TTP. Further mutational analyses demonstrated that both nonamers bind TTP in a cooperative fashion. The functional importance of this ARE was further demonstrated by the ability of unlabelled "cold" WT 3'UTR to compete with labeled WT transcript for binding to TTP, whereas the cold mutant 3'UTR had no effect.

In conclusion, these data demonstrate the specific role for the p38-TTP axis in the post-transcriptional regulation of TF. The functional ARE in this setting is a highly conserved palindromic ARE, that comprises of 2 overlapping nonamers (AUUUAUUUA and UUAUUUAAU) that both appear to be functionally cooperative.

Chapter 4

Results:

PARP-14 cooperates with TTP to regulate TF mRNA stability

4.1 INTRODUCTION

Poly(ADP-ribosyl)ation is a unique post-translational modification where negatively charged ADP-ribose moieties are adducted onto proteins. It is of central importance to a wide variety of cellular processes, e.g. DNA repair, transcriptional regulation, proteasomal protein degradation, vesicle trafficking and apoptosis[425]. This process is catalyzed by a family of NAD+ ADP-ribosyl transferases, the poly(ADP-ribose) polymerases (PARPs). These contain PARP domains that catalyze the formation of ADP-ribose from NAD+, which is then covalently attached to target proteins[367]. PARP-1 has been the subject of extensive research and is of central importance to DNA repair and transcriptional regulation [425]. In contrast, most of the other PARP family proteins are much less well understood. Poly (ADP-ribose) polymerase (PARP)-14 (also known as ADP-Ribosyltransferase Diphteria Toxin-like 8, ARDT8) is a ~205 kDa intracellular protein that has previously been identified as a nuclear coactivator of STAT-6-mediated gene transcription in B cells[406, 407]. Although PARP-14 has a C terminal PARP domain, its enzymatic function is likely to be restricted to ADP-ribosyl monotransferase activity[425].

However, it has recently become clear that several PARP family members, including PARP-14, may have roles in RNA regulation[395, 408]. PARP family members including PARP-14 have been found to localize with components of the stress granule that contains various RNA binding proteins and components of the RNA decay machinery. Work in our laboratory has identified PARP-14 as a novel RNA-binding protein, and specifically plays a role in regulating mRNA stability of the chemokine IP-10 following IFNγ stimulation (unpublished data).

In this chapter, the specific role for PARP-14 is examined, and whether or not it cooperates with TTP to regulate TF mRNA stability. Despite its implication in diverse cellular functions, ADP-ribosylation has not been reported to regulate coagulation and thrombosis. Thus, the role for ADP ribosylation in regulating TF mRNA turnover is investigated.

4.2 METHODS

4.2.1 Primary human monocyte isolation and culture

Monocytes were isolated from citrated venous blood derived from healthy donors. Peripheral blood mononuclear cells (PBMCs) were isolated from the cell fraction by Ficoll–Paque density-gradient centrifugation and CD14+ monocytes were separated using magnetic separation with CD14 MicroBeads and MACS Separator column. Monocytes were plated into tissue culture plates according to the experimental protocol in IMDM with 10% FCS ($25x10^4$ cells/well in 24 well plates or $2x10^4$/well in 96-well plates) and incubated overnight in a 37°C incubator with 5% CO_2 atmosphere, for experiments the following day.

4.2.2 Bone marrow-derived macrophage isolation and culture

WT and *Parp14*$^{-/-}$ mice were sacrificed using cervical dislocation. Bone marrow cells were flushed from the femur and tibia and cultured in bone marrow culture medium for 6 days. On day 6, the cells were harvested, resuspended in the bone marrow culture medium, and plated in culture dishes/flasks as per the experimental protocol ($25x10^4$ cells/well in 24 well plates or $1x10^7$cells/T75 flask) and incubated overnight in a 37°C incubator, for experiments the following day.

4.2.3 RNA extraction and quantitative reverse-transcriptase PCR (qRT-PCR)

RNA was isolated from cells using RNEasy Mini kit and from tissues using RNEasy Mini Fibrous kit according to manufacturer's instructions, incorporating an on-column DNase digestion. Tissues were homogenized using TissueLyser and 5mm stainless steel beads. 1µg of total RNA was used for cDNA synthesis using SuperScript III reverse transcriptase enzyme. Comparative qRT-PCR was performed using SYBR green and gene specific primers (table 2-1). Data was normalized to 2 housekeeping controls, GAPDH and HPRT. For mouse TF mRNA expression, data was validated using 2 primer sets. Relative gene expression was calculated using the ΔΔCt method[409].

4.2.4 mRNA decay experiments

All mRNA decay experiments were performed with an identical protocol. Cells were stimulated with LPS 1μg/mL. Actinomycin D (5μg/mL) was added at 2 hours following LPS stimulation to induce transcriptional arrest. For p38 inhibition, SB203580 was used. For PARP inhibition, PJ34 and 3AB were used. In experiments specifically examining the effect of these signaling inhibitors on mRNA decay, the inhibitors were all added at the time of actinomycin D. Following actinomycin D, RNA was isolated at time 0, 15, 30, 60 and 90 minutes. mRNA was quantified using qRT-PCR, and levels were normalized to levels at time 0. The mRNA decay profiles were modeled mathematically using non-linear regression analysis and mRNA half-lives calculated.

4.2.5 Western blotting analysis

Following the experimental protocol, the cells were lysed with 100μL of Cell Lytic M lysis buffer with 1μL of protease inhibitor cocktail. For extraction of proteins from tissue, Cell Lytic MT lysis buffer was used with mechanical homogenization using TissueLyser and 5mm stainless steel beads. The lysates were centrifuged at 17,000g for 20 minutes at 4ºC to pellet cell debris. The supernatants were carefully removed and stored at -80ºC until analysis. A Novex XCell II mini gel system was used. 20μg of protein was used per lane, and proteins were separated by gel electrophoresis using pre-cast polyacrylamide gels, and electrotransferred to polyvinylidene difluoride membranes. The membranes were blocked using blocking buffer and primary and secondary antibodies were applied in blocking buffer at the appropriate dilutions (table 2-2). Protein bands were detected using chemiluminescence. Protein quantification was performed using densitometry using ImageJ software (National Institutes of Health, Bethesda) normalized to tubulin.

4.2.6 TF activity assays

A turbimetric clot assay was used to determine TF activity. Cells were cultured in 96 well plates (cell density=$2x10^4$ cells per well) and treated with LPS 1μg/mL. The supernatant was removed and cells were washed with PBS twice, prior to the addition of plasma. Organ tissues from mice were homogenized in 15mM N-octyl-glycopyranoside in HN-Buffer. 5μL of homogenate (final concentration of 1mg/mL) was

used for analysis. 100 µL of the citrated PPP (human:mouse plasma = 9:1) was added to the wells and recalcified with 2 µL of 1.0M $CaCl_2$ to initiate clotting. Clot turbidity was measured by absorbance (A_{405}) every minute for 60 minutes in a spectrophotometer with internal thermostatic control at 37°C. T_{lag} was determined and correlated to a TF standard curve generated using relipidated TF to determine TF activity.

4.2.7 Flow cytometric analysis of murine TF

WT and *Parp14*$^{-/-}$ macrophages were stimulated with LPS 1µg/mL for 6 hours, following which the culture medium was removed. The cells were harvested, washed and blocked with goat serum for 30 minutes at 4°C. Primary staining was with either 1µg/ml rabbit anti-mouse TF antibody or 1µg/ml rabbit IgG control antibody for 30 minutes at 4°C. The cells were washed and secondary staining was with 1µg/ml FITC-conjugated F(ab')2 fragment of goat anti-rabbit antibody for 30 minutes at 4°C .The cells were washed and resuspended in 500 µl PBS for flow cytometric analysis. The cells were read on a Coulter EpicsXL flow cytometer, FL1–600V, FL2–600V. The maximum event rate was set to 10,000. Data were analyzed and presented using WinMDI software (Scripps Research Institute, CA).

4.2.8 TNFα ELISA

TNFα proteins levels in cell culture supernatants and mouse sera were measured using a mouse TNFα Duo-set sandwich ELISA kit (RND systems) according to the manufacturer's instructions.

4.2.9 RNP immunoprecipitation

Cell lysates were produced from LPS-stimulated murine macrophages. The cells were seeded in T75 culture flasks at a density of $1x10^7$ cells per flask and stimulated with LPS 1µg/mL for 2 hours. Cells were washed with ice cold PBS, lysed with polysome lysis buffer supplemented with RNase and protease inhibitors and centrifuged at 17000g at 4°C for 30 minutes to pellet cell debris.100 µl (3mg protein) of lysate was incubated for 2 hours with 100 µl of preswollen Protein-G agarose beads precoated with either 20µg of rabbit anti-PARP14 or normal rabbit IgG. The beads were washed with

NT2 buffer and then incubated in 100ml NT2 buffer containing 0.1% SDS and 0.5 mg/ml proteinase K (15minutes, 55°C). The beads were pelleted, and the supernatant carefully removed. RNA was extracted using TRIzol reagent. cDNA synthesis and qRT-PCR was performed using gene-specific primers as above. To determine specificity for mRNA, the samples were run in parallel with non-RT samples to control for genomic DNA contamination. The PCR reaction products were separated in a 2% agarose gel containing ethidium bromide and visualized under UV light.

4.2.10 *In vitro* transcription

The murine and human TF 3'UTRs, truncated and mutant 3'UTR segments were amplified from total murine or human macrophage cDNA with PCR primers listed in tables 2-3 and 2-4 using the Advantage 2 PCR cloning kit and cloned using the TOPO TA Cloning Kit into the pCRII-TOPO vector. The plasmids were purified using Plasmid Miniprep Kit, linearized by restriction digestion using (Hind III or EcoRV for the murine sequences, and Sac1 or EcoRV for human sequences). Biotinylated transcripts were generated using the SP6/T7 transcription kit in the presence of biotinylated oligonucleotides. For competition experiments where cold (non-biotinylated) transcripts were necessary, the in vitro transcription reaction was performed replacing the biotinylated nucleotide mix with a standard non-biotinylated nucleotide mix. The RNA was purified from the reaction mixture using ethanol precipitation.

4.2.11 RNA-biotin pulldown assays

Cell lysates were produced from LPS-stimulated murine macrophages. The cells were seeded in T75 culture flasks at a density of $1x10^7$ cells per flask and stimulated with LPS 1µg/mL for 2 hours. Where PARP inhibition was necessary, PJ34 10µM was added 15 minutes prior to lysis. The adherent cells were harvested, washed with PBS and lysed using 1mL lysis buffer supplemented with RNase and protease inhibitors. 100µl (100µg protein) of lysate was incubated with either the sense or anti-sense biotinylated transcript (2µg) for 1 hour. In the competition experiments, parallel reactions were set up where 1, 5 and 10 fold excess cold transcripts were added in addition to the 2µg of biotinylated transcripts. 20µl of magnetic streptavidin-coated Dynabeads® were added

and incubated at 4°C for 1 hour. The beads were separated using magnetic separation, washed with lysis buffer and boiled in 1x SDS loading buffer at 100°C for 4 minutes. The proteins were detected using Western blotting and immunodetection.

4.2.12 Co-immunoprecipitation assay

Cell lysates were produced from LPS-stimulated murine macrophages. The cells were seeded in T75 culture flasks at a density of $1x10^7$ cells per flask and stimulated with LPS 1µg/mL for 2 hours. For experiments were RNase treatment was necessary, RNase A was added to the lysis buffer (prior to lysis) at a final concentration of 5µg/mL. The lysate was added to either 5µg of goat anti-TTP (N-18) antibody (Santa Cruz) or 5µg IgG control (Santa Cruz) and incubated at 4°C for 1 hour with rotation. 50µL of prepared magnetic protein G beads were added to the antibody-lysate mixture and incubated for 15 minutes at room temperature with rotation. The beads were isolated using magnetic separation and washed with ice cold IP wash buffer (3 times). The proteins bound to the beads were eluted by boiling the beads in 20-30µL 1x SDS loading buffer at 100°C for 4 minutes. The (co-)immunoprecipitated proteins were detected using Western blotting and immunodetection methods as described above.

4.2.13 Statistical analyses

All continuous variables were expressed as either as mean ± SEM or medians, depending on normality tests based on the Shapiro-Wilk statistic. Statistical analyses were performed using GraphPad Prism v5.0 (GraphPad Software, San Diego, CA, USA) and Microsoft Excel 2007 (Microsoft, Washington, USA). Data was analysed using an unpaired Student's t-test (2-tailed) or Mann-Whitney U-test (2 tailed). Statistical significance was set at $p<0.05$.

4.3 RESULTS

4.3.1 LPS induces PARP-14 expression

To determine the kinetics and magnitude of PARP-14 induction, WT murine macrophages were stimulated with LPS 1µg/mL and PARP-14 mRNA and protein levels

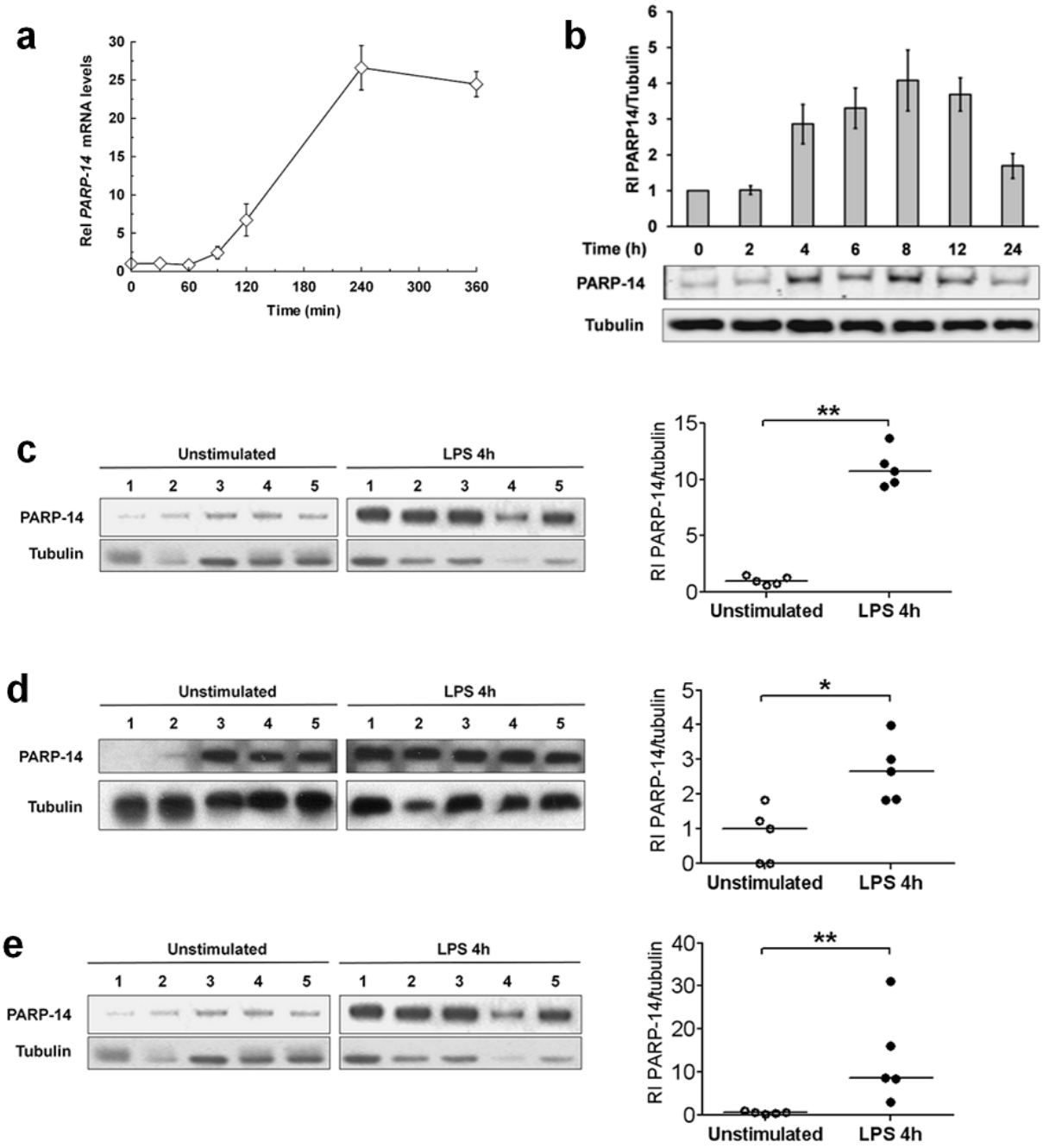

Figure 4-1: Induction of PARP-14 following LPS stimulation *in vitro* and *in vivo*

WT murine macrophages were stimulated with LPS 1µg/mL for times shown following which **(a)** PARP-14 mRNA levels were determined using RT-PCR (n=3); and **(b)** PARP-14 protein levels were determined using western blotting (n=5). Representative blot is shown with densitometric analyses with PARP-14 immunodensity relative to the tubulin immunodensity. This is then normalized to the ratio in unstimulated cells at time=0. Data expressed as mean ± SEM; For determination of in vivo PARP-14 induction , WT mice were stimulated with LPS 5µg i.p. For 4h. Different organs were extracted in unstimulated and LPS-stimulated mice. PARP-14 protein levels were determined using western blotting in the (**c**) heart, **(d)** lungs, and **(e)** liver (all n=5 mice per group). The blots are shown on the left for each organ with densitometric analyses on the right. All blots were run on the same gel, but the unstimulated and 4h samples are separated for clarity. PARP-14 immunodensity relative to the tubulin immunodensity was determined and then ratio was normalized to a single ratio from a mouse in the unstimulated group. Bars are medians. Data analyzed a 2-tailed Mann-Whitney U-test. * $p<0.05$, ** $p<0.01$, *** $p< 0.001$

were quantified. Figure 4-1a,b shows the *in vitro* induction of PARP-14, where PARP-14 mRNA levels peaked at 4 hours, and protein levels peaked at 8 hours following LPS stimulation. Figure 4-1b also demonstrates that PARP-14 protein was detectable at resting basal conditions. PARP-14 induction was also demonstrated *in vivo* by measuring PARP-14 mRNA and protein levels in the heart, lung and liver specimens taken from WT mice in the resting basal state and following LPS stimulation (5μg i.p. for 4 hours) (figure 4-1c-e). Similar to the *in vitro* findings, PARP-14 was also detectable at resting basal conditions *in vivo*.

4.3.2 PARP-14 deficiency increases TF expression

To examine the effect of PARP-14 on TF mRNA expression, WT and *Parp14*$^{-/-}$ macrophages were stimulated with LPS 1μg/mL, and steady state TF mRNA levels were determined (figure 4-2a). TF mRNA levels were significantly increased in Parp14$^{-/-}$ vs. WT macrophages at 2 hours (13.3±2.9 vs. 5.5±0.5 fold induction, p=0.043); at 4 hours (10.2±2.1 vs. 4.0±0.8 fold induction, p=0.026); and at 6 hours (11.8±2.4 vs. 2.7±0.4 fold induction, p=0.013). Whilst there was a trend for the basal TF mRNA levels in unstimulated cells to be higher in *Parp14*$^{-/-}$ macrophages, this was not significant (p=0.07). The TF mRNA levels peaked at 2 hours in both WT and *Parp14*$^{-/-}$ macrophages, but followed by a decline in WT macrophages, whilst remaining relatively stable in *Parp14*$^{-/-}$ macrophages.

To examine the effect of PARP-14 on TF protein expression, TF activity was initially determined. WT and *Parp14*$^{-/-}$ macrophages were stimulated with LPS 1μg/mL, and TF activity was determined at different time points following LPS stimulation (figure 4-2b). TF activity was found to be significantly increased in *Parp14*$^{-/-}$ vs. WT macrophages in unstimulated cells and at every time point following LPS stimulation (all $p<0.05$). In parallel experiments, TF protein was quantified using Western blotting (figures 4-2c,d). TF protein levels were significantly increased in *Parp14*$^{-/-}$ vs. WT macrophages in unstimulated cells and at 2, 4, and 6 hours following LPS stimulation (all $p<0.05$). To further validate, the TF protein data, TF protein was measured using flow cytometric analysis at 6 hours following LPS stimulation (figures 4-2e-g). TF protein was

significantly increased in *Parp14*$^{-/-}$ vs. WT macrophages in both unstimulated cells (3.7±0.1vs. 2.3±0.3, p<0.001) and 6 hours following LPS stimulation (4.6±0.2 vs. 10.6±0.4, p<0.001).

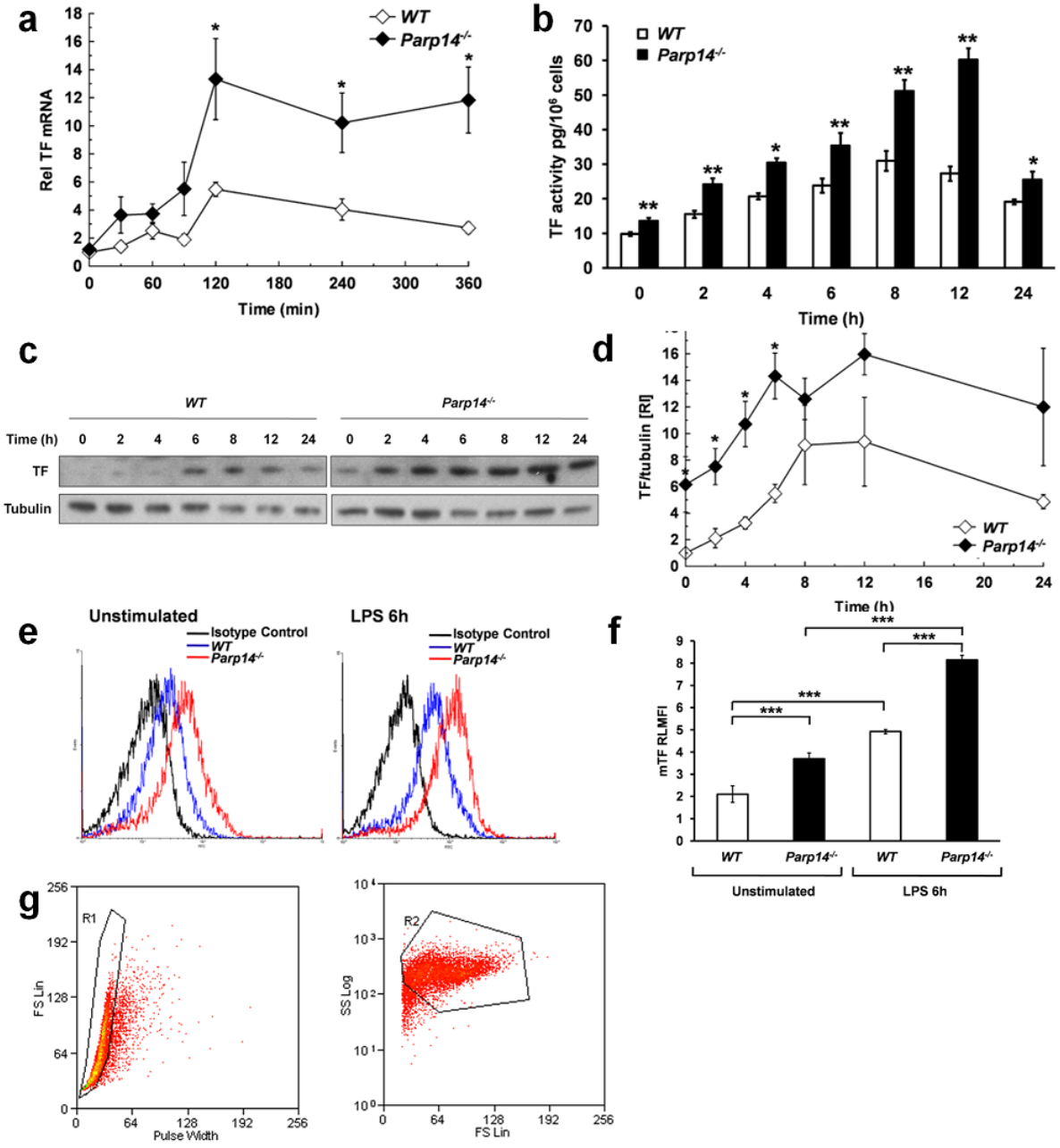

Figure 4-2: The effect of PARP-14 deficiency on TF expression in LPS-stimulated macrophages.
WT and *Parp14*$^{-/-}$ murine macrophages were stimulated with LPS 1µg/mL for times shown following which **(a)** TF mRNA levels were determined using RT-PCR (n=5). TF mRNA levels were normalized to TF mRNA levels for the unstimulated WT sample at time=0; **(b)** TF activity was determined using a turbimetric clot assay, where TF activity was derived from the corresponding TI_{ag} (n=5); **(c)** TF protein levels as determined using Western blotting (n=5). All blots were run on the same gel, but the lanes corresponding to WT and *Parp14*$^{-/-}$ are separated for clarity. Representative blot is shown; **(d)** Densitometric analyses are shown for western blotting experiments with TF immunodensity relative to the tubulin immunodensity normalized to the ratio in unstimulated cells at time=0; **(e)** TF protein expression analyzed using flow cytometric assay with representative histograms from 3 independent experiments; **(f)** Analysis of TF mean fluorescence intensities (MFI) normalised to MFI of isotype control to yield relative MFI (RLMFI) for the representative flow cytometric experiment in (e) with 3-5 experimental replicates; and (g) Gating settings for murine macrophages in the flow cytometry experiments. All data expressed as mean ± SEM and analysed using a 2-tailed Student's t-test. * p<0.05, ** p<0.01, *** p< 0.001

Finally, the effect of increasing LPS concentration on TF mRNA induction was tested (figures 4-3a,b). WT and *Parp14*$^{-/-}$ macrophages were stimulated with LPS 10^{-11}-10^{-5}g/mL and TF mRNA (2 hours) and TF activity (8 hours) were measured. For every respective concentration of LPS, TF mRNA levels were higher in *Parp14*$^{-/-}$ vs. WT macrophages with significant increases at 10^{-8}g/mL (p=0.004), 10^{-6}g/mL (p=0.042) and 10^{-5}g/mL (p=0.028). Similarly, for every respective concentration of LPS, TF activity level was significantly higher in *Parp14*$^{-/-}$ vs. WT macrophages (all p<0.05). A striking observation was that for both TF mRNA and activity levels, the TF response generated with 10^{-5}g/L in WT macrophages was comparable to that generated with 10^{-9}g/L in *Parp14*$^{-/-}$ macrophages, despite a 10,000 fold difference in LPS concentration. These data provided strong evidence that TF expression is increased in *Parp14*$^{-/-}$ vs. WT macrophages following LPS stimulation.

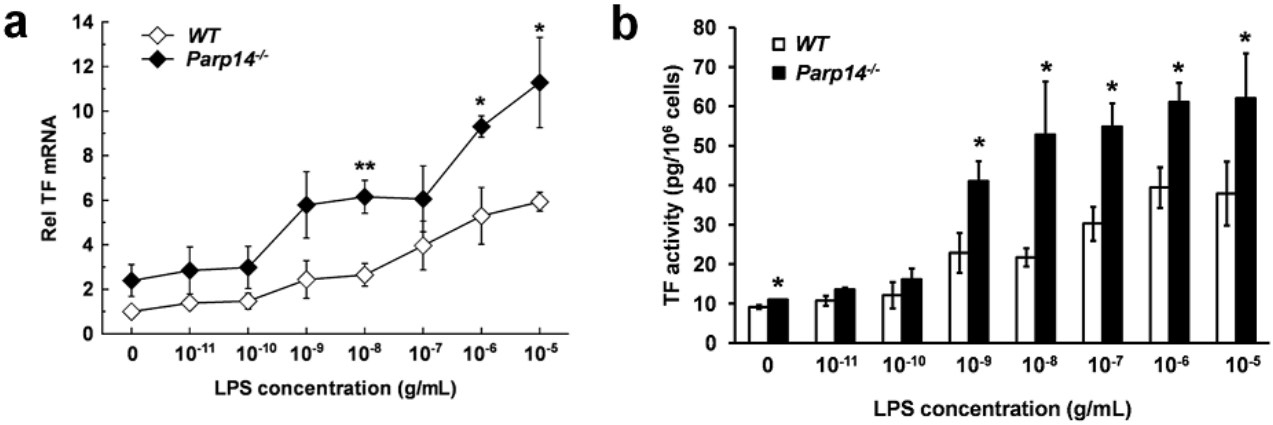

Figure 4-3: The effect of PARP-14 deficiency on TF expression in LPS-stimulated macrophages.
WT and *Parp14*$^{-/-}$ murine macrophages were stimulated with LPS 10^{-5}-10^{-11} g/mL for 2h in **(a)** and 8h in **(b)**. **(a)** TF mRNA levels were determined by RT-PCR and normalized to levels in unstimulated WT macrophages (n=4); and **(b)** TF activity was determined using a turbimetric clot assay, where TF activity was derived from the corresponding TI_{ag} (n=3). All data expressed as mean ± SEM and analysed using a 2-tailed Student's t-test. * p<0.05, ** p<0.01, *** p< 0.001

4.3.3 PARP-14 deficiency increases TF mRNA stability

To test whether, the increased TF expression in *Parp14*$^{-/-}$ macrophages was attributable to an effect on mRNA stability, TF mRNA decay profiles were determined in WT and *Parp14*$^{-/-}$ macrophages (figure 4-4a). TF mRNA stability was significantly increased from 60±5 minutes to 181±11 minutes (p<0.001). Having previously shown that p38 inhibition reduces TF mRNA stability, the effect of p38 inhibition was tested in WT and *Parp14*$^{-/-}$

macrophages (figures 4-4b-d). p38 inhibition using SB203580 1μM reduced TF mRNA stability in WT macrophages, but had no effect in Parp14$^{-/-}$ macrophages (figure 4-4c), comparable to that seen in *Ttp*$^{-/-}$ macrophages (figure 3-7). These data provide evidence that the increased TF expression seen in *Parp14*$^{-/-}$ macrophages, may be attributed, at least in part, to increased TF mRNA stability.

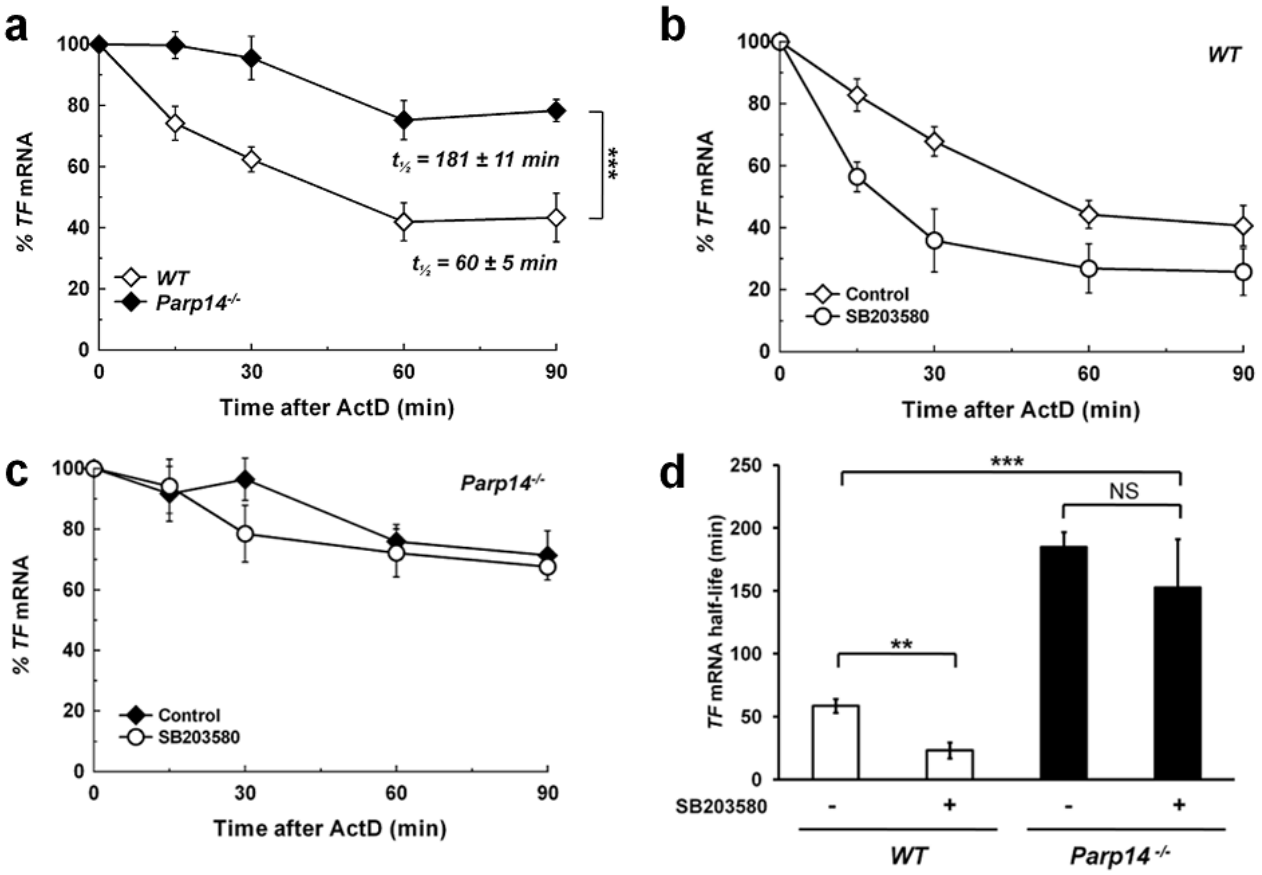

Figure 4-4: The effect of PARP-14 deficiency on TF mRNA stability in LPS-stimulated murine macrophages. WT and *Parp14*$^{-/-}$ murine macrophages were stimulated with LPS 1μg/mL for 2h. Actinomycin D (5μg/mL) was added at 2h to induce transcriptional arrest. Inhibition of p38 was achieved using SB203580 1μM which was added with actinomycin D. TF mRNA levels were determined at each time point and normalized to levels at time point 0 to obtain mRNA decay profiles. The decay profiles were modelled mathematically using non-linear regression analysis to determine mRNA half-life. **(a)** TF mRNA decay profiles in WT vs. *Parp14*$^{-/-}$ macrophages (n=6) and corresponding half-lives shown; **(b)** Effect of p38 inhibition in WT macrophages (n=5); **(c)** Effect of p38 inhibition in *Parp14*$^{-/-}$ macrophages (n=5); and **(d)** Comparison of TF mRNA half lives in WT and *Parp14*$^{-/-}$ macrophages with or without p38 inhibition. Data expressed as mean ± SEM and analysed using a 2-tailed Student's t-test. * $p<0.05$, ** $p<0.01$, *** $p<0.001$. TF mRNA stability is increased in *Parp14*$^{-/-}$ macrophages and p38 inhibition reduces TF mRNA stability in WT but not *Parp14*$^{-/-}$ macrophages.

Given that p38 inhibition had no effect on TF mRNA decay in *Parp14*$^{-/-}$ cells (resembling a *Ttp*$^{-/-}$ phenotype) the possible explanations for the observed increase in TF mRNA stability in *Parp14*$^{-/-}$ macrophages included (a) TTP expression is reduced in *Parp14*$^{-/-}$ cells (thereby reducing the magnitude of the p38-dependent TTP-mediated mRNA degradation), or (b) TTP is unable to interact with TF mRNA in the absence of PARP-14. Thus, the effect of PARP14 on TTP expression was investigated.

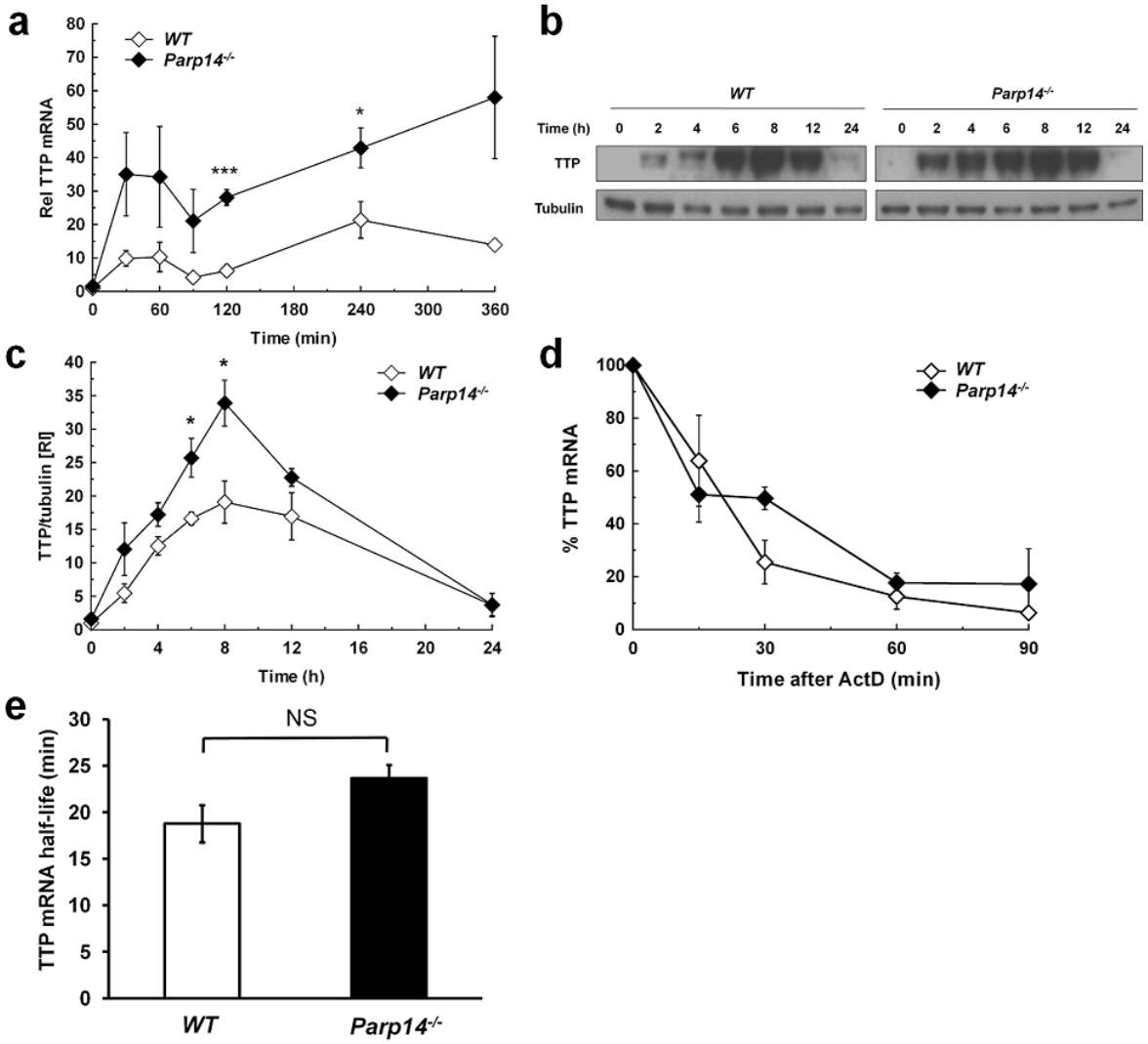

Figure 4-5: The effect of PARP-14 deficiency on TTP expression in LPS-stimulated murine macrophages.
WT and *Parp14*$^{-/-}$ murine macrophages were stimulated with LPS 1µg/mL for times shown. **(a)** TTP mRNA levels were determined using RT-PCR and normalized to levels in unstimulated WT macrophages (n=5); **(b)** TTP protein levels determined using western blotting (n=5). All blots were run on the same gel, but the lanes corresponding to WT and *Parp14*$^{-/-}$ are separated for clarity. Representative blot shown; and quantified in **(c)** using densitometric analysis, where TTP immunodensity relative to the tubulin immunodensity was normalized to the ratio in unstimulated cells at time=0. WT and *Parp14*$^{-/-}$ murine macrophages were stimulated with LPS 1µg/mL for 2h. Actinomycin D (5µg/mL) was added at 2h to induce transcriptional arrest. TTP mRNA levels were determined at each time point and normalized to levels at time point 0 to obtain mRNA decay profiles. The decay profiles were modelled mathematically using non-linear regression analysis to determine mRNA half-life. TTP mRNA decay profiles in WT vs. *Parp14*$^{-/-}$ macrophages (n=6) are shown in **(d)** and corresponding half-lives shown in **(e)**. All data expressed as mean ± SEM and analysed using a 2-tailed Student's t-test. * p<0.05, ** p<0.01, *** p< 0.001. TTP expression is increased in LPS-stimulated *Parp14*$^{-/-}$ macrophages, but this does not appear to be due to an effect on mRNA stability, suggesting a transcriptional mechanism.

WT and *Parp14*$^{-/-}$ macrophages were stimulated with LPS 1µg/mL, and steady state TTP mRNA and protein levels were determined (figures 4-5a-c). TTP mRNA decay was also analyzed at 2 hours following LPS stimulation (figures 4-5d-e). TTP expression was found to be significantly increased in Parp14$^{-/-}$ macrophages both at mRNA and protein level. Given that no significant differences in TTP mRNA stability were observed, these data would imply that this exaggerated TTP response is primarily transcriptional. As TTP expression was actually increased in *Parp14*$^{-/-}$ macrophages, the first of the above 2 explanations could be refuted. The resemblance of a *Ttp*$^{-/-}$ phenotype in *Parp14*$^{-/-}$ macrophages despite increased TTP expression, implied that TTP was unable to mediate its mRNA destabilizing effect, possibly as a result of failure to interact with TF 3'UTR. This was specifically tested below.

4.3.4 PARP-14 deficiency increases TF expression *in vivo*

Having demonstrated increased TF expression in the absence of PARP-14 *in vitro*, the effect of PARP-14 on TF expression was examined *in vivo*, both at resting basal conditions and following LPS stimulation (LPS 5µg i.p. for 4 hours). In addition to determining TF expression from different organs, TF expression was also analyzed in peripheral blood leukocytes to provide a comparison with the effect seen in leukocytes in vitro. WT and *Parp14*$^{-/-}$ mice were sacrificed, citrated venous blood samples were taken and organs (heart, lung, aorta, kidney, liver) were harvested. Blood samples were processed to yield unfractionated leukocyte fractions and sera.

TF mRNA, protein and activity were quantified for all organ tissues, and TF activity was determined for unfractionated leukocytes. There was complete concordance between TF mRNA and TF activity levels throughout all organs, with the exception of the heart following LPS stimulation (figure 4-6, see comments below). In the lungs (figure 4-7), aortae (figure 4-8) and liver (figure 4-9), compared to WT mice, the TF mRNA and activity levels were significantly increased both in the basal state and following LPS stimulation in the *Parp14*$^{-/-}$ mice, with a significant induction in TF response following LPS stimulation, irrespective of genotype. In the kidneys (figure 4-10), the basal TF mRNA and activity levels were similar between WT and *Parp14*$^{-/-}$ mice, but following

LPS stimulation there was significantly greater TF mRNA and activity levels in the *Parp14*$^{-/-}$ mice, again with a significant induction in TF response following LPS stimulation, irrespective of genotype. In the heart, compared to WT mice, TF mRNA and activity levels were significantly increased in *Parp14*$^{-/-}$ mice in the resting basal state. However, following LPS stimulation, a significant reduction in TF mRNA was observed, and the TF activity levels did not change, although still remaining higher in the *Parp14*$^{-/-}$ mice. These anomalous findings for TF expression in the heart following LPS stimulation were in keeping with previously reported studies[173]. Next, TF activity was determined for freshly isolated unfractionated leukocytes from unstimulated and LPS stimulated mice. Although the magnitude of detectable TF activity in peripheral blood leukocytes (which did not contain mcrophages as they had not been allowed to differentiate) was lower than that seen in organ homogenates, in keeping with the organ data, TF activity was increased in *Parp14*$^{-/-}$ mice both at resting basal conditions and following LPS stimulation (figure 4-11a). Taken together, these data indicated that TF expression was increased in *Parp14*$^{-/-}$ mice.

4.3.5 PARP-14 deficiency leads to accelerated thrombus formation *in vivo*

To demonstrate the *in vivo* significance of increased TF expression in the *Parp14*$^{-/-}$ mice, an *in vivo* thrombosis model was used. Using intravital microscopy, in the cremasteric artery model (a murine model for arteriolar thrombosis), time to complete vessel occlusion was determined following ferric chloride vessel injury both in WT and *Parp14*$^{-/-}$ mice at resting basal conditions and following LPS stimulation (LPS 10μg i.p. for 4 hours) (figure 4-11b). At basal levels, no detectable difference was observed between WT and *Parp14*$^{-/-}$ mice. In the WT mice, LPS did not result in a significant reduction in vessel occlusion time. However, in the *Parp14*$^{-/-}$ mice, LPS resulted in significantly accelerated thrombosis with (a) a significant reduction in vessel occlusion time compared to the basal state; and (b) a significant reduction in vessel occlusion time compared to LPS-stimulated WT mice. Collectively, these data demonstrate that PARP-14 deficiency is associated with increased TF expression *in vivo* and increased thrombogenicity in an *in vivo* model of arteriolar thrombosis.

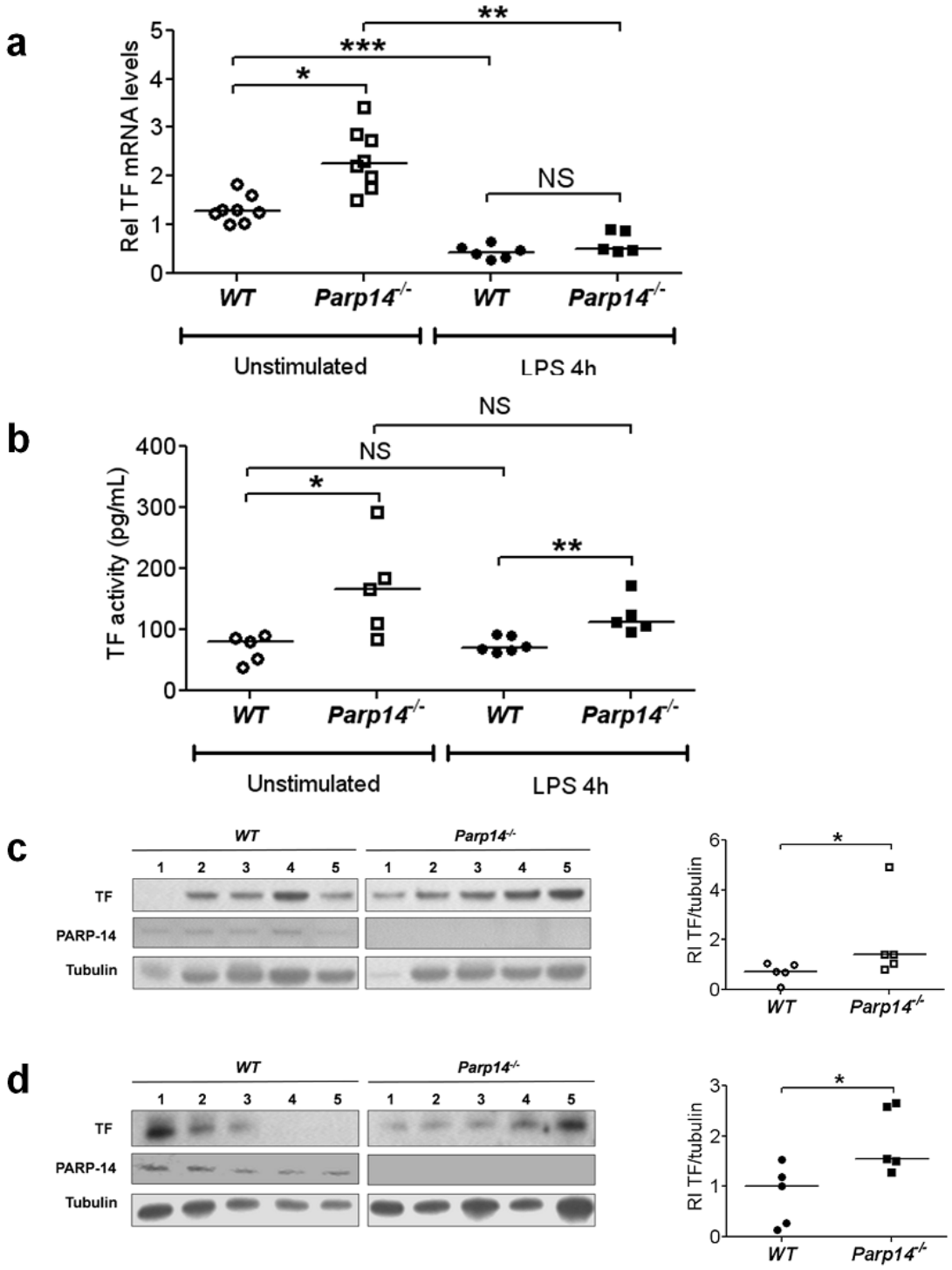

Figure 4-6: The effect of PARP-14 deficiency on TF expression *in vivo* (heart)
WT and *Parp14*$^{-/-}$ murine macrophages were stimulated with LPS 5µg i.p. for 4h and hearts were explanted from unstimulated and LPS-stimulated mice. **(a)** TF mRNA levels were determined using RT-PCR and normalized to a WT mouse in the unstimulated arm of the experiment (n=5-8 mice per group); **(b)** TF activity was determined using a turbimetric clot assay, where TF activity was derived from the corresponding T_{lag} (n=5-6 mice per group); Western blotting analysis of TF protein in **(c)** unstimulated and **(d)** LPS-stimulated mice. Blots are shown on the left and densitometric analyses on the right. All blots were run on the same gel, but the lanes corresponding to WT and *Parp14*$^{-/-}$ are separated for clarity. TF immunodensity relative to the tubulin immunodensity was normalized to the ratio for a WT mouse (n=5 mice per group). All bars represent medians and analysed using a 2-tailed Mann-Whitney U-test. * p<0.05, ** p<0.01, *** p< 0.001.

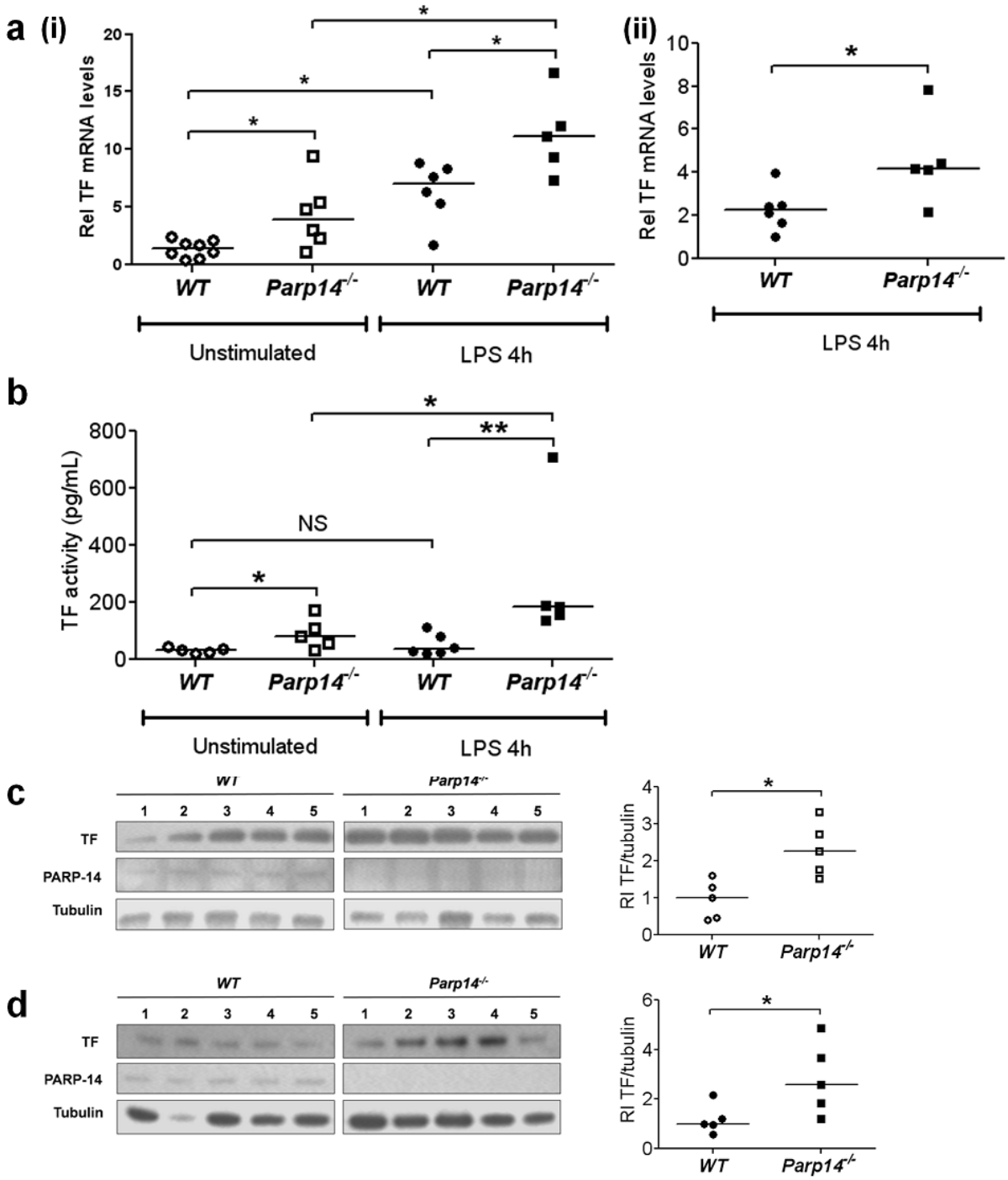

Figure 4-7: The effect of PARP-14 deficiency on TF expression *in vivo* (lung)
WT and *Parp14*$^{-/-}$ murine macrophages were stimulated with LPS 5µg i.p. for 4h and lungs were explanted from unstimulated and LPS-stimulated mice. **(a) (i)** TF mRNA levels were determined using RT-PCR and normalized to a WT mouse in the unstimulated arm of the experiment (n=5-8 mice per group); and **(ii)** Control validation experiment to determine TF mRNA levels in the LPS-stimulated WT and *Parp14*$^{-/-}$ mice using TF primer set 2, using the same cDNA samples as in (i). TF mRNA levels were normalized to a WT mouse. The same pattern is seen using the different primer sets.; **(b)** TF activity was determined using a turbimetric clot assay, where TF activity was derived from the corresponding T_{lag} (n=5-6 mice per group); Western blotting analysis of TF protein in **(c)** unstimulated and **(d)** LPS-stimulated mice. All blots were run on the same gel, but the lanes corresponding to WT and *Parp14*$^{-/-}$ are separated for clarity. Blots are shown on the left and densitometric analyses on the right. TF immunodensity relative to the tubulin immunodensity was normalized to the ratio for a WT mouse (n=5 mice per group). All bars represent medians and analysed using a 2-tailed Mann-Whitney U-test. * $p<0.05$, ** $p<0.01$, *** $p< 0.001$.

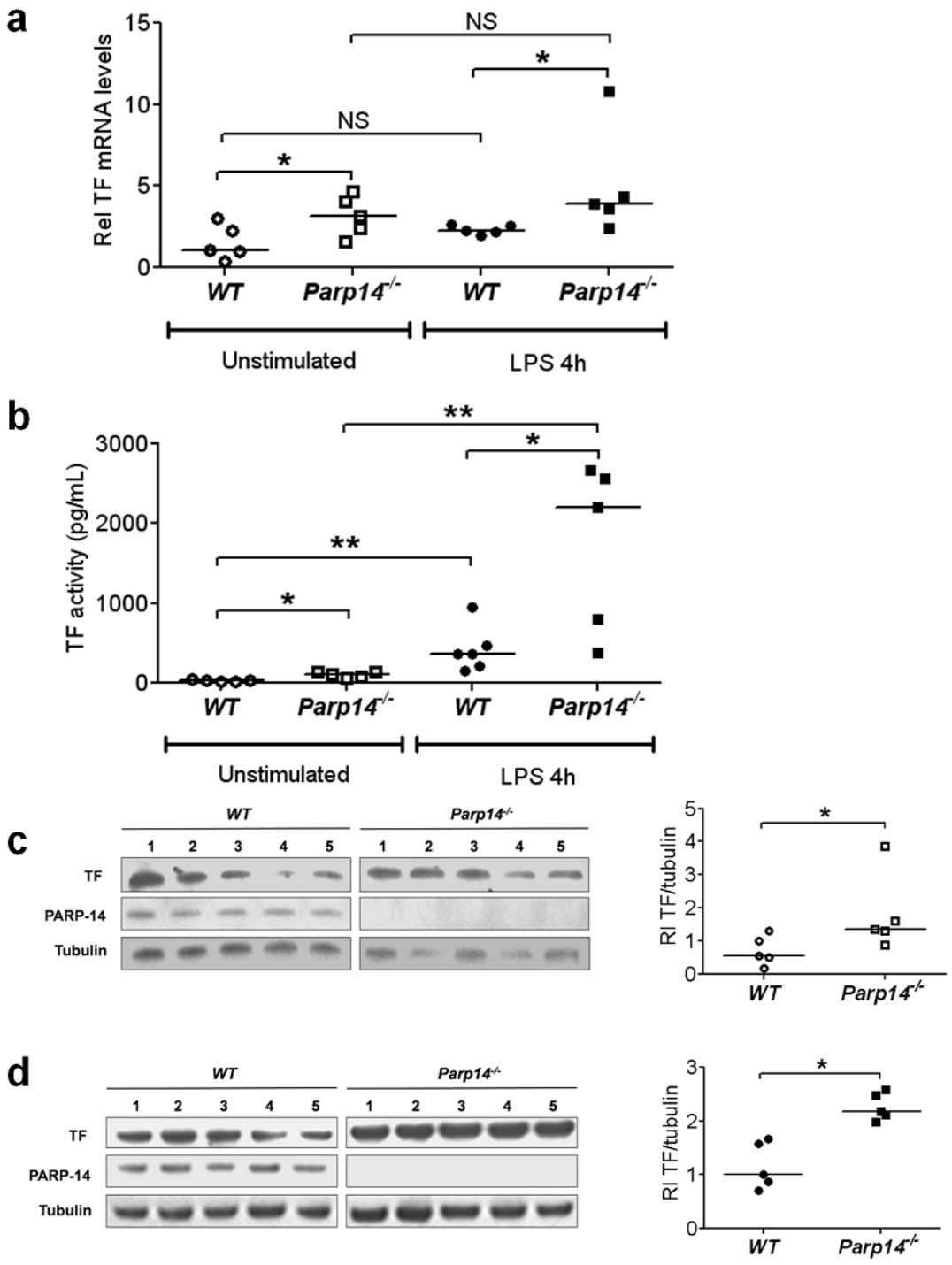

Figure 4-8: The effect of PARP-14 deficiency on TF expression *in vivo* (aorta)
WT and *Parp14*$^{-/-}$ murine macrophages were stimulated with LPS 5µg i.p. for 4h and aortae were explanted from unstimulated and LPS-stimulated mice. **(a)** TF mRNA levels were determined using RT-PCR and normalized to a WT mouse in the unstimulated arm of the experiment (n=5 mice per group); **(b)** TF activity was determined using a turbimetric clot assay, where TF activity was derived from the corresponding T_{lag} (n=5-6 mice per group); Western blotting analysis of TF protein in **(c)** unstimulated and **(d)** LPS-stimulated mice. All blots were run on the same gel, but the lanes corresponding to WT and *Parp14*$^{-/-}$ are separated for clarity. Blots are shown on the left and densitometric analyses on the right. TF immunodensity relative to the tubulin immunodensity was normalized to the ratio for a WT mouse (n=5 mice per group). All bars represent medians and analysed using a 2-tailed Mann-Whitney U-test. * $p<0.05$, ** $p<0.01$, *** $p< 0.001$.

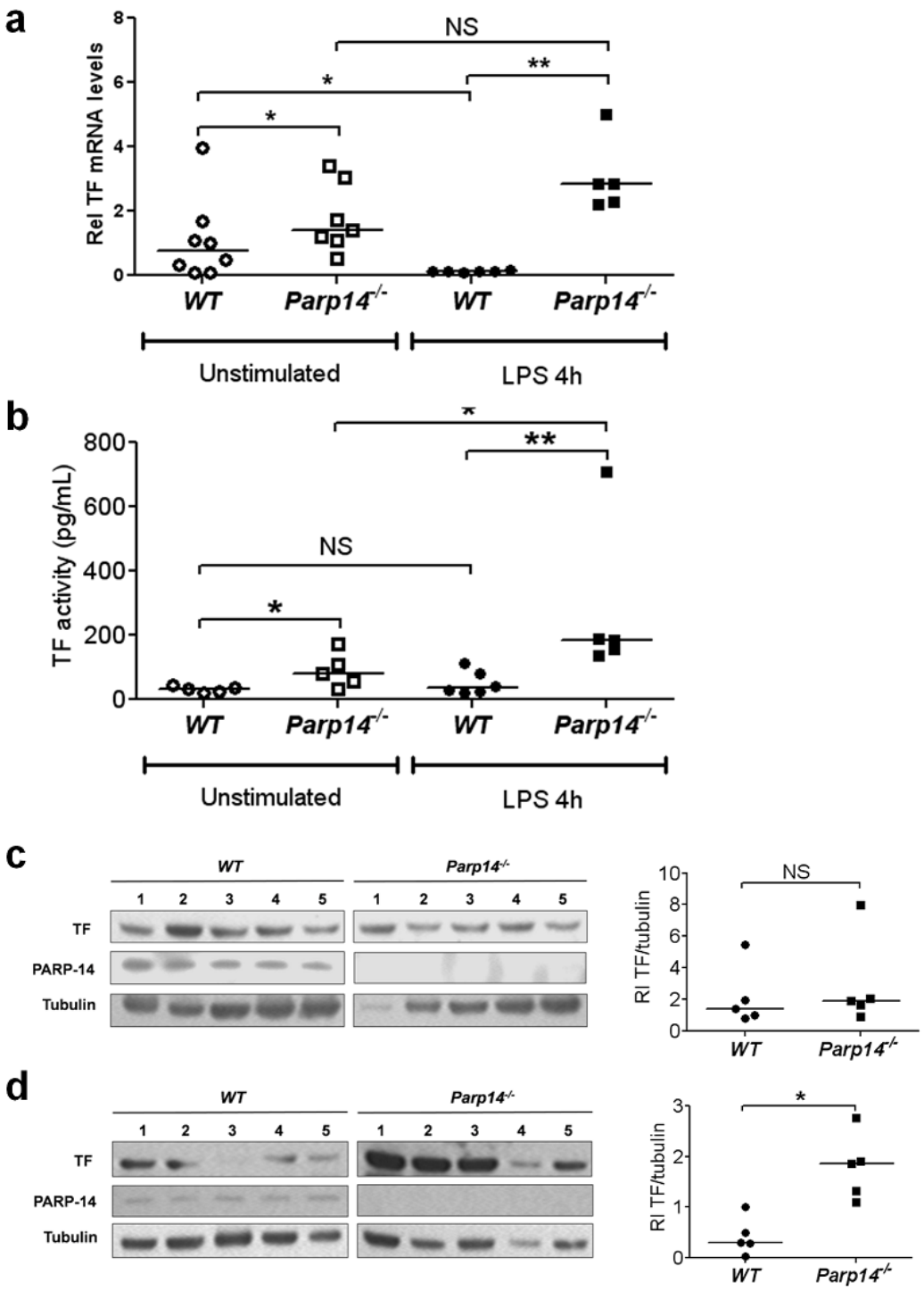

Figure 4-9: The effect of PARP-14 deficiency on TF expression *in vivo* (liver)
WT and *Parp14*$^{-/-}$ murine macrophages were stimulated with LPS 5µg i.p. for 4h and livers were explanted from unstimulated and LPS-stimulated mice. **(a)** TF mRNA levels were determined using RT-PCR and normalized to a WT mouse in the unstimulated arm of the experiment (n=5-8 mice per group); **(b)** TF activity was determined using a turbimetric clot assay, where TF activity was derived from the corresponding T_{lag} (n=5-6 mice per group); Western blotting analysis of TF protein in **(c)** unstimulated and **(d)** LPS-stimulated mice. All blots were run on the same gel, but the lanes corresponding to WT and *Parp14*$^{-/-}$ are separated for clarity. Blots are shown on the left and densitometric analyses on the right. TF immunodensity relative to the tubulin immunodensity was normalized to the ratio for a WT mouse (n=5 mice per group). All bars represent medians and analysed using a 2-tailed Mann-Whitney U-test. * $p<0.05$, ** $p<0.01$, *** $p< 0.001$.

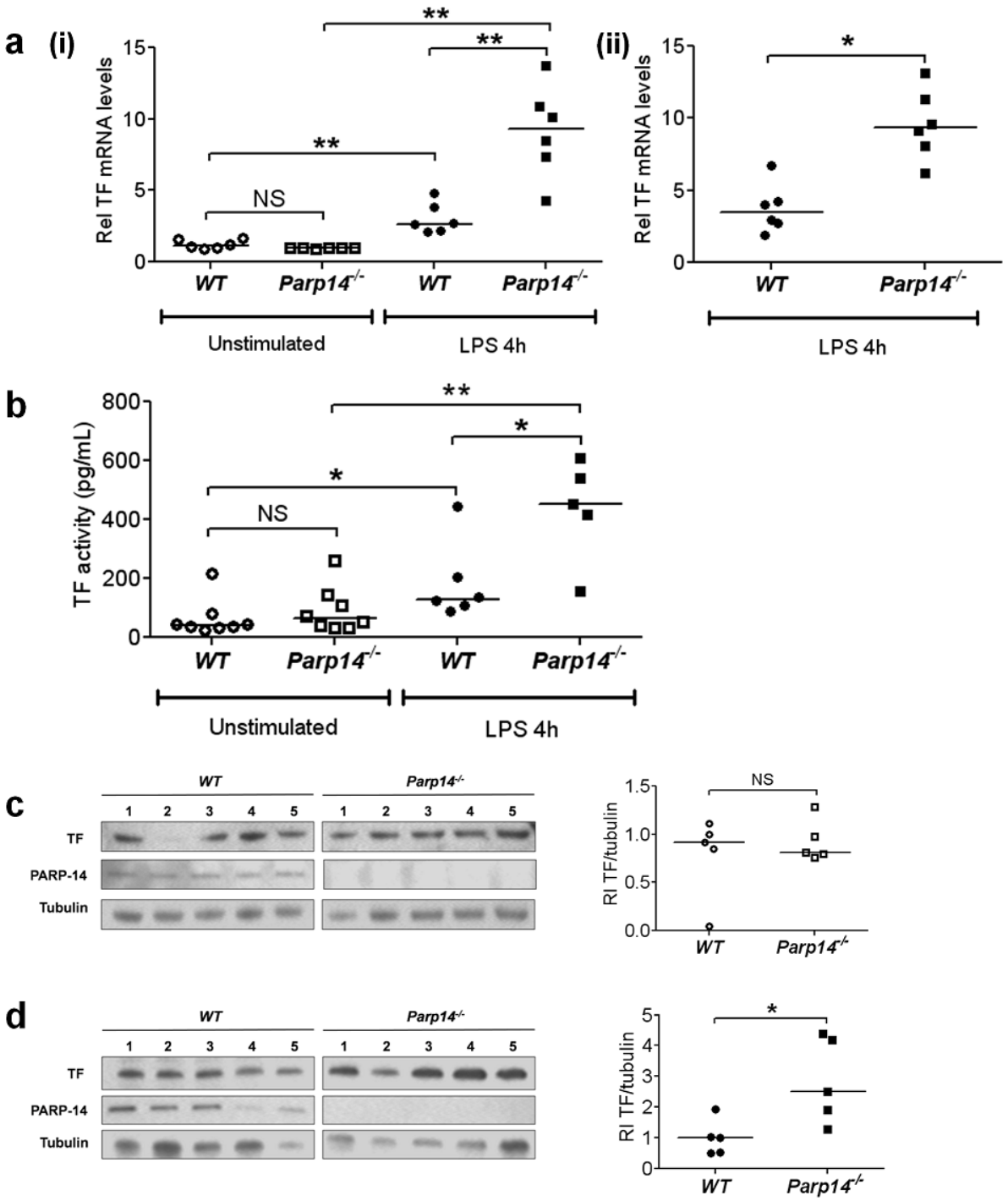

Figure 4-10: The effect of PARP-14 deficiency on TF expression *in vivo* (kidney)
WT and *Parp14*$^{-/-}$ murine macrophages were stimulated with LPS 5µg i.p. for 4h and kidneys were explanted from unstimulated and LPS-stimulated mice. **(a) (i)** TF mRNA levels were determined using RT-PCR and normalized to a WT mouse in the unstimulated arm of the experiment (n=6 mice per group); and **(ii)** Control validation experiment to determine TF mRNA levels in the LPS-stimulated WT and *Parp14*$^{-/-}$ mice using TF primer set 2, using the same cDNA samples as in (i). TF mRNA levels were normalized to a WT mouse. The same pattern is seen using the different primer sets.; **(b)** TF activity was determined using a turbimetric clot assay, where TF activity was derived from the corresponding T_{lag} (n=5-8 mice per group); Western blotting analysis of TF protein in **(c)** unstimulated and **(d)** LPS-stimulated mice. All blots were run on the same gel, but the lanes corresponding to WT and *Parp14*$^{-/-}$ are separated for clarity. Blots are shown on the left and densitometric analyses on the right. TF immunodensity relative to the tubulin immunodensity was normalized to the ratio for a WT mouse (n=5 mice per group). All bars represent medians and analysed using a 2-tailed Mann-Whitney U-test. * $p<0.05$, ** $p<0.01$, *** $p< 0.001$.

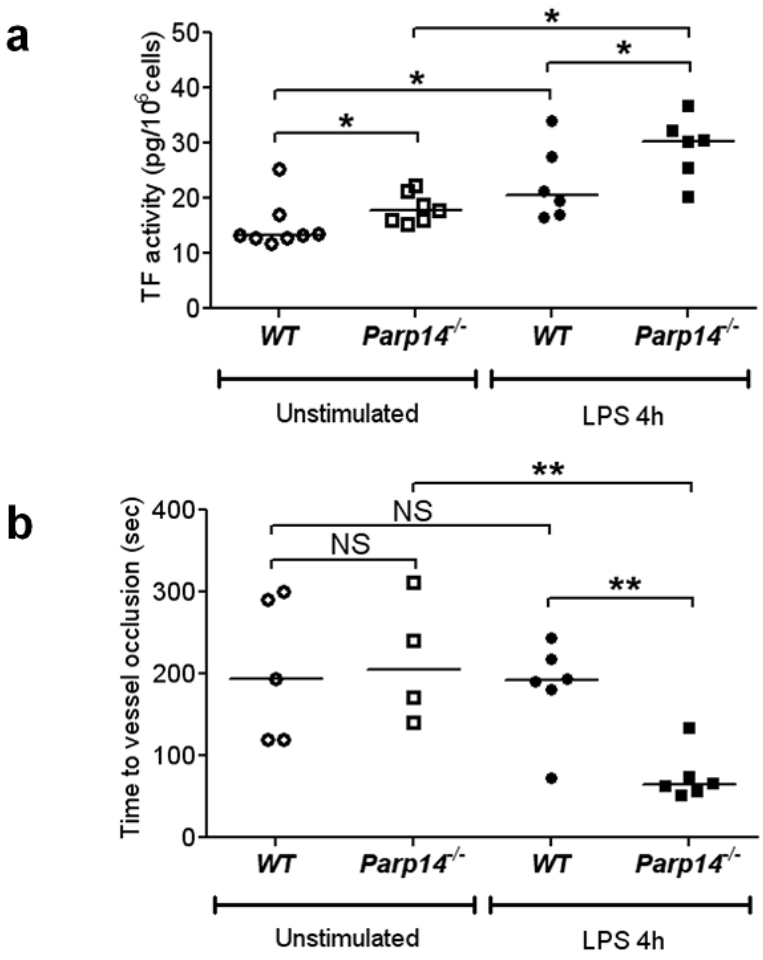

Figure 4-11: The effect of PARP-14 deficiency on procoagulant activity *in vivo*
(a) WT and *Parp14*$^{-/-}$ murine macrophages were stimulated with LPS 5µg i.p. for 4h and peripheral unfractionated leukocytes were isolated. Leukocyte TF activity was determined using a turbimetric clot assay, where TF activity was derived from the corresponding T_{lag} (n=5-6 mice per group); **(b)** *In vivo* thrombogenicity was assessed using intravital microscopy using a ferric chloride model of arteriolar thrombosis and measuring time to complete occlusion of the cremasteric artery. All bars represent medians and analysed using a 2-tailed Mann-Whitney U-test. * $p<0.05$, ** $p<0.01$, *** $p< 0.001$.

4.3.6 PARP-14 interacts with TF mRNA

Having demonstrated that PARP regulates TF mRNA stability, it was crucial to establish whether, indeed, it interacts with TF mRNA. RNP immunoprecipitation assays were performed using a rabbit anti-PARP-14 and rabbit IgG control antibody using lysates prepared from LPS-stimulated WT and *Parp14*$^{-/-}$ macrophages. Following immunoprecipitation of the ribonucleoprotein complexes, the mRNA species bound to PARP-14 were amplified using TF specific primers. HPRT and GAPDH were also amplified using the appropriate primers to control for non-specific pulldown. The PCR

products were visualized on a 2% agarose gel with ethidium bromide. Figure 4-12a demonstrates that TF transcript was bound to PARP-14, which was not observed with the IgG control. Given, that PARP-14 antibody recognizes other non-specific proteins (as seen in Western blot in figure 4-12b), the specificity of PARP-14 for TF mRNA was demonstrated by the inability to detect TF mRNA when using lysates from *Parp14*$^{-/-}$ macrophages. These data confirmed that PARP-14 associates with TF mRNA in murine macrophages.

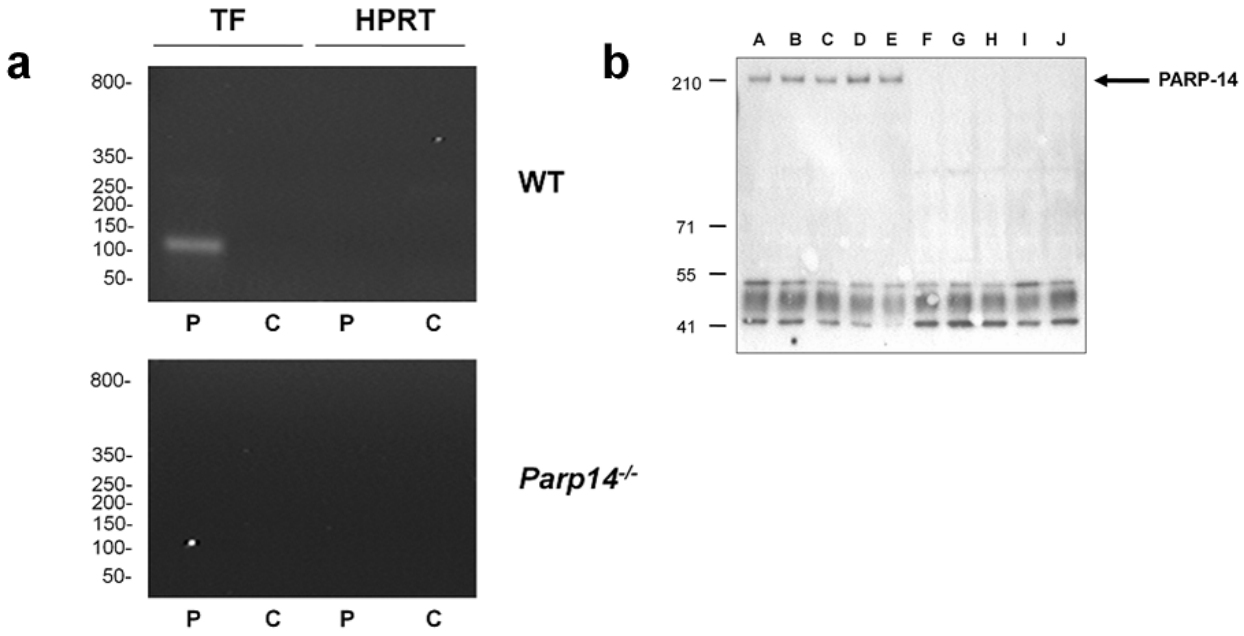

Figure 4-12: PARP-14 interacts with TF mRNA
Interaction of PARP-14 with TF mRNA as shown with RNP immunoprecipitation assays. **(a)** RT-PCR of TF mRNA immunoprecipitated by anti-PARP-14 antibody (P) compared to rabbit IgG control (C) from lysates of LPS-treated WT (top panel) and *Parp14*$^{-/-}$ (lower panel) murine macrophages (1 µg/ml for 2 h). The amplicon length of murine TF PCR product is 105bp. HPRT provides a negative control mRNA (amplicon length=134bp). Representative of 2 independent experiments; **(b)** Western blot demonstrating the non-specific bands seen with the anti-PARP-14 antibody. Macrophages were stimulated with LPS 1 µg/ml for 6h. 15 µg protein lysate per lane. Lanes A-E represent WT macrophages and lanes F-J represent *Parp14*$^{-/-}$ macrophages. Each lane represents a different mouse.

4.3.7 PARP-14 interacts with TF 3'UTR

Having determined that PARP-14 interacts with TF mRNA, to specifically test whether it associates with TF 3'UTR, an RNA-biotin pulldown assay was used. TF 3'UTR sequences for both mouse and human TF 3'UTR were cloned and corresponding biotinylated sense and anti-sense RNA strands were synthesized using *in vitro* transcription. The anti-sense strand served as an internal control for each reaction. The

Figure 4-13: PARP-14 interacts with TF 3'UTR
Interaction of PARP-14 with TF 3'UTR as shown with RNA-biotin pulldown assays. **(a)** Western blots of proteins isolated from lysates of LPS-treated WT macrophages (1 µg/ml for 2 h) by streptavidin beads coated with biotinylated sense (+) or anti-sense (-) murine TF 3'UTR. Tubulin serves as a negative marker for non-specific protein binding to beads; and **(b)** Western blots of proteins isolated from lysates of LPS-treated WT macrophages (1 µg/ml for 2 h) by streptavidin beads coated with biotinylated sense (+) or anti-sense (-) human TF 3'UTR. The TTP-TF 3'UTR interaction demonstrates species cross-reactivity. Representative of 3 independent experiments.

biotinylated RNA strands were incubated with lysates prepared from LPS-stimulated murine macrophages. The biotinylated transcripts were captured using Dynabeads® and the associated proteins resolved by Western blotting. Figure 4-13a shows that PARP-14 associates with murine TF 3'UTR in lysates prepared from WT macrophages. The experiment was controlled by detecting for tubulin which serves as a marker for non-specific binding. The 3'UTR between mouse and human is highly conserved. In the previous chapter, inter-species specificity was shown for TTP-TF 3'UTR binding. To test whether inter-species specificity exists for the PARP-14-TF 3'UTR interaction, an RNA-biotin pulldown assay was performed where biotinylated human 3'UTR sequences were incubated with WT murine macrophage lysates. Figure 4-13b demonstrates that murine PARP-14 interacts with human TF 3'UTR sequence, confirming cross-species specificity for PARP-14 and TF 3'UTR interaction. These data provide evidence that PARP-14 interacts specifically with the 3'UTR of TF.

4.3.8 PARP-14 and TTP form a ternary complex with TF 3'UTR

Both mouse and human TF 3'UTR contain 4 conserved ARE segments. Using truncations and mutational analyses of the murine TF 3'UTR sequence, TTP was found to associate with the final palindromic ARE (AUAAUUUAUUUAAUA), within which 2 overlapping nonamers (AUUUAUUUA and UUAUUUAAU) were found to be functional in mediating TTP binding. Using a similar strategy, the specific binding of PARP-14 to the TF 3'UTR was investigated. RNA-biotin pulldown assays were performed with both sense and anti-sense RNA strands corresponding to the WT TF 3'UTR, truncated and

mutant sequences. Lysates were prepared from LPS-stimulated WT murine macrophages. PARP-14 binding to the TF 3'UTR was found to mirror the binding as observed with TTP. Figure 4-14b shows that both PARP-14 and TTP associate only with transcripts that contains the final ARE. Next, focusing on the final palindromic ARE sequence, PARP-14 binding appeared to bind in a similar pattern to TTP, where PARP-14 binding was not affected by mutations within the palindromic sequence as long as the nonameric sequences were preserved. Mutations of each of the separate nonamers reduced, but did not abolish, PARP-14 binding, but mutations of both nonamers completely abolished PARP-14 binding (figure 4-15a). This was further confirmed using a competition RNA-biotin pulldown assay, where the addition of the cold WT transcripts significantly reduced PARP-14 binding to the biotinylated transcripts captured by the beads. However, the cold mutant transcripts did not affect binding. These data provided evidence that the 2 nonameric sequences within the final palindromic ARE in TF 3'UTR mediate PARP-14 interaction in a cooperative fashion (figure 4-15b).

Given that both PARP-14 and TTP bind the same ARE segment of TF 3'UTR, the inter-dependency for this interaction was next investigated. RNA-biotin pull down assays were performed in LPS-stimulated lysates from WT, *Parp14*$^{-/-}$ and *Ttp*$^{-/-}$ macrophages. The lysates from the *Parp14*$^{-/-}$ and *Ttp*$^{-/-}$ macrophages provide an important experimental tool to investigate protein-RNA binding in the absence of specific proteins, PARP-14 and TTP respectively. Figure 4-16a shows that in the absence of PARP-14, TTP does not bind to the TF 3'UTR. Similarly, in the absence of TTP, PARP-14 binding is significantly reduced. These data demonstrate an inter-dependency for both proteins to bind TF 3'UTR. Next, the specific role for RNA in mediating this interaction was investigated. Co-immunoprecipitation studies were performed, where TTP was immunoprecipitated using a goat anti-TTP antibody and goat IgG control. Figure 4-16b shows that following immunoprecipitation of TTP, PARP-14 could also be co-immunoprecipitated. However, treatment of the lysates with RNase resulted in the loss of PARP-14 in the immunoprecipitate. These data indicate that PARP-14 and TTP form a ternary complex with RNA, where TTP, PARP-14 and RNA are all necessary components for this complex.

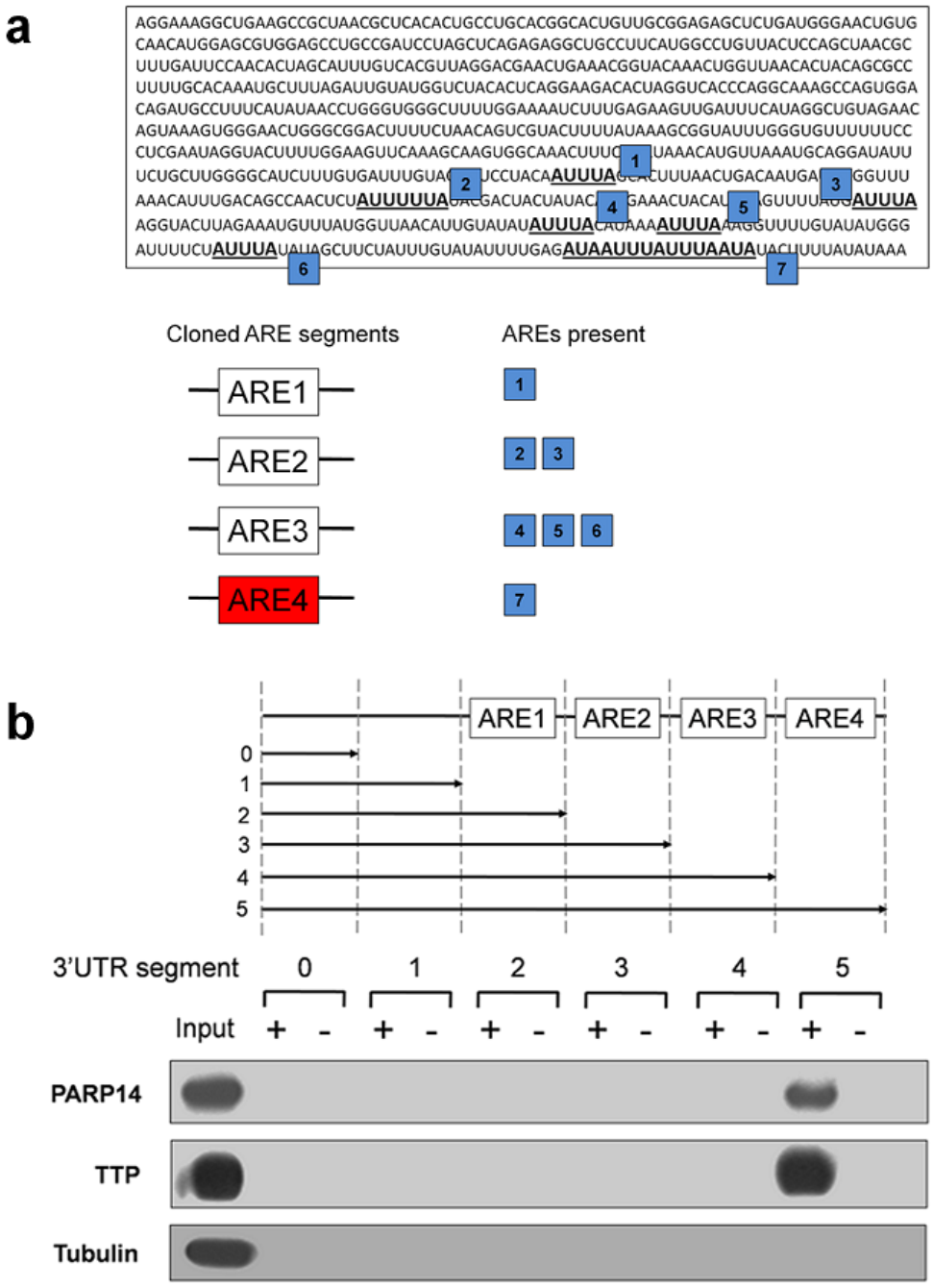

Figure 4-14: The specifics of the interaction between PARP-14, TTP and TF 3'UTR
RNA-biotin pull down assays conducted with lysates of LPS-treated WT macrophages (1 μg/ml for 2 h) by streptavidin beads coated with biotinylated sense (+) or anti-sense (-) human TF 3'UTR. The biotinylated RNA sequences represent different cloned 3'UTR segments. **(a)** Figure showing the cloned ARE segments and the specific AREs contained within. ARE 4 contains the final palindromic ARE sequence; **(b)** RNA – biotin pulldown assays performed for different cloned 3'UTR segments and western blots of proteins isolated. TTP and PARP-14 appear to interact with the 3'UTR sequence that contains the final palindromic ARE. Representative of 2 independent experiments.

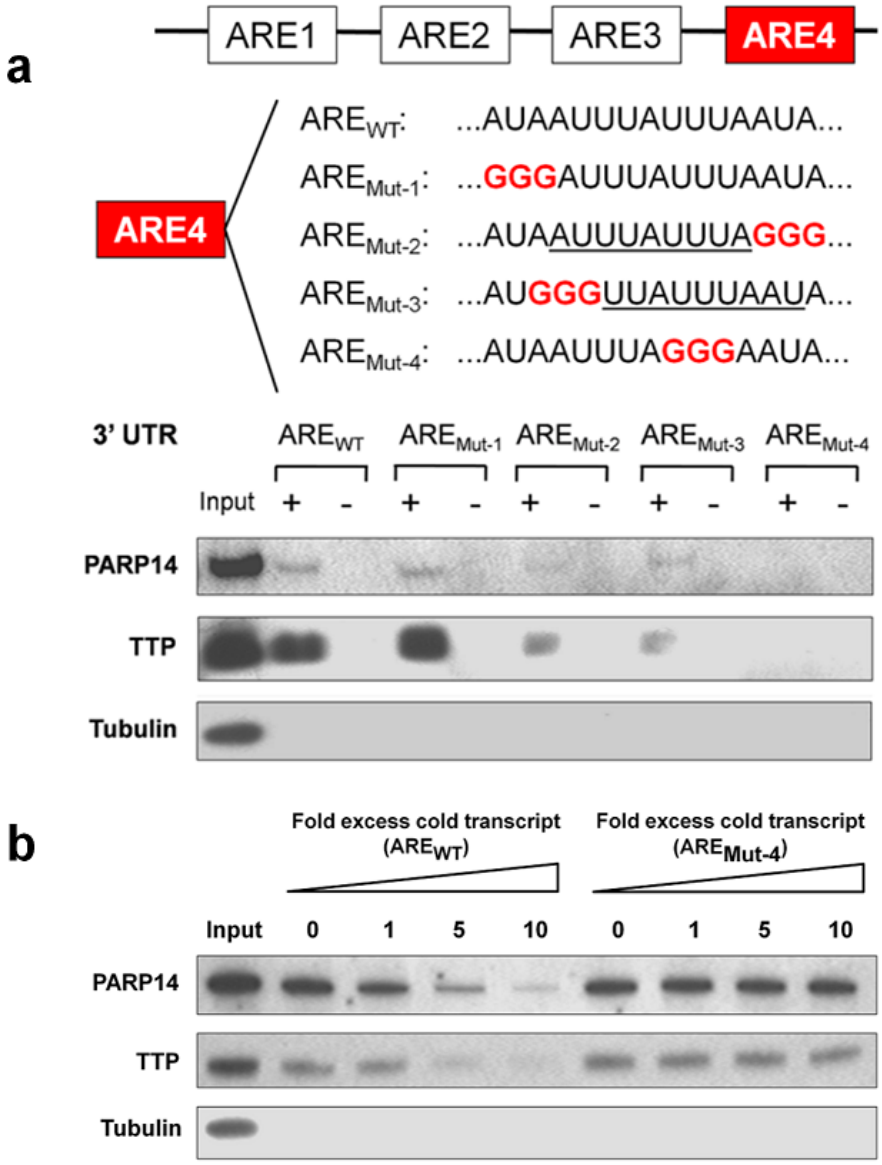

Figure 4-15: Defining the ARE sequences within TF 3'UTR that mediate binding to PARP-14 and TTP The final ARE contains 2 overlapping nonameric sequences with high predictive binding to ARE-binding proteins (underlined). Focusing on this ARE, 4 mutated sequences were generated as shown, and binding to PARP-14 and TTP was interrogated using RNA-biotin pulldown assays. RNA-biotin pull down assays were conducted with lysates of LPS-treated WT macrophages (1 µg/ml for 2 h by streptavidin beads coated with biotinylated sense (+) or anti-sense (-) murine TF 3'UTR (WT or mutant sequences). **(a)** Western blots of proteins isolated. Tubulin acts as a control for non-specific pull-down. PARP-14 and TTP appear to interact with the 3'UTR sequence that contains the final palindromic ARE. Representative of 2 independent experiments. Mutations of each of the separate nonamers reduced, but did not abolish PARP-14 and TTP binding. Mutations of both nonamers by substituting the shared UUU with GGG (ARE_{Mut-4}) completely abolished PARP-14 and TTP binding; **(b)** Competition RNA-biotin pulldown assay was performed, using cold unlabelled transcripts (WT and ARE_{Mut-4}) which if able to bind PARP-14 and TTP would compete with the biotin-labelled WT transcripts coated on the streptavidin beads. Western blots of proteins isolated show that the cold mutant transcripts do not affect PARP-14 and TTP binding, whilst the cold WT transcripts compete with binding. Representative of 2 independent experiments.

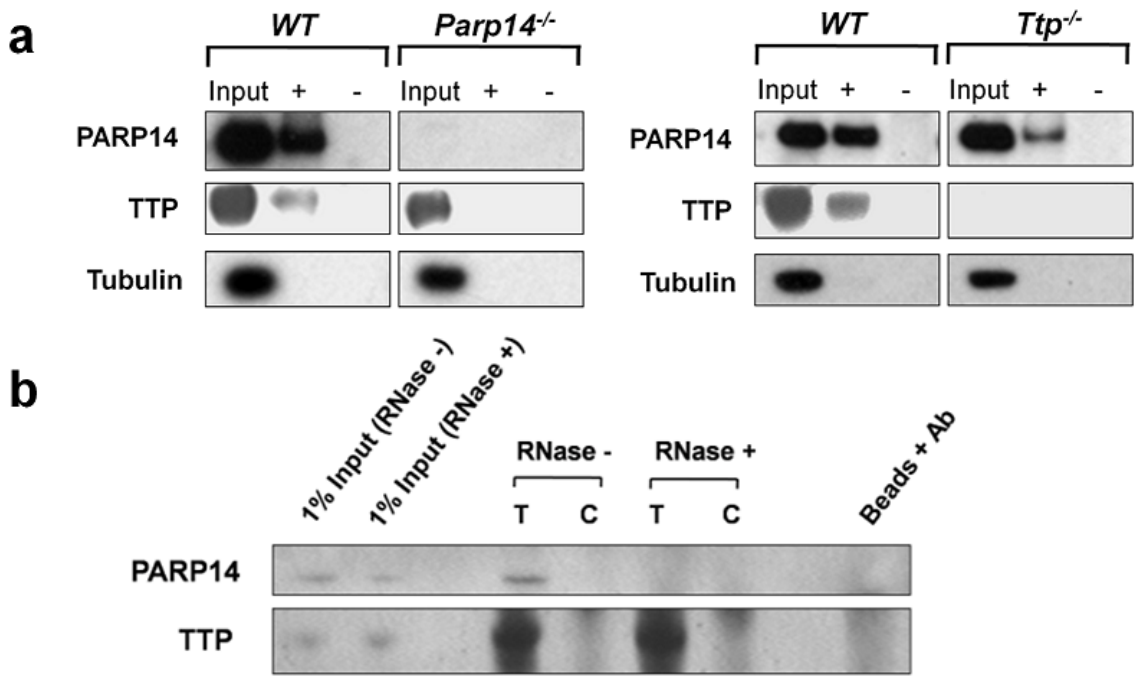

Figure 4-16: PARP-14 and TTP form a ternary complex with TF mRNA
RNA-biotin pull down assays were conducted with lysates of LPS-treated WT, *Parp14*$^{-/-}$ and *Ttp*$^{-/-}$ macrophages (1 µg/ml for 2 h) and streptavidin beads coated with biotinylated sense (+) or anti-sense (-) murine TF 3'UTR. **(a)** Western blots of proteins isolated. All blots were run on the same gel, but the lanes corresponding to WT, *Parp14*$^{-/-}$ *and Ttp*$^{-/-}$ are separated for clarity. Tubulin acts as a control for non-specific pull-down. The panels on the left are representative of 2 independent experiments using WT and *Parp14*$^{-/-}$ lysates, and the panels on the right are representative of 2 independent experiments using WT and *Ttp*$^{-/-}$ lysates. For each experiment all lanes were run on the same gel, but have been separated for clarity. TTP does not bind TF 3'UTR in the absence of PARP-14, and PAPR-14 binding to TF 3'UTR is reduced in the absence of TTP; **(b)** Co-immunoprecipitation assays where western blots of proteins immunoprecipitated from LPS-stimulated WT lysates with anti-TTP antibody (T) or goat IgG control (C) are shown. The figure shows that TTP was successfully pulled down with anti-TTP antibody irrespective of RNase treatment. However, co-immunoprecipitation of PARP-14 was abolished by prior treatment of the lysate with RNase (RNase +). Representative of 2 independent experiments.

4.3.9 PARP-14 enzymatic activity reduces TF mRNA stability

Given that PARP-14 is necessary for TTP binding to the TF 3'UTR and mediating mRNA decay, the specific role for the PARP enzymatic activity of PARP-14 and its relevance to the post-transcriptional regulation of TF mRNA was investigated. TF mRNA decay profiles were determined in WT and *Parp14*$^{-/-}$ macrophages, both in the presence and absence of 2 specific PARP inhibitors, PJ34 10µM and 3AB 1mM (figures 4-17a-c). Parallel experiments were also conducted in WT macrophages where the combined effect of both PARP and p38 inhibition was tested using PJ34 10 µM and

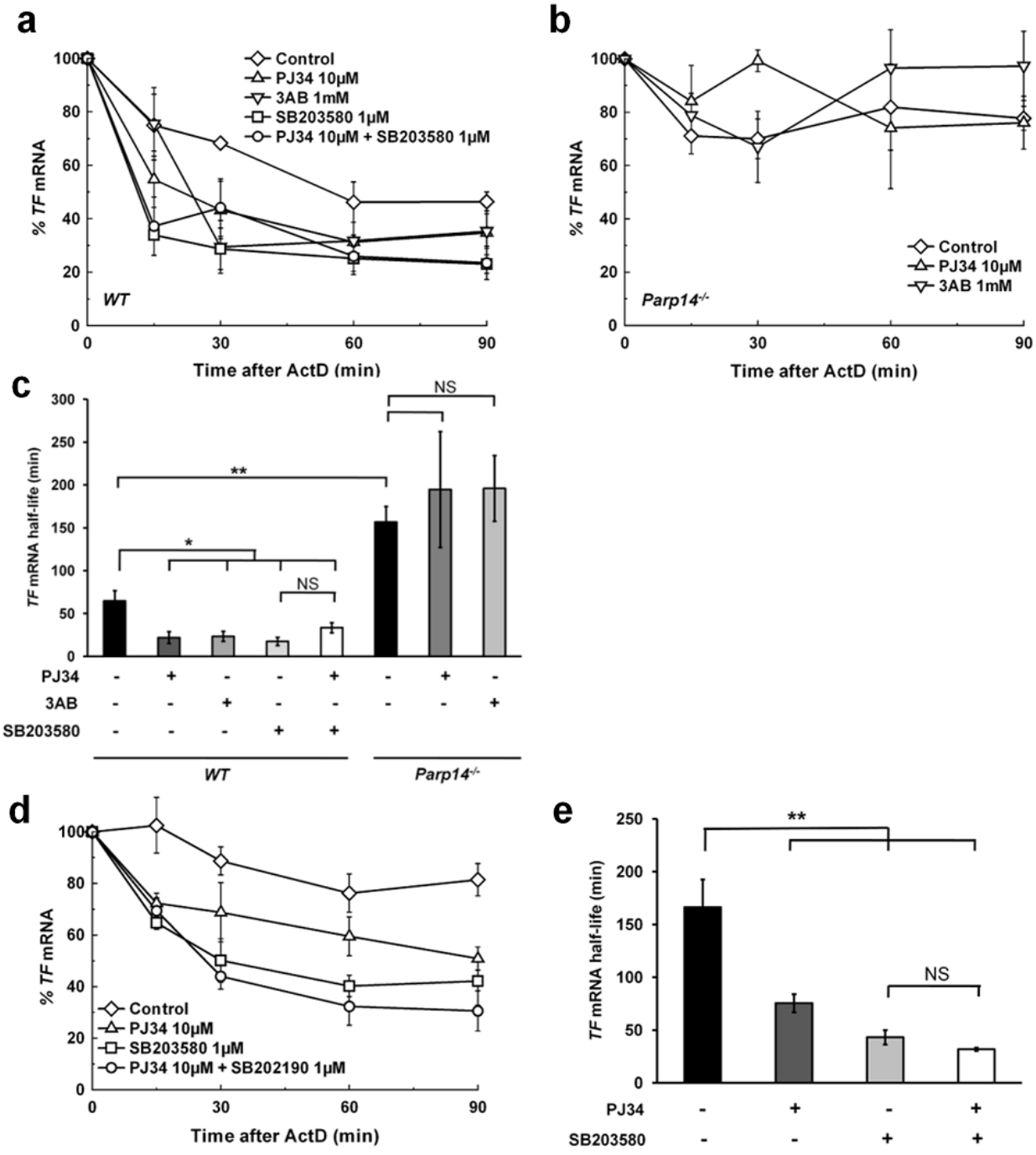

Figure 4-17: The effect of PARP inhibition on TF mRNA stability in LPS-stimulated macrophages
WT or *Parp14*$^{-/-}$ murine macrophages **(a-c)** and human monocytes (**d,e)**, were stimulated with LPS 1μg/mL for 2h. Actinomycin D (5μg/mL) was added at 2h to induce transcriptional arrest. PJ34 10μM, 3AB 1mM and SB203580 1μM were added with actinomycin D. TF mRNA levels were determined at each time point and normalized to levels at time point 0 to obtain mRNA decay profiles. The decay profiles were modelled mathematically using non-linear regression analysis to determine mRNA half-life. TF mRNA decay profiles in WT and *Parp14*$^{-/-}$ macrophages (n=5) are shown in **(a,b)** and corresponding half-lives shown and compared in **(c)**. PARP inhibition accelerated TF mRNA decay in WT cells, comparable to p38 inhibition, but had no effect in *Parp-14*$^{-/-}$ cells. TF mRNA decay profiles in primary human monocytes (n=4) are shown in **(d)** and corresponding half-lives shown and compared in **(e)**; Data expressed as mean ± SEM and analysed using a 2-tailed Student's t-test. * $p<0.05$, ** $p<0.01$, *** $p< 0.001$..

SB203580 1 μM. Macrophages were stimulated with LPS 1μg/mL and TF mRNA decay was determined at 2 hours. The TF mRNA half-life in WT macrophages was 65±12 minutes, and PARP inhibition using the 2 different compounds resulted in a significant reduction in TF mRNA stability (t½=22±7 minutes (p=0.018) and 24±6 minutes (p=0.041) for PJ34 and 3AB respectively). This effect was comparable to that achieved with p38 inhibition (t½=18±5 minutes; p=0.454 compared to PJ34; and p=0.305 compared to 3AB). In the *Parp14*$^{-/-}$ macrophages, PARP inhibition did not have any significant effect on TF mRNA stability. Similarly, the effect of PARP inhibition on TF mRNA stability was also tested in primary human monocytes (figures 4-17d,e). Analogous to the findings in murine macrophages, PARP inhibition with PJ34 10μM resulted in a significant reduction in TF mRNA stability (t½=76±9 minutes vs. 166±26 minutes, PJ34 vs. control, p=0.017). However, the effect of p38 inhibition was greater in human monocytes (t½=43±7 minutes; p=0.008 compared to control; p=0.022 compared to PJ34). Furthermore, combined p38 and PARP inhibition had no additive destabilizing effect. Taken together these data provide preliminary evidence for the importance of the enzymatic activity of PARP-14, and particularly, the role for ADP-ribosylation in the regulation of TF mRNA stability.

The effect of PARP inhibitors on TF mRNA stability was further characterized. To account for the observation that PARP inhibition results in increased TF mRNA decay, one may propose that PARP inhibition may result in either (a) reduced phospho-p38 levels (which may then promote TTP-mediated TF mRNA decay); (b) alter the binding of TTP and/or PAPR-14 to TF 3'UTR; or (c) inhibit ADP-ribosylation of TTP, PARP-14 or other candidate protein which may ultimately increase TF mRNA decay. The first of these hypotheses was tested using western blotting analyses of total and phospho-p38 levels in WT and *Parp14*$^{-/-}$ macrophages following LPS stimulation. As shown in figure 4-18a, there were no significant differences in phospho-p38 levels following LPS stimulation (1μg/mL) in WT and *Parp14*$^{-/-}$ macrophages, indicating PARP-14 in unlikely to affect p38 activity. To specifically examine the role of PARP inhibition on p38 activity, western blotting analyses of total and phospho-p38 levels in WT macrophages was conducted following LPS stimulation (1μg/mL), where cells were stimulated with LPS for

2 hours, and in certain arms of the experiment p38 and PARP inhibition was achieved using SB203580 1μM and PJ34 10μM. These inhibitors were added 15 minutes prior to protein lysate preparation, following which total and phospho-p38 levels were determined using western blotting analysis.

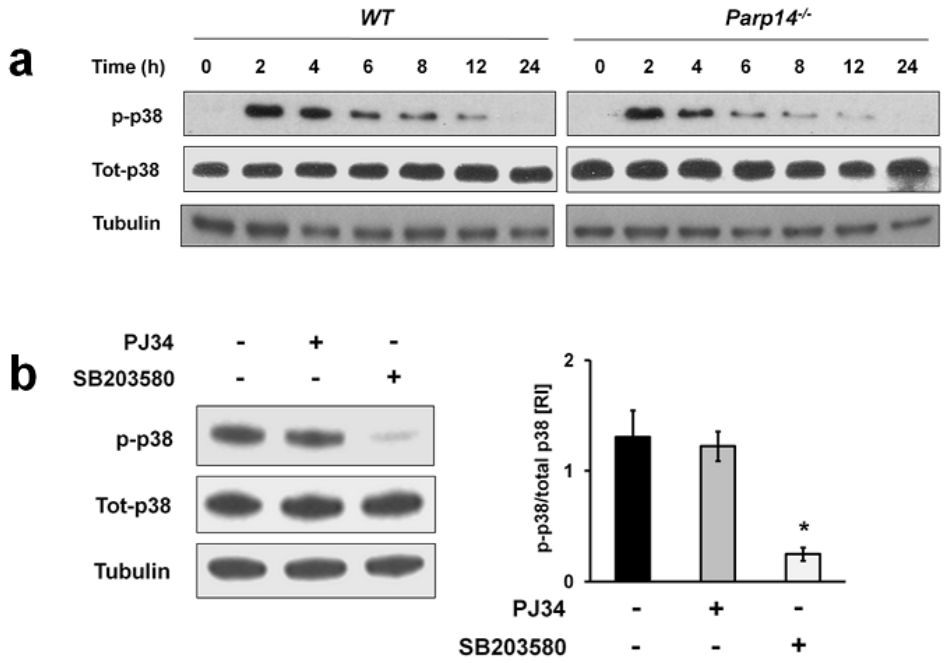

Figure 4-18: The effect of PARP14 deficiency and PARP inhibition on phospho-p38 levels
(a) WT and *Parp14*$^{-/-}$ murine macrophages were stimulated with LPS 1μg/mL for times shown following which total p38 and phospho-p38 protein levels determined using Western blotting (n=3). All blots were run on the same gel, but the lanes corresponding to WT and *Parp14*$^{-/-}$ are separated for clarity. Representative blot is shown. **(b)** WT murine macrophages were stimulated with LPS 1μg/mL for 2h. SB203580 1μM and PJ34 10μM were added 15 minutes prior to lysate preparation (n=3). Representative blot shown on the right with densitometric analyses on the left. The phospho-p38 immunodensity relative to the total p38 immunodensity provided the phospho-p38:total p38 ratio. Data expressed as mean ± SEM and analysed using a 2-tailed Student's t-test. * $p<0.05$, ** $p<0.01$, *** $p< 0.001$, when compared with LPS treated sample only. PARP inhibition did not result in reduction of phospho-p38 levels.

As shown in figure 4-18b, whilst p38 inhibition with SB203580 resulted in a significant reduction in phospho-p38 levels, PARP inhibition did not have an effect. To test the second of the above hypotheses, and to assess whether or not PARP inhibition altered TTP and/or PARP-14 binding to TF 3'UTR, RNA-biotin pulldown assays were used. In these experiments, the preparation of the lysates was critical. WT murine macrophages were cultured with LPS for 105 minutes, and then PJ34 was added to the PARP inhibitor arm of the experiment, with vehicle control to the control arm of the experiment.

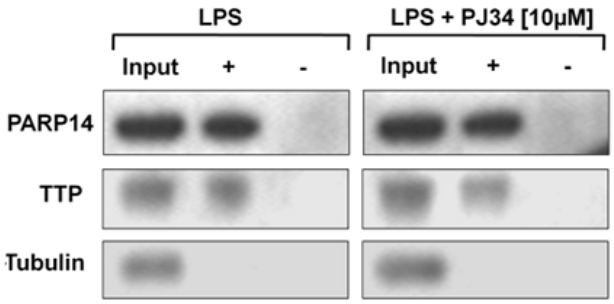

Figure 4-19: PARP-14 inhibition does not affect the binding of TTP or PARP-14 to TF 3'UTR
RNA-biotin pull down assays were conducted with lysates of LPS-treated WT macrophages (1 μg/ml for 2h) and streptavidin beads coated with biotinylated sense (+) or anti-sense (-) murine TF 3'UTR. In lysates with PARP inhibition, PJ34 10μM was added for 15 minutes prior to lysate preparation. Western blots of proteins isolated are shown. All blots were run on the same gel, but the lanes corresponding to LPS and LPS+PJ34 re separated for clarity. Tubulin acts as a control for non-specific pull-down. For each experiment all lanes were run on the same gel, but have been separated for clarity. Representative blot of 3 independent experiments.

The cells were then allowed to incubate for a further 15 minutes prior to preparation of lysates. Using these lysates PARP-14 and TTP binding to TF 3'UTR was assessed with RNA-biotin pulldown assays. Figure 4-19 shows PARP inhibition had no effect on TTP and/or PARP-14 binding to TF 3'UTR. Collectively these data show that PARP-14 and PARP inhibition do not affect p38 activity and, more specifically, PARP inhibition does not alter TTP and PARP-14 binding to TF 3'UTR. These data also indicate that PARP inhibition is likely to affect the ADP-ribosylation of a candidate protein which ultimately results in increased TF mRNA decay. The identification of the candidate protein(s) and the nature of this post-translational modification is beyond the scope of the current investigation and remain the focus of ongoing work.

4.3.10 PARP-14 deficiency does not affect TNFα expression

Having established an inter-dependency of for both PARP-14 and TTP in TTP-mediated TF mRNA decay, the next question was if this would be applicable to other TTP-regulated genes. An important established target for TTP is TNFα. Most of our understanding on TTP function emerges from studies that have used TNFα as the model transcript[426]. Therefore, the role of PARP-14 in TNFα expression was investigated.

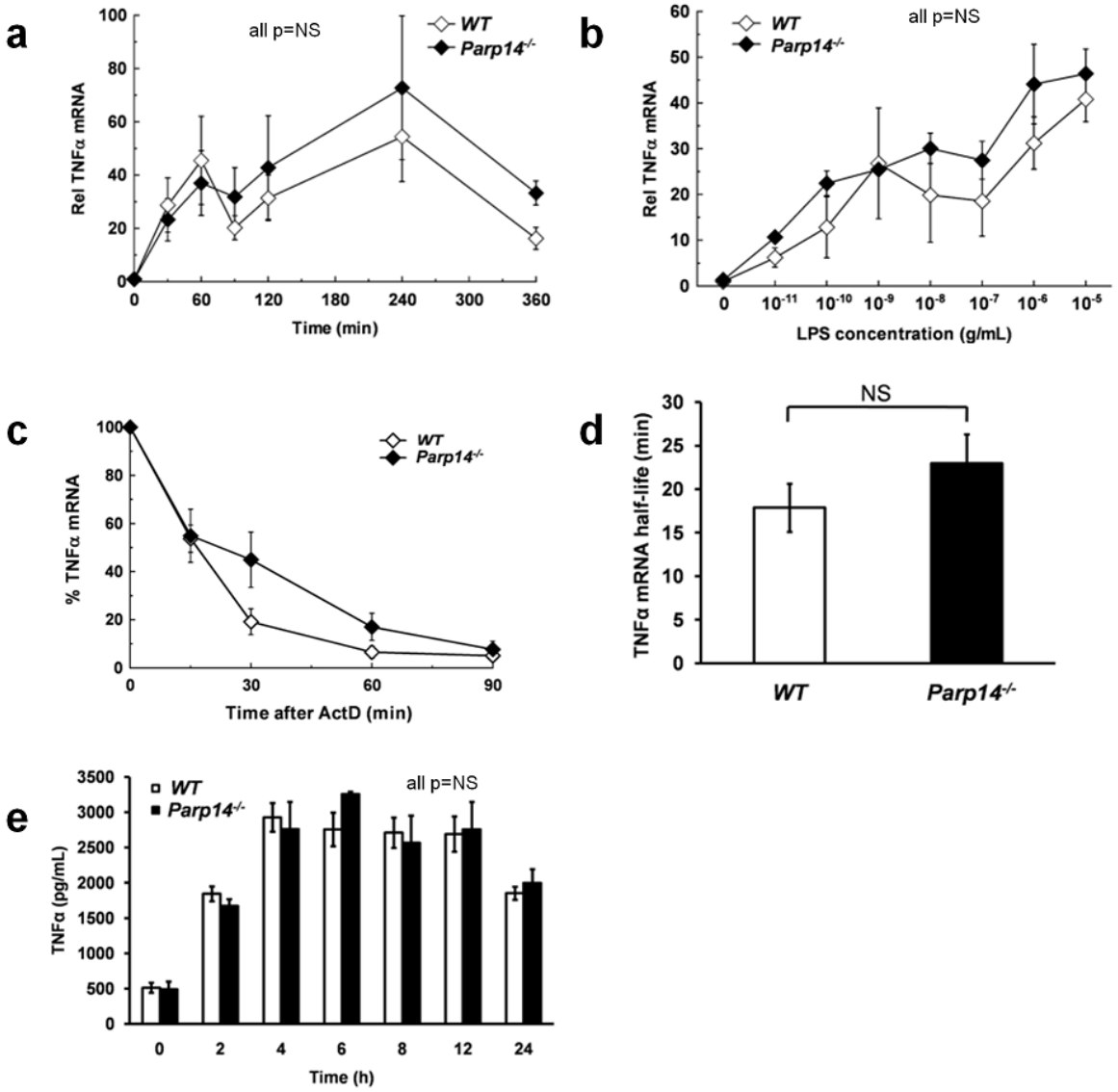

Figure 4-20: The effect of PARP-14 deficiency on TNFα expression in LPS-stimulated macrophages
(a) WT and *Parp14*$^{-/-}$ murine macrophages were stimulated with LPS 1μg/mL for times shown following which TNFα mRNA levels were determined using RT-PCR (n=4). TNFα mRNA levels were normalized to TNFα mRNA levels for the unstimulated WT sample at time=0; **(b)** WT and *Parp14*$^{-/-}$ murine macrophages were stimulated with LPS 10^{-5}-10^{-11} g/mL for 2h and TNFα mRNA levels were determined and normalized to levels in unstimulated WT macrophages (n=4); **(c)** WT and *Parp14*$^{-/-}$ murine macrophages were stimulated with LPS 1μg/mL for 2h. Actinomycin D (5μg/mL) was added at 2h to induce transcriptional arrest. TNFα mRNA levels were determined at each time point and normalized to levels at time point 0 to obtain mRNA decay profiles (n=6). **(d)** The decay profiles were modelled mathematically using non-linear regression analysis to determine mRNA half-lives; (e) WT and *Parp14*$^{-/-}$ murine macrophages were stimulated with LPS 1μg/mL for times shown and TNFα protein levels determined in the cell culture supernatants using ELISA (n=3). Data expressed as mean ± SEM and analysed using a 2-tailed Student's t-test. * p<0.05, ** p<0.01, *** p< 0.001

WT and *Parp14*$^{-/-}$ macrophages were stimulated with LPS 1μg/mL, and steady state TNFα mRNA levels were determined (figure 4-20a). This demonstrated that the TNFα mRNA levels were similar between WT and *Parp14*$^{-/-}$ macrophages. The effect of increasing LPS concentration (10^{-11}-10^{-5}g/mL) on TNFα mRNA induction was also

tested (figure 4-20b), where TNFα mRNA levels were determined at 2 hours following LPS stimulation. Again, this demonstrated no difference in TNFα mRNA levels throughout all concentrations of LPS. Furthermore, examination of TNFα mRNA decay curves at 2 hours following LPS stimulation in WT vs. *Parp14*$^{-/-}$ macrophages found no significant differences in TNFα mRNA half-lives (t½=18±3 vs. 23±3, p=0.281) (figures 4-20c,d). Next, TNFα protein levels in culture supernatants taken from LPS-stimulated WT and *Parp-14*$^{-/-}$ macrophages were analysed by ELISA, and this demonstrated no significant differences between TNFα protein levels (figure 4-20e).

p38 inhibition was found to destabilise TF mRNA in WT, but not *Parp14*$^{-/-}$ macrophages. Although TNFα is a TTP-regulated transcript, it does not behave in a similar manner to TF, as shown in figure 4-21 where p38 inhibition appears to destabilise TNFα mRNA in both WT and *Parp14*$^{-/-}$ macrophages, with a comparable effect in both cells. Taken together, these *in vitro* data demonstrated no significant difference in TNFα expression between WT and *Parp14*$^{-/-}$ macrophages both at mRNA and protein level.

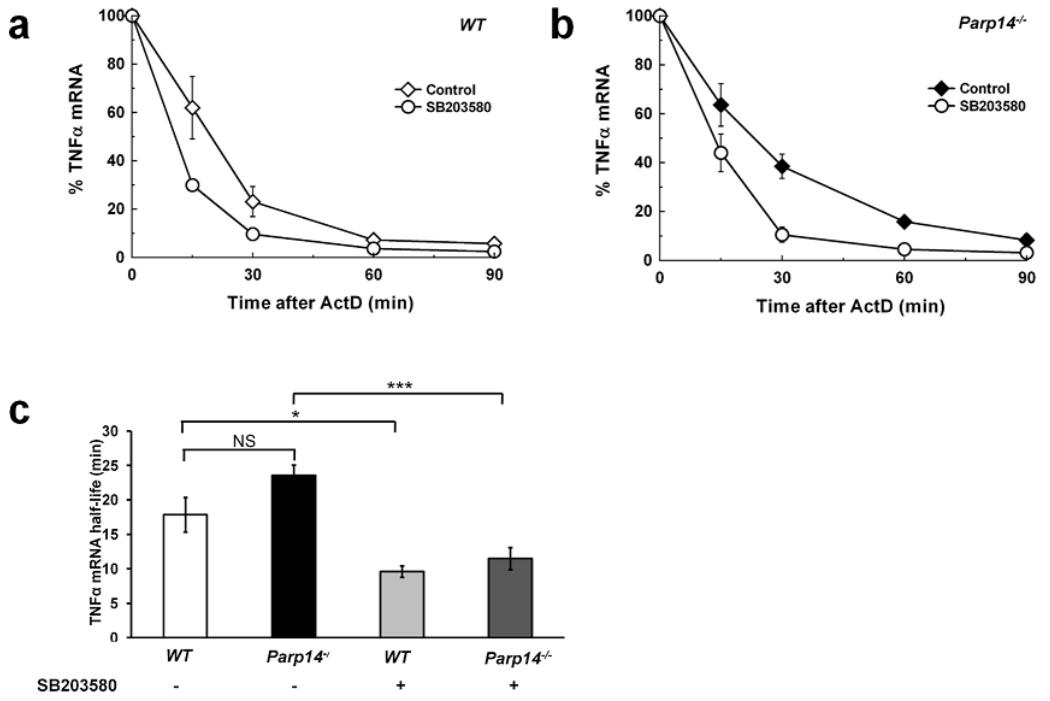

Figure 4-21: The effect of p38 inhibition on TNFα mRNA decay in LPS stimulated WT vs. *Parp14*$^{-/-}$ macrophages
WT and *Parp14*$^{-/-}$ murine macrophages were stimulated with LPS 1μg/mL for 2h. Actinomycin D (5μg/mL) was added at 2h to induce transcriptional arrest. SB203580 was added with actinomycin D. TNFα mRNA levels were determined at each time point and normalized to levels at time point 0 to obtain mRNA decay profiles (n=5). The decay profiles were modelled mathematically using non-linear regression analysis to determine mRNA half-lives. **(a)** TNFα mRNA decay profiles in WT macrophages (n=5); **(b)** TNFα mRNA decay profiles in *Parp14*$^{-/-}$ macrophages (n=5); and **(c)** corresponding TNFα mRNA half-lives. Data expressed as mean ± SEM and analysed using a 2-tailed Student's t-test. * p<0.05, ** p<0.01, *** p< 0.001

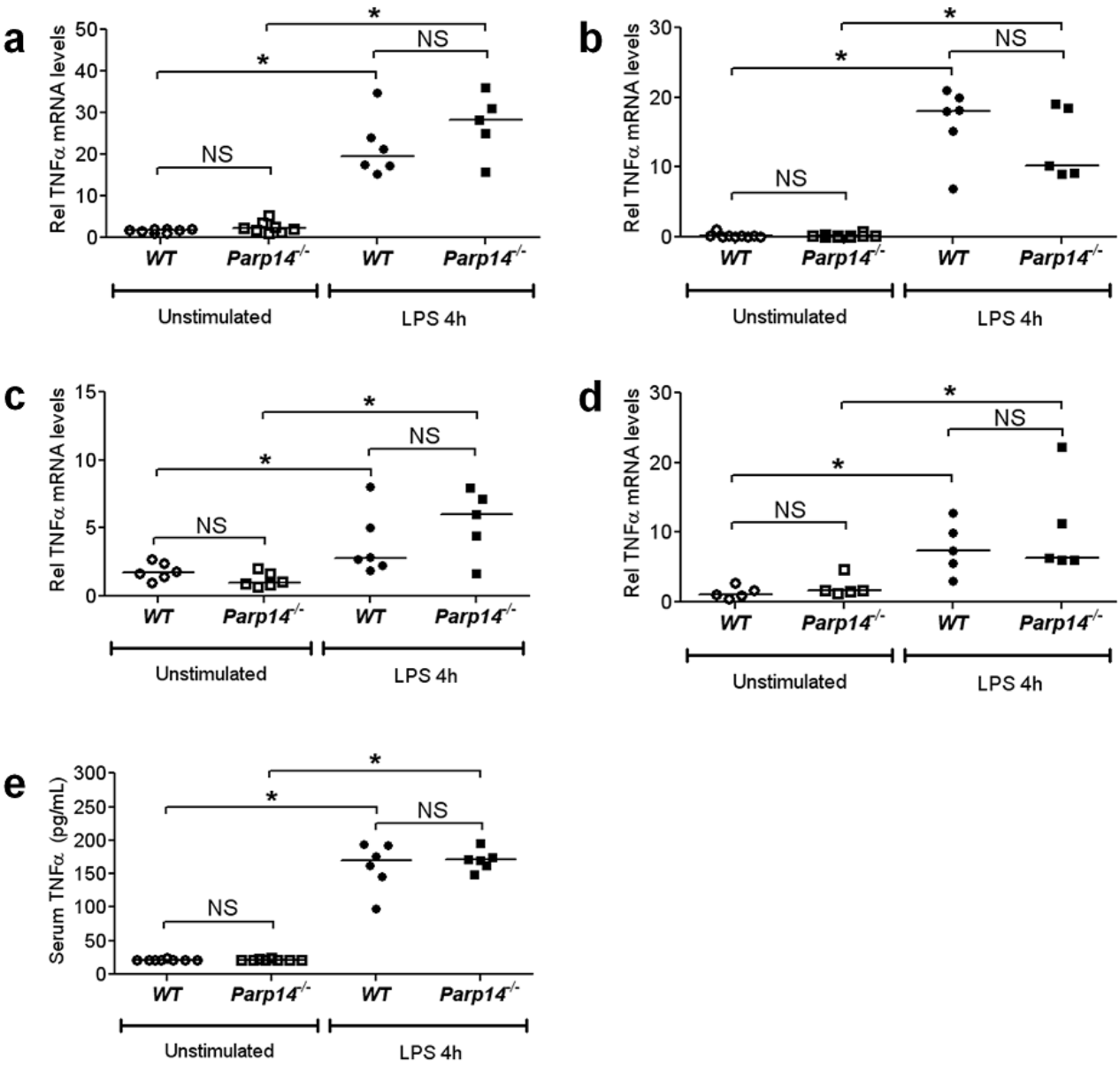

Figure 4-22: The effect of PARP-14 deficiency on TNFα expression *in vivo*
WT and *Parp14*$^{-/-}$ mice were either left unstimulated or stimulated with LPS (5µg i.p. for 4h) and venous blood and organs harvested. The blood was clotted and sera obtained. TNFα mRNA levels within different organs were determined using RT-PCR and normalized to a WT mouse in the unstimulated arm of the experiment (n=5-8 mice per group). TNFα mRNA levels are shown for **(a)** heart; **(b)** lung; **(c)** kidney; and **(d)** aorta. Serum TNFα levels as measured by ELISA, in the similarly treated mice (n=6-8 mice per group), is shown in **(e)**.

Next, the effect of PARP-14 on TNFα expression was determined *in vivo*, both at resting basal conditions and following LPS stimulation (LPS 5µg i.p. for 4 hours). Analysis of TNFα mRNA levels from heart, lung, aorta and kidney demonstrated no significant difference between WT vs. *Parp14*$^{-/-}$ mice both at resting basal conditions and following

LPS, although a significant induction in TNFα mRNA was observed in all organs following LPS stimulation (figures 4-22a-d). Similarly, analysis of sera taken from WT vs. *Parp14*$^{-/-}$ mice showed no significant difference at resting basal conditions and following LPS stimulation (figure 4-22e). These in vitro and in vivo findings provided strong evidence that PARP-14 does not affect TNFα expression.

The effect of PARP inhibition on TNFα mRNA stability was also examined. TNFα mRNA decay profiles were determined in WT macrophages, both in the presence and absence of PJ34 10μM. Parallel experiments were conducted where the combined effect of both PARP and p38 inhibition was tested using PJ34 10 μM and SB203580 1 μM. Macrophages were stimulated with LPS 1μg/mL and TNFα mRNA decay determined at 2 hours. The TNFα mRNA half-life in these set of experiments was 18±4 minutes, with a significant reduction in TNFα mRNA stability with p38 inhibition (t½=6±1 minutes, p=0.02). PARP inhibition did not affect TNFα mRNA stability (t½=18±4 minutes, p=0.999) and had no effect when used in combination with p38 inhibition (t½=9±3 minutes, p=0.339).

These findings were further validated in primary human monocytes. Similar to the findings in murine macrophages, PARP inhibition with PJ34 10μM did not result in a significant difference in TNFα mRNA stability (t½=39±11 minutes vs. 35±7 minutes, control vs. PJ34, p=0.727). p38 inhibition resulted in a significant reduction in TNFα mRNA stability (t½=39±11 minutes, p=0.031), whilst combined p38 and PARP inhibition had no additive destabilizing effect (t½=9±1 minutes, p=0.556). Collectively, these data indicate that whilst TNFα is a TTP-regulated transcript, the presence or absence of PARP-14 does not affect TNFα regulation in a similar pattern to TF with no observed differences in steady state TNFα mRNA levels; TNFα mRNA decay; and TNFα protein levels. Furthermore, PARP inhibition appears to have no effect on TNFα mRNA stability.

Finally, whether or not PARP-14 binds TNFα mRNA was assessed using RNP immunoprecipitation assays. Lysates were prepared from WT, *Ttp*$^{-/-}$ and *Parp14*$^{-/-}$ macrophages treated with LPS (1μg/mL) for 2 hours. RNP immunoprecipitation assays

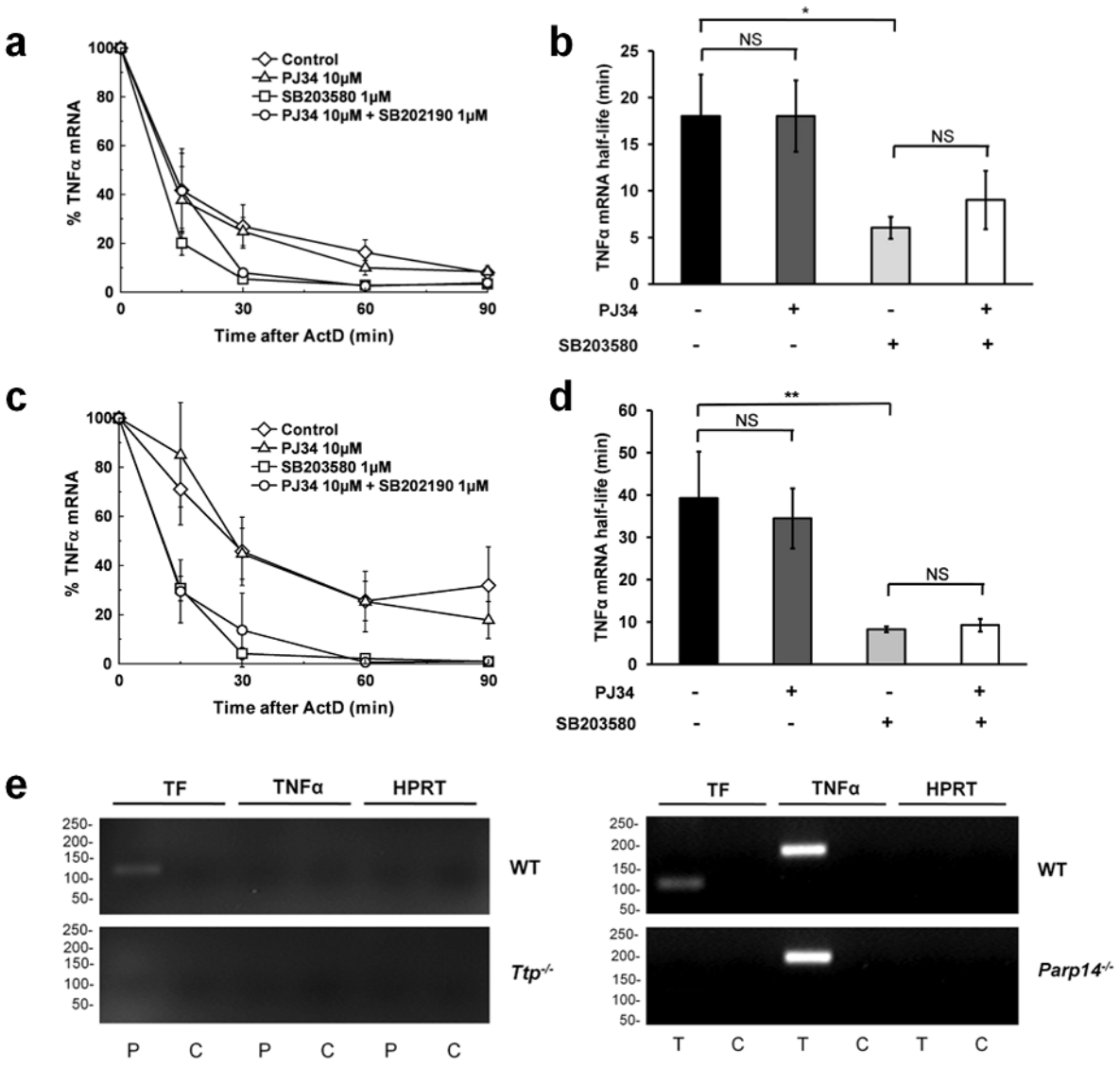

Figure 4-23: PARP inhibition does not alter TNFα mRNA stability and PARP-14 does not bind TNFα mRNA
WT murine macrophages **(a-b)** and human monocytes **(c,d)** were stimulated with LPS 1μg/mL for 2h. Actinomycin D (5μg/mL) was added at 2h to induce transcriptional arrest. PJ34 10μM and SB203580 1μM were added with actinomycin D. TF mRNA levels were determined at each time point and normalized to levels at time point 0 to obtain mRNA decay profiles. The decay profiles were modelled mathematically using non-linear regression analysis to determine mRNA half-life. TF mRNA decay profiles in WT macrophages (n=5) are shown in **(a)** and corresponding half-lives shown and compared in **(b)**. TF mRNA decay profiles in primary human monocytes (n=4) are shown in **(c)** and corresponding half-lives shown and compared in **(d)**. Data expressed as mean ± SEM and analysed using a 2-tailed Student's t-test. * $p<0.05$, ** $p<0.01$, *** $p< 0.001$; **(e)** RNP immunoprecipitation assay where RT-PCR shows that TF mRNA and not TNFα mRNA can be immunoprecipitated by anti-PARP-14 antibody (P) compared to rabbit IgG control (C) from lysates of LPS-treated WT (top left panel) murine macrophages (1 μg/ml for 2h). However, TF mRNA is not immunoprecipitated by anti-PARP-14 from lysates of LPS-treated *Ttp*$^{-/-}$ macrophages (lower left panel). Parallel RNP immunoprecipitation assays using lysates from LPS treated WT and *Parp14*$^{-/-}$ macrophages show that both TF mRNA and TNFα mRNA can be immunoprecipitated by anti-TTP antibody (T) compared to rabbit IgG control (C) from lysates of LPS-treated WT (top right panel) murine macrophages. However, TF mRNA is not immunoprecipitated by anti-TTP from lysates of LPS-treated *Parp14*$^{-/-}$ macrophages (lower right panel). The amplicon length of murine TF PCR product is 105bp and murine TNFα product is 173bp. HPRT provides a negative control mRNA (amplicon length, 134bp). Representative of 2 independent experiments.

were performed using anti-TTP, anti-PARP-14 and rabbit IgG control antibodies (figure 4-23e). This demonstrated 2 key findings, (a) PARP-14 does not bind TNFα mRNA but binds TF mRNA in only in the presence of TTP; and (b) TTP binds TNFα mRNA both in the presence and absence of PARP-14,. This confirms the earlier findings of cooperative binding for TTP and PARP-14 as shown using the RNA-biotin pulldown assays (figure 4-16a), but further demonstrates how the TTP-PARP-14 interaction may provide a means for the differential regulation of TTP-regulated transcripts.

4.4 DISCUSSION

The above data builds upon the findings from Chapter 3, where TTP was found to post-transcriptionally regulate TF expression. In this chapter, a specific role for PARP-14 and ADP ribosylation is demonstrated in TTP-mediated TF mRNA decay. In particular, these data have identified what may be a fundamental mechanism by which mRNA stability is subject to differential regulation in inflammatory processes, as neither PARP-14 deficiency nor PARP inhibition appeared to affect TTP-mediated TNFα mRNA decay. This is the first time that an ADP-ribosyl monotransferase has been shown to regulate mRNA stability under physiological conditions.

Experiments conducted in WT and *Parp14*$^{-/-}$ macrophages demonstrated that a deficiency of PARP-14 resulted in increased TF mRNA, TF protein and TF activity following LPS stimulation. The increased expression of TF mRNA, TF protein and procoagulant activity in *Parp14*$^{-/-}$ macrophages following LPS stimulation was paralleled by increases in TF mRNA, TF protein and TF activity in organs extracted from *Parp14*$^{-/-}$ mice, suggesting PARP-14 serves to set an appropriate level of TF expression. Obviously the organ extracts studied comprised a mixed population of cell types with different basal levels of TF expression and different responses to LPS, which no doubt accounts for the variability between tissues in TF levels. However, the increased TF activity in circulating peripheral blood leukocytes in *Parp14*$^{-/-}$ mice clearly demonstrates the importance of the *in vitro* observations for leukocyte biology *in vivo*. Monocytes are the main source of TF amongst circulating leukocytes[427], but whether the difference

observed between WT and *Parp14*$^{-/-}$ leukocytes in procoagulant activity was solely due to monocyte TF expression remains to be determined. The paradoxical reduction in TF expression in the heart following LPS stimulation has previously been observed[173], but remains unexplained. One can speculate that mechanisms have evolved to protect the heart from enhanced thrombogenicity from endotoxaemia during infections. Further work is needed to establish the differential roles of PARP-14 in TF expression in cells other than monocyte-macrophages, and indeed whether there are differences in this respect between monocyte and macrophage subsets. The functional significance of increased TF expression in *Parp14*$^{-/-}$ mice was supported by intravital microscopy experiments showing accelerated thrombosis *in vivo* as demonstrated by significant reduction in vessel occlusion time in cremaster muscle arterioles following ferric chloride injury. However, a significant reduction in occlusion time in WT mice following LPS challenge was not demonstrated, possibly because of a suboptimal LPS stimulus. Nevertheless, occlusion time was significantly faster in *Parp14*$^{-/-}$ mice after LPS treatment, compared both to that in unstimulated *Parp14*$^{-/-}$ mice and in LPS-stimulated WT mice.

The mechanism by which *Parp14*$^{-/-}$ mice show increased TF expression came from mRNA decay experiments which demonstrated increased TF mRNA stability in *Parp14*$^{-/-}$ macrophages treated with LPS. Subsequent RNP immunoprecipitation and RNA-biotin pulldown assays demonstrated PARP-14 to associate with TF mRNA and specifically with the TF 3'UTR. An interesting finding from RNA-biotin pulldown assays conducted using cellular extracts from WT, *Parp14*$^{-/-}$ and *Ttp*$^{-/-}$ macrophages was that whilst in WT cells both PARP-14 and TTP associate with TF 3'UTR, in *Parp14*$^{-/-}$ cells TTP did not associate with TF 3'UTR and similarly in *Ttp*$^{-/-}$ cells, PARP-14 binding to TF 3'UTR was significantly reduced. This indicated that both proteins appear to bind, somewhat, in a cooperative fashion. This cooperative binding was further demonstrated using RNP immunoprecipitation assays, where anti-TTP antibody was not able to pull down any detectable TF mRNA in *Parp14*$^{-/-}$ cells and anti-PARP14 antibody was not able to pull down any detectable TF mRNA in *Ttp*$^{-/-}$ cells. Further RNA-biotin pull down assays demonstrated TTP and PARP-14 to bind the 3'UTR segment which contained the final

ARE in TF 3'UTR. Focusing mutational analyses on the final palindromic ARE, RNA-biotin pull down assays incorporating WT or mutant AREs demonstrated that this binding was specifically mediated by 2 overlapping nonamer sequences (AUUUAUUUA and UUAUUUAAU) which appear to mediate binding to both TTP and PARP-14 in a cooperative manner, such that mutating either one of these nonamers reduced binding, but mutating both sequences by disrupting the central UUU abolished binding for both proteins. These data would indicate that TTP and PARP14 appear to form a ternary complex with TF mRNA. Subsequent co-immunoprecipitation assays demonstrated that TF mRNA is important for this interaction, as PARP-14 was pulled down along with TTP from WT LPS-stimulated cellular lysates using the anti-TTP antibody. However, treatment of the lysate with RNase to remove any mRNA resulted in loss of PARP-14 from the pulled down complex. This indicated that PARP-14 and TTP are interdependent for binding TF mRNA, with which they appear to form a ternary complex. TTP is known to bind RNA via the centrally placed two ZFs which coordinate Zn in a disc-like structure[428-430]. Furthermore, PARP-14 is likely to bind RNA via its N-terminal RNA recognition motif (RRM)[431]. Although the above data indicate that the two proteins require the central UUU in the conserved ARE, the precise binding sites of the individual proteins within or around the ARE and their means of interacting requires further analysis.

Using two separate inhibitors of PARP domain function (PJ34 and 3AB), mRNA decay experiments in the presence of these compounds demonstrated that TF mRNA stability is also regulated by ADP-ribosylation, consistent with an effect of PARP-14-mediated ADP-ribosyl monotransferase activity. Interestingly, the destabilizing effect on TF mRNA was comparable to that seen with p38 inhibition, and the combination of both p38 and PARP inhibition did not appear to have any additive effect. However, as there are currently no available PARP inhibitors specific for PARP-14, one cannot exclude the possibility that other proteins capable of generating ADP-ribose monomers or polymers might be involved. Nevertheless, whilst a direct role for PARP-14 catalytic function in the system may be implicated by the failure of PARP inhibitors to destabilise TF mRNA in *Parp14*$^{-/-}$ macrophages, it is also important to remember that this is difficult to

interpret, as in the absence of PARP-14, TTP does not bind to TF 3'UTR, so thus irrespective of ADP ribosylation status there will be no TTP-mediated TF mRNA decay. RNA-biotin pull down assay confirmed that PARP inhibition did not affect the interaction of PARP-14 and TTP with the TF 3'UTR. Furthermore, PARP inhibition did not alter the phosphorylation status and thus p38 activity. These results suggest that ADP-ribosylation is likely to alter the function of TTP, PAPR-14 or other unknown candidate protein within the mRNA decay complex. Irrespective of the precise molecular target for ADP-ribosylation, these data certainly suggest that inhibition of ADP-ribosylation provides a pharmacological means to increase TF mRNA degradation. ADP-ribosylation provides a post-translational modification in which negatively charged ADP-ribose moieties are adducted onto acceptor proteins[367]. The identity and site of the protein target(s) of ADP-ribosylation in this system now requires further study, as does establishing how this affects TTP function.

TNFα mRNA is a well-established TTP target, and TNFα mRNA stability is regulated via the p38 MAPK pathway[320, 426]. *Ttp*$^{-/-}$ mice spontaneously develop a chronic inflammatory state that can be prevented by administration of anti-TNFα antibodies[313]. In contrast, *Parp14*$^{-/-}$ mice are apparently healthy and neither PARP-14 deficiency nor PARP inhibition altered TNFα expression. TNFα mRNA half-life was unaffected in the absence of PARP-14. Furthermore, as TNF*α* transcripts were pulled down in a RNP immunoprecipitation assay from WT or *Parp14*$^{-/-}$ cells by anti-TTP but not by anti-PARP-14 antibodies, it seems unlikely that PARP-14 has a role in TTP binding to TNFα 3'UTR mRNA. Similarly, TTP is also a subject to post-transcriptional regulation by itself, and TTP mRNA half-life was unaffected in the absence of PARP-14. Taken together, these data indicate that PARP-14-TTP interaction is not applicable to all TTP-regulated transcripts, and provides compelling evidence for how PARP-14 serves to differentially regulate TTP-regulated transcripts.

In conclusion, these data demonstrate novel interactions between PARP-14, a new protein in post-transcriptional regulation, and TTP, an established protein regulator of mRNA stability, and present evidence that PARP-14 allows the actions of TTP to be

selectively regulated. Thus, whilst the focus has remained on the regulation of TF mRNA turnover, the above findings have significantly wider implications for post-transcriptional regulatory biology in general and TTP-mediated mRNA decay in particular.

Chapter 5

Results:

Glucocorticoids regulate TF mRNA stability via TTP-dependent and TTP-independent pathways

5.1 INTRODUCTION

In chapter 3, the role for TTP in the post-transcriptional regulation of TF expression was presented. TTP exists in two forms: dephosphorylated (active) and phosphorylated (inactive). In the dephosphorylated state, TTP binds to the ARE and promotes rapid degradation of the mRNA. However, phosphorylation of TTP, at Ser^{52} and Ser^{178}, leads to binding of 14-3-3 adaptor proteins that reduce its mRNA destabilizing activity. The phosphatase PP2A competes with 14-3-3 proteins and dephosphorylates TTP. Thus the proportion of TTP in the phosphorylated and dephosphorylated form remains in equilibrium, and the disruption of this equilibrium, through either increased or decreased phosphorylation, is believed to affect the overall activity of TTP.

The p38 signaling pathway is one of the three MAPK pathways that affect gene expression[346]. LPS results in phosphorylation and activation of p38[432], and this mediates both transcriptional and post-transcriptional effects[433]. The p38 pathway confers mRNA stability by activating MAPKAPK-2 that subsequently phosphorylates and inactivates TTP (the primary target for MAPKAPK-2)[363]. The activity of p38 is negatively regulated by a large family of phosphatases, of which MAPK phosphatase 1 or dual specificity phosphatase 1 (DUSP1) is the founding member. DUSP1 dephosphorylates and inactivates MAPKs, and most of its effects are mediated via the inhibition of p38 activity[360, 361, 434].

GCs induce a rapid and sustained expression of DUSP1 in many cell types, resulting in p38 inactivation and mRNA destabilization[435]. GC-induced DUSP1 expression represents an important anti-inflammatory mechanism. Studies using TTP-specific siRNAs and *Ttp*$^{-/-}$ cells have shown that TTP plays an important role in the anti-inflammatory actions of GCs[436, 437]. LPS upregulates TTP expression[438-440] and at the same time increases p38 activity[432]. Whilst, increased p38 signaling further increases TTP expression[441], at the same time it phosphorylates and inactivates it. Thus, following LPS stimulation, the net result is that TTP is predominantly in an inactive state, thereby promoting mRNA stability as part of the acute inflammatory response. The effect of dexamethasone (Dex) on TTP expression in LPS-stimulated cells has been variably

reported, but is likely to depend on the different cells types studied[439, 440]. Nevertheless, it is important to remember, that whilst LPS ± Dex treatment may result in changes in total TTP protein level, it is the net proportion of the active and inactive forms that is likely to affect TTP function, and current evidence indicates that Dex treatment increases the proportion of the active (dephosphorylated) form of TTP.

Current data on the effect of GCs on human monocyte procoagulant activity are ambiguous[442-444]. Muhlfelder and colleagues demonstrated that methylprednisolone reduced procoagulant activity of LPS-stimulated PBMCs[442]. Bottles and colleagues demonstrated that Dex enhanced LPS induction of TF in THP-1 cells and PBMCs, when co-stimulated with LPS and Dex, and that this was not a result of increased mRNA stability, implicating increased gene transcription to play a role[443]. Interestingly, pre-treatment with Dex for 24 hours prior to LPS stimulation, resulted in a reduction in LPS-induced TF response. Reddy and colleagues demonstrated that Dex enhanced LPS induction of TF in THP-1 cells, when pre-incubated with Dex for 30 minutes prior to LPS stimulation. They demonstrated that Dex inhibited TF gene transcription, but increased mRNA stability, with an overall increase in TF expression[444]. Thus there remains some controversy over the effect of GCs on TF regulation in monocytes, and it is likely that experimental conditions, particularly the use of primary human monocytes versus unfractionated PBMCs[445, 446] or THP-1 cells[422], and timing of LPS and GC exposure are crucial.

This chapter builds upon the observation that p38 inhibition reduces TF mRNA stability via the p38-TTP axis. Given that GCs are potent inhibitors of p38 activity and function, the effect of GCs on TF mRNA stability is investigated.

5.2 METHODS

5.2.1 Primary human monocyte isolation and culture

Monocytes were isolated from citrated venous blood derived from healthy donors. PBMCs were isolated from the cell fraction by Ficoll–Paque density-gradient

centrifugation. In experiments where PBMCs were used, the buffy layer was carefully taken, and PBMCs pelleted and washed with PBS twice, before being resuspended in culture medium. In experiments where monocytes were used, CD14+ monocytes were separated from the PBMC fraction using magnetic separation with CD14 MicroBeads and MACS Separator column. Monocytes were plated into tissue culture plates according to the experimental protocol in IMDM with 10% FCS ($25x10^4$ cells/well in 24 well plates or $2x10^4$/well in 96-well plates) and incubated overnight in a 37°C incubator with 5% CO_2 atmosphere, for experiments the following day.

5.2.2 Bone marrow-derived macrophage (BMDM) isolation and culture

WT and *Ttp*$^{-/-}$ mice were sacrificed using cervical dislocation. Bone marrow cells were flushed from the femur and tibia and cultured in bone marrow culture medium for 6 days. On day 6, the cells were harvested, resuspended in the bone marrow culture medium, and plated in culture dishes/flasks as per the experimental protocol ($25x10^4$ cells/well in 24 well plates or $1x10^7$cells/T75 flask) and incubated overnight in a 37°C incubator, for experiments the following day.

5.2.3 Glucocorticoid treatment

Dex was the primary GC used in the experiments. The concentrations used in the experiment below were 10^{-11}-10^{-6}M. A water-soluble preparation was used which necessitated the addition of an equivalent volume of water as vehicle control.

5.2.4 TF activity assays

A turbimetric clot assay was used to determine TF activity. Cells were cultured in 96 well plates (cell density=$2x10^4$ cells per well) and treated with LPS 1μg/mL. Dex 1-1000nm was added in certain experiments. The supernatant was removed and cells were washed with PBS twice, prior to the addition of plasma. 100 μL of the citrated PPP was added to the wells and recalcified with 2 μL of 1.0M $CaCl_2$ to initiate clotting. Clot turbidity was measured by absorbance (A_{405}) every minute for 60 minutes in a spectrophotometer with internal thermostatic control at 37°C. The turbimetric curves

were modeled mathematically and detailed turbimetric analyses were conducted where T_{lag}, V_{max}, ABS_{max}, T_{Vmax} and T_{ABSmax} were measured.

5.2.5 RNA extraction and quantitative reverse-transcriptase PCR (qRT-PCR)

RNA was isolated from cells using RNEasy Mini kit incorporating an on-column DNase digestion. 1µg of total RNA was used for cDNA synthesis using SuperScript III reverse transcriptase enzyme. Comparative qRT-PCR was performed using SYBR green and gene specific primers (table 2-1). Data was normalized to 2 housekeeping controls, GAPDH and HPRT. For mouse TF mRNA expression, data was validated using 2 primer sets. Relative gene expression was calculated using the ΔΔCt method[409].

5.2.6 mRNA decay experiments

All mRNA decay experiments were performed with an identical protocol. Cells were stimulated with LPS 1µg/mL. Actinomycin D (5µg/mL) was added at 2 hours following LPS stimulation to induce transcriptional arrest. For p38 inhibition, SB203580 and SB202190 were used. In experiments specifically examining the effect of these inhibitors on mRNA decay, the inhibitors were all added at the time of actinomycin D. In experiments examining the effect of Dex on mRNA stability, Dex was added 30 minutes after LPS stimulation. Unlike the SB compounds, the effect of Dex is not immediate, and requires induction of anti-inflammatory mediators. On the other hand, adding Dex too early would dampen the TF transcriptional response following LPS stimulation. As a compromise between dampening the initial TF response and allowing sufficient time for induction of anti-inflammatory mediators specifically to examine the effect on mRNA decay, Dex was added 30 minutes after LPS stimulation, and actinomycin D added 2 hours after LPS stimulation. Following actinomycin D, RNA was isolated at time 0, 15, 30, 60 and 90 minutes. mRNA was quantified using qRT-PCR, and levels were normalized to levels at time 0. The mRNA decay profiles were modelled mathematically using non-linear regression analysis and mRNA half-lives calculated. It would be expected that the starting levels of TF mRNA in the Dex arm of the decay experiments would be lower than the control counterparts. However, normalization of TF mRNA levels in each arm to that at their respective time 0 would overcome this problem.

5.2.7 Flow cytometric analysis of TF

The supernatant culture medium was removed and cells washed twice in cold PBS. For detection of surface human TF expression, the cells were incubated with FITC-conjugated TF or FITC-conjugated isotype control antibodies for 30 minutes at 4ºC. The cells were washed with cold PBS and resuspended in 500µL cold PBS and subjected to flow cytometric analysis. The cells were read on a Coulter EpicsXL flow cytometer, FL1–600V, FL2–600V. The maximum event count was set at 10,000. Data were analyzed and presented using WinMDI software (Scripps Research Institute, CA)..

5.2.8 Western blotting analysis

Following the experimental protocol, the cells were lysed with 100µL of Cell Lytic M lysis buffer with 1µL of protease inhibitor cocktail. The lysates were centrifuged at 17,000g for 20 minutes at 4ºC to pellet cell debris. The supernatants were carefully removed and stored at -80ºC until analysis. A Novex XCell II mini gel system was used. 20µg of protein was used per lane, and proteins were separated by gel electrophoresis using pre-cast polyacrylamide gels, and electrotransferred to polyvinylidene difluoride membranes. The membranes were blocked using blocking buffer and primary and secondary antibodies were applied in blocking buffer at the appropriate dilutions (table 2-3). Protein bands were detected using chemiluminescence. Protein quantification was performed using densitometry using ImageJ software (National Institutes of Health, Bethesda, Maryland, USA) normalized to tubulin.

5.2.9 Statistical analyses

All continuous variables were expressed as either as mean ± SEM or medians, depending on normality tests based on the Shapiro-Wilk statistic. Statistical analyses were performed using GraphPad Prism v5.0 (GraphPad Software, San Diego, CA, USA) and Microsoft Excel 2007 (Microsoft, Washington, USA). Where data was expressed as mean ± SEM, the unpaired Student's t-test (2-tailed) was used for comparison. Where the data was expressed as medians the Mann-Whitney U-test (2 tailed) was used. Statistical significance was set at $p<0.05$.

5.3 RESULTS

5.3.1 Dex reduces monocyte procoagulant activity using clot turbimetric analyses

A detailed analysis of the effect of Dex on procoagulant activity of primary human monocytes was conducted using clot turbimetric parameters. The effect of Dex 100nM was first investigated in unstimulated primary human monocytes. LPS is known to enhance monocyte thrombogenicity by increasing TF expression[40], whilst IL-10 has been shown to reduce thrombogenicity by reducing TF expression[73] and increasing TFPI expression[72,73]. Thus both LPS (10ng/mL) and IL-10 (0.5nM) served as important controls for these experiments. Monocytes were cultured with these modulating agents for 24 hours and clot turbimetric profiles determined. The turbimetric curves were modelled mathematically and detailed turbimetric analyses were conducted where T_{lag}, V_{max}, ABS_{max}, T_{Vmax} and T_{ABSmax} were analysed. Figure 5-1 shows that LPS enhances and IL-10 reduces monocyte procoagulant activity (as expected). Furthermore, Dex reduced procoagulant activity in unstimulated primary human monocytes with statistically significant effects on clot turbimetric parameters with an increase in T_{lag} (13.2min vs. 9.1min, p=0.019); decrease in V_{max} (0.03Au/min vs. 0.09Au/min, p=0.049); and decrease in ABS_{max} (0.85Au vs. 1.08Au, p=0.004). A summary of all statistically significant changes in turbimetric parameters is shown in figure 5-1g.

Next, the effect of Dex on monocyte procoagulant activity in LPS-stimulated primary human monocytes was investigated. Previous published data on GCs on LPS-induced procoagulant activity are ambiguous, and this may reflect the timing of GC treatment with respect to LPS-stimulation. Most of the published data used pre-treatment with GCs following which LPS was added. From a therapeutic perspective, if Dex were to reduce procoagulant activity in the context of atherothrombosis or any other inflammatory state, it should do so with cells that are already activated. Given this, Dex was administered after LPS stimulation. Monocytes were stimulated with LPS (1µg/mL) or control for 30 minutes prior to the addition of Dex 100nM or control. Monocytes were cultured with these modulating agents for 24 hours and clot turbimetric profiles were

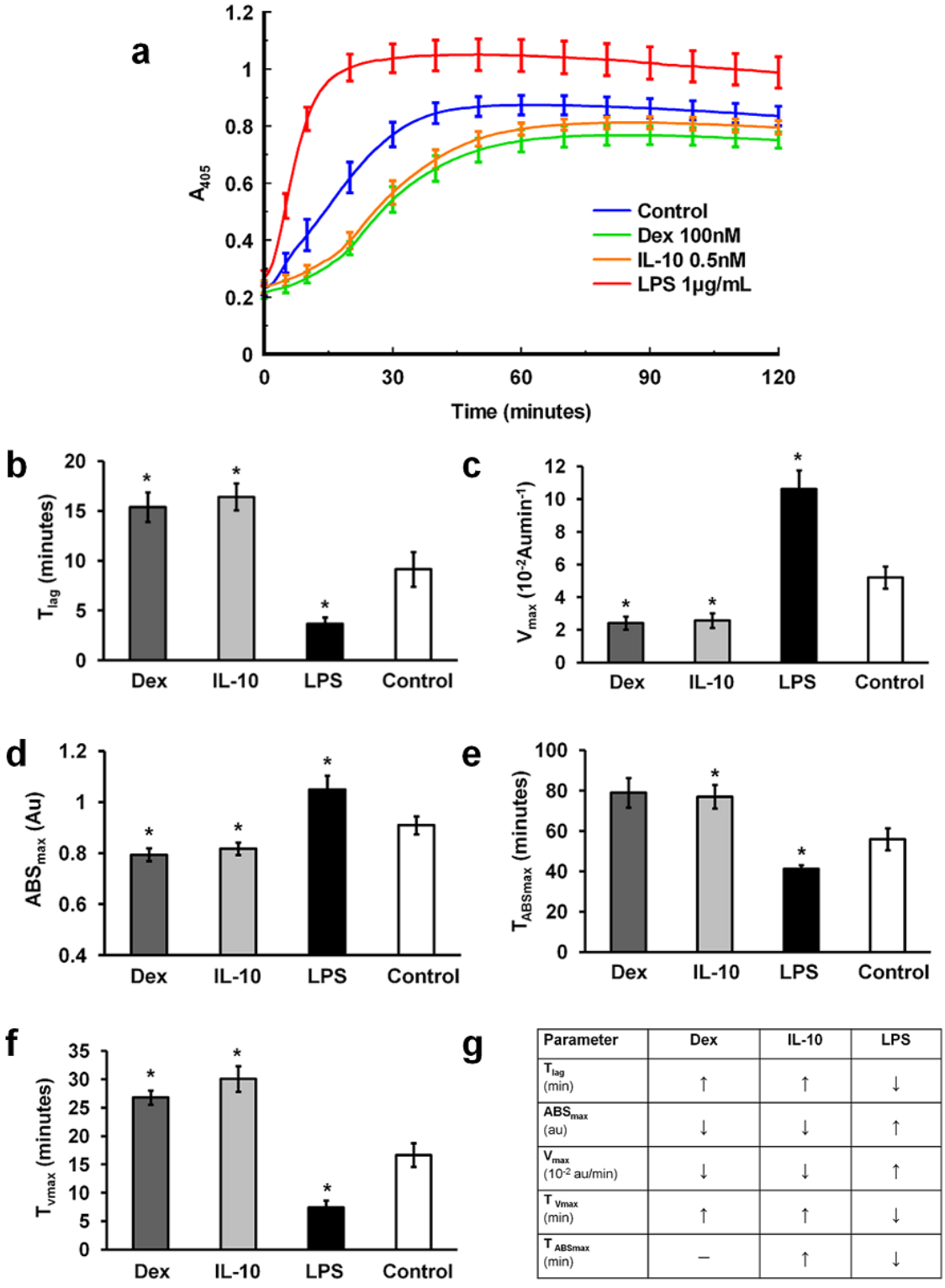

g

Parameter	Dex	IL-10	LPS
T_{lag} (min)	↑	↑	↓
ABS_{max} (au)	↓	↓	↑
V_{max} (10^{-2} au/min)	↓	↓	↑
T_{Vmax} (min)	↑	↑	↓
T_{ABSmax} (min)	–	↑	↓

Figure 5-1: The effect of Dex on monocyte procoagulant activity as determined by clot turbimetric parameters
Primary human monocytes were cultured with either vehicle control, LPS 1µg/mL, IL-10 0.5nM and Dex 100nM for 24h. Clot turbimetric profiles were then determined up to 2h (n=10). The turbimetric curves are shown in **(a)**. The turbimetric curves were modelled mathematically to determine different turbimetric parameters: **(b)** T_{lag}; **(c)** V_{max}; **(d)** ABS_{max}; **(e)** T_{ABSmax}; and **(f)** T_{Vmax}. All data are expressed as mean ± SEM and analysed using a 2-tailed Student's t-test, * $p<0.05$, ** $p<0.01$, *** $p< 0.001$. All statistically significant effects on turbimetric parameters are summarized in **(g)**.

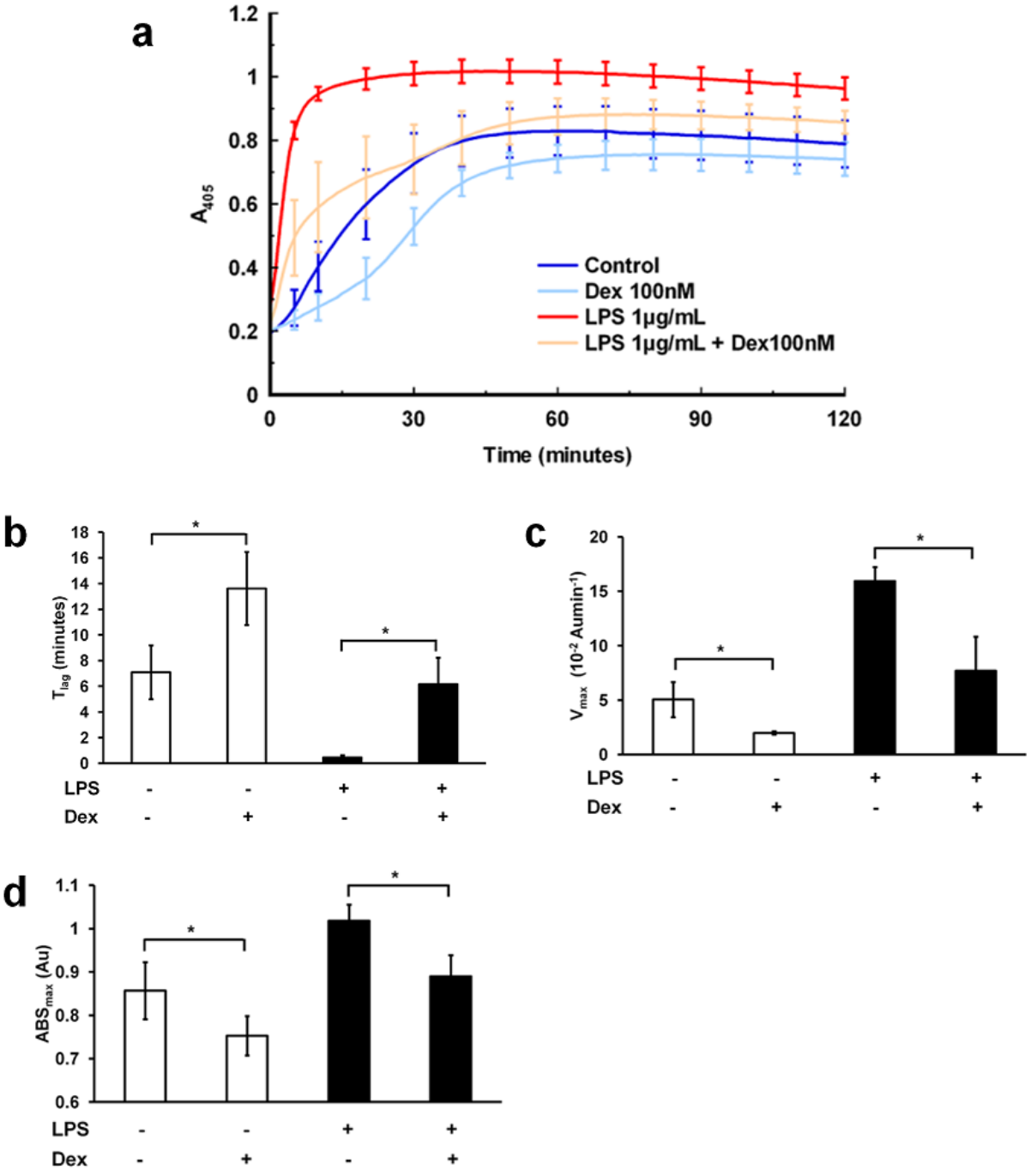

Figure 5-2: The effect of Dex on procoagulant activity of unstimulated and LPS-stimulated monocytes
Primary human monocytes were cultured with either vehicle control or LPS 1µg/mL. After 30min, they were either treated with vehicle control or Dex 100nM. After 24h, clot turbimetric profiles were determined up to 2h (n=5). The turbimetric curves are shown in **(a)**. The turbimetric curves were modelled mathematically to determine different turbimetric parameters: **(b)** T_{lag}; **(c)** V_{max}; and **(d)** ABS_{max}. All data expressed as mean ± SEM and analysed using a 2-tailed Student's t-test, * $p<0.05$, ** $p<0.01$, *** $p< 0.001$. Based on the turbimetric parameters , Dex appears to reduce procoagulant activity of both unstimulated and LPS-stimulated monocytes.

determined. Figure 5-2 shows that Dex reduced procoagulant activity of both unstimulated and LPS stimulated monocytes with statistically significant effects on clot turbimetric parameters (increase in T_{lag}; decrease in V_{max}; and decrease in ABS_{max}).

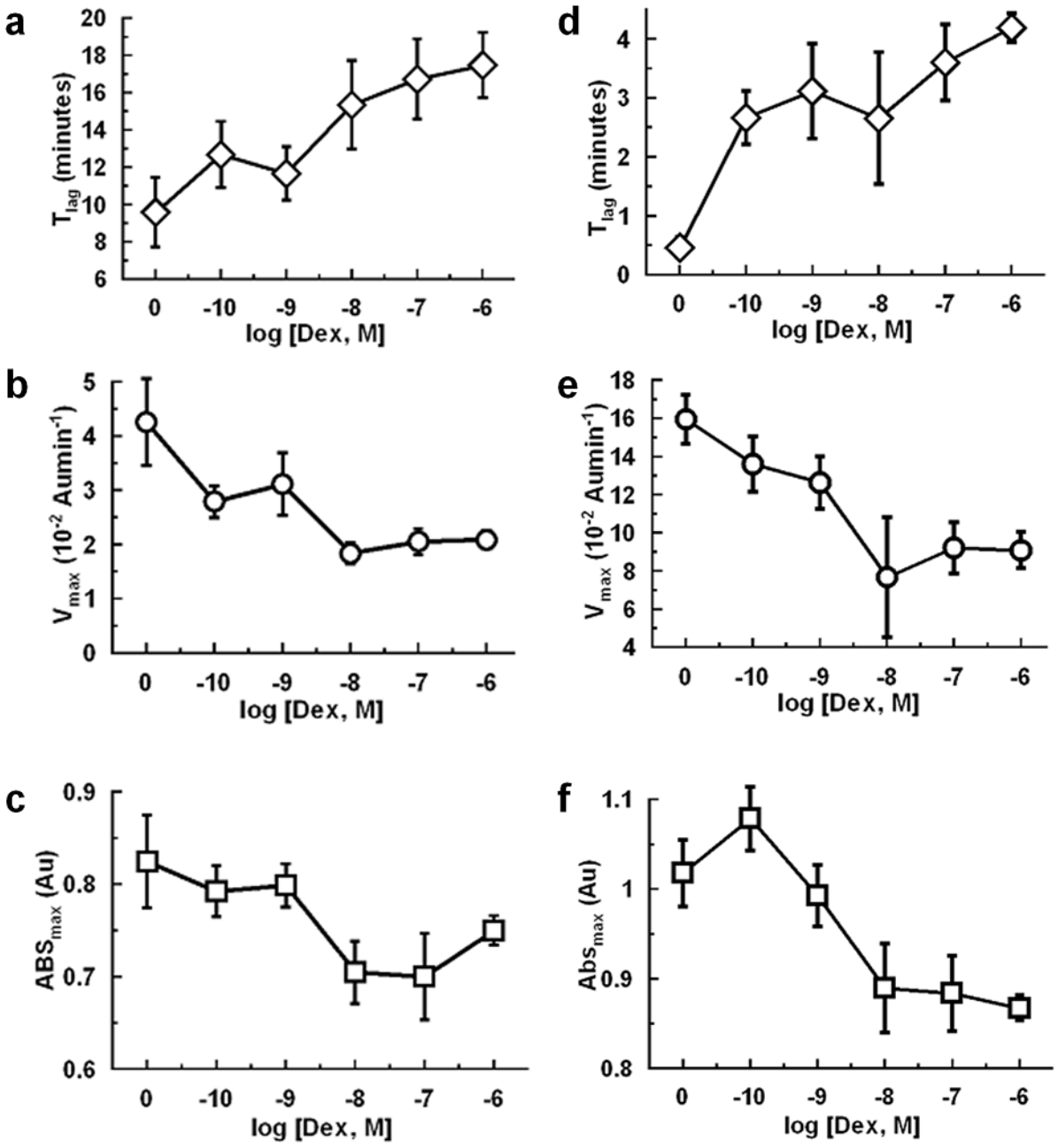

Figure 5-3: The effect of Dex concentration (10^{-10}-10^{-6}M) on procoagulant activity of unstimulated and LPS-stimulated monocytes as determined using clot turbimetric parameters

Primary human monocytes were cultured with either vehicle control **(a-c)** or LPS 1µg/mL **(d-f)**. After 30min, they were either treated with vehicle control or Dex (10^{-10}-10^{-6}M). After 24h, clot turbimetric profiles were determined up to 2h (n=5). The turbimetric curves were modelled mathematically to determine different turbimetric parameters: **(a,d)** T_{lag}; **(b,e)** V_{max}; and **(c,f)** ABS_{max}. All data expressed as mean ± SEM Based on the turbimetric parameters , Dex appears to reduce procoagulant activity of both unstimulated and LPS-stimulated monocytes in a concentration-dependent manner.

Finally, the effect of the Dex concentration on procoagulant activity was investigated in both unstimulated and LPS-stimulated primary human monocytes. Primary human monocytes were cultured with either vehicle control or LPS 1µg/mL, and Dex was added after 30 minutes. Turbimetric profiles were established at 24 hours following LPS stimulation. Figure 5-3 shows the effects of different concentrations of Dex on clot turbimetric parameters in both unstimulated and LPS stimulated monocytes. The turbimetric parameters chosen for this anlaysis were T_{lag}, V_{max}, ABS_{max}. Through a range of Dex concentrations (10^{-10}M to 10^{-6}M), Dex was associated with a concentration-dependent increase in T_{lag}; decrease in V_{max} and decrease in ABS_{max} in both unstimulated and LPS-stimulated monocytes.

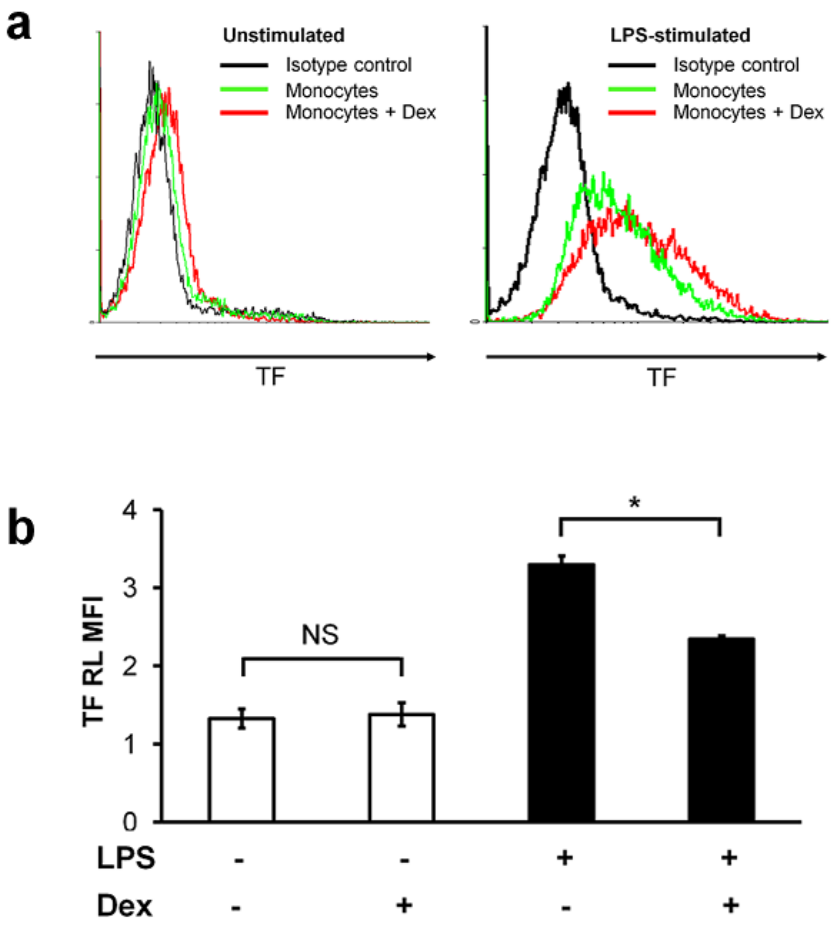

Figure 5-4: The effect of Dex on TF protein expression in unstimulated and LPS-stimulated monocytes
Primary human monocytes were cultured with either vehicle control or LPS 1µg/mL. After 30min, they were either treated with vehicle control or Dex 100nM (n=5). After 24h, TF protein expression analyzed using flow cytometric assay. **(a)** Representative histograms from 5 independent experiments shown; and **(b)** Analysis of TF mean fluorescence intensities (MFI) normalised to MFI of isotype control to yield relative MFI (RLMFI) (n=5). All data expressed as mean ± SEM and analysed using a 2-tailed Student's t-test. * $p<0.05$, ** $p<0.01$, *** $p< 0.001$.

Based on the turbimetric analyses, these data provide consistent evidence that Dex reduces procoagulant activity of both unstimulated and LPS-stimulated primary human monocytes.

5.3.2 Dex reduces LPS-induced TF expression

Having established that Dex reduces monocyte procoagulant activity, the role of Dex on TF expression was next investigated. TF expression was assessed using flow cytometric analyses (figure 5-4). Primary human monocytes were cultured with either vehicle control or LPS 1μg/mL. After 30 minutes, they were either treated with vehicle control or Dex 100nM. After 24 hours, TF protein expression was analyzed using a flow cytometric assay. TF mean fluorescence intensities (MFI) normalised to MFI of isotype control to yield relative MFI (RLMFI). The representative histograms and associated RLMFI values show that in unstimulated monocytes there was very little, if any, TF expressed, and treatment with Dex had no effect on TF expression (RLMFI Dex vs. Control, 1.38 vs. 1.33, p=0.788) . Given that Dex reduces procoagulant activity in the turbimetric clot assay, these results have the following explanations: (a) The levels of TF present in unstimulated monocytes are very low and the effect of Dex on these low levels of TF cannot be detected using flow cytometry; or (b) Dex may be modulating TF-independent pathways of coagulation. The former explanation is unlikely, as shown later with western blotting, that there is no detectable TF protein in unstimulated monocytes, corroborating previous published findings[84]. The TF-independent pathways, particularly in the setting of unstimulated monocytes, raise interesting questions, but are beyond the scope of this investigation. LPS is a strong stimulus for TF expression, and following LPS stimulation, there was a significant increase in TF expression. However, in LPS-stimulated monocytes, treatment with Dex resulted in a significant reduction in TF expression (RLMFI Dex vs. Control, 2.34 vs. 3.30, $p<0.001$). The remainder of this chapter will focus on the effect of Dex on TF expression in LPS-stimulated monocyte-macrophages.

Next, the effect of Dex concentration on TF expression in LPS-stimulated monocytes was investigated. In the above data, procoagulant activity and TF expression has been

evaluated at 24 hours. The effect of Dex was next examined at an earlier time point of 4 hours. Primary human monocytes were cultured with LPS 1μg/mL. After 30 minutes, they were treated with Dex (10^{-10}M to 10^{-6}M). After 4 and 24 hours, TF protein expression was analyzed using a flow cytometric assay (figures 5-5a,b). At both time points, Dex reduced TF expression in a concentration-dependent manner. At 4 hours, Dex produced statistically significant reductions in TF expression at ≥10^{-8}M, whereas at 24 hours, Dex produced statistically significant reductions in TF expression at ≥10^{-11}M. The greater effect in TF reduction with Dex seen at 24 hours is likely to reflect the longer duration of treatment.

To validate findings from flow cytometric assays, the TF protein levels were examined using Western blotting analysis. As above, primary human monocytes were cultured with LPS 1μg/mL. After 30 minutes, they were treated with Dex (10^{-11}M to 10^{-6}M). Lysates were prepared at 24 hours, and TF protein levels were determined. Similar to flow cytometric findings, figure 5-5c shows that Dex reduces TF expression in a concentration-dependent manner using western blotting analysis. When comparing both assays for TF detection at 24 hours, as in figures 5-5d,e, although both test modalities demonstrate the same effect, there are some differences. Dex starts to have a significant effect at lower concentrations (10^{-11}-10^{-10}M) in flow cytometric assays, whereas similar effects with western blotting are seen with higher concentrations of Dex, notably at 10^{-9}-10^{-8}M. This is likely to be explained by the fact that flow cytometry would detect the cell surface TF (cells were not permeabilised), whereas western blotting detects the total cellular TF pool, including intracellular and cell surface TF. Considering T_{lag} as the most sensitive clot turbimetric parameter, the clot turbimetric assay, which is largely a functional assay, indicates that lower concentration of Dex appear to reduce procoagulant activity. As it is the cell surface TF that is of functional significance, there appears to be concordance between clot turbimetric analyses and cell surface TF detected by flow cytometry. At Dex 10^{-11}-10^{-10}M, there appears to be little reduction in total cellular TF as determined by western blotting, whilst a greater reduction in cell surface TF. These findings raise the interesting possibility that Dex may

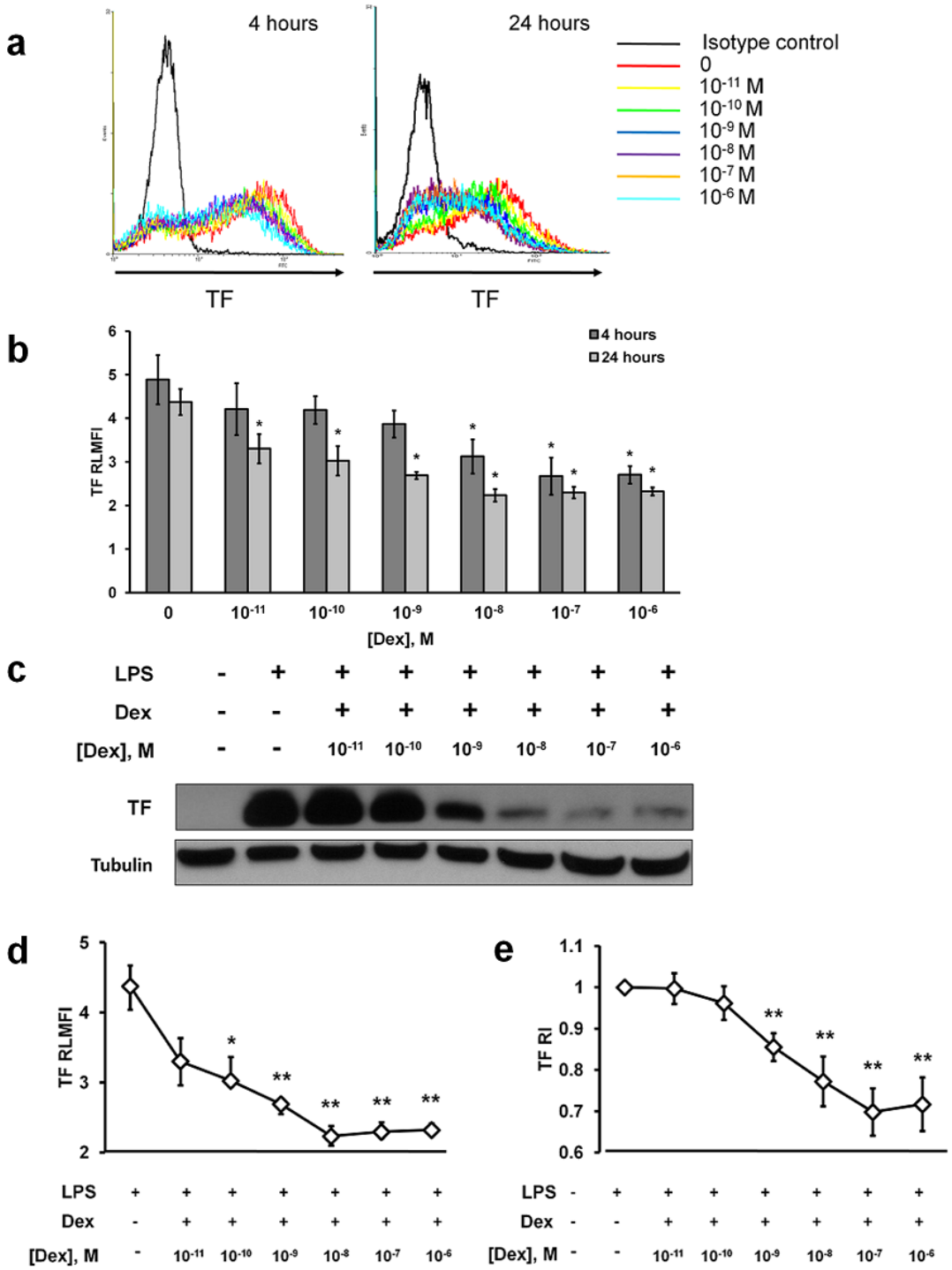

Figure 5-5: The effect of Dex concentration on TF protein expression in LPS-stimulated monocytes
Primary human monocytes were cultured with either vehicle control or LPS 1μg/mL. After 30min, they were either treated with vehicle control or Dex (10^{-10}-10^{-6}M). **(a,b)** TF protein expression analyzed using flow cytometric assay at 4 and 24h (n=3). Representative histograms shown in **(a)**, and analysis of TF mean fluorescence intensities (MFI) normalised to MFI of isotype control to yield relative MFI (RLMFI) shown in **(b)**; **(c)** Western blotting analysis of TF expression following treatment with different concentrations of Dex (n=4). Representative blot shown. The left hand lane represents unstimulated/untreated cells; **(d-e)** Comparison of TF protein levels as determined using flow cytometry and western blotting analysis, with **(d)** TF RLMFI values (n=3) and (d) densitometric analyses for western blotting experiments with TF immunodensity relative to the tubulin immunodensity normalized to the ratio in unstimulated cells (n=4). All data expressed as mean ± SEM and analysed using a 2-tailed Student's t-test. * $p<0.05$, ** $p<0.01$, *** $p< 0.001$, compared to untreated cells.

be acting at a post-translational level and regulating the shuttling of TF from intracellular stores (where it is functionally inactive) to extracellular sites (where it is functionally active). This is beyond the scope of the proposed investigation. Nevertheless, using two different assays, these data provide consistent evidence that Dex reduces TF protein expression in LPS-stimulated monocytes.

In the literature there is variability in the timings of Dex treatment in relation to LPS stimulation and different cells types used. Whether or not these factors may explain differences in the reported effects on TF expression is unknown. To test these factors, the timing of Dex treatment was first examined. Primary human monocytes were cultured with LPS 1µg/mL. Dex 100nM was added either 1 hour pre-, concurrent, or 1 hour post-LPS treatment. TF expression was quantified using flow cytometric analysis. Figure 5-6a shows that irrespective of timing of Dex treatment, Dex treatment resulted in a significant reduction in TF expression in LPS-stimulated monocytes. Next, to test whether the use of unfractionated PBMCs would yield a different finding, similar experiments were conducted in unfractionated PBMCs. Figure 5-6b shows that the effect of Dex in LPS-stimulated PBMCs was similar to that seen in primary human monocytes. Thus, these data indicate that Dex appears to have a universal effect in reducing LPS-induced TF response irrespective of timing of Dex treatment or whether or not monocytes vs. PBMCS are used.

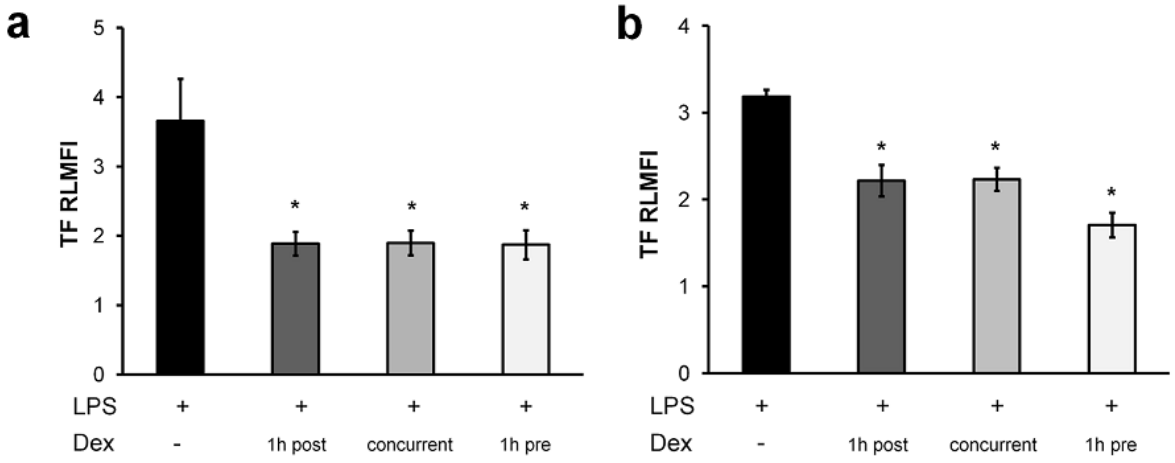

Figure 5-6: The effect of Dex on TF protein expression LPS-stimulated cells
(a) Primary human monocytes (n=4) or **(b)** unfractionated PBMCs (n=4) were cultured with LPS 1µg/mL. Dex 100nM was added at times shown in relation to LPS treatment (1h pre-, concurrent, or 1h post-LPS). TF expression was quantified using flow cytometric analysis at 24h after LPS treatment. TF mean fluorescence intensities (MFI) normalised to MFI of isotype control to yield relative MFI (RLMFI). All data expressed as mean ± SEM and analysed using a 2-tailed Student's t-test. * $p<0.05$, ** $p<0.01$, *** $p< 0.001$, compared to LPS-stimulated cells. Dex produces a reduction in TF protein expression in LPS-stimulated monocytes and unfractionated PBMCs, irrespective of timing of Dex treatment.

Finally, the effect of Dex on TF mRNA expression was tested in LPS-stimulated monocytes. Primary human monocytes were cultured with LPS 1µg/mL. After 30 minutes, they were treated with Dex (10^{-11}M to 10^{-6}M). TF mRNA levels were determined 2 hours after LPS stimulation. Figure 5-7 shows that throughout all concentrations, Dex was associated with a significant reduction in TF mRNA levels. Taking all the data together, these data provide strong evidence that Dex reduces TF expression in LPS-stimulated monocytes at both protein and mRNA level. This reduction in TF expression could reflect (a) reduction in TF transcription; (b) reduction in TF mRNA stability; or (c) both. Given that Dex is a transcriptional regulator, and has previously been shown to reduce TF transcription[444], the observed effect of Dex in the above experiments will certainly have a transcriptional component. However, whether or not TF mRNA stability is also playing a role is unknown. In Chapter 3, the p38-TTP axis was found to regulate TF mRNA at a post-transcriptional level. Given the known effects of Dex on p38 inhibition, it is intriguing to test whether Dex, through inhibition of p38 activity, would also act to reduce TF mRNA stability.

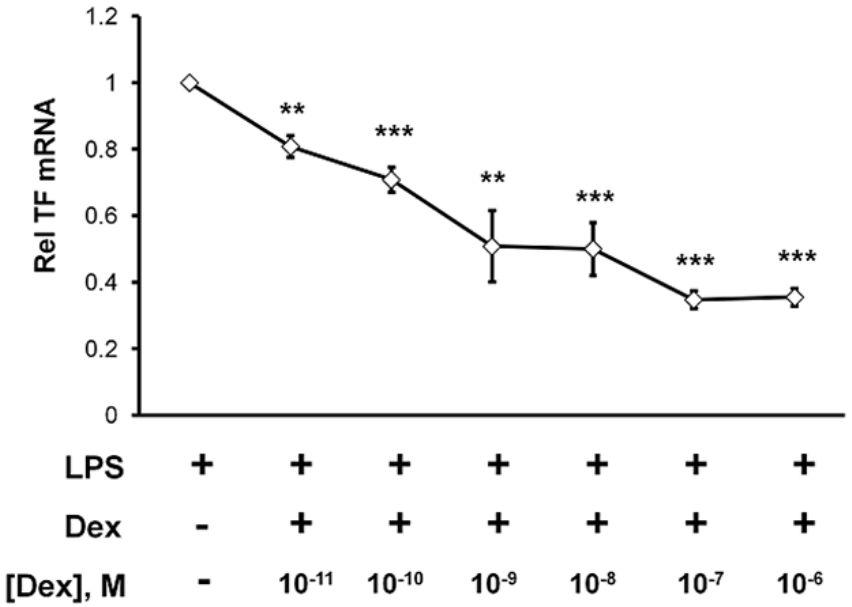

Figure 5-7: The effect of Dex concentration on TF mRNA expression in LPS-stimulated monocytes
Primary human monocytes were cultured with either vehicle control or LPS 1µg/mL. After 30min, they were either treated with vehicle control or Dex (10^{-10}-10^{-6}M). TF mRNA expression was determined using RT-PCR (n=4). mRNA levels were normalized to levels in the LPS-stimulated arm. All data expressed as mean ± SEM and analysed using a 2-tailed Student's t-test. * $p<0.05$, ** $p<0.01$, *** $p< 0.001$, compared to LPS-stimulated cells. Dex produces a concentration-dependent reduction in TF mRNA expression in LPS-stimulated monocytes.

5.3.3 Dex is a negative regulator of p38

Dex is known induce DUSP1, a key phosphatase known to dephosphorylate p38, thereby reducing p38 activity and function. LPS induces DUSP1, which acts as a negative feedback mechanism to limit an over-whelming pro-inflammatory response. Dex is known to further increase LPS-induced DUSP1 expression. To validate these findings, primary human monocytes were cultured with LPS 1µg/mL. After 30 minutes, they were treated with Dex (10^{-11}M to 10^{-6}M). DUSP1, total p38 and phospho-p38 levels were determined using western blotting analysis at 2 hours following LPS stimulation. In parallel experiments, DUSP1 mRNA levels were determined at 2 hours. Dex produced a concentration-dependent increase in DUSP1 expression both at the level of mRNA and protein. This was associated with a decrease in phospho-p38: total p38 ratio (Figure 5-8).

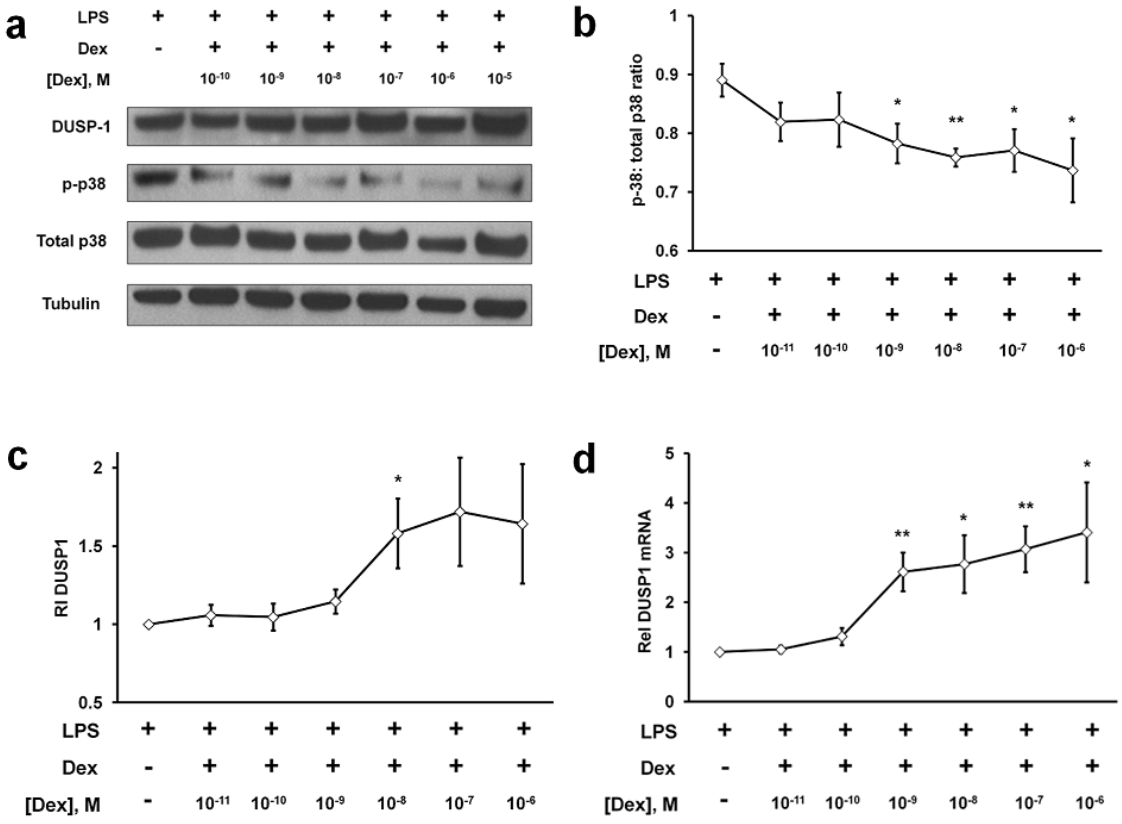

Figure 5-8: The effect of Dex concentration on DUSP1 and p38 expression in LPS-stimulated monocytes
Primary human monocytes were cultured with LPS 1µg/mL. After 30min, they were either treated with vehicle control or Dex (10^{-10}-10^{-6}M). DUSP1, total p38 and phospho-p38 protein levels were determined using western blotting analysis at 2h (n=4). **(a)** Representative blot shown; **(b)** Densitometric analysis where the p-p38: total p38 ratio is derived from p-p38 immunodensity/total p38 immunodensity; **(c)** Densitometric analysis where DUSP1 immunodensity relative to the tubulin immunodensity normalized to the ratio in LPS-stimulated cells; and **(d)** DUSP1 mRNA levels at 2h in cells treated as above (n=4). All data expressed as mean ± SEM and analysed using a 2-tailed Student's t-test. * p<0.05, ** p<0.01, *** p< 0.001, compared to LPS-stimulated cells. Dex produces a concentration-dependent reduction in p-p38: total p38 ratio, with a parallel increase in DUSP1 expression.

5.3.4 Dex increases TTP expression

Next, the effect of Dex on TTP expression was investigated in LPS-stimulated monocytes. As demonstrated previously, LPS induces TTP expression[438-440]. The effect of Dex on TTP expression in this setting is variably reported, and this is likely to reflect the different cell types studied[439, 440]. Primary human monocytes were cultured with LPS 1μg/mL. After 30 minutes, they were treated with Dex (10^{-11}M to 10^{-6}M). TTP protein levels were determined using western blotting analysis at 2 hours following LPS stimulation. Dex produced a concentration-dependent increase in LPS-induced TTP expression (figure 5-9). These data would indicate that Dex may potentially act synergistically to increase TTP-mediated mRNA decay. Firstly, it increases TTP expression resulting in an increase in cellular TTP pool, and secondly, it renders TTP active by reducing p38-mediated phosphorylation. Thus, the net effect is increased amounts of active TTP within the cell, which may potentially mediate target mRNA degradation.

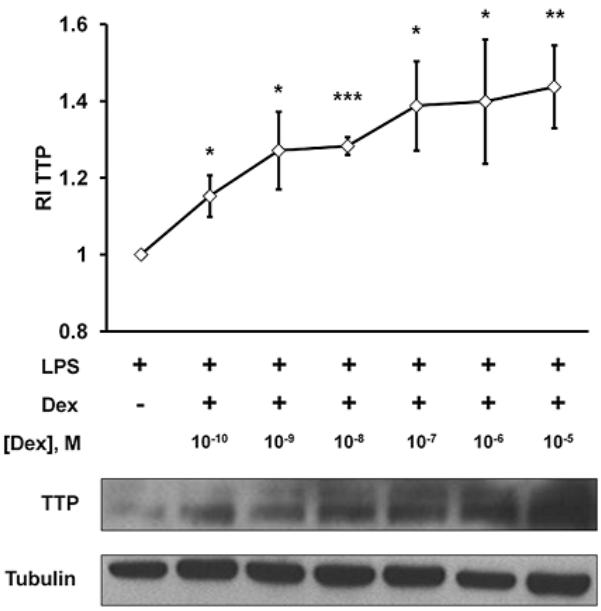

Figure 5-9: The effect of Dex concentration on TTP expression in LPS-stimulated monocytes
Primary human monocytes were cultured with LPS 1μg/mL. After 30min, they were either treated with vehicle control or Dex (10^{-10}-10^{-6}M). TTP protein levels were determined using western blotting analysis at 2h (n=4). Representative blot is shown at the bottom with densitometric analyses shown above where the TTP immunodensity is expressed relative to tubulin immunodensity and then normalized to the ratio in the LPS-stimulated cells. All data expressed as mean ± SEM and analysed using a 2-tailed Student's t-test. * $p<0.05$, ** $p<0.01$, *** $p< 0.001$, compared to LPS-stimulated cells. Dex produces a concentration-dependent increase in TTP expression.

5.3.5 Dex reduces TF mRNA stability

To specifically address whether Dex regulates TF mRNA stability, TF mRNA decay profiles were established following LPS stimulation both in the absence and presence of Dex. Parallel experiments with p38 inhibitors were also conducted to allow comparison. Monocytes were stimulated with LPS (1μg/mL). Dex 100nM was added 30 minutes after LPS. Actinomycin D (5μg/mL) was added at 2 hour to induce transcriptional arrest. SB compounds, SB202474, SB202190 and SB203580 1μM were added concurrently with actinomycin D. Given that all compounds were water soluble, water was added as a vehicle control to the control arm of the experiment. TF mRNA levels were quantified at time 0, 15, 30, 60 and 90 minutes after actinomycin D using RT-PCR and TF mRNA decay profiles determined. The TF mRNA half-life in the control arm of the experiment was 166±30 minutesutes. In the presence of Dex, there was a significant reduction in TF mRNA half-life to 30±7min (p=0.007). This effect was comparable to the effect seen with p38 inhibition (figures 5-10a,b). As Dex is a negative regulator of p38 activity, these data would otherwise be in keeping with the earlier observations that p38 MAPK pathway post-transcriptionally regulates TF mRNA expression. Figure 5-10c shows that unlike SB203580 1μM and SB202190 1μM, in addition to reducing phosphor-p38 levels, Dex also reduced phospho-JNK levels. Although this was not specifically tested, it would be intriguing to assess whether inhibition of JNK also reduced TF mRNA stability.

5.3.6 Dex reduces TF mRNA stability via a TTP-independent mechanism

If Dex reduces TF mRNA stability through p38 inhibition, then one would hypothesize that Dex would not have an effect on TF mRNA stability in the absence of TTP. This would be analogous to the absence of an effect with p38 inhibition seen in *Ttp*$^{-/-}$ macrophages. Thus to test this, the specific role for TTP in Dex-mediated reduction TF mRNA stability was examined. Murine macrophages were stimulated with LPS 1μg/mL. Dex 100nM was added 30 minutes after LPS. Actinomycin D (5μg/mL) was added at 2 hours to induce transcriptional arrest. As above, parallel experiments were also conducted with p38 inhibitors, where SB202190 and SB203580 1μM were added concurrently with actinomycin D. TF mRNA decay profiles were then determined (figures 5-11a-c).

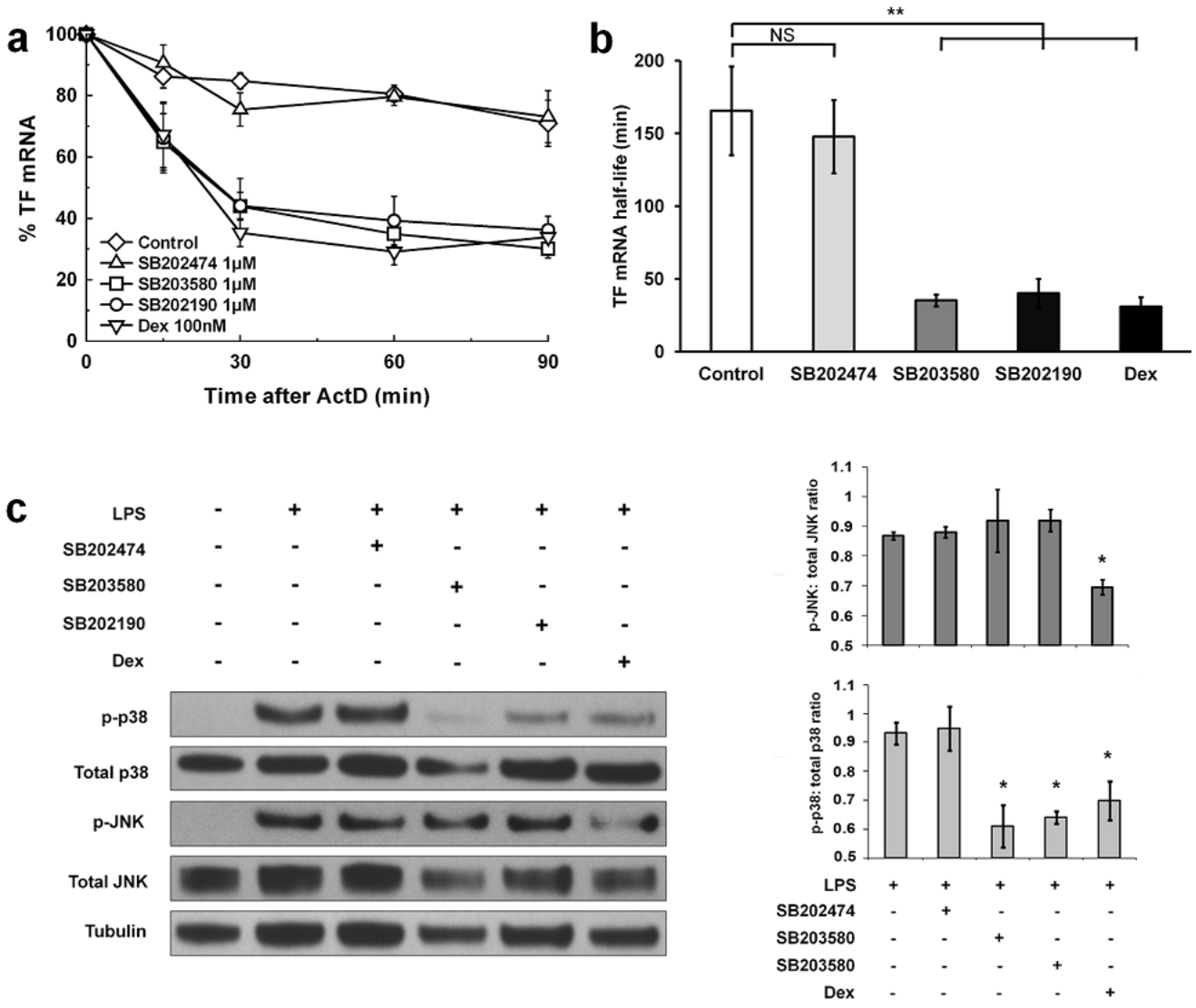

Figure 5-10: The effect of Dex on TF mRNA stability in LPS-stimulated primary human monocytes.
Monocytes were stimulated with LPS 1μg/mL for 2h. Dex 100nM was added 30 minutes after LPS stimulation. Actinomycin D (5μg/mL) was added at 2h to induce transcriptional arrest. In parallel experiments, inhibition of p38 was achieved using SB compounds 1μM which were added with actinomycin D (n=5). **(a)** TF mRNA levels were determined at each time point and normalized to levels at time point 0 to obtain mRNA decay profiles; **(b)** The decay profiles were modelled mathematically using non-linear regression analysis to determine mRNA half-life. Data expressed as mean ± SEM and analysed using a 2-tailed Student's t-test. * $p<0.05$, ** $p<0.01$, *** $p< 0.001$. Dex reduced TF mRNA stability-an effect which was comparable to p38 inhibition; and **(c)** Western blotting analysis to compare the effect of Dex with p38 inhibition on the p38 and JNK MAPK activity. Monocytes were stimulated with LPS 1μg/mL. Different SB compounds (SB202474 1μM, SB203580 1μM and SB202190 1μM) and Dex 100nM were added 30min after LPS. Total p38, phospho-p38, total JNK and phospo-JNK were determined at 2h after LPS stimulation using western blotting. SB203580 1μM, SB202190 1μM and Dex 100nM. Dex 100nM also resulted in reduced a significant reduction in phospho-JNK:total JNK whilst p38 inhibition had no observed effect. Representative blot of 3 independent experiments is shown on the left with densitometric analyses on the right. Data expressed as mean ± SEM and analysed using a 2-tailed Student's t-test. * $p<0.05$, ** $p<0.01$, *** $p< 0.001$ compared to LPS control arm of the experiment. Whilst SB203580 and SB202190 1μM exhibit relative selectivity for p38 inhibition, Dex 100nM reduces both phospho-p38 and phospho-JNK levels.

In WT murine macrophages, the TF mRNA half-life was 97±15 minutes. Dex resulted in a significant reduction in TF mRNA half-life to 41±11min (p=0.017), again comparable to p38 inhibition. These finding mirrored those seen in primary human monocytes (figures 5-10a,b). In *Ttp*$^{-/-}$ macrophages, TF mRNA half-life was 352±82 minutes. Interestingly, whilst p38 inhibitors had no effect on TF mRNA half-life in *Ttp*$^{-/-}$ macrophages, Dex resulted in a significant reduction in TF mRNA half-life to 54±8min (p=0.016). This was an unexpected finding, and these data would indicate that whilst Dex may act to reduce TF mRNA stability through p38 inhibition, other mechanisms must exist that are independent of TTP.

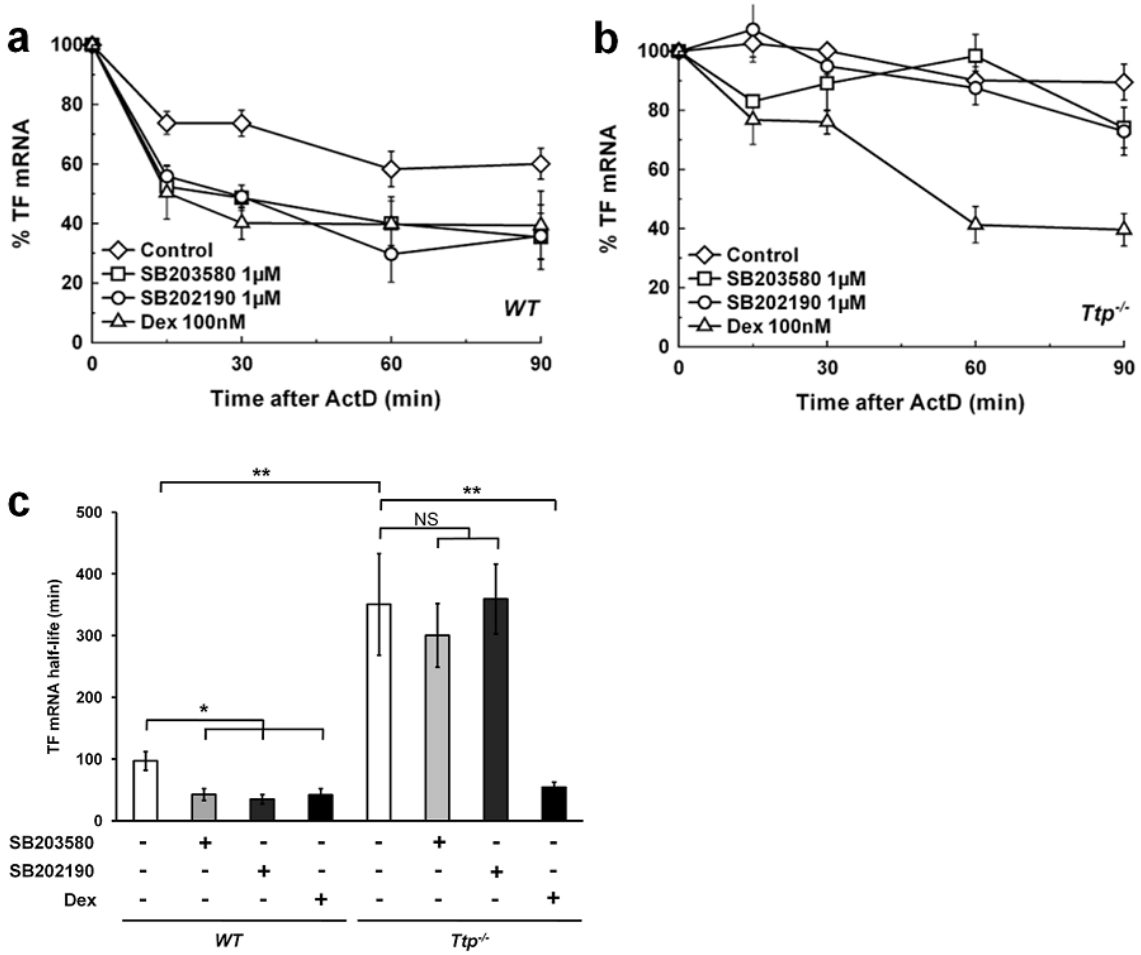

Figure 5-11: The effect of Dex on TF mRNA stability in LPS stimulated WT and *Ttp*$^{-/-}$ murine macrophages. WT and *Ttp*$^{-/-}$ murine macrophages were stimulated with LPS 1µg/mL for 2h. Dex 100nM was added 30mins after LPS stimulation. Actinomycin D (5µg/mL) was added at 2h to induce transcriptional arrest. In parallel experiments to allow comparison, inhibition of p38 was achieved using SB 203580 and SB202190 (both1µM) which were added with actinomycin D (n=5). TF mRNA levels were determined at each time point and normalized to levels at time point 0 to obtain mRNA decay profiles, as shown for **(a)** WT macrophages, and **(b)** *Ttp*$^{-/-}$ macrophages; **(c)** The decay profiles were modelled mathematically using non-linear regression analysis to determine mRNA half-life. Data expressed as mean ± SEM and analysed using a 2-tailed Student's t-test. * p<0.05, ** p<0.01, *** p< 0.001. Dex reduced TF mRNA stability in WT cells-an effect which was comparable to p38 inhibition. However, despite p38 inhibition having no effect on TF mRNA in stability in *Ttp*$^{-/-}$ macrophages, Dex resulted in a reduction in TF mRNA stability in *Ttp*$^{-/-}$ macrophages.

5.4 DISCUSSION

In this chapter, we sought to determine if Dex would reduce TF mRNA stability. The hypothesis was founded upon the fact that Dex is negative regulator of p38 activity and function, and the observation that p38 inhibition reduces TF mRNA stability. The above data has a number of interesting findings. Firstly, Dex reduces TF expression in LPS stimulated monocyte-macrophages. Secondly, indeed, this effect is in part due to a reduction in TF mRNA stability. Thirdly, whilst Dex is a negative regulator of the p38-TTP axis, other TTP-independent mechanisms are likely to contribute to this effect.

Current data on the effect of GCs on monocyte TF expression are ambiguous[442-444]. Earlier studies had demonstrated that methylprednisolone reduced procoagulant activity of LPS-stimulated PBMCs[442]. Contrary to this finding, Dex enhanced LPS induction of TF in THP-1 cells and PBMCs, when co-stimulated with LPS and Dex, and that this was not a result of increased mRNA stability, implicating increased gene transcription to play a role[443]. In another study, Dex also enhanced LPS induction of TF in THP-1 cells, when pre-incubated with Dex for 30 minutes prior to LPS stimulation. Using TF-promoter-LUC constructs, it was shown that Dex inhibited TF gene transcription[444]. This effect of Dex on TF transcription would be in keeping with our current understanding on Dex as the TF promoter contains binding sites for transcription factors AP-1, NF-κB, that mediate the LPS-induced TF response[190, 251, 447], and Dex is known to block NF-κB and AP-1 activity[448]. In this particular study, however, Dex was found to increase TF mRNA stability, with an overall increase in TF expression[444]. These conflicting findings of the effect of Dex on TF expression and TF mRNA stability may be explained by the different cells types studied (primary human monocytes vs. THP-1 cells vs. unfractionated PBMCs). Certainly, there remain important differences between THP-1 cells and primary human monocytes[422]. Another possible explanation could be the timing of Dex treatment. There appears to be variability in the experimental designs of these studies, where Dex is administered prior to or with concurrent LPS treatment. To our knowledge there are no published data on the effect of Dex on TF expression in primary human

monocytes. It was therefore crucial to first characterize the effect of Dex on monocyte procoagulant activity and TF expression.

Using functional clot turbimetric assays, Dex was found to reduce procoagulant activity in both unstimulated and LPS-stimulated monocytes. Subsequent experiments demonstrated Dex reduced TF expression both at mRNA and protein level. An interesting observation was that that Dex reduced procoagulant activity in unstimulated monocytes, despite there being very little, if any, detectable TF in unstimulated monocytes (as shown using western blotting and flow cytometry). This raises the possibility that Dex may modulate TF-independent pathways. Macrophages can initiate coagulation via the Mac-1 (CD11b/CD18, $\alpha_M\beta_2$) receptor[69] and through the expression of factor VII activating protein (FSAP)[72]. Mac-1 can bind to factor X and following exposure to ADP, macrophages can catalyse the activation of cell-bound factor X to factor Xa, independent of TF and factor VIIa[69]. FSAP is a serine protease, secreted by macrophages. The primary substrates for FSAP are factor VII and uPA[72], and therefore, FSAP may play important roles in initiating the extrinsic pathway and mediating fibrinolysis, although there is greater evidence for the latter. Dex has been shown to reduce Mac-1 expression in human eosinophils[449]. Although this has not been demonstrated in monocyte-macrophages, one can postulate that Dex may reduce monocyte procoagulant activity through a reduction in Mac-1 expression. The experimental dissection of the TF-independent pathways was beyond the scope of this study. Another interesting finding stemmed from the direct comparison of TF expression as demonstrated using flow cytometry vs. western blotting. Both assays demonstrated that Dex reduce TF protein expression in LPS-stimulated monocytes. However, flow cytometry detects cell surface TF antigen, whereas western blotting detects the total cellular TF pool. The functional clot turbimetric assays, demonstrated Dex to reduce procoagulant activity at concentrations as low as 10^{-10}M. At this concentration, cell surface TF protein expression was reduced, as shown using flow cytometry, However, at this concentration, there was very little change in the total cellular TF pool, as shown using western blotting. Whilst the differences in sensitivities between the two assays may explain this, one may speculate that Dex may play a role at a post-translational

level and modulate shuttling of TF from the extracellular to the intracellular compartment. Whilst, these alternative explanations are far from conclusive, they are certainly hypothesis generating, and further dissection of these potentially interesting mechanisms are, again, beyond the scope of this study.

Having established that Dex reduces TF expression in LPS stimulated monocytes, whether or not this effect was a result of reduced TF mRNA stability was investigated with TF mRNA decay experiments in both primary human monocytes and WT murine macrophages. These experiments specifically demonstrated that Dex significantly reduced TF mRNA stability, an effect which was comparable to p38 inhibition. This was in keeping with the original hypothesis, as Dex is known to increase DUSP1 expression which in turn dephosphorylates p38, thereby reducing its activity and function. Earlier experiments in *Ttp*$^{-/-}$ murine macrophages had demonstrated that p38 inhibition had no effect on TF mRNA half-life, implicating a TTP-dependent mechanism. On this basis, given that Dex is a negative regulator of p38, one would similarly hypothesize that Dex would not have an effect on TF mRNA stability in *Ttp*$^{-/-}$ macrophages. However, unexpectedly, Dex reduced TF mRNA stability in *Ttp*$^{-/-}$ macrophages. This interesting observation indicates that Dex is additionally likely to regulate TF mRNA stability through other TTP-independent mechanisms, most likely microRNAs or other RNA-binding proteins.

In conclusion, these data demonstrate for the first time that Dex reduces TF expression in LPS-stimulated monocytes. This effect is, in part, due to a reduction in TF mRNA stability – an effect comparable to p38 inhibition. Dex negatively regulates p38 activity through induction of DUSP1 that dephosphorylates p38. Dex also increases TTP expression, and therefore the net effect of Dex is to increase the dephosphorylated (active) form of TTP. Whilst Dex is likely to regulate TF mRNA stability, in part, through the p38-TTP axis, experiments in *Ttp*$^{-/-}$ macrophages demonstrate that other TTP-independent mechanisms are likely to be contributory. The characterization of these TTP-independent pathways warrant further study.

Chapter 6

General Discussion

6.1 Current understanding of the post-transcriptional regulation of TF

Tissue factor (TF) is a 47kDa transmembrane cell surface glycoprotein and is the key trigger for the extrinsic coagulation cascade resulting in thrombus formation[152]. Monocyte-macrophages are an important source of TF in atherothrombosis, both within the plaque and the circulating blood. Throughout plaque formation, the inflammatory milieu induces TF expression in plaque macrophages, foam cells and smooth muscle cells[43]. Within the blood, TF is expressed in circulating monocytes and TF-containing microparticles which are predominantly derived from monocyte-macrophages[77]. Following plaque rupture, TF within the necrotic core is exposed to the flowing blood and initiates thrombosis resulting in acute ischaemia[37, 38] or asymptomatic plaque growth[39]. Activation of PARs by coagulation proteases provide an important means for TF to mediate cross-talk between coagulation and inflammation[71]. TF may also contribute to plaque development through coagulation-independent mechanisms. For example, the TF/VIIa complex has been shown to be a stimulus for smooth muscle migration in atherosclerotic plaques[220, 221]. Furthermore, TF may also promote plaque neovascularization[154], thereby contributing to plaque growth, haemorrhage and instability. Taken together, the multiple roles TF may play in atherothrombosis indicate that a detailed understanding of the mechanisms regulating its expression is essential, not only for understanding pathophysiology but also for the identification of novel therapeutic targets.

The passage of genetic information from DNA through to the effector protein molecule is highly regulated. In addition to transcriptional and translational control, there is overwhelming evidence for the role of mRNA turnover in determining net gene expression. Post-transcriptional controls on mRNA safe-guard against inappropriate transcriptional leak, couple steady-state mRNA levels to transcription, and provide the means for accelerated mRNA decay to terminate gene expression[304]. The mRNA serves as a template for translation, and the level of steady state mRNA present in a cell, depends on the balance between its rate of formation and decay. The concept of mRNA decay gives rise to the concept of mRNA stability and half-life. The regulation of mRNA stability is complex depending on the dynamic interplay between target mRNA

sequence elements; RNA-binding proteins and cofactors; and mRNA degradation machinery. In broadest terms, mRNA stability is governed by specific sequences in the 3'UTR of transcripts and their interaction with different RNA-binding proteins, which depending on their function, mediate either mRNA stabilization or decay. Although the TF transcript is known to be intrinsically unstable[259, 260], little has been known about its post-transcriptional regulation. The TF 3'UTR contains several AREs that may serve as potential binding sites for ARE-binding proteins, and indeed TF mRNA has been assigned to the group III cluster of the ARED database[261]. These AREs are functional and conserved in both human and mouse. Although, the roles for microRNAs in regulating TF mRNA stability have recently been reported[268], the precise molecular mechanisms involved in ARE-mediated TF mRNA decay have not been fully elucidated. Furthermore, whether or not other inducible proteins besides ARE-binding proteins are required is not known.

The data presented in this thesis breaks new ground in two general areas. First, it provides new information on the post-transcriptional regulation of TF, a protein which is central to thrombosis and atherosclerosis. Secondly, it identifies a fundamental mechanism by which mRNA stability is subject to differential regulation in inflammatory processes. These data represent a significant advance in our understanding of the regulation of TF mRNA turnover, and thus post-transcriptional control should be considered alongside transcriptional[177, 249] and post-translational[450] regulation as one of the critical levels at which expression of this important protein is regulated.

6.2 TTP regulates TF mRNA stability

TTP is the most widely studied ARE-binding protein and the optimal ARE-binding site is considered to be UUAUUUA(U/A)(U/A)[264-266]. A similar sequence is present in a palindromic ARE sequence at the distal end of TF 3'UTR. TTP exists in two forms: dephosphorylated (active) and phosphorylated (inactive). The p38 MAPK pathway plays a pivotal role in the regulation of TTP activity. p38 activates MAPKAPK-2, and both MAPKAPK-2 and to a lesser extent p38 can phosphorylate and inactivate TTP[363]. Classically, inhibition of p38 reduces the stability of TTP-regulated transcripts.

Experiments conducted in LPS-stimulated monocyte-macrophage demonstrated that inhibition of p38 reduced TF expression and TF mRNA stability. This was demonstrated using a variety of p38 inhibitors (SB202190, SB203580, BIRB796 and LY2228800). A direct role for TTP was demonstrated by increased TF expression and increased TF mRNA stability in *Ttp*$^{-/-}$ macrophages. The effect of p38 inhibition was most likely to be TTP-dependent as p38 inhibition in *Ttp*$^{-/-}$ macrophages had no effect on TF mRNA stability. This is an important observation as other ARE-binding proteins, e.g. AUF1 and KSRP are also regulated by p38-mediated phosphorylation. Using RNP immunoprecipitation techniques and RNA-biotin pulldown assays a direct interaction between TF 3'UTR and TTP was demonstrated and further mutational analyses highlighted 2 specific overlapping nonameric ARE sequences, AUUUAUUUA and UUAUUUAAU, to mediate TTP binding in a cooperative manner.

This is the first time that TTP has been shown to post-transcriptionally regulate TF expression. Over the recent years, many studies have revealed numerous targets for TTP. Various approaches have been used including small interfering RNA knockdown experiments[451]; "forced" TTP-promoted mRNA degradation, in which overexpression of TTP in transfected cells has been shown to stimulate the breakdown of potential target mRNAs[452-455]; *in vitro* decay studies[456]; and microarray analyses[340]. Specifically, a genome-wide approach combining RNP immunoprecipitation and microarray analysis in RAW264.7 cells, treated with LPS for 2 hours, identified 137 mRNAs as targets for TTP[340]. The major drawback of "forced" TTP expression is that given the major determinant of TTP binding is the ARE binding site sequence and that relatively minor sequence variations might still permit TTP binding, TTP-mediated mRNA decay may still occur if the TTP concentrations are high enough. This may result in identifying false-positive TTP targets. Using the strict criterion that for TTP-regulated transcripts where mRNA stabilization needs to be demonstrated in cells derived from the *Ttp*$^{-/-}$ mice, a microarray analysis of RNA from wild-type and TTP-deficient mouse embryonic fibroblast cell lines after serum stimulation and treatment with actinomycin D, identified 250 mRNAs that were stabilized in the absence of TTP[364]. It is interesting to note that in all reported studies, TF has never been identified as a TTP target. There are a number

of possible explanations. Firstly, there are likely to be important differences in the cells lines used in these studies. In this thesis, primary human and murine macrophages have been used for analysis, and there are no micro-array analyses examining TTP targets specifically in primary human and murine macrophages. Secondly, the stimulants used in these studies are variable, and in this thesis, LPS has been used as the stimulus, as it induces a powerful induction in TF expression. Thirdly, given the kinetics of TF mRNA expression, the duration of stimulation prior to analysis of TF mRNA decay is critical. TF mRNA levels peak early at 2-4 hours and are followed by a rapid decline in levels. In this thesis, the timing for analysis of TF mRNA decay was set at 2 hours, as this represented the time at peak TF mRNA levels, and where the transcripts were relatively stable, allowing detection of changes in mRNA stability in response to different pharmacological inhibitors and/or macrophage phenotypes. For example, if the baseline TF mRNA half-life was very high (stable), then it would be difficult to detect increased mRNA stability, and conversely, if the TF mRNA half-life was very low (unstable), then it would be difficult to detect decreased mRNA stability. It is interesting to note, that in a study examining TF mRNA stability in lung epithelial cells, the TF 3'UTR was shown to bind a 37kDa protein which was postulated to confer instability[267]. Although TTP would be a candidate protein, to date, the identity of this protein has not been reported.

Similarly, p38 inhibition has not previously been shown to regulate TF mRNA stability. There are no specific studies reporting the spectrum of target mRNAs destabilized by p38 inhibition in primary human and murine macrophages. However, a large scale comprehensive analysis examining the effect of p38 inhibition, using SB203580, on mRNA decay of 470 ARE-containing mRNAs in LPS-stimulated THP-1 cells did not identify TF as exhibiting p38-dependent decay[457]. In this study, THP-1 cells were stimulated with LPS for 2 hours prior to transcriptional arrest with actinomycin D, which is comparable to our experimental protocol based on TF mRNA kinetics. However, the results of this study are far from conclusive. For example, IL-3, TNFα, and uPA have been reported to be stabilized by p38 activation[458-460], but this study failed to highlight these mRNAs. This is particularly surprising for TNFα, which is considered to be the

model TTP-regulated transcript. Although the precise basis for these discrepant findings are unclear, it is likely to reflect the different cell lines used.

The TF 3'UTR contains a number of AREs which are conserved in mouse and human. The final palindromic ARE in the 3'UTR is highly conserved throughout different species and was found to be functional in mediating TTP-mediated TF mRNA decay. This observation is consistent with a previous study where the destabilizing element within TF 3'UTR was found to be confined to the last 150bp sequence[260]. In this study, the more upstream 3'UTR sequence was also shown to confer some degree of mRNA instability, and it is possible that this may be due to miRNA, as the mir-19 binding site is located in the more proximal segment of TF 3'UTR[268]. The evidence for mir-19 regulating TF comes from a recent study examining TF expression in breast cancer cells, where the use of luciferase reporter constructs demonstrated that deletion of mir-19 binding site in TF 3'UTR resulted in increased luciferase activity to a level comparable with that of the control construct, which comprised the anti-sense TF 3'UTR sequence[268]. However, one may question this observation, as if the mir-19 binding site is disrupted this should not affect ARE-mediated decay, and one should still expect to have seen reduced luciferase activity compared to the control construct. This may be explained by closer examination of the TF 3'UTR constructs and this reveals that the cloned sequences used in this study were actually devoid of the final 218bp which contains the palindromic ARE. One may presume that the deliberate exclusion of this final ARE-rich sequence in this study would reduce potential confounding and allow easier detection and assessment of miRNA-mediated degradation. Nevertheless, this provides indirect evidence that the non-miRNA-mediated destabilizing elements in TF 3'UTR are likely to be located in final 218 bp sequence.

The *in vitro* analyses in *Ttp*$^{-/-}$ macrophages demonstrated that TTP deficiency results in increased TF expression. Given that TTP deficiency also results in increased TNFα expression and that TNFα, itself, increases TF expression, it is very likely that the increased TF expression seen in *Ttp*$^{-/-}$ cells has a transcriptional component. The effect of TTP deficiency on the TF transcription was not specifically tested. However, the

effect on post-transcriptional regulation can be confidently dissected using mRNA decay experiments with actinomycin D which induces transcriptional arrest. The increased TNFα in *Ttp*$^{-/-}$ mice, however, limits the applicability of these mice in determining TF expression *in vivo*. The increased TNFα *in vivo* can increase TF expression, and thus will have confounded interpretation. This problem may be potentially circumvented by treating mice with TNFα inhibitors[313], however non-specific effects of these inhibitors, particularly on TF expression cannot be excluded. A more robust strategy to determine whether TTP is acting to destabilize TF expression *in vivo* would be to investigate TF expression using triple knock-out mouse (deficient in TTP and both of the known TNFα receptors, TNFR1 and TNFR2)[316, 461, 462]. Mice deficient in TTP and TNFR1, or in TTP and both receptors, are protected from developing the TNF-alpha-induced cachexia and inflammation[316]. Thus the absence of TNFα effects would allow less confounded assessment of the *in vivo* non-transcriptional effects of TTP deficiency on TF expression.

6.3 PARP-14 regulates TF mRNA stability

Poly(ADP-ribosyl)ation is a post-translational modification where negatively charged ADP-ribose moieties are adducted onto proteins and this process is catalyzed by PARPs. Most of our current understanding of PARPs is centred on PARP-1 and PARP-2, that have been shown to regulate transcription, chromosome structure, and DNA damage repair. As such, there is very little data on the functions of other PARP family members. PARP-14, a macroPARP, has been shown to be a co-activator of IL-4/Stat-6-mediated transcription in B lymphocytes[401, 406, 407], acting as a transcriptional switch by ADP-ribosylating HDAC 2 and 3, which are then released from IL-4 responsive promoters to allow access of histone acetyl transferases. Recently, several PARP family members, including PARP-14, have been shown to have roles in RNA regulation[395, 408]. ADP ribosylation plays an important role within the SG where specific PARPs (PARP-5a; PARP-12, PARP-13, PARP-14, PARP-15), and two PARG isoforms (PARG99 and PARG102) have been shown to be SG components. Overexpression of these PARPs results in the de novo formation of SGs, whilst overexpression of the PARG isoforms result in inhibition of SG assembly and knockdown of PARG delays the disassembly of

SG[395]. These data suggest that the levels of ADP-ribose within the cytoplasm are locally regulated for the assembly and maintenance of SG structure. Furthermore, RNA-binding proteins Ago2, G3BP1, and TIA-1 can be modified by ADP ribosylation; and PABP, although not specifically modified by ADP–ribosylation, can bind ADP-ribose moieties[395]. Thus the function of ADP ribosylation in SGs may be analogous to the role in other cellular scaffolds, e.g. at the mitotic spindle, Cajal bodies or at DNA damage sites[396, 397], where the ADP-ribose scaffold in the SG regulates specific interactions between different RNA-binding proteins. The presence of PARGs within the SG further adds regulatory complexity, whereby regulation of ADP-ribose synthesis may ultimately serve to regulate the recruitment of RNA regulatory proteins. ADP ribosylation has been proposed to regulate miRNA function, such that following cellular stress, local high concentrations of ADP-ribose around the Ago2 or miRNA complex may either function to disrupt electrostatic interactions between similarly charged miRNA and mRNA, or cause steric hindrance for effective miRNA silencing[395]. TTP is also an important component of the SG, and it is possible that ADP ribosylation may serve to regulate TTP-mediated mRNA decay either through direct modification of TTP or another member of the mRNA decay complex. APLF is a novel component of the DNA repair machinery and contains two tandem ZF domains that closely resemble the tandem Zn fingers present in TTP. Interestingly, APLF has been shown to bind ADP-ribose moieties via the ZF domains, indicating the potential for TTP to bind sites of ADP-ribosylation[463].

Preliminary experiments in *Parp14*$^{-/-}$ macrophages demonstrated that the absence of PARP-14 resulted in increased TF expression and that this was due to increased TF mRNA stability. Whether or not the absence of PARP-14 also results in increased TF transcription was not specifically tested. Nevertheless, the in vitro findings were supported by in vivo findings of increased TF expression within different organs harvested from unstimulated and LPS-stimulated mice. Clearly, the organ tissues comprised of a number of different cells types besides macrophages, which were the cell type used for conducting the in vitro experiments. Although not specifically tested, this would broadly suggest that PARP-14 may also regulate TF expression in other cell

types. However, the finding that PARP-14 deficiency was associated with increased TF activity in unfractionated peripheral leukocytes in unstimulated and LPS-stimulated mice would specifically support the in vitro findings in macrophages. Importantly, the functional and pathological significance of the increased TF expression seen in *Parp14*$^{-/-}$ mice was demonstrated by intravital microscopy where cremasteric artery occlusion time following ferric chloride injury was accelerated in LPS-stimulated *Parp14*$^{-/-}$ mice. Thrombosis in this model has been shown to be dependent on TF[464-466], although under normal circumstances TF expressed by vascular smooth muscle cells (VSMC) may make the predominant contribution[466]. The ferric chloride induces chemical injury when applied topically to the outer medial/adventitial artery wall, and is referred to as an outside-in model of injury. Ferric chloride reaches the arterial lumen via an endocytic-exocytic pathway resulting in complete denudation of the endothelium and exposure of the blood to medial TF resulting in localised thrombosis[467]. This small animal model of thrombosis is thought to be comparable to arterial thrombosis in large animal models because there are cyclic flow variations induced by the presence of thrombi in arteries after ferric chloride injury[468]. The role of TF has been examined in this model using mice with either a conditional deletion of the TF gene in VSMCs or with increased expression of TFPI in VSMCs[465, 466]. Both studies demonstrated that a reduction of TF activity was associated with an increase in the time to occlusion, indicating that "vessel wall" TF mediates ferric chloride-induced thrombosis. It remains to be determined whether the increased thrombogenicity in this model in *Parp14*$^{-/-}$ mice is due to increased VSMC expression of TF and/or to the increased TF activity as demonstrated in circulating leukocytes. It is also possible that *Parp14*$^{-/-}$ mice may have increased levels of circulating microparticles expressing TF at 4 hours after LPS challenge and that these may contribute to the accelerated thrombosis observed in this model.

Subsequent *in vitro* experiments demonstrated that PARP-14 appears to cooperate with TTP, such that both these proteins appear to form a ternary complex with TF 3'UTR involving the same nonameric ARE sequences as determined for TTP. RNA-biotin pulldown assays demonstrated that in the absence of PARP-14, TTP does not appear to interact with TF 3'UTR, although low-affinity binding cannot be excluded. Similarly, in

the absence of TTP, the binding of PARP-14 to TF 3'UTR is reduced. Although TTP expression appears to be increased in *Parp14*$^{-/-}$ cells, the TF mRNA is stable, indicating that TTP is not able to exert its TF mRNA destabilizing function. One may postulate that altered TTP phosphorylation may limit TTP-binding, but this is unlikely as specific experiments using p38 inhibition demonstrated that the TTP phosphorylation status should not affect TTP-binding. This is in keeping with previously reported studies[331]. Furthermore, phospho-p38 levels were found to be similar in the absence and presence of PARP-14. To definitively determine if PARP-14 alters the phosphorylation status of TTP, one would need to perform a phosphorylation blot specifically for TTP phosphorylation at Ser-52 and Ser-178 sites[20, 21]. However, there are no reliable antibodies available to conduct such analysis.

This is first time a PARP family member has been shown to cooperate with an established RNA-binding protein and regulate mRNA stability. Both TNFα and TTP (itself) are established targets for TTP, and both TNFα and TTP mRNA stability was unaffected by the absence or presence of PARP-14. Given that TF, a TTP regulated transcript was found to be co-regulated by PARP-14 at the level of mRNA stability, these also data provide evidence, for the first time, how the effects of TTP may differentially regulated. One may postulate that PARP-14 serves as an accessory protein that regulates TTP binding to a subset of TTP-regulated transcripts where TTP binding has insufficient affinity because of the specific ARE sequence and/or RNA folded structure. Whether or not an alternative accessory protein(s) is required for optimal TTP binding to TNFα mRNA 3'UTR and other PARP-14- independent TTP target transcripts remains to be determined. Further work will also be directed at determining the subset mRNA transcripts, or RNA regulon[469], coregulated by PARP-14 and TTP and whether these encode a set of functionally-related proteins that might all be simultaneously regulated. The presence of the PARP domain and its catalytic activity adds further complexity to the post-transcriptional regulatory mechanisms. Using PARP inhibitors, PJ34 and 3AB, mRNA decay experiments in human monocytes and WT murine macrophages demonstrated that PARP inhibition reduced TF mRNA stability. The drawback of these compounds is that these are non-specific inhibitors and not

specific for PARP-14. However, some degree of specificity for PARP-14-TTP interaction may be conferred by experiments where PARP inhibition had no effect on TF mRNA stability in *Parp14*$^{-/-}$ cells. Conversely, one may argue that in the absence of either TTP or PARP-14 these proteins are not able to bind to TF 3'UTR, and thus the absence of an effect of PARP inhibition would be expected in *Parp14*$^{-/-}$ and *Ttp*$^{-/-}$ cells. A definitive role for PARP-14 can only be established using PARP-14 specific inhibitors, and these compounds are currently in development. Nevertheless, these experiments confirmed that the PARP inhibitors are not having a non-specific effect on mRNA decay, given the absence of a TF mRNA destabilizing effect in *Parp14*$^{-/-}$ cells. Interestingly, the effect of PARP inhibition did not appear to have an effect on TNFα mRNA stability, again lending further lends support to the fact that these compounds are not having a generalized non-specific effect on mRNA decay, but more importantly demonstrates how ADP-ribosylation may potentially serve to differentially regulate TTP-regulated transcripts.

Therefore the data presented in this thesis support two distinct roles for PARP-14 in the regulation of TF mRNA stability. Firstly, PARP-14 is an accessory protein required for TTP to bind TF mRNA. Secondly, the PARP catalytic activity of PARP-14 serves to stabilize TF mRNA, such that inhibition of PARP activity results in increased TF mRNA decay. The precise role of ADP-ribosylation in this system is not clear, but it is possible that PARP-14-mediated ADP ribosylation is modifying TTP or another candidate protein in the mRNA decay complex to ultimately inhibit TTP-mediated mRNA decay. The precise molecular targets for ADP-ribosylation in this system remain the focus of ongoing work. One mechanism for TTP-mediated decay is interfering with mRNA circularization, by binding to PABP and displacing it from the poly(A) tail thereby promoting 3′-to-5′ degradation. Given that PABP can be ADP-ribosylated, it is intriguing to speculate that ADP-ribosylation of PABP may hinder TTP binding thereby limiting TF mRNA decay.

6.4 A proposed model for the regulation of TF mRNA stability

Taken together, the data presented in this thesis indicates that both p38-mediated phosphorylation and PARP-14-mediated ADP-ribosylation regulate TF mRNA stability.

A proposed model of how these two events co-regulate TF mRNA stability is presented in figure 6-1. As portrayed graphically, TF mRNA is stabilised in *Parp14*$^{-/-}$ and *Ttp*$^{-/-}$ cells

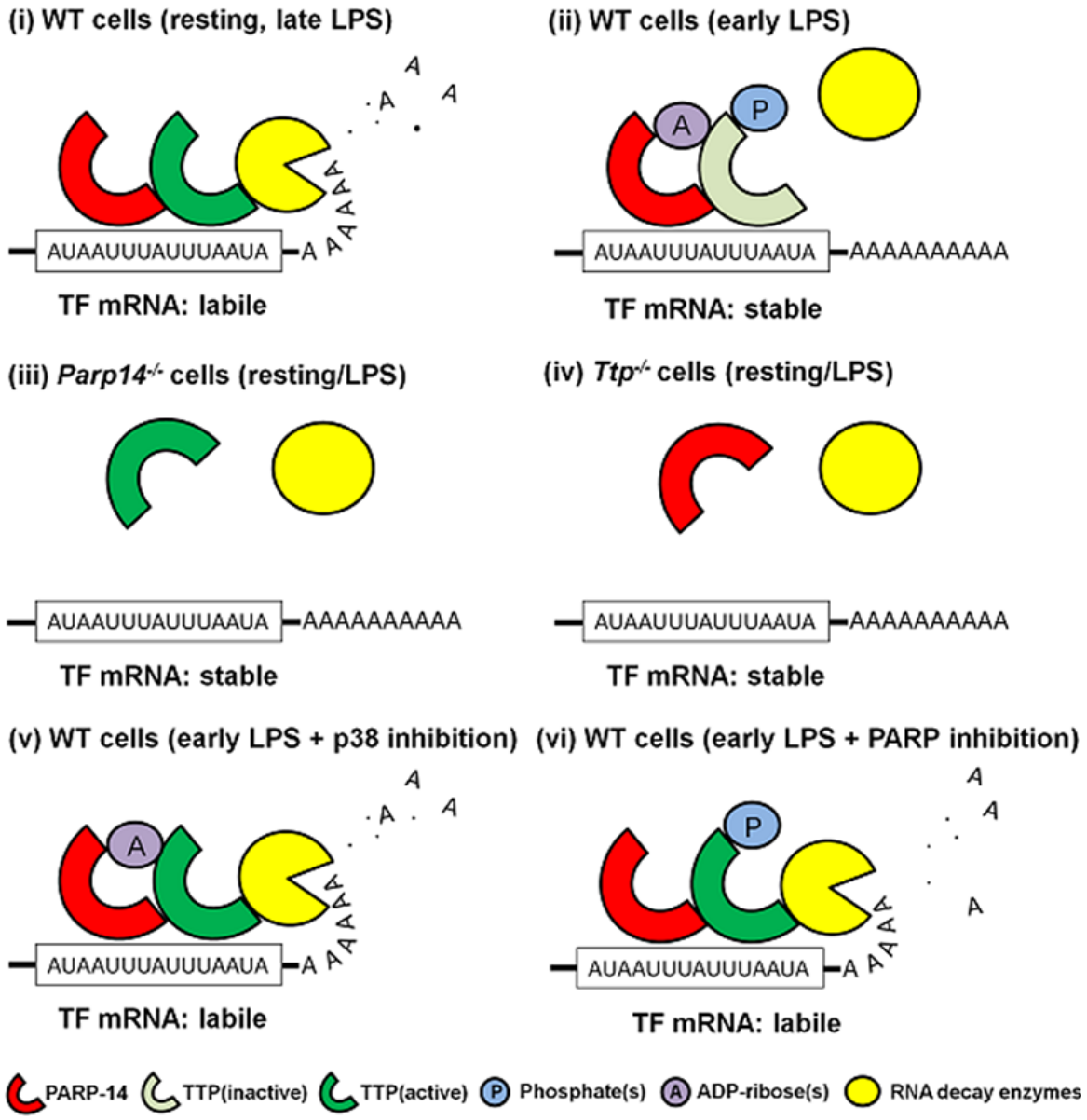

Figure 6-1: A hypothetical working model for the regulation of TF mRNA stability
In this working model, both PARP-14 and TTP are necessary for both these proteins to bind TF 3'UTR **(i, ii)**. Thus in *Parp14*$^{-/-}$ or *Ttp*$^{-/-}$ cells, this complex cannot form and TF mRNA is stable **(iii,iv)**. Both p38-mediated phosphorylation and PARP-14-mediated ADP ribosylation events are necessary to inhibit TTP-mediated TFmRNA decay. Thus in the resting state or late in the LPS response , the absence of either one of these events renders TF mRNA labile **(i)**. In the earlier phase of LPS stimulation, both p38-mediated phosphorylation and PARP-14-mediated ADP ribosylation events act to render TTP inactive and TF mRNA stable. This allows a TF mRNA response to occur following LPS stimulation **(ii)**. However, pharmacological inhibition of either p38-mediated phosphorylation and/or PARP-14-mediated ADP ribosylation renders TTP active and TF mRNA labile. **(v, vi)**

due to impaired binding of TTP and PARP-14 respectively. In WT cells, both PARP enzymatic activity and p38 activity are necessary for inactivating TTP-mediated mRNA decay and thus increasing TF mRNA stability during LPS induction. Thus inhibition of either PARP-14 mediated ADP-ribosylation and/or p38-mediated phosphorylation results in increased TTP-mediated TF mRNA decay. It is known that TF mRNA levels are "super-induced" and mRNA stability prolonged by stimulating monocytes in the presence of the protein synthesis inhibitor cycloheximide, suggesting down-regulation of mRNA stability with time by an induced repressor protein(s)[260, 447]. Previous observations showing the inducibility of TTP and the above data on PARP-14 support their involvement in this. Thus, it has already been established that TTP expression is transcriptionally regulated by a variety of agonists, including LPS[470]. This allows the quantity of TTP to match the increased number of target mRNA appearing as part of transcriptional responses to these agents, and provides a mechanism for accelerated mRNA decay to terminate gene expression as part of feedback inhibition. Expression of TTP is very low to absent in resting macrophages but was shown to be induced by LPS as previously observed[320]. PARP-14 was found to be increased by LPS in murine macrophages with similar kinetics to TTP. Furthermore, PARP-14 and TTP proteins were increased together *in vivo* in multiple organs following LPS treatment. Overall, these data therefore show that both PARP-14 and TTP are coregulated by an LPS-mediated signalling pathway, leading to increased availability of these two RNA-binding proteins to post-transcriptionally regulate TF expression.

6.5 Glucocorticoids reduce TF mRNA stability

Following the observation that p38 inhibition reduces TF mRNA stability via the p38-TTP axis, and given that GCs are potent inhibitors of p38 activity and function, the effect of GCs on TF mRNA stability was investigated. Previous data on the effects of GCs on LPS-stimulated monocyte-macrophage TF expression is ambiguous, and there are no conclusive data on the effects of GCs on TF expression in primary monocyte-macrophages[442-444]. Initial experiments provided compelling evidence that Dex reduces TF expression in LPS-stimulated monocyte-macrophages. In keeping with an inhibitory effect on p38 activity, Dex was found to reduce TF mRNA stability. An interesting

observation came from mRNA decay experiments in WT vs. *Ttp*$^{-/-}$ macrophages in the absence and presence of Dex, where unlike p38 inhibition, Dex was still able to de-stabilize the TF transcript in *Ttp*$^{-/-}$ macrophages. These data indicate that Dex is likely to regulate TF mRNA turnover through both TTP-dependent and TTP-independent mechanisms. The most likely candidates are miRNAs and/or other RNA binding proteins.

miRNAs are small non-coding RNA molecules that act as post-transcriptional repressors by binding to AREs within 3' UTRs of their target genes and either block translation or promote mRNA degradation[280]. Recently, GCs have been shown to regulate miRNA expression in acute lymphoblastic leukaemic cells[471]. Whilst, GC-regulated miRNAs have been identified in alveolar macrophages from asthmatic patients following inhaled GC therapy[472], to date, miRNA profiling has not been performed in Dex-treated primary human monocytes. A bioinformatics search has shown that 20miRNAs have TF mRNA as predicted target (figure 6-2). miRNAs have been shown to regulate many genes, and recently the first miRNA (mir19) to regulate TF expression has been identified in breast cancer cells[268]. Whether Dex regulates TF expression in monocytes at the level of miRNAs, and whether or not mir19 is implicated, are yet unanswered questions and remain the focus of further investigation.

Modulation of gene transcription is considered to be the central feature of GC-mediated gene regulation[473]. Binding of GC to the glucocorticoid receptor (GR) induces its dissociation from a cytoplasmic multimeric complex of chaperone proteins and its translocation to the nucleus, where it dimerizes and acts as a transcription factor, through binding to a glucocorticoid response element (GRE) within the 5′ promoter region of target genes[474, 475]. The GR can also bind different transcription factors such as AP-1, NF-κB subunits and members of STAT and Forkhead box families, resulting in transcriptional inhibition of proinflammatory genes[473, 475]. However, the effect of GCs is now increasingly recognized to occur through the regulation of mRNA turnover. Examples of genes regulated by GCs at a post-transcriptional level include TNFα, GM-CSF, COX-2, IL-4Rα, IL-6, iNOS, vascular endothelial growth factor (VEGF), CCL11, CCL2 and CCL7 and many others[436, 476-478]. As mentioned above, most studied RNA-

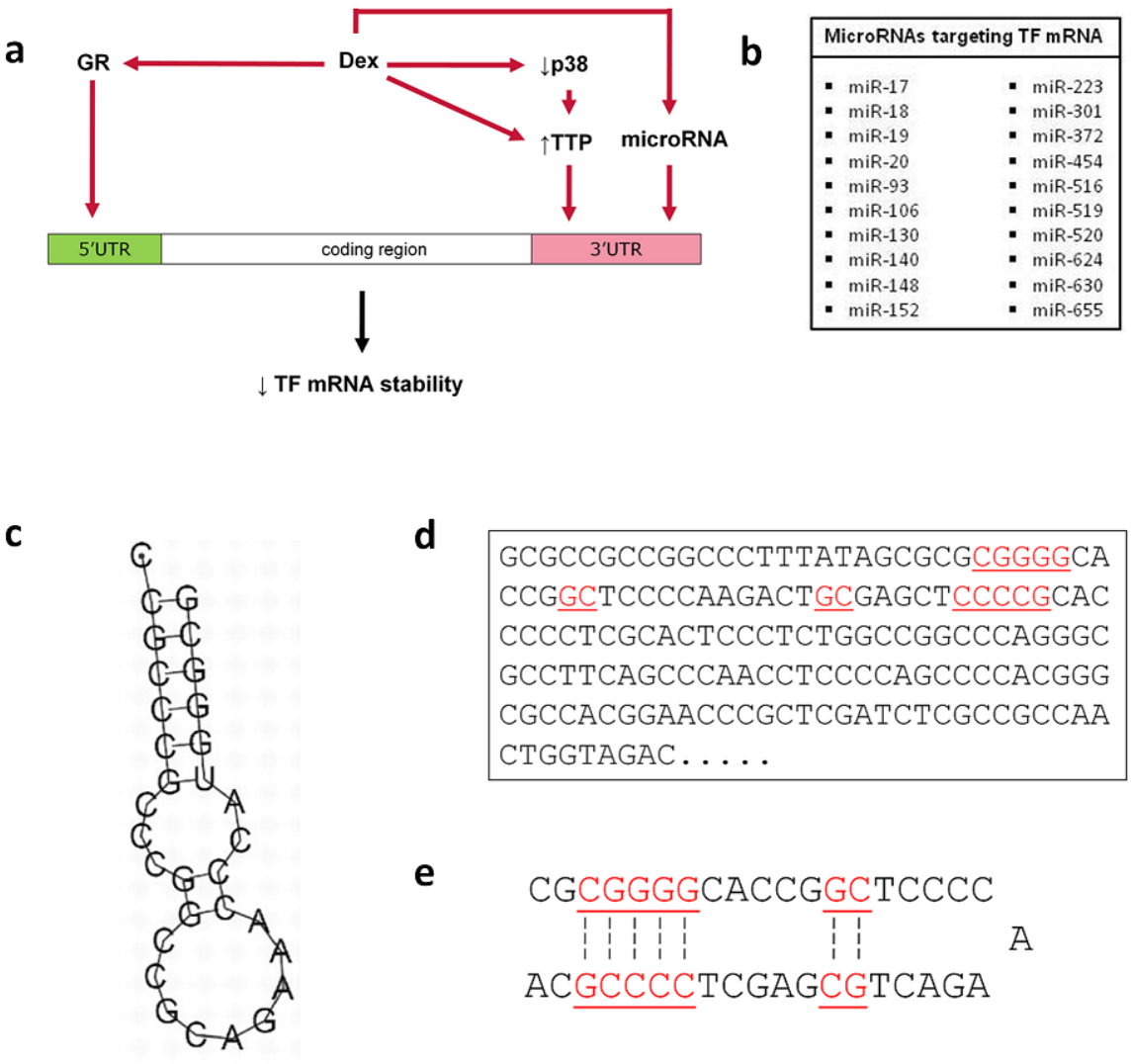

Figure 6-2: A hypothetical working model for the effect of Dex on TF mRNA stability
(a) A hypothetical working model where Dex regulates the p38-TTP axis and microRNAs to target the 3'UTR of TF. Dex binds with GR which targets the 5'UTR; **(b)** Potential microRNAs that may regulate TF. A bioinformatics search conducted using the miRGen database (http://www.diana.pcbi.upenn.edu/miRGen/v3/miRGen.html) highlights 20 microRNAs with TF mRNA as a predicted target; **(c)** An example of GR binding motif as present in CCL2 mRNA. The GR motif is a GC-rich segment with a short stem forming two contiguous loops; **(d)** The 5'UTR sequence of human TF 5'UTR. The GC rich sequences that form the potential GR-binding site are highlighted in red; and **(e)** The proposed GR binding motif in human TF 5'UTR.

binding proteins bind to AREs in the 3'UTR of target mRNAs. However, these specific regulatory elements are not exclusive to the 3'UTR. Research in the last decade has identified a growing number of additional non-ARE destabilizing elements within the 5' and 3'UTR of many genes[479-481]. It has been shown that the GR can interact with CCL2 mRNA in rat smooth muscle cells[482]. The GR has recently been shown to bind 5'UTR of CCL2 and CCL7 mRNA in human airway epithelial cells[483]. Using computational

analyses a novel GC-rich motif in the 5'UTR was found to bind GR, and this sequence was present in the 5' UTRs of 7889 predicted mRNA targets, or in the entire sequences of 25,672 predicted mRNA targets (21% of the UniGene transcript pool)[483]. Interestingly, the GR binding motif is also found in TF 5'UTR. This raises the possibility that the GR may contribute to the acceleration of TF mRNA decay seen above in the *Ttp*$^{-/-}$ macrophages. A hypothetical working model for the role of Dex in the post-transcriptional regulation of TF is presented in figure 6-2.

6.6 Therapeutic targeting of TF expression

Given that the TF pathway is the primary mechanism for initiating thrombosis, the TF pathway is an attractive therapeutic target. The development of new pharmacological approaches to target TF-mediated coagulation at several different levels remains an exciting research field. It is well established that other anti-thrombotic approaches such as glycoprotein IIb/IIIa blockade and inhibition of thrombin increase bleeding time and the risk for bleeding. A remarkable feature of anti-thrombotic therapies targeting TF, e.g. FVIIa or the TF-FVIIa complex, is that the antithrombotic effect is similar to heparin or warfarin but with less severe bleeding tendencies[484-487].

One approach has been to directly target the TF molecule using anti-TF monoclonal antibodies (D3H44, AP-1)[63, 488-490]. Antagonizing membrane-bound TF through the administration of a recombinant truncated extracellular form of TF (hTFAA) has been shown to limit thrombosis in animal models without significantly increasing bleeding risk[485, 486]. This recombinant peptide has been further modified (hTFAA-3) to enhance its affinity for FVIIa[491]. A small-molecule TF inhibitor PHA-927F, has also been shown to limit thrombosis in a primate model of acute thrombosis without increasing bleeding risk[492]. Another approach has been to target the activated form of FVII by administering active site-inactivated FVIIa (FVIIa$_i$, FFR-rFVIIa, DEGR-FVIIa, or ASIS)[493, 494]. FVIIa$_i$ is an active site-blocked version of rFVIIa that is rendered catalytically inactive, and acts as a competitive inhibitor of TF. The resulting TF-FVIIa$_i$ complex is very stable and incapable of activating the downstream coagulation cascade. ASIS competes with FVIIa for complex formation and does not replace FVIIa already bound to TF[495]. Intravenous,

topical and intracarotid administration of $FVIIa_i$ in various animal models has demonstrated good antithrombotic effects[496-498]. Similarly, small protein inhibitors of the TF•FVIIa complex (XK1 and rNAPc2) have been shown to have antithrombotic effects in animal models[499, 500]. Recombinant TFPI (rTFPI) (e.g. Tifacogin and Ixolaris) has been shown to limit thrombosis in various animal models and to inhibit thrombin generation in human volunteers infused with endotoxin[501-505]. Clinical application of rTFPI has predominantly focused on treatment of sepsis rather than thrombosis due to the requirement of large doses of rTFPI to inhibit thrombus formation[506]. The effect of local overexpression of the TFPI gene has also been investigated using a 'hemagglutinating virus of Japan'–artificial viral envelope liposome-mediated TFPI gene therapy in rabbits[507].

Over the recent years, post-transcriptional regulation has emerged as an important determinant of gene expression. In the current advancing era of molecular biology, targeting post-transcriptional pathways is now emerging as a promising therapeutic strategy in a wide spectrum of diseases[508, 509]. Inhibition of TF expression at the post-transcriptional level may be accomplished by several different methods. Various approaches using ribozyme, antisense and RNA interference technologies have been reported. Delivery of antisense nucleic acid molecules into the cells results in hybridization between the antisense molecule and the TF mRNA thereby preventing translation. Administration of antisense TF oligonucleotides has been demonstrated to limit thrombosis in various animal models[510, 511]. However, the stoichiometric nature of antisense therapy limits their usefulness in situations characterized by very high levels of mRNA induction, as seen with TF[512]. Catalytic RNA, or ribozymes, are a class of RNA molecules that possess enzymatic properties[512, 513]. Ribozymes are thought to be more useful than conventional antisense RNAs and DNAs, since ribozymes possess the properties of antisense RNA with the additional ability of catalytic cleavage[512]. TF gene silencing using RNA interference, has also been reported, but has limited efficiency[514]. The main limitation for these approaches is the development of an efficient and safe delivery mechanism.

The data presented in this thesis advances our understanding of the post-transcriptional regulation of TF and presents a novel role for PARP-14 and ADP-ribosylation in selectively regulating TF mRNA turnover. This raises the possibility of pharmacological therapies that may *"selectively"* target TF expression. There has already been considerable pharmaceutical interest in p38 MAPK as a target for drug development for treating inflammatory diseases [515-517], and one might predict that destabilisation of TF mRNA and a reduction in TF expression and activity would give these compounds anti-thrombotic as well as anti-inflammatory properties. However, therapeutic targeting of pro-inflammatory pathways such as NFkB or p38 MAPK pathways, contrary to intuitive thinking as having potential anti-inflammatory and anti-thrombotic effects, would have diverse non-specific and potentially undesirable effects due to the important roles played by these pathways in both inflammatory and anti-inflammatory signalling. Having shown that the PARP-14-TTP interaction applies to TF but not TNFα regulation, this selectivity for TTP targets shows great promise for PARP-14 inhibitors as therapeutic agents. Specific PARP-14 inhibitors[518] might be advantageous in having less ubiquitous effects compared to p38 MAPK inhibition. As TF not only activates blood coagulation but is also pro-inflammatory via activation of PARs by thrombin[28], PARP-14 inhibition may have wider therapeutic effects in atherothrombosis, severe sepsis and cancer where the pathology is linked to increased TF expression.

6.7 Limitations

This study has a number of limitations. LPS has been used as the model stimulus as it produces a strong and consistent induction in TF. Whilst endotoxaemia is atherogenic[519] and may precipitate ACS[520], it may be of limited relevance to cardiovascular disease and atherosclerosis in general. It would have been ideal to test other stimuli relevant to cardiovascular disease, e.g. CD40L, TNFα and IL-1. To investigate the effect of TTP and PARP-14 deficiency on TF expression, transgenic mice (*Ttp*$^{-/-}$ and *Parp14*$^{-/-}$) were used. Whilst transgenic mice are a powerful tool to investigate the effect of a target protein, the major drawback is the potential for any unknown genetic compensation. To further confirm the effects of TTP and PARP-14 deficiency on TF expression and TF mRNA stability, experiments should also have

been conducted in human monocytes or WT murine macrophages using siRNA technology. However, the off-target effects of siRNA approaches would remain a potential problem. The majority of the experiments, particularly the determination of the mechanisms underlying the PARP-14-TTP interaction have been conducted *in vitro*. Whilst, the *in vitro* findings of increased TF expression and thrombogenicity were confirmed in vivo, whether or not the *in vitro* mechanisms reflect the *in vivo* mechanisms for mRNA stability remain to be determined. This will always be a limitation of any *in vitro* analysis. However, most of our understanding of the mechanisms regulating mRNA stability is derived from *in vitro* studies, and as such, determining *in vivo* molecular mechanisms regulating mRNA stability is somewhat challenging[270]. All the *in vitro* work was conducted in monocyte-macrophages, and the observed mechanisms were not tested in other cell types. However, the *in vivo* organ analyses were in keeping with the *in vitro* monocyte-macrophage results, and given the multiple cell types besides macrophages that make up the organs, it is likely that these mechanisms may be broadly applicable to other cell types. The p38 inhibitors used in this study were experimentally controlled for by using the inactive analogue compound SB202474. However, despite analyses demonstrating specificity for p38, one cannot definitively exclude non-specific effects, especially as dedicated kinase assays to demonstrate specificity were not used. The PARP inhibitors used in this study are not specific for PARP-14, and this has been acknowledged. The concentration of PARP inhibitors used in this study are based on those in previously reported studies. However, the efficacy of these compounds would have best been demonstrated using dedicated PARP assays.

6.8 Future directions

(a) To determine whether TTP can be ADP-ribosylated

The novel finding that the PARP-14-TTP interaction selectively regulates TF mRNA stability needs further clarification. Whilst the inhibition of ADP-ribosylation appears to increase TF mRNA decay, the effect of ADP-ribosylation on TTP or other proteins in the mRNA decay complex requires further study. In the first instance this can be assessed by immunoprecipitation of candidate target proteins, including TTP, and assessing ADP-ribosylation using mass spectrometry.

(b) To determine the subset of TTP-regulated transcripts co-regulated by PARP-14

Whilst the PARP-14-TTP interaction does not appear to regulate TNFα mRNA, the pool of mRNA or subset of TTP-regulated transcripts that may also be regulated by PARP-14 remain to be determined. Although the putative ARE sequences in mediating PARP-14-TTP interaction have been identified, the detailed analysis of how PARP-14 interacts with mRNA needs to be conducted. To establish which other genes are coregulated by PARP-14 and TTP, PAR-CLIP (Photo-Activatable Ribonuceoside Cross-Linking and ImmunoPrecipitation) and "next generation" RNA sequencing can be used. This technique chemically cross-links RNA-binding proteins to RNA prior to immunoprecipitation, and has the advantage over simple RNP immunoprecipitation in allowing the identification of protein-RNA interactions that are of insufficiently high affinity to be survive conventional immunoprecipitation protocols[521]. Furthermore, PAR-CLIP reduces the false-positive hits due to indirect interactions identified by pulling down large RNA-protein complexes. A major added advantage of PAR-CLIP is that it also enables the identification of protein contact points on mRNA, as T to C mutations occur at cross-linking sites[521]. Using a PAR-CLIP protocol, immunoprecipitation with anti-PARP-14 and anti-TTP antibodies can determine the mRNAs bound to these proteins. Based on T to C cDNA mutations that occur at cross-linking sites, a common RNA footprint(s) for PARP-14 binding can be determined, albeit recognising the possibility that tertiary RNA structure may be more important than precise nucleotide sequence. Following this, the putative PARP-14 binding sites may be validated on selected PARP-14 target mRNA by appropriately mutating the 3'UTR and assessing effects on mRNA-PARP-14 interactions using RNP immunoprecipitation and RNA-biotin pulldown assays.

(c) To determine the role of PARP-14 catalytic activity

A major limitation of the PARP inhibitors is lack of specificity for PARP-14. Although PARP-14 specific compounds are in development, they are not currently available for use. Another way to address this problem is to generate of catalytically-inactive PARP-14 knock-in mouse. Rather than make a PARP-14 mutant mouse (*Parp-14*^{mut}) lacking

the PARP domain, one can simply mutate the conserved glutamate in the 5th conserved β strand, which is critical for catalytic function in several enzymatically-active PARP protein, including PARP-14[522-524]. This is less likely to cause non-specific steric confounding effects compared to a PARP domain deletion, and this mutant should predict the effects of drug targeting PARP-14 catalytic activity. These mice can then be used in a similar way for conducting the *in vitro* and *in vivo* work as above.

(d) To determine the effects of PARP-14 deficiency and PARP-14 catalytic activity on thrombosis and atherosclerosis in hyperlipidaemic mice

There is good evidence that hyperlipidaemia leads to a procoagulant state, both in humans and mice[231, 525]. Furthermore, this has been linked to an increase in circulating TF, both on circulating monocytes and microparticles[231]. Given that a deficiency of PARP-14 increases LPS-induced TF expression, replacing the "LPS" stimulus with "hypercholesterolaemia" and assessing whether TF expression is increased in the context of PARP-14 deficiency would provide a more suitable disease model for thrombosis and atherosclerosis. One can hypothesise that *Parp14*$^{-/-}$ mice will show accelerated atherosclerosis, possibly with a novel thrombotic phenotype related to the inappropriately high TF levels, whereas *Parp14*^{mut} *mice* will be protected. However, as PARP-14 also regulates IFNγ-driven genes, its effects on atherosclerosis will probably be more complex than acting via a single pathway. This can be examined further by cross-breeding *Parp14*$^{-/-}$ mice with *Ldlr*$^{-/-}$ mice and obtaining double knock-out mice. By establishing a breeding colony of *Ldlr*$^{-/-}$ homozygous / *Parp-14*$^{-/+}$ mice, one can compare *Ldlr*$^{-/-}$ homozygous / *Parp14*$^{-/-}$ mice *versus* *Ldlr*$^{-/-}$ homozygous / *Parp14*$^{+/+}$ offspring. Similarly, *Parp14*^{mut} homozygous mice can be cross-bred with *Ldlr*$^{-/-}$ mice to obtain a double homozygous colony. These can then be bred with heterozygous Cre-expressing mice, with a view to comparing *Ldlr*$^{-/-}$ homozygous / *Parp14*^{mut} mice which do not express Cre (i.e. inactive knock-in) versus mice homozygous for Cre (i.e. active knock-in). These mice would provide a valuable resource for evaluating the effect of PARP-14 deficiency and/or PARP-14 catalytic activity on thrombosis and atherosclerosis (using intravascular thrombosis models) and on atherosclerotic lesion and morphology (using lesional immunohistochemistry).

Chapter 7

Conclusions

The primary aim of this thesis was to determine the molecular mechanisms regulating TF mRNA decay. TF is a key stimulus for thrombus formation, with diverse effects in the context of cardiovascular disease. Most of our understanding is centred on the transcriptional regulation of TF. Despite the fact that that the TF transcript is reported to be intrinsically unstable, the molecular mechanisms governing its post-transcriptional regulation are poorly understood.

The data presented in this thesis have shown that TTP, an important well-studied mRNA binding protein, interacts with PARP-14, a new protein in post-transcriptional biology, to regulate TF mRNA stability in LPS-stimulated monocyte-macrophages, such that TF expression and TF mRNA stability are increased in the absence of either of these proteins. These findings are supported by *in vivo* demonstration of increased TF expression and thrombogenicity in PARP-14 deficient mice. Both TTP and PARP-14 appear to bind cooperatively with TF mRNA and the final palindromic sequence in the TF 3'UTR (AUAAUUUAUUUAAUA) which contains 2 overlapping AUUUAUUUA and UUAUUUAAU nonamers, both of which appear to be critical in mediating this interaction.

The TTP-PARP-14 interaction allows pharmacological modulation of TF mRNA stability. As TTP regulates TF mRNA stability, TF mRNA decay can be accelerated with p38 inhibition – an effect classically seen with TTP-regulated transcript. PARP-14 appears to have two distinct roles in regulating TF mRNA turnover. Firstly, it serves as an accessory protein required for TTP to bind TF mRNA. Secondly, the PARP catalytic activity of PARP-14 serves to stabilize TF mRNA, such that inhibition of ADP-ribosylation results in increased TF mRNA decay. Thus one may propose that both PARP-14 mediated ADP-ribosylation and and p38-mediated phosphorylation events are necessary for inactivating TTP-mediated TF mRNA decay. Furthermore, the PARP-14-TTP interaction applies to TF but not TNFα or TTP, which are other TTP-regulated transcripts. This selectivity for TTP targets shows great promise for PARP-14 inhibitors as therapeutic agents, potentially, with less ubiquitous effects.

These data have also shown for the first time that Dex reduces TF expression in LPS-stimulated monocyte-macrophages. Dex is negative regulator of p38 activity, and is known to increase TTP-mediated mRNA decay. However, the unexpected observation that Dex reduces TF mRNA stability in TTP-deficient cells indicates that Dex is acting to regulate TF mRNA stability through both TTP-dependent and TTP-independent mechanisms, perhaps involving miRNAs or other RNA-binding proteins.

Collectively, these data provide novel molecular mechanisms governing the regulation of TF mRNA turnover, and represent a significant advance in our understanding of the regulation of TF. A better understanding of the regulation of TF holds considerable therapeutic potential. As TF not only activates blood coagulation but is also pro-inflammatory via activation of PARs, targeting TF may have wider therapeutic effects in pathological states such as atherothrombosis, sepsis and cancer which are associated with increased TF expression.

References

1. Ross R, Glomset JA. The pathogenesis of atherosclerosis (first of two parts). *The New England journal of medicine*. 1976;295:369-377
2. Ross R, Glomset JA. The pathogenesis of atherosclerosis (second of two parts). *The New England journal of medicine*. 1976;295:420-425
3. Schwartz CJ, Valente AJ, Sprague EA, Kelley JL, Nerem RM. The pathogenesis of atherosclerosis: An overview. *Clinical cardiology*. 1991;14:I1-16
4. Ross R. Atherosclerosis--an inflammatory disease. *The New England journal of medicine*. 1999;340:115-126
5. Altman R. Risk factors in coronary atherosclerosis athero-inflammation: The meeting point. *Thrombosis journal*. 2003;1:4
6. Organization WH. Who cardiovascular factsheet no.317. 2012;2012
7. Townsend N WK, Bhatnagar P, Smolina K, Nichols M, Leal J, Luengo-Fernandez R, Rayner M. Coronary heart disease statistics 2012 edition. 2012
8. Hansson GK. Inflammation, atherosclerosis, and coronary artery disease. *The New England journal of medicine*. 2005;352:1685-1695
9. Poole JC, Florey HW. Changes in the endothelium of the aorta and the behaviour of macrophages in experimental atheroma of rabbits. *The Journal of pathology and bacteriology*. 1958;75:245-251
10. Jaffe EA. Cell biology of endothelial cells. *Human pathology*. 1987;18:234-239
11. Pearson JD. Endothelial cell function and thrombosis. *Bailliere's best practice & research. Clinical haematology*. 1999;12:329-341
12. Davignon J, Ganz P. Role of endothelial dysfunction in atherosclerosis. *Circulation*. 2004;109:III27-32
13. Ni W, Egashira K, Kitamoto S, Kataoka C, Koyanagi M, Inoue S, Imaizumi K, Akiyama C, Nishida KI, Takeshita A. New anti-monocyte chemoattractant protein-1 gene therapy attenuates atherosclerosis in apolipoprotein e-knockout mice. *Circulation*. 2001;103:2096-2101
14. Aiello RJ, Bourassa PA, Lindsey S, Weng W, Natoli E, Rollins BJ, Milos PM. Monocyte chemoattractant protein-1 accelerates atherosclerosis in apolipoprotein e-deficient mice. *Arterioscler Thromb Vasc Biol*. 1999;19:1518-1525
15. Boring L, Gosling J, Cleary M, Charo IF. Decreased lesion formation in ccr2-/- mice reveals a role for chemokines in the initiation of atherosclerosis. *Nature*. 1998;394:894-897
16. Nageh MF, Sandberg ET, Marotti KR, Lin AH, Melchior EP, Bullard DC, Beaudet AL. Deficiency of inflammatory cell adhesion molecules protects against atherosclerosis in mice. *Arterioscler Thromb Vasc Biol*. 1997;17:1517-1520
17. Poston RN, Haskard DO, Coucher JR, Gall NP, Johnson-Tidey RR. Expression of intercellular adhesion molecule-1 in atherosclerotic plaques. *The American journal of pathology*. 1992;140:665-673
18. Bogen S, Pak J, Garifallou M, Deng X, Muller WA. Monoclonal antibody to murine pecam-1 (cd31) blocks acute inflammation in vivo. *The Journal of experimental medicine*. 1994;179:1059-1064
19. Smith JD, Trogan E, Ginsberg M, Grigaux C, Tian J, Miyata M. Decreased atherosclerosis in mice deficient in both macrophage colony-stimulating factor (op) and apolipoprotein e. *Proceedings of the National Academy of Sciences of the United States of America*. 1995;92:8264-8268
20. Peiser L, Mukhopadhyay S, Gordon S. Scavenger receptors in innate immunity. *Current opinion in immunology*. 2002;14:123-128
21. Brown MS, Ho YK, Goldstein JL. The cholesteryl ester cycle in macrophage foam cells. Continual hydrolysis and re-esterification of cytoplasmic cholesteryl esters. *The Journal of biological chemistry*. 1980;255:9344-9352

22. Warner GJ, Stoudt G, Bamberger M, Johnson WJ, Rothblat GH. Cell toxicity induced by inhibition of acyl coenzyme a:Cholesterol acyltransferase and accumulation of unesterified cholesterol. *The Journal of biological chemistry*. 1995;270:5772-5778
23. Glass CK, Witztum JL. Atherosclerosis. The road ahead. *Cell*. 2001;104:503-516
24. Tabas I. Free cholesterol-induced cytotoxicity a possible contributing factor to macrophage foam cell necrosis in advanced atherosclerotic lesions. *Trends in cardiovascular medicine*. 1997;7:256-263
25. Davie EW, Fujikawa K, Kisiel W. The coagulation cascade: Initiation, maintenance, and regulation. *Biochemistry*. 1991;30:10363-10370
26. Dubois C, Panicot-Dubois L, Merrill-Skoloff G, Furie B, Furie BC. Glycoprotein vi-dependent and -independent pathways of thrombus formation in vivo. *Blood*. 2006;107:3902-3906
27. Ruggeri ZM. Old concepts and new developments in the study of platelet aggregation. *The Journal of clinical investigation*. 2000;105:699-701
28. Coughlin SR. Protease-activated receptors in hemostasis, thrombosis and vascular biology. *Journal of thrombosis and haemostasis : JTH*. 2005;3:1800-1814
29. Vu TK, Hung DT, Wheaton VI, Coughlin SR. Molecular cloning of a functional thrombin receptor reveals a novel proteolytic mechanism of receptor activation. *Cell*. 1991;64:1057-1068
30. Du X, Gu M, Weisel JW, Nagaswami C, Bennett JS, Bowditch R, Ginsberg MH. Long range propagation of conformational changes in integrin alpha iib beta 3. *The Journal of biological chemistry*. 1993;268:23087-23092
31. Davi G, Patrono C. Platelet activation and atherothrombosis. *The New England journal of medicine*. 2007;357:2482-2494
32. Furie B, Furie BC. Mechanisms of thrombus formation. *The New England journal of medicine*. 2008;359:938-949
33. Gailani D, Renne T. Intrinsic pathway of coagulation and arterial thrombosis. *Arterioscler Thromb Vasc Biol*. 2007;27:2507-2513
34. Broze GJ, Jr. The role of tissue factor pathway inhibitor in a revised coagulation cascade. *Seminars in hematology*. 1992;29:159-169
35. Ofosu FA, Liu L, Freedman J. Control mechanisms in thrombin generation. *Seminars in thrombosis and hemostasis*. 1996;22:303-308
36. Esmon CT. Regulation of blood coagulation. *Biochimica et biophysica acta*. 2000;1477:349-360
37. Fuster V, Stein B, Ambrose JA, Badimon L, Badimon JJ, Chesebro JH. Atherosclerotic plaque rupture and thrombosis. Evolving concepts. *Circulation*. 1990;82:II47-59
38. Davies MJ, Thomas A. Thrombosis and acute coronary-artery lesions in sudden cardiac ischemic death. *The New England journal of medicine*. 1984;310:1137-1140
39. Virmani R, Kolodgie FD, Burke AP, Farb A, Schwartz SM. Lessons from sudden coronary death: A comprehensive morphological classification scheme for atherosclerotic lesions. *Arterioscler Thromb Vasc Biol*. 2000;20:1262-1275
40. Kolodgie FD, Gold HK, Burke AP, Fowler DR, Kruth HS, Weber DK, Farb A, Guerrero LJ, Hayase M, Kutys R, Narula J, Finn AV, Virmani R. Intraplaque hemorrhage and progression of coronary atheroma. *The New England journal of medicine*. 2003;349:2316-2325
41. Falk E, Shah PK, Fuster V. Coronary plaque disruption. *Circulation*. 1995;92:657-671
42. Hackett D, Davies G, Maseri A. Pre-existing coronary stenoses in patients with first myocardial infarction are not necessarily severe. *European heart journal*. 1988;9:1317-1323
43. Guyton JR, Klemp KF. Development of the lipid-rich core in human atherosclerosis. *Arterioscler Thromb Vasc Biol*. 1996;16:4-11

44. Shah PK. Mechanisms of plaque vulnerability and rupture. *Journal of the American College of Cardiology*. 2003;41:15S-22S
45. Libby P, Aikawa M. Stabilization of atherosclerotic plaques: New mechanisms and clinical targets. *Nature medicine*. 2002;8:1257-1262
46. van der Wal AC, Becker AE, van der Loos CM, Das PK. Site of intimal rupture or erosion of thrombosed coronary atherosclerotic plaques is characterized by an inflammatory process irrespective of the dominant plaque morphology. *Circulation*. 1994;89:36-44
47. Libby P. Inflammation in atherosclerosis. *Nature*. 2002;420:868-874
48. Burleigh MC, Briggs AD, Lendon CL, Davies MJ, Born GV, Richardson PD. Collagen types i and iii, collagen content, gags and mechanical strength of human atherosclerotic plaque caps: Span-wise variations. *Atherosclerosis*. 1992;96:71-81
49. Felton CV, Crook D, Davies MJ, Oliver MF. Relation of plaque lipid composition and morphology to the stability of human aortic plaques. *Arterioscler Thromb Vasc Biol*. 1997;17:1337-1345
50. Kockx MM, Knaapen MW. The role of apoptosis in vascular disease. *The Journal of pathology*. 2000;190:267-280
51. Amento EP, Ehsani N, Palmer H, Libby P. Cytokines and growth factors positively and negatively regulate interstitial collagen gene expression in human vascular smooth muscle cells. *Arteriosclerosis and thrombosis : a journal of vascular biology / American Heart Association*. 1991;11:1223-1230
52. Bobik A, Agrotis A, Kanellakis P, Dilley R, Krushinsky A, Smirnov V, Tararak E, Condron M, Kostolias G. Distinct patterns of transforming growth factor-beta isoform and receptor expression in human atherosclerotic lesions. Colocalization implicates tgf-beta in fibrofatty lesion development. *Circulation*. 1999;99:2883-2891
53. Sugiyama S, Kugiyama K, Aikawa M, Nakamura S, Ogawa H, Libby P. Hypochlorous acid, a macrophage product, induces endothelial apoptosis and tissue factor expression: Involvement of myeloperoxidase-mediated oxidant in plaque erosion and thrombogenesis. *Arterioscler Thromb Vasc Biol*. 2004;24:1309-1314
54. Shah PK, Falk E, Badimon JJ, Fernandez-Ortiz A, Mailhac A, Villareal-Levy G, Fallon JT, Regnstrom J, Fuster V. Human monocyte-derived macrophages induce collagen breakdown in fibrous caps of atherosclerotic plaques. Potential role of matrix-degrading metalloproteinases and implications for plaque rupture. *Circulation*. 1995;92:1565-1569
55. Sukhova GK, Schonbeck U, Rabkin E, Schoen FJ, Poole AR, Billinghurst RC, Libby P. Evidence for increased collagenolysis by interstitial collagenases-1 and -3 in vulnerable human atheromatous plaques. *Circulation*. 1999;99:2503-2509
56. Sukhova GK, Shi GP, Simon DI, Chapman HA, Libby P. Expression of the elastolytic cathepsins s and k in human atheroma and regulation of their production in smooth muscle cells. *The Journal of clinical investigation*. 1998;102:576-583
57. Galis ZS, Khatri JJ. Matrix metalloproteinases in vascular remodeling and atherogenesis: The good, the bad, and the ugly. *Circulation research*. 2002;90:251-262
58. Herman MP, Sukhova GK, Libby P, Gerdes N, Tang N, Horton DB, Kilbride M, Breitbart RE, Chun M, Schonbeck U. Expression of neutrophil collagenase (matrix metalloproteinase-8) in human atheroma: A novel collagenolytic pathway suggested by transcriptional profiling. *Circulation*. 2001;104:1899-1904
59. Geng YJ, Libby P. Evidence for apoptosis in advanced human atheroma. Colocalization with interleukin-1 beta-converting enzyme. *The American journal of pathology*. 1995;147:251-266
60. Newby AC. Dual role of matrix metalloproteinases (matrixins) in intimal thickening and atherosclerotic plaque rupture. *Physiological reviews*. 2005;85:1-31
61. Hasko G, Pacher P, Deitch EA, Vizi ES. Shaping of monocyte and macrophage function by adenosine receptors. *Pharmacology & therapeutics*. 2007;113:264-275

62. Simon DI, Ezratty AM, Francis SA, Rennke H, Loscalzo J. Fibrin(ogen) is internalized and degraded by activated human monocytoid cells via mac-1 (cd11b/cd18): A nonplasmin fibrinolytic pathway. *Blood*. 1993;82:2414-2422
63. Giesen PL, Rauch U, Bohrmann B, Kling D, Roque M, Fallon JT, Badimon JJ, Himber J, Riederer MA, Nemerson Y. Blood-borne tissue factor: Another view of thrombosis. *Proceedings of the National Academy of Sciences of the United States of America*. 1999;96:2311-2315
64. Raghunath PN, Tomaszewski JE, Brady ST, Caron RJ, Okada SS, Barnathan ES. Plasminogen activator system in human coronary atherosclerosis. *Arterioscler Thromb Vasc Biol*. 1995;15:1432-1443
65. Mansilla S, Boulaftali Y, Venisse L, Arocas V, Meilhac O, Michel JB, Jandrot-Perrus M, Bouton MC. Macrophages and platelets are the major source of protease nexin-1 in human atherosclerotic plaque. *Arterioscler Thromb Vasc Biol*. 2008;28:1844-1850
66. Schonbeck U, Libby P. The cd40/cd154 receptor/ligand dyad. *Cellular and molecular life sciences : CMLS*. 2001;58:4-43
67. van Gils JM, Zwaginga JJ, Hordijk PL. Molecular and functional interactions among monocytes, platelets, and endothelial cells and their relevance for cardiovascular diseases. *Journal of leukocyte biology*. 2009;85:195-204
68. Crawley J, Lupu F, Westmuckett AD, Severs NJ, Kakkar VV, Lupu C. Expression, localization, and activity of tissue factor pathway inhibitor in normal and atherosclerotic human vessels. *Arterioscler Thromb Vasc Biol*. 2000;20:1362-1373
69. Altieri DC, Morrissey JH, Edgington TS. Adhesive receptor mac-1 coordinates the activation of factor x on stimulated cells of monocytic and myeloid differentiation: An alternative initiation of the coagulation protease cascade. *Proceedings of the National Academy of Sciences of the United States of America*. 1988;85:7462-7466
70. Fernandez-Ortiz A, Badimon JJ, Falk E, Fuster V, Meyer B, Mailhac A, Weng D, Shah PK, Badimon L. Characterization of the relative thrombogenicity of atherosclerotic plaque components: Implications for consequences of plaque rupture. *Journal of the American College of Cardiology*. 1994;23:1562-1569
71. Coughlin SR. Thrombin signalling and protease-activated receptors. *Nature*. 2000;407:258-264
72. Kanse SM, Parahuleva M, Muhl L, Kemkes-Matthes B, Sedding D, Preissner KT. Factor vii-activating protease (fsap): Vascular functions and role in atherosclerosis. *Thrombosis and haemostasis*. 2008;99:286-289
73. Rittersma SZ, van der Wal AC, Koch KT, Piek JJ, Henriques JP, Mulder KJ, Ploegmakers JP, Meesterman M, de Winter RJ. Plaque instability frequently occurs days or weeks before occlusive coronary thrombosis: A pathological thrombectomy study in primary percutaneous coronary intervention. *Circulation*. 2005;111:1160-1165
74. Kramer MC, van der Wal AC, Koch KT, Ploegmakers JP, van der Schaaf RJ, Henriques JP, Baan J, Jr., Rittersma SZ, Vis MM, Piek JJ, Tijssen JG, de Winter RJ. Presence of older thrombus is an independent predictor of long-term mortality in patients with st-elevation myocardial infarction treated with thrombus aspiration during primary percutaneous coronary intervention. *Circulation*. 2008;118:1810-1816
75. Kramer MC, van der Wal AC, Koch KT, Rittersma SZ, Li X, Ploegmakers HP, Henriques JP, van der Schaaf RJ, Baan J, Jr., Vis MM, Meesterman MG, Piek JJ, Tijssen JG, de Winter RJ. Histopathological features of aspirated thrombi after primary percutaneous coronary intervention in patients with st-elevation myocardial infarction. *PloS one*. 2009;4:e5817
76. Verouden NJ, Kramer MC, Li X, Meuwissen M, Koch KT, Henriques JP, Baan J, Vis MM, Piek JJ, van der Wal AC, Tijssen JG, de Winter RJ. Histopathology of aspirated thrombus and its association with st-segment recovery in patients undergoing primary

percutaneous coronary intervention with routine thrombus aspiration. *Catheterization and cardiovascular interventions : official journal of the Society for Cardiac Angiography & Interventions*. 2011;77:35-42
77. Morel O, Toti F, Hugel B, Bakouboula B, Camoin-Jau L, Dignat-George F, Freyssinet JM. Procoagulant microparticles: Disrupting the vascular homeostasis equation? *Arterioscler Thromb Vasc Biol*. 2006;26:2594-2604
78. Hron G, Kollars M, Weber H, Sagaster V, Quehenberger P, Eichinger S, Kyrle PA, Weltermann A. Tissue factor-positive microparticles: Cellular origin and association with coagulation activation in patients with colorectal cancer. *Thrombosis and haemostasis*. 2007;97:119-123
79. Del Conde I, Shrimpton CN, Thiagarajan P, Lopez JA. Tissue-factor-bearing microvesicles arise from lipid rafts and fuse with activated platelets to initiate coagulation. *Blood*. 2005;106:1604-1611
80. Meisel SR, Xu XP, Edgington TS, Dimayuga P, Kaul S, Lee S, Fishbein MC, Cercek B, Shah PK. Differentiation of adherent human monocytes into macrophages markedly enhances tissue factor protein expression and procoagulant activity. *Atherosclerosis*. 2002;161:35-43
81. Bruemmer D, Riggers U, Holzmeister J, Grill M, Lippek F, Settmacher U, Regitz-Zagrosek V, Fleck E, Graf K. Expression of cd40 in vascular smooth muscle cells and macrophages is associated with early development of human atherosclerotic lesions. *The American journal of cardiology*. 2001;87:21-27
82. Mach F, Schonbeck U, Sukhova GK, Bourcier T, Bonnefoy JY, Pober JS, Libby P. Functional cd40 ligand is expressed on human vascular endothelial cells, smooth muscle cells, and macrophages: Implications for cd40-cd40 ligand signaling in atherosclerosis. *Proceedings of the National Academy of Sciences of the United States of America*. 1997;94:1931-1936
83. Li D, Liu L, Chen H, Sawamura T, Mehta JL. Lox-1, an oxidized ldl endothelial receptor, induces cd40/cd40l signaling in human coronary artery endothelial cells. *Arterioscler Thromb Vasc Biol*. 2003;23:816-821
84. Mach F, Schonbeck U, Bonnefoy JY, Pober JS, Libby P. Activation of monocyte/macrophage functions related to acute atheroma complication by ligation of cd40: Induction of collagenase, stromelysin, and tissue factor. *Circulation*. 1997;96:396-399
85. Miller DL, Yaron R, Yellin MJ. Cd40l-cd40 interactions regulate endothelial cell surface tissue factor and thrombomodulin expression. *Journal of leukocyte biology*. 1998;63:373-379
86. Croce K, Libby P. Intertwining of thrombosis and inflammation in atherosclerosis. *Current opinion in hematology*. 2007;14:55-61
87. Kaikita K, Takeya M, Ogawa H, Suefuji H, Yasue H, Takahashi K. Co-localization of tissue factor and tissue factor pathway inhibitor in coronary atherosclerosis. *The Journal of pathology*. 1999;188:180-188
88. Caplice NM, Mueske CS, Kleppe LS, Simari RD. Presence of tissue factor pathway inhibitor in human atherosclerotic plaques is associated with reduced tissue factor activity. *Circulation*. 1998;98:1051-1057
89. Badimon JJ, Lettino M, Toschi V, Fuster V, Berrozpe M, Chesebro JH, Badimon L. Local inhibition of tissue factor reduces the thrombogenicity of disrupted human atherosclerotic plaques: Effects of tissue factor pathway inhibitor on plaque thrombogenicity under flow conditions. *Circulation*. 1999;99:1780-1787
90. Higuchi DA, Wun TC, Likert KM, Broze GJ, Jr. The effect of leukocyte elastase on tissue factor pathway inhibitor. *Blood*. 1992;79:1712-1719

91. Petersen LC, Bjorn SE, Nordfang O. Effect of leukocyte proteinases on tissue factor pathway inhibitor. *Thrombosis and haemostasis*. 1992;67:537-541
92. Martorell L, Martinez-Gonzalez J, Rodriguez C, Gentile M, Calvayrac O, Badimon L. Thrombin and protease-activated receptors (pars) in atherothrombosis. *Thrombosis and haemostasis*. 2008;99:305-315
93. Colognato R, Slupsky JR, Jendrach M, Burysek L, Syrovets T, Simmet T. Differential expression and regulation of protease-activated receptors in human peripheral monocytes and monocyte-derived antigen-presenting cells. *Blood*. 2003;102:2645-2652
94. Johansson U, Lawson C, Dabare M, Syndercombe-Court D, Newland AC, Howells GL, Macey MG. Human peripheral blood monocytes express protease receptor-2 and respond to receptor activation by production of il-6, il-8, and il-1{beta}. *Journal of leukocyte biology*. 2005;78:967-975
95. Raza SL, Nehring LC, Shapiro SD, Cornelius LA. Proteinase-activated receptor-1 regulation of macrophage elastase (mmp-12) secretion by serine proteinases. *The Journal of biological chemistry*. 2000;275:41243-41250
96. Minami T, Sugiyama A, Wu SQ, Abid R, Kodama T, Aird WC. Thrombin and phenotypic modulation of the endothelium. *Arterioscler Thromb Vasc Biol*. 2004;24:41-53
97. Kaplanski G, Marin V, Fabrigoule M, Boulay V, Benoliel AM, Bongrand P, Kaplanski S, Farnarier C. Thrombin-activated human endothelial cells support monocyte adhesion in vitro following expression of intercellular adhesion molecule-1 (icam-1; cd54) and vascular cell adhesion molecule-1 (vcam-1; cd106). *Blood*. 1998;92:1259-1267
98. Kruithof EK, Mestries JC, Gascon MP, Ythier A. The coagulation and fibrinolytic responses of baboons after in vivo thrombin generation--effect of interleukin 6. *Thrombosis and haemostasis*. 1997;77:905-910
99. Rabiet MJ, Plantier JL, Rival Y, Genoux Y, Lampugnani MG, Dejana E. Thrombin-induced increase in endothelial permeability is associated with changes in cell-to-cell junction organization. *Arterioscler Thromb Vasc Biol*. 1996;16:488-496
100. Brass LF. Thrombin and platelet activation. *Chest*. 2003;124:18S-25S
101. Wu CC, Hwang TL, Liao CH, Kuo SC, Lee FY, Teng CM. The role of par4 in thrombin-induced thromboxane production in human platelets. *Thrombosis and haemostasis*. 2003;90:299-308
102. Andrews RK, Shen Y, Gardiner EE, Dong JF, Lopez JA, Berndt MC. The glycoprotein ib-ix-v complex in platelet adhesion and signaling. *Thrombosis and haemostasis*. 1999;82:357-364
103. Schroeck F, Arroyo de Prada N, Sperl S, Schmitt M, Viktor M. Interaction of plasminogen activator inhibitor type-1 (pai-1) with vitronectin (vn): Mapping the binding sites on pai-1 and vn. *Biological chemistry*. 2002;383:1143-1149
104. Evans DL, McGrogan M, Scott RW, Carrell RW. Protease specificity and heparin binding and activation of recombinant protease nexin i. *The Journal of biological chemistry*. 1991;266:22307-22312
105. Pratt CW, Church FC. General features of the heparin-binding serpins antithrombin, heparin cofactor ii and protein c inhibitor. *Blood coagulation & fibrinolysis : an international journal in haemostasis and thrombosis*. 1993;4:479-490
106. Boulaftali Y, Adam F, Venisse L, Ollivier V, Richard B, Taieb S, Monard D, Favier R, Alessi MC, Bryckaert M, Arocas V, Jandrot-Perrus M, Bouton MC. Anticoagulant and antithrombotic properties of platelet protease nexin-1. *Blood*. 2010;115:97-106
107. Parahuleva MS, Kanse SM, Parviz B, Barth A, Tillmanns H, Bohle RM, Sedding DG, Holschermann H. Factor seven activating protease (fsap) expression in human monocytes and accumulation in unstable coronary atherosclerotic plaques. *Atherosclerosis*. 2008;196:164-171

108. Muhl L, Nykjaer A, Wygrecka M, Monard D, Preissner KT, Kanse SM. Inhibition of pdgf-bb by factor vii-activating protease (fsap) is neutralized by protease nexin-1, and the fsap-inhibitor complexes are internalized via lrp. *The Biochemical journal*. 2007;404:191-196
109. Shibamiya A, Muhl L, Tannert-Otto S, Preissner KT, Kanse SM. Nucleic acids potentiate factor vii-activating protease (fsap)-mediated cleavage of platelet-derived growth factor-bb and inhibition of vascular smooth muscle cell proliferation. *The Biochemical journal*. 2007;404:45-50
110. Falati S, Liu Q, Gross P, Merrill-Skoloff G, Chou J, Vandendries E, Celi A, Croce K, Furie BC, Furie B. Accumulation of tissue factor into developing thrombi in vivo is dependent upon microparticle p-selectin glycoprotein ligand 1 and platelet p-selectin. *The Journal of experimental medicine*. 2003;197:1585-1598
111. Ploug M, Ronne E, Behrendt N, Jensen AL, Blasi F, Dano K. Cellular receptor for urokinase plasminogen activator. Carboxyl-terminal processing and membrane anchoring by glycosyl-phosphatidylinositol. *The Journal of biological chemistry*. 1991;266:1926-1933
112. Li Q, Laumonnier Y, Syrovets T, Simmet T. Plasmin triggers cytokine induction in human monocyte-derived macrophages. *Arterioscler Thromb Vasc Biol*. 2007;27:1383-1389
113. Robbie LA, Booth NA, Brown AJ, Bennett B. Inhibitors of fibrinolysis are elevated in atherosclerotic plaque. *Arterioscler Thromb Vasc Biol*. 1996;16:539-545
114. Andreasen PA, Georg B, Lund LR, Riccio A, Stacey SN. Plasminogen activator inhibitors: Hormonally regulated serpins. *Molecular and cellular endocrinology*. 1990;68:1-19
115. Schwartz CJ, Valente AJ, Kelley JL, Sprague EA, Edwards EH. Thrombosis and the development of atherosclerosis: Rokitansky revisited. *Seminars in thrombosis and hemostasis*. 1988;14:189-195
116. Massague J. The transforming growth factor-beta family. *Annual review of cell biology*. 1990;6:597-641
117. Jiang Z, Seo JY, Ha H, Lee EA, Kim YS, Han DC, Uh ST, Park CS, Lee HB. Reactive oxygen species mediate tgf-beta1-induced plasminogen activator inhibitor-1 upregulation in mesangial cells. *Biochemical and biophysical research communications*. 2003;309:961-966
118. Fox R, Nhan TQ, Law GL, Morris DR, Liles WC, Schwartz SM. Psgl-1 and mtor regulate translation of rock-1 and physiological functions of macrophages. *The EMBO journal*. 2007;26:505-515
119. Carmeliet P, Schoonjans L, Kieckens L, Ream B, Degen J, Bronson R, De Vos R, van den Oord JJ, Collen D, Mulligan RC. Physiological consequences of loss of plasminogen activator gene function in mice. *Nature*. 1994;368:419-424
120. Ploplis VA, Carmeliet P, Vazirzadeh S, Van Vlaenderen I, Moons L, Plow EF, Collen D. Effects of disruption of the plasminogen gene on thrombosis, growth, and health in mice. *Circulation*. 1995;92:2585-2593
121. Simon DI, Ezratty AM, Loscalzo J. The fibrin(ogen)olytic properties of cathepsin d. *Biochemistry*. 1994;33:6555-6563
122. Simon DI, Rao NK, Xu H, Wei Y, Majdic O, Ronne E, Kobzik L, Chapman HA. Mac-1 (cd11b/cd18) and the urokinase receptor (cd87) form a functional unit on monocytic cells. *Blood*. 1996;88:3185-3194
123. Plow EF, Edgington TS. An alternative pathway for fibrinolysis. I. The cleavage of fibrinogen by leukocyte proteases at physiologic ph. *The Journal of clinical investigation*. 1975;56:30-38

124. Plow EF. Leukocyte elastase release during blood coagulation. A potential mechanism for activation of the alternative fibrinolytic pathway. *The Journal of clinical investigation*. 1982;69:564-572
125. Weitz JI, Huang AJ, Landman SL, Nicholson SC, Silverstein SC. Elastase-mediated fibrinogenolysis by chemoattractant-stimulated neutrophils occurs in the presence of physiologic concentrations of antiproteinases. *The Journal of experimental medicine*. 1987;166:1836-1850
126. Machovich R, Owen WG. An elastase-dependent pathway of plasminogen activation. *Biochemistry*. 1989;28:4517-4522
127. Kolev K, Tenekedjiev K, Komorowicz E, Machovich R. Functional evaluation of the structural features of proteases and their substrate in fibrin surface degradation. *The Journal of biological chemistry*. 1997;272:13666-13675
128. Takada A, Sugawara Y, Takada Y. Degradation of glu- and lys-plasminogen by elastase in the presence or absence of tranexamic acid. *Thromb Res*. 1988;50:285-294
129. Schmidt W, Egbring R, Havemann K. Effect of elastase-like and chymotrypsin-like neutral proteases from human granulocytes on isolated clotting factors. *Thromb Res*. 1975;6:315-329
130. Henriksson P, Nilsson IM, Ohlsson K, Stenberg P. Granulocyte elastase activation and degradation of factor xiii. *Thromb Res*. 1980;18:343-351
131. Brower MS, Walz DA, Garry KE, Fenton JW, 2nd. Human neutrophil elastase alters human alpha-thrombin function: Limited proteolysis near the gamma-cleavage site results in decreased fibrinogen clotting and platelet-stimulatory activity. *Blood*. 1987;69:813-819
132. Nagase H, Visse R, Murphy G. Structure and function of matrix metalloproteinases and timps. *Cardiovascular research*. 2006;69:562-573
133. Newby AC. Metalloproteinase expression in monocytes and macrophages and its relationship to atherosclerotic plaque instability. *Arterioscler Thromb Vasc Biol*. 2008;28:2108-2114
134. Malik N, Greenfield BW, Wahl AF, Kiener PA. Activation of human monocytes through cd40 induces matrix metalloproteinases. *Journal of immunology (Baltimore, Md. : 1950)*. 1996;156:3952-3960
135. Chase AJ, Bond M, Crook MF, Newby AC. Role of nuclear factor-kappa b activation in metalloproteinase-1, -3, and -9 secretion by human macrophages in vitro and rabbit foam cells produced in vivo. *Arterioscler Thromb Vasc Biol*. 2002;22:765-771
136. Feinberg MW, Jain MK, Werner F, Sibinga NE, Wiesel P, Wang H, Topper JN, Perrella MA, Lee ME. Transforming growth factor-beta 1 inhibits cytokine-mediated induction of human metalloelastase in macrophages. *The Journal of biological chemistry*. 2000;275:25766-25773
137. Lacraz S, Nicod L, Galve-de Rochemonteix B, Baumberger C, Dayer JM, Welgus HG. Suppression of metalloproteinase biosynthesis in human alveolar macrophages by interleukin-4. *The Journal of clinical investigation*. 1992;90:382-388
138. Shimizu K, Shichiri M, Libby P, Lee RT, Mitchell RN. Th2-predominant inflammation and blockade of ifn-gamma signaling induce aneurysms in allografted aortas. *The Journal of clinical investigation*. 2004;114:300-308
139. Tedgui A, Mallat Z. Cytokines in atherosclerosis: Pathogenic and regulatory pathways. *Physiological reviews*. 2006;86:515-581
140. Wu L, Fan J, Matsumoto S, Watanabe T. Induction and regulation of matrix metalloproteinase-12 by cytokines and cd40 signaling in monocyte/macrophages. *Biochemical and biophysical research communications*. 2000;269:808-815
141. Moreau M, Brocheriou I, Petit L, Ninio E, Chapman MJ, Rouis M. Interleukin-8 mediates downregulation of tissue inhibitor of metalloproteinase-1 expression in cholesterol-

loaded human macrophages: Relevance to stability of atherosclerotic plaque. *Circulation*. 1999;99:420-426
142. Newby AC. Matrix metalloproteinases regulate migration, proliferation, and death of vascular smooth muscle cells by degrading matrix and non-matrix substrates. *Cardiovascular research*. 2006;69:614-624
143. Fredholm BB, Abbracchio MP, Burnstock G, Dubyak GR, Harden TK, Jacobson KA, Schwabe U, Williams M. Towards a revised nomenclature for p1 and p2 receptors. *Trends in pharmacological sciences*. 1997;18:79-82
144. Wright SD, Weitz JI, Huang AJ, Levin SM, Silverstein SC, Loike JD. Complement receptor type three (cd11b/cd18) of human polymorphonuclear leukocytes recognizes fibrinogen. *Proceedings of the National Academy of Sciences of the United States of America*. 1988;85:7734-7738
145. Altieri DC, Bader R, Mannucci PM, Edgington TS. Oligospecificity of the cellular adhesion receptor mac-1 encompasses an inducible recognition specificity for fibrinogen. *The Journal of cell biology*. 1988;107:1893-1900
146. Loike JD, Sodeik B, Cao L, Leucona S, Weitz JI, Detmers PA, Wright SD, Silverstein SC. Cd11c/cd18 on neutrophils recognizes a domain at the n terminus of the a alpha chain of fibrinogen. *Proceedings of the National Academy of Sciences of the United States of America*. 1991;88:1044-1048
147. Diamond MS, Springer TA. A subpopulation of mac-1 (cd11b/cd18) molecules mediates neutrophil adhesion to icam-1 and fibrinogen. *The Journal of cell biology*. 1993;120:545-556
148. Nham SU. Characteristics of fibrinogen binding to the domain of cd11c, an alpha subunit of p150,95. *Biochemical and biophysical research communications*. 1999;264:630-634
149. Fan ST, Edgington TS. Integrin regulation of leukocyte inflammatory functions. Cd11b/cd18 enhancement of the tumor necrosis factor-alpha responses of monocytes. *Journal of immunology (Baltimore, Md. : 1950)*. 1993;150:2972-2980
150. Perez RL, Roman J. Fibrin enhances the expression of il-1 beta by human peripheral blood mononuclear cells. Implications in pulmonary inflammation. *Journal of immunology (Baltimore, Md. : 1950)*. 1995;154:1879-1887
151. Smiley ST, King JA, Hancock WW. Fibrinogen stimulates macrophage chemokine secretion through toll-like receptor 4. *Journal of immunology (Baltimore, Md. : 1950)*. 2001;167:2887-2894
152. Mackman N, Morrissey JH, Fowler B, Edgington TS. Complete sequence of the human tissue factor gene, a highly regulated cellular receptor that initiates the coagulation protease cascade. *Biochemistry*. 1989;28:1755-1762
153. Bazan JF. Structural design and molecular evolution of a cytokine receptor superfamily. *Proceedings of the National Academy of Sciences of the United States of America*. 1990;87:6934-6938
154. Carmeliet P, Mackman N, Moons L, Luther T, Gressens P, Van Vlaenderen I, Demunck H, Kasper M, Breier G, Evrard P, Muller M, Risau W, Edgington T, Collen D. Role of tissue factor in embryonic blood vessel development. *Nature*. 1996;383:73-75
155. Mackman N, Imes S, Maske WH, Taylor B, Lusis AJ, Drake TA. Structure of the murine tissue factor gene. Chromosome location and conservation of regulatory elements in the promoter. *Arteriosclerosis and thrombosis : a journal of vascular biology / American Heart Association*. 1992;12:474-483
156. Harlos K, Martin DM, O'Brien DP, Jones EY, Stuart DI, Polikarpov I, Miller A, Tuddenham EG, Boys CW. Crystal structure of the extracellular region of human tissue factor. *Nature*. 1994;370:662-666

157. Morrissey JH, Fakhrai H, Edgington TS. Molecular cloning of the cdna for tissue factor, the cellular receptor for the initiation of the coagulation protease cascade. *Cell*. 1987;50:129-135
158. Spicer EK, Horton R, Bloem L, Bach R, Williams KR, Guha A, Kraus J, Lin TC, Nemerson Y, Konigsberg WH. Isolation of cdna clones coding for human tissue factor: Primary structure of the protein and cdna. *Proceedings of the National Academy of Sciences of the United States of America*. 1987;84:5148-5152
159. Petersen LC, Valentin S, Hedner U. Regulation of the extrinsic pathway system in health and disease: The role of factor viia and tissue factor pathway inhibitor. *Thromb Res*. 1995;79:1-47
160. Ruf W, Edgington TS. Structural biology of tissue factor, the initiator of thrombogenesis in vivo. *FASEB journal : official publication of the Federation of American Societies for Experimental Biology*. 1994;8:385-390
161. Bach R, Konigsberg WH, Nemerson Y. Human tissue factor contains thioester-linked palmitate and stearate on the cytoplasmic half-cystine. *Biochemistry*. 1988;27:4227-4231
162. Contrino J, Hair G, Kreutzer DL, Rickles FR. In situ detection of tissue factor in vascular endothelial cells: Correlation with the malignant phenotype of human breast disease. *Nature medicine*. 1996;2:209-215
163. Drake TA, Morrissey JH, Edgington TS. Selective cellular expression of tissue factor in human tissues. Implications for disorders of hemostasis and thrombosis. *The American journal of pathology*. 1989;134:1087-1097
164. Flossel C, Luther T, Muller M, Albrecht S, Kasper M. Immunohistochemical detection of tissue factor (tf) on paraffin sections of routinely fixed human tissue. *Histochemistry*. 1994;101:449-453
165. Fleck RA, Rao LV, Rapaport SI, Varki N. Localization of human tissue factor antigen by immunostaining with monospecific, polyclonal anti-human tissue factor antibody. *Thromb Res*. 1990;59:421-437
166. Wilcox JN, Smith KM, Schwartz SM, Gordon D. Localization of tissue factor in the normal vessel wall and in the atherosclerotic plaque. *Proceedings of the National Academy of Sciences of the United States of America*. 1989;86:2839-2843
167. Kato K, Elsayed YA, Namoto M, Nakagawa K, Sueishi K. Enhanced expression of tissue factor activity in the atherosclerotic aortas of cholesterol-fed rabbits. *Thromb Res*. 1996;82:335-347
168. Semeraro N, Triggiani R, Montemurro P, Cavallo LG, Colucci M. Enhanced endothelial tissue factor but normal thrombomodulin in endotoxin-treated rabbits. *Thromb Res*. 1993;71:479-486
169. Todoroki H, Nakamura S, Higure A, Okamoto K, Takeda S, Nagata N, Itoh H, Ohsato K. Neutrophils express tissue factor in a monkey model of sepsis. *Surgery*. 2000;127:209-216
170. Erlich J, Fearns C, Mathison J, Ulevitch RJ, Mackman N. Lipopolysaccharide induction of tissue factor expression in rabbits. *Infection and immunity*. 1999;67:2540-2546
171. Pawlinski R, Pedersen B, Kehrle B, Aird WC, Frank RD, Guha M, Mackman N. Regulation of tissue factor and inflammatory mediators by egr-1 in a mouse endotoxemia model. *Blood*. 2003;101:3940-3947
172. Hara S, Asada Y, Hatakeyama K, Marutsuka K, Sato Y, Kisanuki A, Sumiyoshi A. Expression of tissue factor and tissue factor pathway inhibitor in rats lungs with lipopolysaccharide-induced disseminated intravascular coagulation. *Laboratory investigation; a journal of technical methods and pathology*. 1997;77:581-589

173. Mackman N, Sawdey MS, Keeton MR, Loskutoff DJ. Murine tissue factor gene expression in vivo. Tissue and cell specificity and regulation by lipopolysaccharide. *The American journal of pathology*. 1993;143:76-84
174. Steffel J, Hermann M, Greutert H, Gay S, Luscher TF, Ruschitzka F, Tanner FC. Celecoxib decreases endothelial tissue factor expression through inhibition of c-jun terminal nh2 kinase phosphorylation. *Circulation*. 2005;111:1685-1689
175. Brox JH, Osterud B, Bjorklid E, Fenton JW, 2nd. Production and availability of thromboplastin in endothelial cells: The effects of thrombin, endotoxin and platelets. *British journal of haematology*. 1984;57:239-246
176. Napoleone E, Di Santo A, Lorenzet R. Monocytes upregulate endothelial cell expression of tissue factor: A role for cell-cell contact and cross-talk. *Blood*. 1997;89:541-549
177. Bavendiek U, Libby P, Kilbride M, Reynolds R, Mackman N, Schonbeck U. Induction of tissue factor expression in human endothelial cells by cd40 ligand is mediated via activator protein 1, nuclear factor kappa b, and egr-1. *The Journal of biological chemistry*. 2002;277:25032-25039
178. Eto M, Kozai T, Cosentino F, Joch H, Luscher TF. Statin prevents tissue factor expression in human endothelial cells: Role of rho/rho-kinase and akt pathways. *Circulation*. 2002;105:1756-1759
179. Steffel J, Akhmedov A, Greutert H, Luscher TF, Tanner FC. Histamine induces tissue factor expression: Implications for acute coronary syndromes. *Circulation*. 2005;112:341-349
180. Drake TA, Hannani K, Fei HH, Lavi S, Berliner JA. Minimally oxidized low-density lipoprotein induces tissue factor expression in cultured human endothelial cells. *The American journal of pathology*. 1991;138:601-607
181. Camera M, Giesen PL, Fallon J, Aufiero BM, Taubman M, Tremoli E, Nemerson Y. Cooperation between vegf and tnf-alpha is necessary for exposure of active tissue factor on the surface of human endothelial cells. *Arterioscler Thromb Vasc Biol*. 1999;19:531-537
182. Moosbauer C, Morgenstern E, Cuvelier SL, Manukyan D, Bidzhekov K, Albrecht S, Lohse P, Patel KD, Engelmann B. Eosinophils are a major intravascular location for tissue factor storage and exposure. *Blood*. 2007;109:995-1002
183. Muller I, Klocke A, Alex M, Kotzsch M, Luther T, Morgenstern E, Zieseniss S, Zahler S, Preissner K, Engelmann B. Intravascular tissue factor initiates coagulation via circulating microvesicles and platelets. *FASEB journal : official publication of the Federation of American Societies for Experimental Biology*. 2003;17:476-478
184. Chung J, Koyama T, Ohsawa M, Shibamiya A, Hoshi A, Hirosawa S. 1,25(oh)(2)d(3) blocks tnf-induced monocytic tissue factor expression by inhibition of transcription factors ap-1 and nf-kappab. *Laboratory investigation; a journal of technical methods and pathology*. 2007;87:540-547
185. Guha M, Mackman N. The phosphatidylinositol 3-kinase-akt pathway limits lipopolysaccharide activation of signaling pathways and expression of inflammatory mediators in human monocytic cells. *The Journal of biological chemistry*. 2002;277:32124-32132
186. Ernofsson M, Siegbahn A. Platelet-derived growth factor-bb and monocyte chemotactic protein-1 induce human peripheral blood monocytes to express tissue factor. *Thromb Res*. 1996;83:307-320
187. He M, He X, Xie Q, Chen F, He S. Angiotensin ii induces the expression of tissue factor and its mechanism in human monocytes. *Thromb Res*. 2006;117:579-590
188. Lewis JC, Bennett-Cain AL, DeMars CS, Doellgast GJ, Grant KW, Jones NL, Gupta M. Procoagulant activity after exposure of monocyte-derived macrophages to minimally

oxidized low density lipoprotein. Co-localization of tissue factor antigen and nascent fibrin fibers at the cell surface. *The American journal of pathology*. 1995;147:1029-1040
189. Cermak J, Key NS, Bach RR, Balla J, Jacob HS, Vercellotti GM. C-reactive protein induces human peripheral blood monocytes to synthesize tissue factor. *Blood*. 1993;82:513-520
190. Brand K, Fowler BJ, Edgington TS, Mackman N. Tissue factor mrna in thp-1 monocytic cells is regulated at both transcriptional and posttranscriptional levels in response to lipopolysaccharide. *Molecular and cellular biology*. 1991;11:4732-4738
191. Crossman DC, Carr DP, Tuddenham EG, Pearson JD, McVey JH. The regulation of tissue factor mrna in human endothelial cells in response to endotoxin or phorbol ester. *The Journal of biological chemistry*. 1990;265:9782-9787
192. Osterud B, Bjorklid E. The tissue factor pathway in disseminated intravascular coagulation. *Seminars in thrombosis and hemostasis*. 2001;27:605-617
193. Ritis K, Doumas M, Mastellos D, Micheli A, Giaglis S, Magotti P, Rafail S, Kartalis G, Sideras P, Lambris JD. A novel c5a receptor-tissue factor cross-talk in neutrophils links innate immunity to coagulation pathways. *Journal of immunology (Baltimore, Md. : 1950)*. 2006;177:4794-4802
194. Panes O, Matus V, Saez CG, Quiroga T, Pereira J, Mezzano D. Human platelets synthesize and express functional tissue factor. *Blood*. 2007;109:5242-5250
195. Perez-Pujol S, Aras O, Lozano M, Cocking-Johnson D, Key NS, White JG, McCullough J, Escolar G. Stored platelets contain residual amounts of tissue factor: Evidence from studies on platelet concentrates stored for prolonged periods. *Transfusion*. 2005;45:572-579
196. Rauch U, Bonderman D, Bohrmann B, Badimon JJ, Himber J, Riederer MA, Nemerson Y. Transfer of tissue factor from leukocytes to platelets is mediated by cd15 and tissue factor. *Blood*. 2000;96:170-175
197. Misumi K, Ogawa H, Yasue H, Soejima H, Suefuji H, Nishiyama K, Takazoe K, Kugiyama K, Tsuji I, Kumeda K, Nakamura S. Comparison of plasma tissue factor levels in unstable and stable angina pectoris. *The American journal of cardiology*. 1998;81:22-26
198. Suefuji H, Ogawa H, Yasue H, Kaikita K, Soejima H, Motoyama T, Mizuno Y, Oshima S, Saito T, Tsuji I, Kumeda K, Kamikubo Y, Nakamura S. Increased plasma tissue factor levels in acute myocardial infarction. *American heart journal*. 1997;134:253-259
199. Amengual O, Atsumi T, Khamashta MA, Hughes GR. The role of the tissue factor pathway in the hypercoagulable state in patients with the antiphospholipid syndrome. *Thrombosis and haemostasis*. 1998;79:276-281
200. Key NS, Slungaard A, Dandelet L, Nelson SC, Moertel C, Styles LA, Kuypers FA, Bach RR. Whole blood tissue factor procoagulant activity is elevated in patients with sickle cell disease. *Blood*. 1998;91:4216-4223
201. Asakura H, Kamikubo Y, Goto A, Shiratori Y, Yamazaki M, Jokaji H, Saito M, Uotani C, Kumabashiri I, Morishita E, et al. Role of tissue factor in disseminated intravascular coagulation. *Thromb Res*. 1995;80:217-224
202. Bogdanov VY, Balasubramanian V, Hathcock J, Vele O, Lieb M, Nemerson Y. Alternatively spliced human tissue factor: A circulating, soluble, thrombogenic protein. *Nature medicine*. 2003;9:458-462
203. Censarek P, Bobbe A, Grandoch M, Schror K, Weber AA. Alternatively spliced human tissue factor (ashtf) is not pro-coagulant. *Thrombosis and haemostasis*. 2007;97:11-14
204. Schecter AD, Giesen PL, Taby O, Rosenfield CL, Rossikhina M, Fyfe BS, Kohtz DS, Fallon JT, Nemerson Y, Taubman MB. Tissue factor expression in human arterial smooth muscle cells. Tf is present in three cellular pools after growth factor stimulation. *The Journal of clinical investigation*. 1997;100:2276-2285

205. Bach RR. Tissue factor encryption. *Arterioscler Thromb Vasc Biol*. 2006;26:456-461
206. Le DT, Rapaport SI, Rao LV. Relations between factor viia binding and expression of factor viia/tissue factor catalytic activity on cell surfaces. *The Journal of biological chemistry*. 1992;267:15447-15454
207. Bach RR, Moldow CF. Mechanism of tissue factor activation on hl-60 cells. *Blood*. 1997;89:3270-3276
208. Bach R, Rifkin DB. Expression of tissue factor procoagulant activity: Regulation by cytosolic calcium. *Proceedings of the National Academy of Sciences of the United States of America*. 1990;87:6995-6999
209. Greeno EW, Bach RR, Moldow CF. Apoptosis is associated with increased cell surface tissue factor procoagulant activity. *Laboratory investigation; a journal of technical methods and pathology*. 1996;75:281-289
210. Ahamed J, Versteeg HH, Kerver M, Chen VM, Mueller BM, Hogg PJ, Ruf W. Disulfide isomerization switches tissue factor from coagulation to cell signaling. *Proceedings of the National Academy of Sciences of the United States of America*. 2006;103:13932-13937
211. Chen VM, Ahamed J, Versteeg HH, Berndt MC, Ruf W, Hogg PJ. Evidence for activation of tissue factor by an allosteric disulfide bond. *Biochemistry*. 2006;45:12020-12028
212. Reinhardt C, von Bruhl ML, Manukyan D, Grahl L, Lorenz M, Altmann B, Dlugai S, Hess S, Konrad I, Orschiedt L, Mackman N, Ruddock L, Massberg S, Engelmann B. Protein disulfide isomerase acts as an injury response signal that enhances fibrin generation via tissue factor activation. *The Journal of clinical investigation*. 2008;118:1110-1122
213. Cho J, Furie BC, Coughlin SR, Furie B. A critical role for extracellular protein disulfide isomerase during thrombus formation in mice. *The Journal of clinical investigation*. 2008;118:1123-1131
214. Pendurthi UR, Ghosh S, Mandal SK, Rao LV. Tissue factor activation: Is disulfide bond switching a regulatory mechanism? *Blood*. 2007;110:3900-3908
215. Kothari H, Nayak RC, Rao LV, Pendurthi UR. Cystine 186-cystine 209 disulfide bond is not essential for the procoagulant activity of tissue factor or for its de-encryption. *Blood*. 2010;115:4273-4283
216. Daleke DL. Regulation of phospholipid asymmetry in the erythrocyte membrane. *Current opinion in hematology*. 2008;15:191-195
217. Bach RR, Monroe D. What is wrong with the allosteric disulfide bond hypothesis? *Arterioscler Thromb Vasc Biol*. 2009;29:1997-1998
218. Kaikita K, Ogawa H, Yasue H, Takeya M, Takahashi K, Saito T, Hayasaki K, Horiuchi K, Takizawa A, Kamikubo Y, Nakamura S. Tissue factor expression on macrophages in coronary plaques in patients with unstable angina. *Arterioscler Thromb Vasc Biol*. 1997;17:2232-2237
219. Lee CW, Park CS, Hwang I, Lee H, Park DW, Kang SJ, Lee SW, Kim YH, Park SW, Park SJ. Comparison of ruptured coronary plaques in patients with unstable and stable clinical presentation. *Journal of thrombosis and thrombolysis*. 2011;32:150-157
220. Kamikubo Y, Nakahara Y, Takemoto S, Hamuro T, Miyamoto S, Funatsu A. Human recombinant tissue-factor pathway inhibitor prevents the proliferation of cultured human neonatal aortic smooth muscle cells. *FEBS letters*. 1997;407:116-120
221. Sato Y, Kataoka H, Asada Y, Marutsuka K, Kamikubo Y, Koono M, Sumiyoshi A. Overexpression of tissue factor pathway inhibitor in aortic smooth muscle cells inhibits cell migration induced by tissue factor/factor viia complex. *Thromb Res*. 1999;94:401-406
222. El-Ghoroury EA, El-Din HG, Abdel-Kader M, Ragab S. Study of factor vii, tissue factor pathway inhibitor and monocyte tissue factor in noninsulin-dependent diabetes mellitus.

Blood coagulation & fibrinolysis : an international journal in haemostasis and thrombosis. 2008;19:7-13
223. Diamant M, Nieuwland R, Pablo RF, Sturk A, Smit JW, Radder JK. Elevated numbers of tissue-factor exposing microparticles correlate with components of the metabolic syndrome in uncomplicated type 2 diabetes mellitus. *Circulation*. 2002;106:2442-2447
224. Lim HS, Blann AD, Lip GY. Soluble cd40 ligand, soluble p-selectin, interleukin-6, and tissue factor in diabetes mellitus: Relationships to cardiovascular disease and risk factor intervention. *Circulation*. 2004;109:2524-2528
225. Vaidyula VR, Rao AK, Mozzoli M, Homko C, Cheung P, Boden G. Effects of hyperglycemia and hyperinsulinemia on circulating tissue factor procoagulant activity and platelet cd40 ligand. *Diabetes*. 2006;55:202-208
226. Boeri D, Almus FE, Maiello M, Cagliero E, Rao LV, Lorenzi M. Modification of tissue-factor mrna and protein response to thrombin and interleukin 1 by high glucose in cultured human endothelial cells. *Diabetes*. 1989;38:212-218
227. Bierhaus A, Illmer T, Kasper M, Luther T, Quehenberger P, Tritschler H, Wahl P, Ziegler R, Muller M, Nawroth PP. Advanced glycation end product (age)-mediated induction of tissue factor in cultured endothelial cells is dependent on rage. *Circulation*. 1997;96:2262-2271
228. Bierhaus A, Chevion S, Chevion M, Hofmann M, Quehenberger P, Illmer T, Luther T, Berentshtein E, Tritschler H, Muller M, Wahl P, Ziegler R, Nawroth PP. Advanced glycation end product-induced activation of nf-kappab is suppressed by alpha-lipoic acid in cultured endothelial cells. *Diabetes*. 1997;46:1481-1490
229. Ichikawa K, Yoshinari M, Iwase M, Wakisaka M, Doi Y, Iino K, Yamamoto M, Fujishima M. Advanced glycosylation end products induced tissue factor expression in human monocyte-like u937 cells and increased tissue factor expression in monocytes from diabetic patients. *Atherosclerosis*. 1998;136:281-287
230. Bea F, Blessing E, Shelley MI, Shultz JM, Rosenfeld ME. Simvastatin inhibits expression of tissue factor in advanced atherosclerotic lesions of apolipoprotein e deficient mice independently of lipid lowering: Potential role of simvastatin-mediated inhibition of egr-1 expression and activation. *Atherosclerosis*. 2003;167:187-194
231. Owens AP, 3rd, Passam FH, Antoniak S, Marshall SM, McDaniel AL, Rudel L, Williams JC, Hubbard BK, Dutton JA, Wang J, Tobias PS, Curtiss LK, Daugherty A, Kirchhofer D, Luyendyk JP, Moriarty PM, Nagarajan S, Furie BC, Furie B, Johns DG, Temel RE, Mackman N. Monocyte tissue factor-dependent activation of coagulation in hypercholesterolemic mice and monkeys is inhibited by simvastatin. *The Journal of clinical investigation*. 2012;122:558-568
232. Viswambharan H, Ming XF, Zhu S, Hubsch A, Lerch P, Vergeres G, Rusconi S, Yang Z. Reconstituted high-density lipoprotein inhibits thrombin-induced endothelial tissue factor expression through inhibition of rhoa and stimulation of phosphatidylinositol 3-kinase but not akt/endothelial nitric oxide synthase. *Circulation research*. 2004;94:918-925
233. Felmeden DC, Spencer CG, Chung NA, Belgore FM, Blann AD, Beevers DG, Lip GY. Relation of thrombogenesis in systemic hypertension to angiogenesis and endothelial damage/dysfunction (a substudy of the anglo-scandinavian cardiac outcomes trial [ascot]). *The American journal of cardiology*. 2003;92:400-405
234. Taubman MB, Marmur JD, Rosenfield CL, Guha A, Nichtberger S, Nemerson Y. Agonist-mediated tissue factor expression in cultured vascular smooth muscle cells. Role of ca2+ mobilization and protein kinase c activation. *The Journal of clinical investigation*. 1993;91:547-552
235. Napoleone E, Di Santo A, Camera M, Tremoli E, Lorenzet R. Angiotensin-converting enzyme inhibitors downregulate tissue factor synthesis in monocytes. *Circulation research*. 2000;86:139-143

236. Sambola A, Osende J, Hathcock J, Degen M, Nemerson Y, Fuster V, Crandall J, Badimon JJ. Role of risk factors in the modulation of tissue factor activity and blood thrombogenicity. *Circulation*. 2003;107:973-977
237. Annex BH, Denning SM, Channon KM, Sketch MH, Jr., Stack RS, Morrissey JH, Peters KG. Differential expression of tissue factor protein in directional atherectomy specimens from patients with stable and unstable coronary syndromes. *Circulation*. 1995;91:619-622
238. Ardissino D, Merlini PA, Ariens R, Coppola R, Bramucci E, Mannucci PM. Tissue-factor antigen and activity in human coronary atherosclerotic plaques. *Lancet*. 1997;349:769-771
239. Brambilla M, Camera M, Colnago D, Marenzi G, De Metrio M, Giesen PL, Balduini A, Veglia F, Gertow K, Biglioli P, Tremoli E. Tissue factor in patients with acute coronary syndromes: Expression in platelets, leukocytes, and platelet-leukocyte aggregates. *Arterioscler Thromb Vasc Biol*. 2008;28:947-953
240. Lee KW, Blann AD, Lip GY. Plasma markers of endothelial damage/dysfunction, inflammation and thrombogenesis in relation to timi risk stratification in acute coronary syndromes. *Thrombosis and haemostasis*. 2005;94:1077-1083
241. Soejima H, Ogawa H, Yasue H, Kaikita K, Nishiyama K, Misumi K, Takazoe K, Miyao Y, Yoshimura M, Kugiyama K, Nakamura S, Tsuji I, Kumeda K. Heightened tissue factor associated with tissue factor pathway inhibitor and prognosis in patients with unstable angina. *Circulation*. 1999;99:2908-2913
242. Palmerini T, Coller BS, Cervi V, Tomasi L, Marzocchi A, Marrozzini C, Leone O, Piccioli M, Branzi A. Monocyte-derived tissue factor contributes to stent thrombosis in an in vitro system. *Journal of the American College of Cardiology*. 2004;44:1570-1577
243. Malarstig A, Tenno T, Johnston N, Lagerqvist B, Axelsson T, Syvanen AC, Wallentin L, Siegbahn A. Genetic variations in the tissue factor gene are associated with clinical outcome in acute coronary syndrome and expression levels in human monocytes. *Arterioscler Thromb Vasc Biol*. 2005;25:2667-2672
244. Mackman N. Regulation of the tissue factor gene. *Thrombosis and haemostasis*. 1997;78:747-754
245. Eilertsen KE, Osterud B. Tissue factor: (patho)physiology and cellular biology. *Blood coagulation & fibrinolysis : an international journal in haemostasis and thrombosis*. 2004;15:521-538
246. Armesilla AL, Lorenzo E, Gomez del Arco P, Martinez-Martinez S, Alfranca A, Redondo JM. Vascular endothelial growth factor activates nuclear factor of activated t cells in human endothelial cells: A role for tissue factor gene expression. *Molecular and cellular biology*. 1999;19:2032-2043
247. Bird AP. Cpg-rich islands and the function of DNA methylation. *Nature*. 1986;321:209-213
248. Krikun G, Schatz F, Mackman N, Guller S, Demopoulos R, Lockwood CJ. Regulation of tissue factor gene expression in human endometrium by transcription factors sp1 and sp3. *Molecular endocrinology (Baltimore, Md.)*. 2000;14:393-400
249. Oeth P, Parry GC, Mackman N. Regulation of the tissue factor gene in human monocytic cells. Role of ap-1, nf-kappa b/rel, and sp1 proteins in uninduced and lipopolysaccharide-induced expression. *Arterioscler Thromb Vasc Biol*. 1997;17:365-374
250. Parry GC, Mackman N. Transcriptional regulation of tissue factor expression in human endothelial cells. *Arterioscler Thromb Vasc Biol*. 1995;15:612-621
251. Mackman N, Brand K, Edgington TS. Lipopolysaccharide-mediated transcriptional activation of the human tissue factor gene in thp-1 monocytic cells requires both activator protein 1 and nuclear factor kappa b binding sites. *The Journal of experimental medicine*. 1991;174:1517-1526

252. Cui MZ, Parry GC, Oeth P, Larson H, Smith M, Huang RP, Adamson ED, Mackman N. Transcriptional regulation of the tissue factor gene in human epithelial cells is mediated by sp1 and egr-1. *The Journal of biological chemistry*. 1996;271:2731-2739
253. Mechtcheriakova D, Wlachos A, Holzmuller H, Binder BR, Hofer E. Vascular endothelial cell growth factor-induced tissue factor expression in endothelial cells is mediated by egr-1. *Blood*. 1999;93:3811-3823
254. Cui MZ, Parry GC, Edgington TS, Mackman N. Regulation of tissue factor gene expression in epithelial cells. Induction by serum and phorbol 12-myristate 13-acetate. *Arteriosclerosis and thrombosis : a journal of vascular biology / American Heart Association*. 1994;14:807-814
255. Houston P, Dickson MC, Ludbrook V, White B, Schwachtgen JL, McVey JH, Mackman N, Reese JM, Gorman DG, Campbell C, Braddock M. Fluid shear stress induction of the tissue factor promoter in vitro and in vivo is mediated by egr-1. *Arterioscler Thromb Vasc Biol*. 1999;19:281-289
256. Mechtcheriakova D, Schabbauer G, Lucerna M, Clauss M, De Martin R, Binder BR, Hofer E. Specificity, diversity, and convergence in vegf and tnf-alpha signaling events leading to tissue factor up-regulation via egr-1 in endothelial cells. *FASEB journal : official publication of the Federation of American Societies for Experimental Biology*. 2001;15:230-242
257. Blum S, Issbruker K, Willuweit A, Hehlgans S, Lucerna M, Mechtcheriakova D, Walsh K, von der Ahe D, Hofer E, Clauss M. An inhibitory role of the phosphatidylinositol 3-kinase-signaling pathway in vascular endothelial growth factor-induced tissue factor expression. *The Journal of biological chemistry*. 2001;276:33428-33434
258. Steffel J, Latini RA, Akhmedov A, Zimmermann D, Zimmerling P, Luscher TF, Tanner FC. Rapamycin, but not fk-506, increases endothelial tissue factor expression: Implications for drug-eluting stent design. *Circulation*. 2005;112:2002-2011
259. Scarpati EM, Wen D, Broze GJ, Jr., Miletich JP, Flandermeyer RR, Siegel NR, Sadler JE. Human tissue factor: Cdna sequence and chromosome localization of the gene. *Biochemistry*. 1987;26:5234-5238
260. Ahern SM, Miyata T, Sadler JE. Regulation of human tissue factor expression by mrna turnover. *The Journal of biological chemistry*. 1993;268:2154-2159
261. Bakheet T, Frevel M, Williams BR, Greer W, Khabar KS. Ared: Human au-rich element-containing mrna database reveals an unexpectedly diverse functional repertoire of encoded proteins. *Nucleic acids research*. 2001;29:246-254
262. Scarpati EM, Sadler JE. Regulation of endothelial cell coagulant properties. Modulation of tissue factor, plasminogen activator inhibitors, and thrombomodulin by phorbol 12-myristate 13-acetate and tumor necrosis factor. *The Journal of biological chemistry*. 1989;264:20705-20713
263. Yamazaki S, Takeshige K. Protein synthesis inhibitors enhance the expression of mrnas for early inducible inflammatory genes via mrna stabilization. *Biochimica et biophysica acta*. 2008;1779:108-114
264. Lagnado CA, Brown CY, Goodall GJ. Auuua is not sufficient to promote poly(a) shortening and degradation of an mrna: The functional sequence within au-rich elements may be uuauuua(u/a)(u/a). *Molecular and cellular biology*. 1994;14:7984-7995
265. Lewis T, Gueydan C, Huez G, Toulme JJ, Kruys V. Mapping of a minimal au-rich sequence required for lipopolysaccharide-induced binding of a 55-kda protein on tumor necrosis factor-alpha mrna. *The Journal of biological chemistry*. 1998;273:13781-13786
266. Zubiaga AM, Belasco JG, Greenberg ME. The nonamer uuauuuauu is the key au-rich sequence motif that mediates mrna degradation. *Molecular and cellular biology*. 1995;15:2219-2230

267. Shetty S, Bhandary YP, Shetty SK, Velusamy T, Shetty P, Bdeir K, Gyetko MR, Cines DB, Idell S, Neuenschwander PF, Ruppert C, Guenther A, Abraham E, Shetty RS. Induction of tissue factor by urokinase in lung epithelial cells and in the lungs. *American journal of respiratory and critical care medicine*. 2010;181:1355-1366
268. Zhang X, Yu H, Lou JR, Zheng J, Zhu H, Popescu NI, Lupu F, Lind SE, Ding WQ. Microrna-19 (mir-19) regulates tissue factor expression in breast cancer cells. *The Journal of biological chemistry*. 2011;286:1429-1435
269. Brenner S, Jacob F, Meselson M. An unstable intermediate carrying information from genes to ribosomes for protein synthesis. *Nature*. 1961;190:576-581
270. Ross J. Mrna stability in mammalian cells. *Microbiological reviews*. 1995;59:423-450
271. Chen CY, Shyu AB. Au-rich elements: Characterization and importance in mrna degradation. *Trends in biochemical sciences*. 1995;20:465-470
272. Wilson T, Treisman R. Removal of poly(a) and consequent degradation of c-fos mrna facilitated by 3' au-rich sequences. *Nature*. 1988;336:396-399
273. Conne B, Stutz A, Vassalli JD. The 3' untranslated region of messenger rna: A molecular 'hotspot' for pathology? *Nature medicine*. 2000;6:637-641
274. Yang E, van Nimwegen E, Zavolan M, Rajewsky N, Schroeder M, Magnasco M, Darnell JE, Jr. Decay rates of human mrnas: Correlation with functional characteristics and sequence attributes. *Genome research*. 2003;13:1863-1872
275. Shaw G, Kamen R. A conserved au sequence from the 3' untranslated region of gm-csf mrna mediates selective mrna degradation. *Cell*. 1986;46:659-667
276. Halees AS, El-Badrawi R, Khabar KS. Ared organism: Expansion of ared reveals au-rich element cluster variations between human and mouse. *Nucleic acids research*. 2008;36:D137-140
277. Chen CY, Shyu AB. Selective degradation of early-response-gene mrnas: Functional analyses of sequence features of the au-rich elements. *Molecular and cellular biology*. 1994;14:8471-8482
278. Barreau C, Paillard L, Osborne HB. Au-rich elements and associated factors: Are there unifying principles? *Nucleic acids research*. 2005;33:7138-7150
279. Fan XC, Steitz JA. Overexpression of hur, a nuclear-cytoplasmic shuttling protein, increases the in vivo stability of are-containing mrnas. *The EMBO journal*. 1998;17:3448-3460
280. Bartel DP. Micrornas: Genomics, biogenesis, mechanism, and function. *Cell*. 2004;116:281-297
281. Lee Y, Kim M, Han J, Yeom KH, Lee S, Baek SH, Kim VN. Microrna genes are transcribed by rna polymerase ii. *The EMBO journal*. 2004;23:4051-4060
282. Lagos-Quintana M, Rauhut R, Meyer J, Borkhardt A, Tuschl T. New micrornas from mouse and human. *RNA (New York, N.Y.)*. 2003;9:175-179
283. Lee Y, Ahn C, Han J, Choi H, Kim J, Yim J, Lee J, Provost P, Radmark O, Kim S, Kim VN. The nuclear rnase iii drosha initiates microrna processing. *Nature*. 2003;425:415-419
284. Lund E, Guttinger S, Calado A, Dahlberg JE, Kutay U. Nuclear export of microrna precursors. *Science (New York, N.Y.)*. 2004;303:95-98
285. Hutvagner G, McLachlan J, Pasquinelli AE, Balint E, Tuschl T, Zamore PD. A cellular function for the rna-interference enzyme dicer in the maturation of the let-7 small temporal rna. *Science (New York, N.Y.)*. 2001;293:834-838
286. Hammond SM, Boettcher S, Caudy AA, Kobayashi R, Hannon GJ. Argonaute2, a link between genetic and biochemical analyses of rnai. *Science (New York, N.Y.)*. 2001;293:1146-1150
287. Hutvagner G, Simard MJ. Argonaute proteins: Key players in rna silencing. *Nature reviews. Molecular cell biology*. 2008;9:22-32

288. Ding L, Han M. Gw182 family proteins are crucial for microrna-mediated gene silencing. *Trends Cell Biol*. 2007;17:411-416
289. Eulalio A, Huntzinger E, Izaurralde E. Gw182 interaction with argonaute is essential for mirna-mediated translational repression and mrna decay. *Nature structural & molecular biology*. 2008;15:346-353
290. Wightman B, Burglin TR, Gatto J, Arasu P, Ruvkun G. Negative regulatory sequences in the lin-14 3'-untranslated region are necessary to generate a temporal switch during caenorhabditis elegans development. *Genes & development*. 1991;5:1813-1824
291. Saxena S, Jonsson ZO, Dutta A. Small rnas with imperfect match to endogenous mrna repress translation. Implications for off-target activity of small inhibitory rna in mammalian cells. *The Journal of biological chemistry*. 2003;278:44312-44319
292. Brennecke J, Stark A, Russell RB, Cohen SM. Principles of microrna-target recognition. *PLoS biology*. 2005;3:e85
293. Kim HH, Kuwano Y, Srikantan S, Lee EK, Martindale JL, Gorospe M. Hur recruits let-7/risc to repress c-myc expression. *Genes & development*. 2009;23:1743-1748
294. Bhattacharyya SN, Habermacher R, Martine U, Closs EI, Filipowicz W. Relief of microrna-mediated translational repression in human cells subjected to stress. *Cell*. 2006;125:1111-1124
295. Kedde M, Strasser MJ, Boldajipour B, Oude Vrielink JA, Slanchev K, le Sage C, Nagel R, Voorhoeve PM, van Duijse J, Orom UA, Lund AH, Perrakis A, Raz E, Agami R. Rna-binding protein dnd1 inhibits microrna access to target mrna. *Cell*. 2007;131:1273-1286
296. Jing Q, Huang S, Guth S, Zarubin T, Motoyama A, Chen J, Di Padova F, Lin SC, Gram H, Han J. Involvement of microrna in au-rich element-mediated mrna instability. *Cell*. 2005;120:623-634
297. Gallie DR. The cap and poly(a) tail function synergistically to regulate mrna translational efficiency. *Genes & development*. 1991;5:2108-2116
298. Wang Z, Kiledjian M. The poly(a)-binding protein and an mrna stability protein jointly regulate an endoribonuclease activity. *Molecular and cellular biology*. 2000;20:6334-6341
299. Yamashita A, Chang TC, Yamashita Y, Zhu W, Zhong Z, Chen CY, Shyu AB. Concerted action of poly(a) nucleases and decapping enzyme in mammalian mrna turnover. *Nature structural & molecular biology*. 2005;12:1054-1063
300. Tucker M, Valencia-Sanchez MA, Staples RR, Chen J, Denis CL, Parker R. The transcription factor associated ccr4 and caf1 proteins are components of the major cytoplasmic mrna deadenylase in saccharomyces cerevisiae. *Cell*. 2001;104:377-386
301. Steiger M, Carr-Schmid A, Schwartz DC, Kiledjian M, Parker R. Analysis of recombinant yeast decapping enzyme. *RNA (New York, N.Y.)*. 2003;9:231-238
302. Houseley J, LaCava J, Tollervey D. Rna-quality control by the exosome. *Nature reviews. Molecular cell biology*. 2006;7:529-539
303. Liu H, Rodgers ND, Jiao X, Kiledjian M. The scavenger mrna decapping enzyme dcps is a member of the hit family of pyrophosphatases. *The EMBO journal*. 2002;21:4699-4708
304. Garneau NL, Wilusz J, Wilusz CJ. The highways and byways of mrna decay. *Nature reviews. Molecular cell biology*. 2007;8:113-126
305. Lai WS, Stumpo DJ, Blackshear PJ. Rapid insulin-stimulated accumulation of an mrna encoding a proline-rich protein. *The Journal of biological chemistry*. 1990;265:16556-16563
306. Ma Q, Herschman HR. A corrected sequence for the predicted protein from the mitogen-inducible tis11 primary response gene. *Oncogene*. 1991;6:1277-1278
307. DuBois RN, McLane MW, Ryder K, Lau LF, Nathans D. A growth factor-inducible nuclear protein with a novel cysteine/histidine repetitive sequence. *The Journal of biological chemistry*. 1990;265:19185-19191

308. Varnum BC, Lim RW, Sukhatme VP, Herschman HR. Nucleotide sequence of a cdna encoding tis11, a message induced in swiss 3t3 cells by the tumor promoter tetradecanoyl phorbol acetate. *Oncogene*. 1989;4:119-120
309. Frederick ED, Ramos SB, Blackshear PJ. A unique c-terminal repeat domain maintains the cytosolic localization of the placenta-specific tristetraprolin family member zfp36l3. *The Journal of biological chemistry*. 2008;283:14792-14800
310. Ciais D, Cherradi N, Feige JJ. Multiple functions of tristetraprolin/tis11 rna-binding proteins in the regulation of mrna biogenesis and degradation. *Cellular and molecular life sciences : CMLS*. 2013;70:2031-2044
311. Stoecklin G, Stubbs T, Kedersha N, Wax S, Rigby WF, Blackwell TK, Anderson P. Mk2-induced tristetraprolin:14-3-3 complexes prevent stress granule association and are-mrna decay. *The EMBO journal*. 2004;23:1313-1324
312. Schmidlin M, Lu M, Leuenberger SA, Stoecklin G, Mallaun M, Gross B, Gherzi R, Hess D, Hemmings BA, Moroni C. The are-dependent mrna-destabilizing activity of brf1 is regulated by protein kinase b. *The EMBO journal*. 2004;23:4760-4769
313. Taylor GA, Carballo E, Lee DM, Lai WS, Thompson MJ, Patel DD, Schenkman DI, Gilkeson GS, Broxmeyer HE, Haynes BF, Blackshear PJ. A pathogenetic role for tnf alpha in the syndrome of cachexia, arthritis, and autoimmunity resulting from tristetraprolin (ttp) deficiency. *Immunity*. 1996;4:445-454
314. Stumpo DJ, Byrd NA, Phillips RS, Ghosh S, Maronpot RR, Castranio T, Meyers EN, Mishina Y, Blackshear PJ. Chorioallantoic fusion defects and embryonic lethality resulting from disruption of zfp36l1, a gene encoding a ccch tandem zinc finger protein of the tristetraprolin family. *Molecular and cellular biology*. 2004;24:6445-6455
315. Stumpo DJ, Broxmeyer HE, Ward T, Cooper S, Hangoc G, Chung YJ, Shelley WC, Richfield EK, Ray MK, Yoder MC, Aplan PD, Blackshear PJ. Targeted disruption of zfp36l2, encoding a ccch tandem zinc finger rna-binding protein, results in defective hematopoiesis. *Blood*. 2009;114:2401-2410
316. Carballo E, Blackshear PJ. Roles of tumor necrosis factor-alpha receptor subtypes in the pathogenesis of the tristetraprolin-deficiency syndrome. *Blood*. 2001;98:2389-2395
317. Douni E, Akassoglou K, Alexopoulou L, Georgopoulos S, Haralambous S, Hill S, Kassiotis G, Kontoyiannis D, Pasparakis M, Plows D, Probert L, Kollias G. Transgenic and knockout analyses of the role of tnf in immune regulation and disease pathogenesis. *Journal of inflammation*. 1995;47:27-38
318. Kontoyiannis D, Pasparakis M, Pizarro TT, Cominelli F, Kollias G. Impaired on/off regulation of tnf biosynthesis in mice lacking tnf au-rich elements: Implications for joint and gut-associated immunopathologies. *Immunity*. 1999;10:387-398
319. Carballo E, Gilkeson GS, Blackshear PJ. Bone marrow transplantation reproduces the tristetraprolin-deficiency syndrome in recombination activating gene-2 (-/-) mice. Evidence that monocyte/macrophage progenitors may be responsible for tnfalpha overproduction. *The Journal of clinical investigation*. 1997;100:986-995
320. Carballo E, Lai WS, Blackshear PJ. Feedback inhibition of macrophage tumor necrosis factor-alpha production by tristetraprolin. *Science (New York, N.Y.)*. 1998;281:1001-1005
321. Chrestensen CA, Schroeder MJ, Shabanowitz J, Hunt DF, Pelo JW, Worthington MT, Sturgill TW. Mapkap kinase 2 phosphorylates tristetraprolin on in vivo sites including ser178, a site required for 14-3-3 binding. *The Journal of biological chemistry*. 2004;279:10176-10184
322. Hitti E, Iakovleva T, Brook M, Deppenmeier S, Gruber AD, Radzioch D, Clark AR, Blackshear PJ, Kotlyarov A, Gaestel M. Mitogen-activated protein kinase-activated protein kinase 2 regulates tumor necrosis factor mrna stability and translation mainly by

altering tristetraprolin expression, stability, and binding to adenine/uridine-rich element. *Molecular and cellular biology*. 2006;26:2399-2407
323. Johnson BA, Stehn JR, Yaffe MB, Blackwell TK. Cytoplasmic localization of tristetraprolin involves 14-3-3-dependent and -independent mechanisms. *The Journal of biological chemistry*. 2002;277:18029-18036
324. Sun L, Stoecklin G, Van Way S, Hinkovska-Galcheva V, Guo RF, Anderson P, Shanley TP. Tristetraprolin (ttp)-14-3-3 complex formation protects ttp from dephosphorylation by protein phosphatase 2a and stabilizes tumor necrosis factor-alpha mrna. *The Journal of biological chemistry*. 2007;282:3766-3777
325. Ciais D, Cherradi N, Feige J-J. Multiple functions of tristetraprolin/tis11 rna-binding proteins in the regulation of mrna biogenesis and degradation. *Cell. Mol. Life Sci.* 2013;70:2031-2044
326. Clement SL, Scheckel C, Stoecklin G, Lykke-Andersen J. Phosphorylation of tristetraprolin by mk2 impairs au-rich element mrna decay by preventing deadenylase recruitment. *Molecular and cellular biology*. 2011;31:256-266
327. Rowlett RM, Chrestensen CA, Schroeder MJ, Harp MG, Pelo JW, Shabanowitz J, DeRose R, Hunt DF, Sturgill TW, Worthington MT. Inhibition of tristetraprolin deadenylation by poly(a) binding protein. *American journal of physiology. Gastrointestinal and liver physiology*. 2008;295:G421-430
328. Kedar VP, Darby MK, Williams JG, Blackshear PJ. Phosphorylation of human tristetraprolin in response to its interaction with the cbl interacting protein cin85. *PloS one*. 2010;5:e9588
329. Zheng D, Ezzeddine N, Chen CY, Zhu W, He X, Shyu AB. Deadenylation is prerequisite for p-body formation and mrna decay in mammalian cells. *The Journal of cell biology*. 2008;182:89-101
330. Schwede A, Ellis L, Luther J, Carrington M, Stoecklin G, Clayton C. A role for caf1 in mrna deadenylation and decay in trypanosomes and human cells. *Nucleic acids research*. 2008;36:3374-3388
331. Marchese FP, Aubareda A, Tudor C, Saklatvala J, Clark AR, Dean JL. Mapkap kinase 2 blocks tristetraprolin-directed mrna decay by inhibiting caf1 deadenylase recruitment. *The Journal of biological chemistry*. 2010;285:27590-27600
332. Eulalio A, Behm-Ansmant I, Izaurralde E. P bodies: At the crossroads of post-transcriptional pathways. *Nature reviews. Molecular cell biology*. 2007;8:9-22
333. Lykke-Andersen J, Wagner E. Recruitment and activation of mrna decay enzymes by two are-mediated decay activation domains in the proteins ttp and brf-1. *Genes & development*. 2005;19:351-361
334. Fenger-Gron M, Fillman C, Norrild B, Lykke-Andersen J. Multiple processing body factors and the are binding protein ttp activate mrna decapping. *Molecular cell*. 2005;20:905-915
335. Chen CY, Gherzi R, Ong SE, Chan EL, Raijmakers R, Pruijn GJ, Stoecklin G, Moroni C, Mann M, Karin M. Au binding proteins recruit the exosome to degrade are-containing mrnas. *Cell*. 2001;107:451-464
336. Hau HH, Walsh RJ, Ogilvie RL, Williams DA, Reilly CS, Bohjanen PR. Tristetraprolin recruits functional mrna decay complexes to are sequences. *Journal of cellular biochemistry*. 2007;100:1477-1492
337. Lai WS, Kennington EA, Blackshear PJ. Tristetraprolin and its family members can promote the cell-free deadenylation of au-rich element-containing mrnas by poly(a) ribonuclease. *Molecular and cellular biology*. 2003;23:3798-3812
338. Kedersha N, Stoecklin G, Ayodele M, Yacono P, Lykke-Andersen J, Fritzler MJ, Scheuner D, Kaufman RJ, Golan DE, Anderson P. Stress granules and processing

bodies are dynamically linked sites of mrnp remodeling. *The Journal of cell biology*. 2005;169:871-884
339. Emmons J, Townley-Tilson WH, Deleault KM, Skinner SJ, Gross RH, Whitfield ML, Brooks SA. Identification of ttp mrna targets in human dendritic cells reveals ttp as a critical regulator of dendritic cell maturation. *RNA (New York, N.Y.)*. 2008;14:888-902
340. Stoecklin G, Tenenbaum SA, Mayo T, Chittur SV, George AD, Baroni TE, Blackshear PJ, Anderson P. Genome-wide analysis identifies interleukin-10 mrna as target of tristetraprolin. *The Journal of biological chemistry*. 2008;283:11689-11699
341. Fechir M, Linker K, Pautz A, Hubrich T, Forstermann U, Rodriguez-Pascual F, Kleinert H. Tristetraprolin regulates the expression of the human inducible nitric-oxide synthase gene. *Molecular pharmacology*. 2005;67:2148-2161
342. Kedar VP, Zucconi BE, Wilson GM, Blackshear PJ. Direct binding of specific auf1 isoforms to tandem zinc finger domains of tristetraprolin (ttp) family proteins. *The Journal of biological chemistry*. 2012;287:5459-5471
343. Murata T, Hikita K, Kaneda N. Transcriptional activation function of zinc finger protein tis11 and its negative regulation by phorbol ester. *Biochemical and biophysical research communications*. 2000;274:526-532
344. Liang J, Lei T, Song Y, Yanes N, Qi Y, Fu M. Rna-destabilizing factor tristetraprolin negatively regulates nf-kappab signaling. *The Journal of biological chemistry*. 2009;284:29383-29390
345. Schichl YM, Resch U, Hofer-Warbinek R, de Martin R. Tristetraprolin impairs nf-kappab/p65 nuclear translocation. *The Journal of biological chemistry*. 2009;284:29571-29581
346. Cuadrado A, Nebreda AR. Mechanisms and functions of p38 mapk signalling. *The Biochemical journal*. 2010;429:403-417
347. Jiang Y, Chen C, Li Z, Guo W, Gegner JA, Lin S, Han J. Characterization of the structure and function of a new mitogen-activated protein kinase (p38beta). *The Journal of biological chemistry*. 1996;271:17920-17926
348. Lechner C, Zahalka MA, Giot JF, Moller NP, Ullrich A. Erk6, a mitogen-activated protein kinase involved in c2c12 myoblast differentiation. *Proceedings of the National Academy of Sciences of the United States of America*. 1996;93:4355-4359
349. Mertens S, Craxton M, Goedert M. Sap kinase-3, a new member of the family of mammalian stress-activated protein kinases. *FEBS letters*. 1996;383:273-276
350. Goedert M, Cuenda A, Craxton M, Jakes R, Cohen P. Activation of the novel stress-activated protein kinase sapk4 by cytokines and cellular stresses is mediated by skk3 (mkk6); comparison of its substrate specificity with that of other sap kinases. *The EMBO journal*. 1997;16:3563-3571
351. Jiang Y, Gram H, Zhao M, New L, Gu J, Feng L, Di Padova F, Ulevitch RJ, Han J. Characterization of the structure and function of the fourth member of p38 group mitogen-activated protein kinases, p38delta. *The Journal of biological chemistry*. 1997;272:30122-30128
352. Enslen H, Raingeaud J, Davis RJ. Selective activation of p38 mitogen-activated protein (map) kinase isoforms by the map kinase kinases mkk3 and mkk6. *The Journal of biological chemistry*. 1998;273:1741-1748
353. Alonso G, Ambrosino C, Jones M, Nebreda AR. Differential activation of p38 mitogen-activated protein kinase isoforms depending on signal strength. *The Journal of biological chemistry*. 2000;275:40641-40648
354. Brancho D, Tanaka N, Jaeschke A, Ventura JJ, Kelkar N, Tanaka Y, Kyuuma M, Takeshita T, Flavell RA, Davis RJ. Mechanism of p38 map kinase activation in vivo. *Genes & development*. 2003;17:1969-1978

355. Cuevas BD, Abell AN, Johnson GL. Role of mitogen-activated protein kinase kinase kinases in signal integration. *Oncogene*. 2007;26:3159-3171
356. Zhang YY, Mei ZQ, Wu JW, Wang ZX. Enzymatic activity and substrate specificity of mitogen-activated protein kinase p38alpha in different phosphorylation states. *The Journal of biological chemistry*. 2008;283:26591-26601
357. Lindqvist A, de Bruijn M, Macurek L, Bras A, Mensinga A, Bruinsma W, Voets O, Kranenburg O, Medema RH. Wip1 confers g2 checkpoint recovery competence by counteracting p53-dependent transcriptional repression. *The EMBO journal*. 2009;28:3196-3206
358. Farooq A, Zhou MM. Structure and regulation of mapk phosphatases. *Cellular signalling*. 2004;16:769-779
359. Lang R, Hammer M, Mages J. Dusp meet immunology: Dual specificity mapk phosphatases in control of the inflammatory response. *Journal of immunology (Baltimore, Md. : 1950)*. 2006;177:7497-7504
360. Owens DM, Keyse SM. Differential regulation of map kinase signalling by dual-specificity protein phosphatases. *Oncogene*. 2007;26:3203-3213
361. Camps M, Nichols A, Arkinstall S. Dual specificity phosphatases: A gene family for control of map kinase function. *FASEB journal : official publication of the Federation of American Societies for Experimental Biology*. 2000;14:6-16
362. Zeng Y, Sankala H, Zhang X, Graves PR. Phosphorylation of argonaute 2 at serine-387 facilitates its localization to processing bodies. *The Biochemical journal*. 2008;413:429-436
363. Sandler H, Stoecklin G. Control of mrna decay by phosphorylation of tristetraprolin. *Biochemical Society transactions*. 2008;36:491-496
364. Lai WS, Parker JS, Grissom SF, Stumpo DJ, Blackshear PJ. Novel mrna targets for tristetraprolin (ttp) identified by global analysis of stabilized transcripts in ttp-deficient fibroblasts. *Molecular and cellular biology*. 2006;26:9196-9208
365. Worthington MT, Pelo JW, Sachedina MA, Applegate JL, Arseneau KO, Pizarro TT. Rna binding properties of the au-rich element-binding recombinant nup475/tis11/tristetraprolin protein. *The Journal of biological chemistry*. 2002;277:48558-48564
366. Linker K, Pautz A, Fechir M, Hubrich T, Greeve J, Kleinert H. Involvement of ksrp in the post-transcriptional regulation of human inos expression-complex interplay of ksrp with ttp and hur. *Nucleic acids research*. 2005;33:4813-4827
367. Diefenbach J, Burkle A. Introduction to poly(adp-ribose) metabolism. *Cellular and molecular life sciences : CMLS*. 2005;62:721-730
368. Berger F, Ramirez-Hernandez MH, Ziegler M. The new life of a centenarian: Signalling functions of nad(p). *Trends in biochemical sciences*. 2004;29:111-118
369. Christmann M, Tomicic MT, Roos WP, Kaina B. Mechanisms of human DNA repair: An update. *Toxicology*. 2003;193:3-34
370. Menissier de Murcia J, Ricoul M, Tartier L, Niedergang C, Huber A, Dantzer F, Schreiber V, Ame JC, Dierich A, LeMeur M, Sabatier L, Chambon P, de Murcia G. Functional interaction between parp-1 and parp-2 in chromosome stability and embryonic development in mouse. *The EMBO journal*. 2003;22:2255-2263
371. Hassa PO, Hottiger MO. The functional role of poly(adp-ribose)polymerase 1 as novel coactivator of nf-kappab in inflammatory disorders. *Cellular and molecular life sciences : CMLS*. 2002;59:1534-1553
372. Hassa PO, Buerki C, Lombardi C, Imhof R, Hottiger MO. Transcriptional coactivation of nuclear factor-kappab-dependent gene expression by p300 is regulated by poly(adp)-ribose polymerase-1. *The Journal of biological chemistry*. 2003;278:45145-45153

373. Mayer-Kuckuk P, Ullrich O, Ziegler M, Grune T, Schweiger M. Functional interaction of poly(adp-ribose) with the 20s proteasome in vitro. *Biochemical and biophysical research communications*. 1999;259:576-581
374. Yu SW, Wang H, Poitras MF, Coombs C, Bowers WJ, Federoff HJ, Poirier GG, Dawson TM, Dawson VL. Mediation of poly(adp-ribose) polymerase-1-dependent cell death by apoptosis-inducing factor. *Science (New York, N.Y.)*. 2002;297:259-263
375. Chambon P, Weill JD, Mandel P. Nicotinamide mononucleotide activation of new DNA-dependent polyadenylic acid synthesizing nuclear enzyme. *Biochemical and biophysical research communications*. 1963;11:39-43
376. Sallmann FR, Vodenicharov MD, Wang ZQ, Poirier GG. Characterization of sparp-1. An alternative product of parp-1 gene with poly(adp-ribose) polymerase activity independent of DNA strand breaks. *The Journal of biological chemistry*. 2000;275:15504-15511
377. Ruf A, Mennissier de Murcia J, de Murcia G, Schulz GE. Structure of the catalytic fragment of poly(ad-ribose) polymerase from chicken. *Proceedings of the National Academy of Sciences of the United States of America*. 1996;93:7481-7485
378. Oliver AW, Ame JC, Roe SM, Good V, de Murcia G, Pearl LH. Crystal structure of the catalytic fragment of murine poly(adp-ribose) polymerase-2. *Nucleic acids research*. 2004;32:456-464
379. Ame JC, Spenlehauer C, de Murcia G. The parp superfamily. *BioEssays : news and reviews in molecular, cellular and developmental biology*. 2004;26:882-893
380. Schreiber V, Dantzer F, Ame JC, de Murcia G. Poly(adp-ribose): Novel functions for an old molecule. *Nature reviews. Molecular cell biology*. 2006;7:517-528
381. Ame JC, Rolli V, Schreiber V, Niedergang C, Apiou F, Decker P, Muller S, Hoger T, Menissier-de Murcia J, de Murcia G. Parp-2, a novel mammalian DNA damage-dependent poly(adp-ribose) polymerase. *The Journal of biological chemistry*. 1999;274:17860-17868
382. Sbodio JI, Chi NW. Identification of a tankyrase-binding motif shared by irap, tab182, and human trf1 but not mouse trf1. Numa contains this rxxpdg motif and is a novel tankyrase partner. *The Journal of biological chemistry*. 2002;277:31887-31892
383. Ladurner AG. Inactivating chromosomes: A macro domain that minimizes transcription. *Molecular cell*. 2003;12:1-3
384. Ogata N, Ueda K, Kagamiyama H, Hayaishi O. Adp-ribosylation of histone h1. Identification of glutamic acid residues 2, 14, and the cooh-terminal lysine residue as modification sites. *The Journal of biological chemistry*. 1980;255:7616-7620
385. Ogata N, Ueda K, Hayaishi O. Adp-ribosylation of histone h2b. Identification of glutamic acid residue 2 as the modification site. *The Journal of biological chemistry*. 1980;255:7610-7615
386. Kiehlbauch CC, Aboul-Ela N, Jacobson EL, Ringer DP, Jacobson MK. High resolution fractionation and characterization of adp-ribose polymers. *Analytical biochemistry*. 1993;208:26-34
387. Ruf A, Rolli V, de Murcia G, Schulz GE. The mechanism of the elongation and branching reaction of poly(adp-ribose) polymerase as derived from crystal structures and mutagenesis. *Journal of molecular biology*. 1998;278:57-65
388. Brochu G, Duchaine C, Thibeault L, Lagueux J, Shah GM, Poirier GG. Mode of action of poly(adp-ribose) glycohydrolase. *Biochimica et biophysica acta*. 1994;1219:342-350
389. Slade D, Dunstan MS, Barkauskaite E, Weston R, Lafite P, Dixon N, Ahel M, Leys D, Ahel I. The structure and catalytic mechanism of a poly(adp-ribose) glycohydrolase. *Nature*. 2011;477:616-620
390. Meyer-Ficca ML, Meyer RG, Coyle DL, Jacobson EL, Jacobson MK. Human poly(adp-ribose) glycohydrolase is expressed in alternative splice variants yielding isoforms that localize to different cell compartments. *Experimental cell research*. 2004;297:521-532

391. Cervantes-Laurean D, Jacobson EL, Jacobson MK. Glycation and glycoxidation of histones by adp-ribose. *The Journal of biological chemistry*. 1996;271:10461-10469
392. Bernet D, Pinto RM, Costas MJ, Canales J, Cameselle JC. Rat liver mitochondrial adp-ribose pyrophosphatase in the matrix space with low km for free adp-ribose. *The Biochemical journal*. 1994;299 (Pt 3):679-682
393. Oka S, Kato J, Moss J. Identification and characterization of a mammalian 39-kda poly(adp-ribose) glycohydrolase. *The Journal of biological chemistry*. 2006;281:705-713
394. Stilmann M, Hinz M, Arslan SC, Zimmer A, Schreiber V, Scheidereit C. A nuclear poly(adp-ribose)-dependent signalosome confers DNA damage-induced ikappab kinase activation. *Molecular cell*. 2009;36:365-378
395. Leung AK, Vyas S, Rood JE, Bhutkar A, Sharp PA, Chang P. Poly(adp-ribose) regulates stress responses and microrna activity in the cytoplasm. *Molecular cell*. 2011;42:489-499
396. Chang P, Jacobson MK, Mitchison TJ. Poly(adp-ribose) is required for spindle assembly and structure. *Nature*. 2004;432:645-649
397. Kotova E, Jarnik M, Tulin AV. Poly (adp-ribose) polymerase 1 is required for protein localization to cajal body. *PLoS genetics*. 2009;5:e1000387
398. Wang Z, Michaud GA, Cheng Z, Zhang Y, Hinds TR, Fan E, Cong F, Xu W. Recognition of the iso-adp-ribose moiety in poly(adp-ribose) by wwe domains suggests a general mechanism for poly(adp-ribosyl)ation-dependent ubiquitination. *Genes & development*. 2012;26:235-240
399. Aravind L. The wwe domain: A common interaction module in protein ubiquitination and adp ribosylation. *Trends in biochemical sciences*. 2001;26:273-275
400. Kang HC, Lee YI, Shin JH, Andrabi SA, Chi Z, Gagne JP, Lee Y, Ko HS, Lee BD, Poirier GG, Dawson VL, Dawson TM. Iduna is a poly(adp-ribose) (par)-dependent e3 ubiquitin ligase that regulates DNA damage. *Proceedings of the National Academy of Sciences of the United States of America*. 2011;108:14103-14108
401. Goenka S, Boothby M. Selective potentiation of stat-dependent gene expression by collaborator of stat6 (coast6), a transcriptional cofactor. *Proceedings of the National Academy of Sciences of the United States of America*. 2006;103:4210-4215
402. Maris C, Dominguez C, Allain FH. The rna recognition motif, a plastic rna-binding platform to regulate post-transcriptional gene expression. *The FEBS journal*. 2005;272:2118-2131
403. Clery A, Blatter M, Allain FH. Rna recognition motifs: Boring? Not quite. *Current opinion in structural biology*. 2008;18:290-298
404. Gibson TJ, Thompson JD, Heringa J. The kh domain occurs in a diverse set of rna-binding proteins that include the antiterminator nusa and is probably involved in binding to nucleic acid. *FEBS letters*. 1993;324:361-366
405. Valverde R, Edwards L, Regan L. Structure and function of kh domains. *The FEBS journal*. 2008;275:2712-2726
406. Cho SH, Goenka S, Henttinen T, Gudapati P, Reinikainen A, Eischen CM, Lahesmaa R, Boothby M. Parp-14, a member of the b aggressive lymphoma family, transduces survival signals in primary b cells. *Blood*. 2009;113:2416-2425
407. Mehrotra P, Riley JP, Patel R, Li F, Voss L, Goenka S. Parp-14 functions as a transcriptional switch for stat6-dependent gene activation. *The Journal of biological chemistry*. 2011;286:1767-1776
408. Leung A, Todorova T, Ando Y, Chang P. Poly(adp-ribose) regulates post-transcriptional gene regulation in the cytoplasm. *RNA biology*. 2012;9:542-548
409. Livak KJ, Schmittgen TD. Analysis of relative gene expression data using real-time quantitative pcr and the 2(-delta delta c(t)) method. *Methods (San Diego, Calif.)*. 2001;25:402-408

410. Rothberger H, Zimmerman TS, Vaughan JH. Increased production and expression of tissue thromboplastin-like procoagulant activity in vitro by allogeneically stimulated human leukocytes. *The Journal of clinical investigation*. 1978;62:649-655
411. Undas A, Celinska-Lowenhoff M, Lowenhoff T, Szczeklik A. Statins, fenofibrate, and quinapril increase clot permeability and enhance fibrinolysis in patients with coronary artery disease. *Journal of thrombosis and haemostasis : JTH*. 2006;4:1029-1036
412. Smith SA, Morrissey JH. Polyphosphate enhances fibrin clot structure. *Blood*. 2008;112:2810-2816
413. Kadish JL, Wenc KM, Dvorak HF. Tissue factor activity of normal and neoplastic cells: Quantitation and species specificity. *Journal of the National Cancer Institute*. 1983;70:551-557
414. Al-Souhibani N, Al-Ahmadi W, Hesketh JE, Blackshear PJ, Khabar KS. The rna-binding zinc-finger protein tristetraprolin regulates au-rich mrnas involved in breast cancer-related processes. *Oncogene*. 2010;29:4205-4215
415. Anyanful A, Ono K, Johnsen RC, Ly H, Jensen V, Baillie DL, Ono S. The rna-binding protein sup-12 controls muscle-specific splicing of the adf/cofilin pre-mrna in c. Elegans. *The Journal of cell biology*. 2004;167:639-647
416. Gavins FN, Chatterjee BE. Intravital microscopy for the study of mouse microcirculation in anti-inflammatory drug research: Focus on the mesentery and cremaster preparations. *Journal of pharmacological and toxicological methods*. 2004;49:1-14
417. Lindenblatt N, Bordel R, Schareck W, Menger MD, Vollmar B. Vascular heme oxygenase-1 induction suppresses microvascular thrombus formation in vivo. *Arterioscler Thromb Vasc Biol*. 2004;24:601-606
418. Boyle JJ, Harrington HA, Piper E, Elderfield K, Stark J, Landis RC, Haskard DO. Coronary intraplaque hemorrhage evokes a novel atheroprotective macrophage phenotype. *The American journal of pathology*. 2009;174:1097-1108
419. Qian X, Ning H, Zhang J, Hoft DF, Stumpo DJ, Blackshear PJ, Liu J. Posttranscriptional regulation of il-23 expression by ifn-gamma through tristetraprolin. *Journal of immunology (Baltimore, Md. : 1950)*. 2011;186:6454-6464
420. Matetzky S, Tani S, Kangavari S, Dimayuga P, Yano J, Xu H, Chyu KY, Fishbein MC, Shah PK, Cercek B. Smoking increases tissue factor expression in atherosclerotic plaques: Implications for plaque thrombogenicity. *Circulation*. 2000;102:602-604
421. King EM, Kaur M, Gong W, Rider CF, Holden NS, Newton R. Regulation of tristetraprolin expression by interleukin-1 beta and dexamethasone in human pulmonary epithelial cells: Roles for nuclear factor-kappa b and p38 mitogen-activated protein kinase. *The Journal of pharmacology and experimental therapeutics*. 2009;330:575-585
422. Kohro T, Tanaka T, Murakami T, Wada Y, Aburatani H, Hamakubo T, Kodama T. A comparison of differences in the gene expression profiles of phorbol 12-myristate 13-acetate differentiated thp-1 cells and human monocyte-derived macrophage. *Journal of atherosclerosis and thrombosis*. 2004;11:88-97
423. Sawaoka H, Dixon DA, Oates JA, Boutaud O. Tristetraprolin binds to the 3'-untranslated region of cyclooxygenase-2 mrna. A polyadenylation variant in a cancer cell line lacks the binding site. *The Journal of biological chemistry*. 2003;278:13928-13935
424. Brewer BY, Ballin JD, Fialcowitz-White EJ, Blackshear PJ, Wilson GM. Substrate dependence of conformational changes in the rna-binding domain of tristetraprolin assessed by fluorescence spectroscopy of tryptophan mutants. *Biochemistry*. 2006;45:13807-13817
425. Gibson BA, Kraus WL. New insights into the molecular and cellular functions of poly(adp-ribose) and parps. *Nature reviews. Molecular cell biology*. 2012;13:411-424
426. Mahtani KR, Brook M, Dean JL, Sully G, Saklatvala J, Clark AR. Mitogen-activated protein kinase p38 controls the expression and posttranslational modification of

tristetraprolin, a regulator of tumor necrosis factor alpha mrna stability. *Molecular and cellular biology*. 2001;21:6461-6469
427. Shantsila E, Lip GY. The role of monocytes in thrombotic disorders. Insights from tissue factor, monocyte-platelet aggregates and novel mechanisms. *Thrombosis and haemostasis*. 2009;102:916-924
428. Worthington MT, Amann BT, Nathans D, Berg JM. Metal binding properties and secondary structure of the zinc-binding domain of nup475. *Proceedings of the National Academy of Sciences of the United States of America*. 1996;93:13754-13759
429. Amann BT, Worthington MT, Berg JM. A cys3his zinc-binding domain from nup475/tristetraprolin: A novel fold with a disklike structure. *Biochemistry*. 2003;42:217-221
430. Lai WS, Carballo E, Thorn JM, Kennington EA, Blackshear PJ. Interactions of ccch zinc finger proteins with mrna. Binding of tristetraprolin-related zinc finger proteins to au-rich elements and destabilization of mrna. *The Journal of biological chemistry*. 2000;275:17827-17837
431. Dang W MY, Inoue M, Kigawa T, Shirouzu M, Terada T, Yokoyama S Riken Structural Genomics/proteomics Initiative (Rsgi). Solution structure of rrm domain in parp14. 2005
432. Akira S, Takeda K, Kaisho T. Toll-like receptors: Critical proteins linking innate and acquired immunity. *Nature immunology*. 2001;2:675-680
433. Clark A. Post-transcriptional regulation of pro-inflammatory gene expression. *Arthritis research*. 2000;2:172-174
434. Clark AR, Lasa M. Crosstalk between glucocorticoids and mitogen-activated protein kinase signalling pathways. *Current opinion in pharmacology*. 2003;3:404-411
435. Zhao Q, Shepherd EG, Manson ME, Nelin LD, Sorokin A, Liu Y. The role of mitogen-activated protein kinase phosphatase-1 in the response of alveolar macrophages to lipopolysaccharide: Attenuation of proinflammatory cytokine biosynthesis via feedback control of p38. *The Journal of biological chemistry*. 2005;280:8101-8108
436. Smoak K, Cidlowski JA. Glucocorticoids regulate tristetraprolin synthesis and posttranscriptionally regulate tumor necrosis factor alpha inflammatory signaling. *Molecular and cellular biology*. 2006;26:9126-9135
437. Ishmael FT, Fang X, Galdiero MR, Atasoy U, Rigby WF, Gorospe M, Cheadle C, Stellato C. Role of the rna-binding protein tristetraprolin in glucocorticoid-mediated gene regulation. *Journal of immunology (Baltimore, Md. : 1950)*. 2008;180:8342-8353
438. Fairhurst AM, Connolly JE, Hintz KA, Goulding NJ, Rassias AJ, Yeager MP, Rigby W, Wallace PK. Regulation and localization of endogenous human tristetraprolin. *Arthritis research & therapy*. 2003;5:R214-225
439. Sauer I, Schaljo B, Vogl C, Gattermeier I, Kolbe T, Muller M, Blackshear PJ, Kovarik P. Interferons limit inflammatory responses by induction of tristetraprolin. *Blood*. 2006;107:4790-4797
440. Jalonen U, Lahti A, Korhonen R, Kankaanranta H, Moilanen E. Inhibition of tristetraprolin expression by dexamethasone in activated macrophages. *Biochemical pharmacology*. 2005;69:733-740
441. Tchen CR, Brook M, Saklatvala J, Clark AR. The stability of tristetraprolin mrna is regulated by mitogen-activated protein kinase p38 and by tristetraprolin itself. *The Journal of biological chemistry*. 2004;279:32393-32400
442. Muhlfelder TW, Niemetz J, Kang S. Glucocorticoids inhibit the generation of leukocyte procoagulant (tissue factor) activity. *Blood*. 1982;60:1169-1172
443. Bottles KD, Morrissey JH. Dexamethasone enhances agonist induction of tissue factor in monocytes but not in endothelial cells. *Blood coagulation & fibrinolysis : an international journal in haemostasis and thrombosis*. 1993;4:405-414

444. Reddy KV, Bhattacharjee G, Schabbauer G, Hollis A, Kempf K, Tencati M, O'Connell M, Guha M, Mackman N. Dexamethasone enhances lps induction of tissue factor expression in human monocytic cells by increasing tissue factor mrna stability. *Journal of leukocyte biology*. 2004;76:145-151
445. van der Logt CP, Dirven RJ, Reitsma PH, Bertina RM. Expression of tissue factor and tissue factor pathway inhibitor in monocytes in response to bacterial lipopolysaccharide and phorbolester. *Blood coagulation & fibrinolysis : an international journal in haemostasis and thrombosis*. 1994;5:211-220
446. Cadroy Y, Dupouy D, Boneu B, Plaisancie H. Polymorphonuclear leukocytes modulate tissue factor production by mononuclear cells: Role of reactive oxygen species. *Journal of immunology (Baltimore, Md. : 1950)*. 2000;164:3822-3828
447. Gregory SA, Morrissey JH, Edgington TS. Regulation of tissue factor gene expression in the monocyte procoagulant response to endotoxin. *Molecular and cellular biology*. 1989;9:2752-2755
448. Jeon YJ, Han SH, Lee YW, Lee M, Yang KH, Kim HM. Dexamethasone inhibits il-1 beta gene expression in lps-stimulated raw 264.7 cells by blocking nf-kappa b/rel and ap-1 activation. *Immunopharmacology*. 2000;48:173-183
449. Das AM, Lim LH, Flower RJ, Perretti M. Dexamethasone reduces cell surface levels of cd11b on human eosinophils. *Mediators of inflammation*. 1997;6:363-367
450. Egorina EM, Sovershaev MA, Osterud B. Regulation of tissue factor procoagulant activity by post-translational modifications. *Thromb Res*. 2008;122:831-837
451. Gringhuis SI, Garcia-Vallejo JJ, van Het Hof B, van Dijk W. Convergent actions of i kappa b kinase beta and protein kinase c delta modulate mrna stability through phosphorylation of 14-3-3 beta complexed with tristetraprolin. *Molecular and cellular biology*. 2005;25:6454-6463
452. Stoecklin G, Ming XF, Looser R, Moroni C. Somatic mrna turnover mutants implicate tristetraprolin in the interleukin-3 mrna degradation pathway. *Molecular and cellular biology*. 2000;20:3753-3763
453. Stoecklin G, Stoeckle P, Lu M, Muehlemann O, Moroni C. Cellular mutants define a common mrna degradation pathway targeting cytokine au-rich elements. *RNA (New York, N.Y.)*. 2001;7:1578-1588
454. Yu H, Stasinopoulos S, Leedman P, Medcalf RL. Inherent instability of plasminogen activator inhibitor type 2 mrna is regulated by tristetraprolin. *The Journal of biological chemistry*. 2003;278:13912-13918
455. Brooks SA, Connolly JE, Rigby WF. The role of mrna turnover in the regulation of tristetraprolin expression: Evidence for an extracellular signal-regulated kinase-specific, au-rich element-dependent, autoregulatory pathway. *Journal of immunology (Baltimore, Md. : 1950)*. 2004;172:7263-7271
456. Briata P, Ilengo C, Corte G, Moroni C, Rosenfeld MG, Chen CY, Gherzi R. The wnt/beta-catenin-->pitx2 pathway controls the turnover of pitx2 and other unstable mrnas. *Molecular cell*. 2003;12:1201-1211
457. Frevel MA, Bakheet T, Silva AM, Hissong JG, Khabar KS, Williams BR. P38 mitogen-activated protein kinase-dependent and -independent signaling of mrna stability of au-rich element-containing transcripts. *Molecular and cellular biology*. 2003;23:425-436
458. Brook M, Sully G, Clark AR, Saklatvala J. Regulation of tumour necrosis factor alpha mrna stability by the mitogen-activated protein kinase p38 signalling cascade. *FEBS letters*. 2000;483:57-61
459. Ming XF, Stoecklin G, Lu M, Looser R, Moroni C. Parallel and independent regulation of interleukin-3 mrna turnover by phosphatidylinositol 3-kinase and p38 mitogen-activated protein kinase. *Molecular and cellular biology*. 2001;21:5778-5789

460. Montero L, Nagamine Y. Regulation by p38 mitogen-activated protein kinase of adenylate- and uridylate-rich element-mediated urokinase-type plasminogen activator (upa) messenger rna stability and upa-dependent in vitro cell invasion. *Cancer research*. 1999;59:5286-5293
461. Carballo E, Lai WS, Blackshear PJ. Evidence that tristetraprolin is a physiological regulator of granulocyte-macrophage colony-stimulating factor messenger rna deadenylation and stability. *Blood*. 2000;95:1891-1899
462. Ghosh S, Hoenerhoff MJ, Clayton N, Myers P, Stumpo DJ, Maronpot RR, Blackshear PJ. Left-sided cardiac valvulitis in tristetraprolin-deficient mice: The role of tumor necrosis factor alpha. *The American journal of pathology*. 2010;176:1484-1493
463. Rulten SL, Cortes-Ledesma F, Guo L, Iles NJ, Caldecott KW. Aplf (c2orf13) is a novel component of poly(adp-ribose) signaling in mammalian cells. *Molecular and cellular biology*. 2008;28:4620-4628
464. Kuijpers MJ, Munnix IC, Cosemans JM, Vlijmen BV, Reutelingsperger CP, Egbrink MO, Heemskerk JW. Key role of platelet procoagulant activity in tissue factor-and collagen-dependent thrombus formation in arterioles and venules in vivo differential sensitivity to thrombin inhibition. *Microcirculation (New York, N.Y. : 1994)*. 2008;15:269-282
465. Pan S, Kleppe LS, Witt TA, Mueske CS, Simari RD. The effect of vascular smooth muscle cell-targeted expression of tissue factor pathway inhibitor in a murine model of arterial thrombosis. *Thrombosis and haemostasis*. 2004;92:495-502
466. Wang L, Miller C, Swarthout RF, Rao M, Mackman N, Taubman MB. Vascular smooth muscle-derived tissue factor is critical for arterial thrombosis after ferric chloride-induced injury. *Blood*. 2009;113:705-713
467. Tseng MT, Dozier A, Haribabu B, Graham UM. Transendothelial migration of ferric ion in fecl3 injured murine common carotid artery. *Thromb Res*. 2006;118:275-280
468. Farrehi PM, Ozaki CK, Carmeliet P, Fay WP. Regulation of arterial thrombolysis by plasminogen activator inhibitor-1 in mice. *Circulation*. 1998;97:1002-1008
469. Keene JD. Rna regulons: Coordination of post-transcriptional events. *Nature reviews. Genetics*. 2007;8:533-543
470. Chen YL, Huang YL, Lin NY, Chen HC, Chiu WC, Chang CJ. Differential regulation of are-mediated tnfalpha and il-1beta mrna stability by lipopolysaccharide in raw264.7 cells. *Biochemical and biophysical research communications*. 2006;346:160-168
471. Rainer J, Ploner C, Jesacher S, Ploner A, Eduardoff M, Mansha M, Wasim M, Panzer-Grumayer R, Trajanoski Z, Niederegger H, Kofler R. Glucocorticoid-regulated micrornas and mirtrons in acute lymphoblastic leukemia. *Leukemia*. 2009;23:746-752
472. Williams AE, Larner-Svensson H, Perry MM, Campbell GA, Herrick SE, Adcock IM, Erjefalt JS, Chung KF, Lindsay MA. Microrna expression profiling in mild asthmatic human airways and effect of corticosteroid therapy. *PloS one*. 2009;4:e5889
473. Adcock IM, Ito K, Barnes PJ. Glucocorticoids: Effects on gene transcription. *Proceedings of the American Thoracic Society*. 2004;1:247-254
474. Bhavsar P, Hew M, Khorasani N, Torrego A, Barnes PJ, Adcock I, Chung KF. Relative corticosteroid insensitivity of alveolar macrophages in severe asthma compared with non-severe asthma. *Thorax*. 2008;63:784-790
475. Rhen T, Cidlowski JA. Antiinflammatory action of glucocorticoids--new mechanisms for old drugs. *The New England journal of medicine*. 2005;353:1711-1723
476. Stellato C. Glucocorticoid actions on airway epithelial responses in immunity: Functional outcomes and molecular targets. *The Journal of allergy and clinical immunology*. 2007;120:1247-1263; quiz 1264-1245
477. Stellato C. Post-transcriptional and nongenomic effects of glucocorticoids. *Proceedings of the American Thoracic Society*. 2004;1:255-263

478. Stellato C, Matsukura S, Fal A, White J, Beck LA, Proud D, Schleimer RP. Differential regulation of epithelial-derived c-c chemokine expression by il-4 and the glucocorticoid budesonide. *Journal of immunology (Baltimore, Md. : 1950)*. 1999;163:5624-5632
479. Vavassori S, Covey LR. Post-transcriptional regulation in lymphocytes: The case of cd154. *RNA biology*. 2009;6:259-265
480. Chen CY, Gherzi R, Andersen JS, Gaietta G, Jurchott K, Royer HD, Mann M, Karin M. Nucleolin and yb-1 are required for jnk-mediated interleukin-2 mrna stabilization during t-cell activation. *Genes & development*. 2000;14:1236-1248
481. Yarovinsky TO, Butler NS, Monick MM, Hunninghake GW. Early exposure to il-4 stabilizes il-4 mrna in cd4+ t cells via rna-binding protein hur. *Journal of immunology (Baltimore, Md. : 1950)*. 2006;177:4426-4435
482. Dhawan L, Liu B, Blaxall BC, Taubman MB. A novel role for the glucocorticoid receptor in the regulation of monocyte chemoattractant protein-1 mrna stability. *The Journal of biological chemistry*. 2007;282:10146-10152
483. Ishmael FT, Fang X, Houser KR, Pearce K, Abdelmohsen K, Zhan M, Gorospe M, Stellato C. The human glucocorticoid receptor as an rna-binding protein: Global analysis of glucocorticoid receptor-associated transcripts and identification of a target rna motif. *Journal of immunology (Baltimore, Md. : 1950)*. 2011;186:1189-1198
484. Pawashe AB, Golino P, Ambrosio G, Migliaccio F, Ragni M, Pascucci I, Chiariello M, Bach R, Garen A, Konigsberg WK, et al. A monoclonal antibody against rabbit tissue factor inhibits thrombus formation in stenotic injured rabbit carotid arteries. *Circulation research*. 1994;74:56-63
485. Kelley RF, Refino CJ, O'Connell MP, Modi N, Sehl P, Lowe D, Pater C, Bunting S. A soluble tissue factor mutant is a selective anticoagulant and antithrombotic agent. *Blood*. 1997;89:3219-3227
486. Himber J, Refino CJ, Burcklen L, Roux S, Kirchhofer D. Inhibition of arterial thrombosis by a soluble tissue factor mutant and active site-blocked factors ixa and xa in the guinea pig. *Thrombosis and haemostasis*. 2001;85:475-481
487. Cirillo P, Golino P, Ragni M, D'Andrea D, Calabro P, Corcione N, Vigorito F, Ravera M, Chiariello M. Long-lasting antithrombotic effects of a single dose of human recombinant, active site-blocked factor vii: Insights into possible mechanism(s) of action. *Journal of thrombosis and haemostasis : JTH*. 2003;1:992-998
488. Jang IK, Gold HK, Leinbach RC, Fallon JT, Collen D, Wilcox JN. Antithrombotic effect of a monoclonal antibody against tissue factor in a rabbit model of platelet-mediated arterial thrombosis. *Arteriosclerosis and thrombosis : a journal of vascular biology / American Heart Association*. 1992;12:948-954
489. Ragni M, Cirillo P, Pascucci I, Scognamiglio A, D'Andrea D, Eramo N, Ezekowitz MD, Pawashe AB, Chiariello M, Golino P. Monoclonal antibody against tissue factor shortens tissue plasminogen activator lysis time and prevents reocclusion in a rabbit model of carotid artery thrombosis. *Circulation*. 1996;93:1913-1918
490. Presta L, Sims P, Meng YG, Moran P, Bullens S, Bunting S, Schoenfeld J, Lowe D, Lai J, Rancatore P, Iverson M, Lim A, Chisholm V, Kelley RF, Riederer M, Kirchhofer D. Generation of a humanized, high affinity anti-tissue factor antibody for use as a novel antithrombotic therapeutic. *Thrombosis and haemostasis*. 2001;85:379-389
491. Yang J, Lee GF, Riederer MA, Kelley RF. Enhancing the anticoagulant potency of soluble tissue factor mutants by increasing their affinity to factor viia. *Thrombosis and haemostasis*. 2002;87:450-458
492. Suleymanov OD, Szalony JA, Salyers AK, LaChance RM, Parlow JJ, South MS, Wood RS, Nicholson NS. Pharmacological interruption of acute thrombus formation with minimal hemorrhagic complications by a small molecule tissue factor/factor viia inhibitor: Comparison to factor xa and thrombin inhibition in a nonhuman primate thrombosis

model. *The Journal of pharmacology and experimental therapeutics*. 2003;306:1115-1121
493. Kirchhofer D, Tschopp TB, Baumgartner HR. Active site-blocked factors viia and ixa differentially inhibit fibrin formation in a human ex vivo thrombosis model. *Arterioscler Thromb Vasc Biol*. 1995;15:1098-1106
494. Wildgoose P, Berkner KL, Kisiel W. Synthesis, purification, and characterization of an arg152----glu site-directed mutant of recombinant human blood clotting factor vii. *Biochemistry*. 1990;29:3413-3420
495. Valentin S, Reutlingsperger CP, Nordfang O, Lindhout T. Inhibition of factor x activation at extracellular matrix of fibroblasts during flow conditions: A comparison between tissue factor pathway inhibitor and inactive factor viia. *Thrombosis and haemostasis*. 1995;74:1478-1485
496. Golino P, Ragni M, Cirillo P, D'Andrea D, Scognamiglio A, Ravera A, Buono C, Ezban M, Corcione N, Vigorito F, Condorelli M, Chiariello M. Antithrombotic effects of recombinant human, active site-blocked factor viia in a rabbit model of recurrent arterial thrombosis. *Circulation research*. 1998;82:39-46
497. Golino P, Ragni M, Cirillo P, Scognamiglio A, Ravera A, Buono C, Guarino A, Piro O, Lambiase C, Botticella F, Ezban M, Condorelli M, Chiariello M. Recombinant human, active site-blocked factor viia reduces infarct size and no-reflow phenomenon in rabbits. *American journal of physiology. Heart and circulatory physiology*. 2000;278:H1507-1516
498. Golino P, Ragni M, Cirillo P, D'Andrea D, Ravera M, Calabro P, Ezban M, Tommasini P, Chiariello M. Effects of recombinant active site-blocked activated factor vii in rabbit models of carotid stenosis and myocardial infarction. *Blood coagulation & fibrinolysis : an international journal in haemostasis and thrombosis*. 2000;11 Suppl 1:S149-158
499. Moons AH, Peters RJ, Cate H, Bauer KA, Vlasuk GP, Buller HR, Levi M. Recombinant nematode anticoagulant protein c2, a novel inhibitor of tissue factor-factor viia activity, abrogates endotoxin-induced coagulation in chimpanzees. *Thrombosis and haemostasis*. 2002;88:627-631
500. Szalony JA, Taite BB, Girard TJ, Nicholson NS, LaChance RM. Pharmacological intervention at disparate sites in the coagulation cascade: Comparison of anti-thrombotic efficacy vs bleeding propensity in a rat model of acute arterial thrombosis. *Journal of thrombosis and thrombolysis*. 2002;14:113-121
501. St Pierre J, Yang LY, Tamirisa K, Scherrer D, De Ciechi P, Eisenberg P, Tolunay E, Abendschein D. Tissue factor pathway inhibitor attenuates procoagulant activity and upregulation of tissue factor at the site of balloon-induced arterial injury in pigs. *Arterioscler Thromb Vasc Biol*. 1999;19:2263-2268
502. Creasey AA, Chang AC, Feigen L, Wun TC, Taylor FB, Jr., Hinshaw LB. Tissue factor pathway inhibitor reduces mortality from escherichia coli septic shock. *The Journal of clinical investigation*. 1993;91:2850-2860
503. Asada Y, Hara S, Tsuneyoshi A, Hatakeyama K, Kisanuki A, Marutsuka K, Sato Y, Kamikubo Y, Sumiyoshi A. Fibrin-rich and platelet-rich thrombus formation on neointima: Recombinant tissue factor pathway inhibitor prevents fibrin formation and neointimal development following repeated balloon injury of rabbit aorta. *Thrombosis and haemostasis*. 1998;80:506-511
504. Roque M, Reis ED, Fuster V, Padurean A, Fallon JT, Taubman MB, Chesebro JH, Badimon JJ. Inhibition of tissue factor reduces thrombus formation and intimal hyperplasia after porcine coronary angioplasty. *Journal of the American College of Cardiology*. 2000;36:2303-2310
505. Abraham E, Reinhart K, Svoboda P, Seibert A, Olthoff D, Dal Nogare A, Postier R, Hempelmann G, Butler T, Martin E, Zwingelstein C, Percell S, Shu V, Leighton A, Creasey AA. Assessment of the safety of recombinant tissue factor pathway inhibitor in

patients with severe sepsis: A multicenter, randomized, placebo-controlled, single-blind, dose escalation study. *Critical care medicine*. 2001;29:2081-2089
506. Rauch U, Osende JI, Fuster V, Badimon JJ, Fayad Z, Chesebro JH. Thrombus formation on atherosclerotic plaques: Pathogenesis and clinical consequences. *Annals of internal medicine*. 2001;134:224-238
507. Yin X, Yutani C, Ikeda Y, Enjyoji K, Ishibashi-Ueda H, Yasuda S, Tsukamoto Y, Nonogi H, Kaneda Y, Kato H. Tissue factor pathway inhibitor gene delivery using hvj-ave liposomes markedly reduces restenosis in atherosclerotic arteries. *Cardiovascular research*. 2002;56:454-463
508. van Rooij E, Purcell AL, Levin AA. Developing microrna therapeutics. *Circulation research*. 2012;110:496-507
509. Peltz SW, Welch EM, Trotta CR, Davis T, Jacobson A. Targeting post-transcriptional control for drug discovery. *RNA biology*. 2009;6:329-334
510. Zhang Y, Deng Y, Wendt T, Liliensiek B, Bierhaus A, Greten J, He W, Chen B, Hach-Wunderle V, Waldherr R, Ziegler R, Mannel D, Stern DM, Nawroth PP. Intravenous somatic gene transfer with antisense tissue factor restores blood flow by reducing tumor necrosis factor-induced tissue factor expression and fibrin deposition in mouse meth-a sarcoma. *The Journal of clinical investigation*. 1996;97:2213-2224
511. Stephens AC, Rivers RP. Suppression of human monocyte tissue factor synthesis by antisense oligodeoxynucleotide. *Thromb Res*. 1997;85:387-398
512. Cavusoglu E, Chen I, Rappaport J, Marmur JD. Inhibition of tissue factor gene induction and activity using a hairpin ribozyme. *Circulation*. 2002;105:2282-2287
513. Jankowsky E, Schwenzer B. Oligonucleotide facilitators enable a hammerhead ribozyme to cleave long rna substrates with multiple-turnover activity. *European journal of biochemistry / FEBS*. 1998;254:129-134
514. Holen T, Amarzguioui M, Wiiger MT, Babaie E, Prydz H. Positional effects of short interfering rnas targeting the human coagulation trigger tissue factor. *Nucleic acids research*. 2002;30:1757-1766
515. Melloni C, Sprecher DL, Sarov-Blat L, Patel MR, Heitner JF, Hamm CW, Aylward P, Tanguay JF, DeWinter RJ, Marber MS, Lerman A, Hasselblad V, Granger CB, Newby LK. The study of losmapimod treatment on inflammation and infarctsize (solstice): Design and rationale. *American heart journal*. 2012;164:646-653 e643
516. Kumar S, Boehm J, Lee JC. P38 map kinases: Key signalling molecules as therapeutic targets for inflammatory diseases. *Nature reviews. Drug discovery*. 2003;2:717-726
517. Lee JC, Kumar S, Griswold DE, Underwood DC, Votta BJ, Adams JL. Inhibition of p38 map kinase as a therapeutic strategy. *Immunopharmacology*. 2000;47:185-201
518. Wahlberg E, Karlberg T, Kouznetsova E, Markova N, Macchiarulo A, Thorsell AG, Pol E, Frostell A, Ekblad T, Oncu D, Kull B, Robertson GM, Pellicciari R, Schuler H, Weigelt J. Family-wide chemical profiling and structural analysis of parp and tankyrase inhibitors. *Nature biotechnology*. 2012;30:283-288
519. Wiedermann CJ, Kiechl S, Dunzendorfer S, Schratzberger P, Egger G, Oberhollenzer F, Willeit J. Association of endotoxemia with carotid atherosclerosis and cardiovascular disease: Prospective results from the bruneck study. *Journal of the American College of Cardiology*. 1999;34:1975-1981
520. Corrales-Medina VF, Madjid M, Musher DM. Role of acute infection in triggering acute coronary syndromes. *The Lancet infectious diseases*. 2010;10:83-92
521. Hafner M, Landthaler M, Burger L, Khorshid M, Hausser J, Berninger P, Rothballer A, Ascano M, Jr., Jungkamp AC, Munschauer M, Ulrich A, Wardle GS, Dewell S, Zavolan M, Tuschl T. Transcriptome-wide identification of rna-binding protein and microrna target sites by par-clip. *Cell*. 2010;141:129-141

522. Kleine H, Poreba E, Lesniewicz K, Hassa PO, Hottiger MO, Litchfield DW, Shilton BH, Luscher B. Substrate-assisted catalysis by parp10 limits its activity to mono-adp-ribosylation. *Molecular cell*. 2008;32:57-69
523. Goenka S, Cho SH, Boothby M. Collaborator of stat6 (coast6)-associated poly(adp-ribose) polymerase activity modulates stat6-dependent gene transcription. *The Journal of biological chemistry*. 2007;282:18732-18739
524. Otto H, Reche PA, Bazan F, Dittmar K, Haag F, Koch-Nolte F. In silico characterization of the family of parp-like poly(adp-ribosyl)transferases (parts). *BMC genomics*. 2005;6:139
525. Lacoste L, Lam JY, Hung J, Letchacovski G, Solymoss CB, Waters D. Hyperlipidemia and coronary disease. Correction of the increased thrombogenic potential with cholesterol reduction. *Circulation*. 1995;92:3172-3177

Appendix

The following achievements have been accomplished as a result of the work presented in this thesis:

1. PRIZES AND AWARDS

2009 **British Heart Foundation Scholarship**

2010 **British Heart Foundation Clinical Research Fellowship**

2012 **BAS/BSCR/BCS Young Investigator Award (runner-up)**

2012 **BAS/BSCR Travel Award**

2012 **RNA Society Harden Award**

2012 **Royal Society of Medicine President's Medal (finalist)**

2013 **ACC Young Investigator Award (winner)**
(ACCF/Herman K. Gold Award in Molecular and Cellular Cardiology)

2. ABSTRACTS (POSTER PRESENTATIONS)

Dexamethasone reduces monocyte thrombogenecity via tissue factor-dependent and tissue factor-independent pathways
Iqbal MB, Johns M, Laffan MA, Boyle JJ, Haskard DO.
British Atherosclerosis Society Meeting 2010. Oxford (Atherosclerosis 2010; 213(1):E6)

Tristeraprolin post-transcriptionally regulates tissue factor expression in primary human and murine macrophages
Iqbal MB, Dean J, Burke N, Clark AR, Johns M, Haskard DO
72nd Harden Conference of the RNA Society Meeting 2012, Cambridge

Poly(ADP-ribose)-polymerase-14 (PARP-14) post-transcriptionally regulates macrophage tissue factor expression through interaction with tristetraprolin
Iqbal MB**,** Johns M, Burke N, Dean J, Yu SC, Boothby M, Haskard DO
72nd Harden Conference of the RNA Society Meeting 2012, Cambridge

Regulation of macrophage CXCL10 chemokine expression by Poly(ADP-ribose)-polymerase-14 (PARP-14): a novel RNA binding protein
Johns M, Iqbal MB, Yu SC, Burke N, Chu SH, Boothby M, Haskard DO
72nd Harden Conference of the RNA Society Meeting 2012, Cambridge

A novel KH-like domain accounts for the subcellular localization of Poly(ADP-Ribose) Polymerase-14 (PARP)-14 in cytoplasmic granules
Yu SC, Johns M, Iqbal MB, Burke N, Haskard DO
72nd Harden Conference of the RNA Society Meeting 2012, Cambridge

Poly(ADP-ribose) polymerase -14 interacts with tristetraprolin to selectively regulate tissue factor mRNA stability: a novel role for ADP-ribosylation in regulating mRNA turnover and thrombosis
Iqbal MB, Johns M, Liu Y, Yu SC, Hyde GD, Laffan MA, Marchese FP, Cho SH, Clark AR, Gavins FN, Blackshear PJ, Mackman N, Dean JL, Boothby M, Haskard DO
BAS/BSCR/BCS Meeting, 3th-4th Jun 2013, London

3. ABSTRACTS (ORAL PRESENTATIONS)

Tristeraprolin regulates tissue factor mRNA stability in macrophages
Iqbal MB, Dean J, Burke N, Clark AR, Johns M, Haskard DO
BAS/BSCR/BCS Meeting 2012, Manchester

Post-transcriptional regulation of tissue factor expression: novel mechanisms regulating thrombosis
Iqbal MB, Johns M, Burke N, Clark AR, M Boothby, Dean J, Haskard DO
Royal Society of Medicine 2012. London.

Poly(ADP-ribose)-polymerase-14 (PARP-14) post-transcriptionally regulates macrophage tissue factor expression through interaction with tristetraprolin
Iqbal MB, Johns M, Burke N, Clark AR, M Boothby, Dean J, Haskard DO
British Atherosclerosis Society Meeting 2012. Cambridge

Tristetraprolin and Poly(ADP-ribose)-polymerase-14 post-transcriptionally regulates macrophage tissue factor expression: novel mechanisms for regulating thrombosis
Iqbal MB, Johns M, Burke N, Clark AR, Dean J, M Boothby, Gavins F, Haskard DO
AHA 2012 Annual Scientific Session, 3rd-7th Nov 2012. Los Angeles, CA.

Poly(ADP-ribose)-polymerase-14 cooperates with tristetraprolin to control tissue factor mRNA stability: a novel role for ADP ribosylation in regulating thrombosis
Iqbal MB, Johns M, Liu Y, Yu SC, Hyde GD, Laffan MA, Marchese FP, Cho SH, Clark AR, Gavins FN, Blackshear PJ, Mackman N, Dean JL, Boothby M, Haskard DO
ACC 2013 Annual Scientific Sessions, 9th-11th Mar 2013. San Francisco, CA.

Poly(ADP-ribose) polymerase -14 interacts with tristetraprolin to selectively regulate tissue factor mRNA stability: a novel role for ADP-ribosylation in regulating mRNA turnover and thrombosis
Iqbal MB, Johns M, Liu Y, Yu SC, Hyde GD, Laffan MA, Marchese FP, Cho SH, Clark AR, Gavins FN, Blackshear PJ, Mackman N, Dean JL, Boothby M, Haskard DO
ESC Congress 2013, 31st Aug – 4th Sep 2013, Amsterdam, Netherlands

4. PEER-REVIEWED JOURNAL PUBLICATIONS

Poly(ADP-ribose)-polymerase-14 cooperates with tristetraprolin to control tissue factor mRNA stability
Iqbal MB, Johns M, Liu Y, Yu SC, Hyde GD, Laffan MA, Marchese FP, Cho SH, Clark AR, Gavins FN, Woollard K, Blackshear PJ, Mackman N, Dean JL, Boothby M, Haskard DO
Submitted to Blood (under review)